RESEARCH

UDOT CONNECTING COMMUNITIES

Utah Department of Transportation - Research Division
4501 South 2700 West, Box 148410 - Salt Lake City, Utah 84114-8410

Report No. UT-09.08

SEISMIC VULNERABILITY ASSESSMENT AND RETROFIT RECOMMENDATIONS FOR STATE HIGHWAY BRIDGES: CASE STUDIES

Prepared For:

Utah Department of Transportation
Research Division

Submitted by:

Department of Civil & Environmental Engineering, Utah State University

Authored by:

Abdollah Shafieezadeh
Wenying Hu
Emrah Erduran
Keri L. Ryan

February, 2009

DISCLAIMER

The authors alone are responsible for the preparation and accuracy of the information, data, analysis, discussions, recommendations, and conclusions presented herein. The contents do not necessarily reflect the views, opinions, endorsements, or policies of the Utah Department of Transportation of the US Department of Transportation. The Utah Department of Transportation makes no representation or warranty of any kind, and assumes no liability therefore.

THIS PAGE INTENTIONALLY LEFT BLANK

Report Documentation Page (FHWA Abstract Page)

1. Report No. UT- 09-08	2. Government Accession No.	3. Recipient's Catalog No.
4. Title and Subtitle SEISMIC VULNERABILITY ASSESSMENT AND RETROFIT RECOMMENDATIONS FOR STATE HIGHWAY BRIDGES: CASE STUDIES		5. Report Date May, 2009 6. Performing Organization Code
7. Author Abdollah Shafieezadeh, Wenying Hu, Emrah Erduran, Keri L. Ryan		8. Performing Organization Report No. N/A
9. Performing Organization Name and Address Utah State University Department of Civil and Environmental Engineering 4110 Old Main Hill Logan, UT 84322-4110		10. Work Unit No. 11. Contract or Grant No. 07-9035
12. Sponsoring Agency Name and Address Utah Department of Transportation 4501 South 2700 West Salt Lake City, Utah 84114-8410		13.Type of Report & Period Covered Final Report 09/2006-04/2009 14. Sponsoring Agency Code PIC No. UT06.801
15. Supplementary Notes Prepared in cooperation with the Utah Department of Transportation Research Division		

16. Abstract

Much of Utah's population dwells in a seismically active region, and many of the bridges connecting transportation lifelines predate the rigorous seismic design standards that have been developed in the past 10-20 years. Other states in the west have instituted seismic retrofit programs in response to damage to transportation networks in past California earthquakes. In a parallel report, seismic retrofit guidelines were developed for Utah based on the Seismic Retrofitting Manual for Highway Structures published by FHWA. In this report, representative case study bridges are evaluated in detail using the guidelines. The case study evaluations include the following for each bridge: (1) selection and presentation of analysis method, (2) development of numerical model in LARSA 4D and/or additional programs as needed, (3) evaluation of the seismic response of the unretrofitted bridge, (4) design of a possible retrofit scheme. The bridges evaluated include a four-span simply supported prestressed concrete girder bridge, a four-span continuous concrete T-beam, and an eight-span curved steel girder bridge with in-span pin and hanger joints. A variety of different evaluation methods are presented including linear response spectrum analysis for demand assessment, capacity spectrum method and pushover analysis for capacity assessment, and nonlinear response history analysis. A variety of retrofit techniques are presented including column jacketing, cable restrainers, selectively closing pin and hanger joints, and seismic isolation. The varied examples and techniques presented in this report are meant to be representative of assessment and applicable retrofit approaches for many of the bridges in the state inventory that may be seismically deficient.

17. Key Words Seismic retrofit, nonlinear analysis, column jacketing, seismic isolation, LARSA-4D		18. Distribution Statement UDOT Research Division 4501 south 2700 West-box 148410 Salt Lake City, Utah 84114		23. Registrant's Seal
19. Security Classification Unclassified	20. Security Classification Unclassified	21. No. of Pages 221	22. Price	

THIS PAGE INTENTIONALLY LEFT BLANK

ACKNOWLEDGMENTS

This research was made possible with funding from the Utah Department of Transportation and the Utah Transportation Center at Utah State University. We are very grateful for this support. We wish to recognize the following individuals of the Technical Advisory Committee, who were helpful in guiding the project, and spent extra time engaging in fruitful technical discussions.

Ray Cook	UDOT Structures
Hugh Boyle	Baker Corporation
Daniel Hsiao	UDOT Research

In addition, we wish to recognize Dr Ali Karakaplan of LARSA Corporation and Professor Mettupalayam Sivaselvan of the University of Colorado, Boulder, who provided guidance in the use of nonlinear analysis capabilities of LARSA 4D.

Finally, we recognize the following individuals from Caltrans that took the time to meet with us, give us an overview of California's retrofit program, and provide some general suggestions for developing a retrofit program in Utah.

Mark Yashinsky	Earthquake Engr. – Post EQ Recovery
Rand Held	Structures Local Assistance
Craig Whitten	Earthquake Engr. - Design
Don Lee	Earthquake Engr. – Isolation
Mark Mahan	Earthquake Engr. – Design
Cynthia MacLeay	Earthquake Engr. – Prioritization
Gary Goff	Structures Local Assistance

THIS PAGE INTENTIONALLY LEFT BLANK

TABLE OF CONTENTS

LIST OF TABLES xii
LIST OF FIGURES xv
EXECUTIVE SUMMARY 1
1. Clearfield Interchange Overpass, So. Layton to Hill Field Interchange 9
1.1 Existing Structure 9
1.2 Determination of Seismic Retrofit Category (SRC) 9
1.3 Overview of Evaluation Methods 10
1.4 Creating a LARSA Model 11
1.4.1 Superstructure Elements 12
1.4.2 Substructure Elements 15
1.4.3 Foundation Elements 16
1.4.4 Abutment Springs 17
1.4.5 Summary of the LARSA Bridge Model 19
1.5 Evaluation of the Bridge for the LL Ground Motion 20
1.5.1 Component Capacity Evaluation 21
1.5.2 Structure Demand Evaluation 22
1.5.3 Evaluation of Capacity/Demand Ratios 23
1.6 Evaluation of the Bridge for the UL Ground Motion 24
1.6.1 Capacity Evaluation 24
1.6.2 Pushover Analysis with LARSA 25
1.6.4 Analysis Results and Discussion 28
1.7 Bridge Retrofit using Seismic Isolation 29
Appendix 1. Detailed Analysis for Clearfield Interchange Overpass 33
Appendix 1A. Determination of Seismic Retrofit Category 33
Appendix 1B. Element Properties in LARSA Model 36
Appendix 1C. Column and Footing Moment Capacities 45
Appendix 1D. Elastic Moment Demands for LL Evaluation 51
Appendix 1E. Capacity/Demand Ratios for LL Evaluation 54
Appendix 1F. Deformation Capacity of Columns 64
Appendix 1G. Excel Worksheet for Iterative Demand Analysis 75
Appendix 1H. Design and Evaluation of Isolation Systems 80

2. Church Street Underpass, So. Layton to Hill Field Interchange 91
2.1 Existing Structure..... 91
2.2 Determination of Seismic Retrofit Category (SRC) 91
2.3 Overview of Evaluation Methods 92
2.4 Creating a LARSA Model 93
2.4.1 Superstructure Elements 94
2.4.2 Substructure Elements 95
2.4.3 Foundation Elements 96
2.4.4 Abutment Springs 97
2.4.5 Summary of the LARSA Bridge Model 98
2.5 Evaluation of the Bridge for the LL Ground Motion..... 100
2.5.1 Component Capacity Evaluation 101
2.5.2 Structure Demand Evaluation 102
2.5.3 Evaluation of Capacity/Demand Ratios..... 103
2.6 Evaluation of the Bridge for the UL Ground Motion 104
2.6.1 Bridge Capacity Evaluation 104
2.6.2 Bridge Demand Evaluation..... 108
2.7 Proposed Retrofit Measures and Evaluation..... 112
Appendix 2. Detailed Analysis for Church Street Underpass 114
Appendix 2A. Determination of Seismic Retrofit Category..... 114
Appendix 2B. Element Properties in LARSA Model..... 116
Appendix 2C. Column and Footing Moment Capacities..... 123
Appendix 2D. Elastic Moment Demands for LL Evaluation 131
Appendix 2E. Capacity/Demand Ratios for LL Evaluation 133
Appendix 2F. Capacity Spectrum Evaluation for Upper Level Ground Motion (Method D1) 145
Appendix 2G. Design of Steel Shell for Retrofitting..... 149
3. B-Ramp Over I-215 and I-80..... 155
3.1 Introduction..... 155
3.2 Existing Bridge Structure..... 157
3.3 Overview of Evaluation Methods 158
3.3.1 Selection of Ground Motions for Response History Analysis..... 159

3.4 Development and Verification of Pin/Hanger Element 161
3.5 Evaluation of the Unretrofitted Bridge 163
3.5.1 Model Description 163
3.5.2 Analysis Results 167
3.6 Proposed Retrofit Solutions 169
3.6.1 Fixing All the Hanger Joints 169
3.6.2 Partial Joint Fixity and Column Isolation 169
3.6.3 Column Jacketing 174
3.7 Evaluation of Retrofit Solutions 175
3.8 Design of Cable Restrainers 178
Appendix 3. Detailed Analysis for B-Bent Over I-215 and I-80 182
Appendix 3A. Determination of Seismic Retrofit Category 182
Appendix 3B. Verification Studies of Pin-Hanger Element 184
Appendix 3C. Modeling Considerations 195
Appendix 3D. Restrainer Cable Design 200
REFERENCES 203

THIS PAGE INTENTIONALLY LEFT BLANK

LIST OF TABLES

Table 1.4.1 LARSA modeling and analysis files for bridge example 1 12
Table 1.6.1 Comparison of displacement capacities and demands in bent local directions 28
Table 1.7.1 Deformation response of the isolated bridge from response spectrum analysis..... 32
Table 1A.1 Blow count number of soil..... 35
Table 1B.1 Natural periods of bridge in tension and compression model..... 45
Table 1C.1 Column and footing overstrength moments..... 46
Table 1C.2 Revised column and footing overstrength moments (iteration 1)..... 48
Table 1C.3 Revised column and footing overstrength moments (iteration 2)..... 49
Table 1D.1 Maximum elastic moment demands for compression model 51
Table 1D.2 Maximum elastic moment demands for tension model 52
Table 1D.3 Maximum elastic moment demands 53
Table 1E.1 Ultimate moment capacity/elastic moment demand ratios 54
Table 1E.2 C/D ratios for columns and footings. 60
Table 1E.3 C/D ratios for column shear 62
Table 1E.4 Capacity/demand ratios for abutments 63
Table 1E.5 Capacity/demand ratios for the as-built bridge. 64
Table 1F.1 Neutral axis depth in columns 67
Table 1F.2 Plastic curvature capacity of columns. 73
Table 1F.3 Total rotational capacity of columns. 73
Table 1F.4 Allowable drift in each bent 74
Table 1F.5 Allowable drift in each bent 75
Table 1G.1 Bent deformations in global X and Y-directions 79
Table 1G.2 Bent deformations in bent longitudinal and transverse directions..... 80
Table 1H.1 Design shear forces for isolators..... 81
Table 1H.2 Equivalent moment of inertia for isolators 87
Table 1H.3 Equivalent moments of inertia selected for economy of design 88
Table 2.4.1 LARSA modeling and analysis files for bridge example 2 94
Table 2.6.1 Displacement response of bridge..... 112
Table 2B.1 Natural periods of bridge in tension and compression model..... 123
Table 2C.1 Column and footing overstrength moments..... 125

Table 2C.2 Revised column and footing overstrength moments (iteration 1). 127
Table 2C.3 Revised column and footing overstrength moments (iteration 2) 128
Table 2D.1 Maximum elastic moment demands for compression model 131
Table 2D.2 Maximum elastic moment demands for tension model 132
Table 2E.1 Ultimate moment capacity/demand ratios for compression model 133
Table 2E.2 Ultimate moment capacity/demand ratios for tension model 134
Table 2E.3 C/D ratios for plastic hinging at column base (compression model) 136
Table 2E.4 C/D ratios for plastic hinging at the column base (tension model) 137
Table 2E.5 C/D ratios for plastic hinging at the column top (tension model) 140
Table 2E.6 C/D ratios for plastic hinging at column top (compression model) 140
Table 2E.7 C/D ratios for column shear (compression model) 142
Table 2E.8 C/D ratios for column shear (tension model) 142
Table 2E.9 C/D ratios for abutment displacement 144
Table 2F.1 Stiffness and natural period of the bridge 146
Table 2F.2 Elastic bridge response 146
Table 2F.3 Nominal yield moment of the columns 147
Table 2F.4 Summary of iterations to calculate spectral displacement 148
Table 2G.1 Values of plastic curvature and plastic rotation capacity (t= 10 mm) 151
Table 2G.2 Plastic rotation demand 152
Table 2G.3 Values of plastic curvature and plastic rotation capacity (t= 6 mm) 152
Table 3.3.1 Properties of ground motions used in the study 161
Table 3.5.1 Summary of bent element properties 165
Table 3.5.2 Mean pounding force at each gap 168
Table 3.5.3 Columns deformation response 168
Table 3.5.4 Hanger longitudinal strains 169
Table 3.6.1 Calculations to determine isolator properties. 173
Table 3.6.2 Summary of jacketed column properties 174

LIST OF FIGURES

Figure 1.4.1. Girder-bent-column connection details.(solid lines show the model)..... 14
Figure 1.4.2. Definition of L, b_0, and *Edge* for longitudinal and transverse directions..... 14
Figure 1.4.3. Composite section with girder and effective deck width 15
Figure 1.4.4. Methods to evaluate pile group stiffness (Figure 6-18 of FHWA, 2006) 17
Figure 1.4.5. Calculation of abutment passive pressure (Figure 6-23 of FHWA, 2006)..... 18
Figure 1.4.6. Geometry for abutment springs..... 19
Figure 1.4.7. 3D rendering of LARSA bridge model excluding composite section geometry 20
Figure 1.4.8. Elevation rendering of LARSA bridge model..... 20
Figure 1.6.1. Sketch of column displaced shape and contributions to column displacement 27
Figure 1A.1. Acceleration design spectra for LL and UL ground motions..... 36
Figure 1B.1. Calculating rotational stiffness of pile group..... 39
Figure 1B.2. Abutment plan 43
Figure 1C.1. Column interaction diagram 50
Figure 1C.2. Computing pile-footing moment capacity using statics (From FHWA, 2006) 50
Figure 1G.1. General bridge information for spreadsheet utility 76
Figure 1G.2. Results in the first iteration for compression model..... 78
Figure 1G.3. Results of the last iteration for compression model. 78
Figure 1G.4. Results of the last iteration for tension model. 78
Figure 1H.1. Hybrid design spectrum for the first iteration 89
Figure 2.4.1. Methods to evaluate pile group stiffness (Figure 6-18 of FHWA, 2006) 96
Figure 2.4.2. Calculation of abutment passive pressure (Figure 6-23 of FHWA, 2006)..... 98
Figure 2.4.3. Elevation rendering of LARSA bridge model..... 99
Figure 2.4.4. 3D rendering of LARSA bridge model 99
Figure 2.4.5. Skeleton rendering of LARSA bridge model indicating nodes and elements..... 100
Figure 2.6.1. Capacity curve to be used in capacity spectrum method..... 105
Figure 2.6.2. Longitudinal uniform loading of LARSA bridge model..... 106
Figure 2.6.3. Transverse uniform loading of LARSA bridge model..... 107
Figure 2.6.4. Response spectrum in spectral acceleration vs. natural period format..... 109
Figure 2.6.5. Response spectrum in spectral acceleration vs. spectral displacement format 109
Figure 2.6.6. Illustration of iterative procedure..... 111

Figure 2.7.1. Typical steel shell retrofit of round column (Figure 9-9 of FHWA, 2006)..... 113
Figure 2A.1. The seismic design response spectrum (Lower Level ground motion)..... 115
Figure 2A.2. The seismic design response spectrum (Upper Level ground motion) 116
Figure 2B.1. Calculating rotational stiffness of pile group..... 119
Figure 2C.1. Column moment and shear to satisfy equilibrium..... 126
Figure 2C.2. Bent equilibrium to determine axial force due to overturning 126
Figure 2C.3. Column interaction diagrams..... 129
Figure 2C.4. Computing pile-footing moment capacity using statics 130
Figure 3.1.1. Typical pin-hanger joint details..... 156
Figure 3.3.1. Seismic hazard deaggregation for 2475 year event at the bridge location..... 160
Figure 3.3.2. Median response spectra of the ground motions along with the design spectrum 161
Figure 3.4.1. The pin-hanger joint model 162
Figure 3.5.1. The cross section of deck. 164
Figure 3.5.2. Moment-curvature curves of the two typical columns. 166
Figure 3.6.1. (a) Locking all pin-hanger joints, and (b) selectively locking pin-hanger joints with seismic isolation..... 170
Figure 3.6.2. Free vibration analysis of bridge segments for positive and negative impulses ... 171
Figure 3.6.3. Free vibration analysis on the isolated bridge 173
Figure 3.6.4. Moment – curvature diagram of jacketed columns 175
Figure 3.7.1. Average pounding forces in the gaps. 176
Figure 3.7.2. Average deformation demands in the hangers. 176
Figure 3.7.3. Average plastic rotation DCR's for all bridges 177
Figure 3B.1. Pin-hanger joint model for the analytical force-deformation derivation. 185
Figure 3B.2. Pin-hanger joint model in LARSA and OpenSees. 186
Figure 3B.3. Imposed end displacement..... 186
Figure 3B.4. Force-deformation curves for static cyclic loading. 187
Figure 3B.5. Input acceleration in x-direction. 188
Figure 3B.6. Time history of the deformation response in X direction. 188
Figure 3B.7. Force-deformation curves for dynamic loading. 189
Figure 3B.8. Force and deformation response of the element in X direction versus time. 189
Figure 3B.9. Input acceleration in y-direction. 191
Figure 3B.10. Force-deformation curves for dynamic loading. 192

Figure 3B.11. X and y-deformation responses of the pin-hanger element versus time..... 193
Figure 3B.12. Pin-hanger joint model with adjacent beam elements. 193
Figure 3B.13. Force-deformation and deformation time history response of the pin-hanger model with adjacent frame elements. 194

EXECUTIVE SUMMARY

Three Utah state highway bridges were investigated in detail to determine their seismic deficiencies. The bridges were analyzed by different methods recommended in recently published guidelines (FHWA, 2006) that have been evaluated in detail for the state of Utah (Wilson and Ryan, 2009). The bridges were evaluated to an Upper Level ground motion with a no collapse performance objective and a Lower Level ground motion under a serviceability performance objective. A detailed model of each bridge that represents its dynamic behavior was created in LARSA 4D from the bridge plans. The evaluation emphasizes nonlinear analysis to determine the capacities of the existing bridges. Additional computational tools were used to supplement the analyses as necessary. Various retrofit approaches are recommended including seismic isolation, column jacketing, locking motion joints, and using cable restrainers to limit joint separation.

Bridge 1: Four-Span Simply Supported Reinforced Concrete Girder Bridge

The first bridge considered is a freeway undercrossing on I-15 near the town of Clearfield constructed in the 1960's. Two essentially identical four span prestressed reinforced concrete girder bridges pass over surface streets – one in each direction. The bridge spans are simply supported and each span has a different length. The superstructure is supported by 7 prestressed girders, except for the longest span, which uses 9 prestressed girders. The superstructure is supported on elastomeric bearings, which are not explicitly modeled. Each bent consists of three reinforced concrete columns of circular cross section. The columns are 30 inch diameter and reinforced with 10 #11 longitudinal bars. The main reinforcing steel is lap spliced just above the footings, and the column transverse steel consists of #4 hoops at 12 in. Abutments are seat type supported on 50-ton piles with approach retaining walls. They are oriented in parallel to bent caps with the skew angle of 34°57'. All columns are supported on pile caps aligned parallel to the bent caps. A standard 5 pile design is used for middle columns while a 4 pile design is used for exterior columns. Piles design load are 50 tons and are assumed to be rigidly connected to the pile cap.

The bridge was evaluated for a fully operational performance objective (Performance Level 3) for the Lower Level motion, which is a 500 year return period earthquake, and for a life safety performance objective (Performance Level 1) for the Upper Level motion, which is a 2500 year return period earthquake. The Seismic Hazard Levels for the Upper Level and Lower Level

motions are functions of the site response spectra and site class. The site class was determined from the boring data and, being on the border between D and E, is taken to be E. Based on a Seismic Hazard Level of IV, the Seismic Retrofit Category (SRC) is C for both Upper Level and Lower Level motions.

For the Lower Level motion, the bridge was evaluated using Method C, which evaluates capacity/demand ratios for each bridge component. Method C requires a linear elastic analysis of the complete bridge to determine the demands of individual components, while the capacities of columns, footings, etc. are determined individually by hand calculations or software. For the Upper Level motion, the bridge was evaluated by pushover analysis of individual events (Method D2) to determine the capacity, in combination with multi-mode linear response spectrum analysis of the complete bridge to determine the demand. The demand assessment is an iterative procedure whereby the footing and abutment stiffnesses are iteratively decreased to limit the forces transferred to the columns. The elastic displacement demands determined through this procedure represent the true inelastic displacement demands according to the equal displacement rule.

A complete model of the bridge was developed in LARSA for demand analysis. Superstructure elements were modeled individually using LARSA Section Composer, and represent the composite stiffness of the girders with deck overlay. Cracked section properties were used to model the columns and bent caps, and the column flexural stiffness was based on the computed nominal moment capacity and yield displacement, determined from a section analysis that accounts for the column axial load. A fully coupled 6x6 foundation stiffness matrix was developed to represent pile groups below columns. Abutments were modeled by individual springs connected to end nodes transversely distributed over the end of the bridge, wherein spring stiffnesses were based on the passive soil pressures of the back walls and wing walls plus pile group stiffness. The bridge was analyzed using both a compression model (span hinges closed) and tension model (span hinges open).

For capacity evaluation, pushover analysis of individual bents was performed in directions both parallel and normal to the bent. In pushover analysis, the lateral forces are incrementally increased while dead loads are held constant. The analysis is displacement controlled and continues until one of several deformation limit states is reached. An alternative nonlinear model of each of the bridge bents was created in LARSA for the pushover analysis. The columns were modeled using a hysteretic beam element, which is a concentrated plasticity

element. The element utilizes user defined moment-curvature curves at various axial loads to determine the behavior of the hinge. These curves were determined by section analysis using Xtract. Bilinear springs were created to model the foundation elements.

The results of the component procedure for the Lower Level motion indicated that capacity/demand ratios for column and footing moments, column shear, anchorage and splice length for column longitudinal reinforcement were all well below 1.0. This suggests that the bridge responded well into the inelastic range, which means (1) the component procedure may be overconservative, and (2) the objective to keep the bridge elastic in the 500 year return period event should be reevaluated. From evaluation to the Upper Level motion, several pier demands determined from elastic response spectrum analysis well exceeded the capacities determined from the pushover analysis.

Seismic isolation was selected as the primary retrofit strategy for this bridge. Seismic isolation is a feasible choice because it uses expansion joints at the bent caps and at the abutments, such that the elastomeric bearings can be replaced with isolation bearings. For the Upper Level motion, seismic isolation will reduce the bridge demands through period lengthening and energy dissipation such that no further strengthening or ductility enhancement is required. In this bridge, the clearance between the abutments and the backwall is inadequate to accommodate the seismic displacement, but it is acceptable to allow the backwall to be damaged and make the necessary repairs to provide additional clearance following an earthquake.

Design properties for the seismic isolation bearings were determined through an iterative analysis procedure. Initially, isolation properties (effective stiffness and effective damping) were chosen that depend on assumed displacement demands. The bridge model was updated to reflect the isolator properties, and response spectrum analysis was performed to determine new demands. The procedure was repeated until the computed demands match the assumed demands from the previous iteration. Isolation bearings were not designed in detail. The converged pier deformation demands of the bridge retrofitted with seismic isolation were well within the capacity limits for the Upper Level ground motion. Although the bridge was not reanalyzed for the Lower Level motion, the isolated bridge is unlikely to suffer serious damage in a more frequent event.

Bridge 2: Four-Span Continuous Concrete T-beam Bridge

The second bridge considered is a freeway overcrossing on I-15 near the town of Layton, constructed in late 1960's. The exterior spans are 35', while the interior spans are 80'-6", and

the bridge has a horizontal skew of 30°36'. The superstructure consists of a 7.5 inch thick reinforced concrete slab supported on four rectangle reinforced concrete girders spaced at 10 ft-8 in. The superstructure is fixed in the transverse direction and contains hinges in the longitudinal direction at each of the four piers. All piers are multi-column bents with three identical 30 inch diameter circular reinforced concrete columns. Each column is supported on a standard pile group with four piles. The end abutments are integral.

This bridge has similar characteristics to the first bridge in terms of importance (standard), age, location (seismicity) and site class. Therefore, it was also determined to be in SRC C, and was evaluated for a fully operational performance objective for the Lower Level (500 year return period) motion, and for a life safety performance objective for the Upper Level (2500 return period) motion.

Like the first example, this bridge was evaluated using Method C, the component capacity/demand method, for the Lower Level motion. For the Upper Level motion, the bridge was evaluated by the Capacity Spectrum Method (Method D2) to determine the capacity, in combination with the Uniform Load Method of the complete bridge to determine the demand. In the Capacity Spectrum Method, a capacity curve for the bridge is developed by hand calculations, and the demand is determined through a single mode response spectrum analysis using equivalent damping. The demand is updated iteratively until the intersection point of the demand and the capacity curve is found.

Because of its regularity and in-plane rigidity, a "spine" model was used, where the bridge superstructure was modeled with single beam elements, representing the composite stiffness of the cross section. A parametric section was defined that allowed girder depth to vary over the length of the bridge. Beam elements were used to model the bent caps and bridge columns based on cracked section properties, except for the column flexural stiffness, which was based on nominal moment capacity as described for the first bridge. Joints were connected at element centerlines and member end offsets were used to account for joint penetration regions. Pile group foundation spring stiffness matrices and individual abutment springs were developed as described for the first bridge.

Since the analysis of this bridge to the Lower Level ground motion is very similar to the first bridge, and the selection of a retrofit measure was controlled by the Upper Level ground motion, only the Upper Level analysis is summarized here. For the capacity spectrum method, a bilinear capacity curve for the bridge was developed that plots applied lateral load against

displacement of a reference degree of freedom. The capacity curve was characterized by initial stiffness (determined from analysis of the bridge model with uniformly applied lateral load), yield strength (computed as the sum of individual column strengths based on their nominal moment capacity), postyield stiffness (taken as 5% of the initial stiffness), and a deformation capacity (based on limiting plastic hinge rotation for this bridge). The demand of the bridge is represented by spectral response, wherein the nonlinear response is accounted for by an equivalent linear system with effective stiffness and effective damping. The effective stiffness is the secant stiffness from 0 to the corresponding point on the capacity curve, and the effective damping is estimated based on the ductility. The response spectrum can be plotted as spectral acceleration versus spectral displacement such that it has the same ordinates as the capacity curve. The equivalent linear properties were iteratively calculated until the intersecting points of the capacity and demand curve are found. Based on this procedure, the bridge displacement demands exceeded the capacity for both the tension and compression models, transverse and longitudinal directions, by amounts ranging from 35 to 75%.

Since the capacity limit state for the Upper Level ground motion was based on a plastic hinge rotation, increasing the ductility and overall displacement capacity of the columns is judged to be the preferred retrofit approach. Partial steel jacketing is recommended to increase the volumetric ratio of transverse reinforcement, increase the ultimate compression strain, and ultimately allow for a larger rotation capacity. Steel jackets will also address the inadequate splice length detected in the Lower Level analysis. Calculations demonstrated that the recommended minimum shell thickness of 10 mm, applied over 32 inch length at the top and bottom of the columns, provides sufficient and reserve ductility capacity for life safety response in the Upper Level ground motion.

Bridge 3: Eight-Span Steel Curved Girder Bridge with Pin-Hanger Assemblies

The third bridge investigated within the scope of this study is an eight span highway overcrossing curved girder bridge crossing over I-215 and I-80 in Salt Lake City. The bridge was constructed in 1985 and represents a class of US bridges that utilize pin-hanger assemblies in some of the spans. The bridge path is a sector of a circle with the radius of 1432 ft and the length of 1430.5 ft. The superstructure in all the spans consists of 4 welded I-section steel girders with reinforced concrete deck overlay at a width of 22.5 ft normal to the bridge path. Geotechnical details provided in the design drawings indicate that the bridge rests on type E soil. Pin-hanger assemblies were provided in four of the spans to prevent formation of stresses due to

thermal expansion. Girders are continuous between the pin-hanger joints and their rotation at columns location is constrained to the column end rotation.

The pin-hanger connection consists of an upper pin, a lower pin and two hangers that together connect the web of a suspended beam to the web of a cantilever beam. The pin-hanger joint provides free rotation by the loose fit of pins into the web of girders, and under typical thermal cycles do not transfer stresses to the deck elements. However, external factors such as weather, deicing salts, and corrosion may cause the locking of pins, formation of bending moments, and unforeseen stresses forming in the hangers. Under seismic excitation, longitudinal forces may lead to differential motion of the spans between the pin-hanger joints, including pounding and local damage at the point of contact. Pin-hanger connections are no longer permitted due to several deficiencies that have been observed.

Another potential problem as far as the seismic behavior of the bridge is concerned may stem from the very low concrete strength and the associated lack of ductility and stiffness in the bridge piers. The yield strength of reinforcement and structural steel can also be considered to be lower than modern standards.

Because of the curvature of the bridge and the importance of accurately modeling the dynamic behavior, including pounding, of the pin-hanger joints, we elected to evaluate the bridge with nonlinear response history analysis methods. Response history analysis is generally reserved for irregular bridges in SRC D, wherein this bridge is categorized in SRC D only if it is considered to be *essential*. In our judgment, the bridge may be considered essential because it connects two major freeway interchanges, and response history analysis is appropriate here. This bridge was only evaluated for the Upper Level ground motion.

The model of the pin-hanger joint was developed and tested in LARSA. The pin-hanger connection was modeled using a corotational truss element that accounts for large deformation kinematics, and pounding of adjacent spans was modeled using a linear gap element with tangent stiffness proportional damping. Convergence difficulties were encountered with the hanger element in LARSA, and an alternative program OpenSees was selected for dynamic analysis. The model of the bridge was created in LARSA and imported to OpenSees, which utilized LARSA bridge path and automatic meshing to define the geometry and connectivity. Elastic frame elements were used to model the superstructure, wherein a single composite section was created to represent the girders and deck. Columns were modeled using concentrated plasticity elements with resultant moment-curvature defined through section analysis. A coupled spring

stiffness matrix was created to model the abutments, and foundations were fixed below the columns. Seven ground motions were selected for dynamic analysis according to the site class, distance, and magnitude consistent with seismic deaggregation data for a return period of 2475 years. The motions were amplitude scaled to match the target spectrum.

Nonlinear response history analyses conducted on the bridge in its current form revealed that pounding of the decks at all four hinge locations is to be expected. Furthermore, the plastic rotation demands in the columns of the bridge were observed to exceed the associated capacities by large amounts, implying a high probability of collapse under a 2475 year event. As such, retrofit schemes that aim to improve the seismic performance of the bridge were developed and evaluated.

The first retrofit scheme proposes to lock all the hanger connections such that the pounding of the adjacent decks will be eliminated. Furthermore, the redundancy of the bridge is also increased, particularly at the end spans that are effectively simply supported. Locking all connections may cause the stresses resulting from thermal cycles to be unacceptably large, and does not provide any solution to the lack of ductility in the bridge columns.

The second retrofit scheme eliminates (locks) two of the pin-hanger joints, and aims to match the periods of the remaining three segments such that they vibrate in phase longitudinally and pounding of the spans is eliminated. The first and third segments have similar properties, and seismic isolators were used to lengthen the period of the middle span. The retrofit scheme also does not address the lack of ductility in the columns.

The third retrofit scheme proposes to retrofit the columns with an additional concrete layer inside a steel jacket. The high strength concrete layer provides additional stiffness to reduce column displacement demands, while the steel jacket enhances confinement and ductility capacity. The first and last joints are also locked in this retrofit scheme.

Nonlinear response history analyses conducted on the proposed retrofit schemes revealed that the first and second schemes did not lead to a significant improvement in the seismic performance of the bridge. Although, pounding of the decks were prevented when all the joints were locked, the plastic rotation demands in the columns were not reduced under the associated capacities. Matching the vibration periods to prevent pounding was observed to be ineffective, particularly once the bridge behavior becomes nonlinear. The plastic rotation demands in the columns for this retrofit scheme also exceeded the capacities. Jacketing the columns, however, was observed to significantly improve the bridge response. The highest plastic rotation demand

capacity ratio was limited to 0.40, indicating that failure of the columns under a 2475 year event would be highly unlikely with the proposed column retrofit. Despite this significant improvement in the column behavior, this retrofit scheme was not sufficient to prevent pounding of the adjacent decks due to the very small gap size provided. The hangers were not predicted to fail; however, due to uncertainty in the pounding model, cable restrainers are proposed as an additional measure of safety.

Conclusions and Recommendations

The potential destruction of the infrastructure from a large earthquake is a major threat that cannot be ignored. According to seismicity studies, the occurrence of a large event on the Wasatch fault is likely within the next 100 to 200 years. Precautionary action should be taken to seismically upgrade important bridge structures for collapse prevention before a major event occurs.

The first two bridges examined in this report are typical of much of Utah's bridge inventory. Two relatively low cost retrofit options were studied that can be applied to most of these typical bridges. The first option uses seismic isolation bearings to reduce the demands. Seismic isolation bearings can be used when the bridge has seat type abutments and expansion joints between bridge spans, wherein the original bearings are replaced with isolation bearings. The second option uses steel jacketing to enhance the ductility capacity of the columns. While the bridge evaluated here was continuous, if the bridge has simple spans, cable restrainers and or seat extenders should also be considered to prevent deck unseating.

The extensive analysis methods that were demonstrated in this report are probably not necessary for every single bridge. For instance, if the strategic decision was made to upgrade all concrete bridges on the I-15 corridor with steel jackets and cable restrainers, conservative designs could be developed for each of the components based on analysis of one or two bridges, and thereafter applied to all the bridges. Such a strategy would be very cost effective and time efficient.

The third bridge examined, the long-span curved girder bridge with pin-hanger connections, required a more extensive and costly retrofit approach. Apparently, Utah has several bridges that could be upgraded with the same techniques. Although the proposed upgrade is more expensive, the expense is justified when the bridge represents a major artery connecting two important interstates.

1. Clearfield Interchange Overpass, So. Layton to Hill Field Interchange

1.1 Existing Structure

The bridge considered is a four span reinforced concrete bridge that is part of I-15. Two essentially identical bridges (one each for traffic in the northbound and southbound direction) pass over surface streets in the middle two spans. Only one bridge is analyzed here since the plans for the two bridges are identical. The overcrossing was constructed in the early 1960's. The bridge spans are simply supported and each span has a different length. A considerable skew of 34°57' is present.

The cross section of the superstructure has constant width (52' normal to longitudinal direction) and constant depth. However, three spans of the superstructure use 7 prestressed girders and the longest span uses 9 prestressed girders. Girders are simply supported on the bent caps and longitudinally fixed indicating that they cannot carry moment at the joints but are capable of transferring longitudinal forces. The cast-in-place and prestressed concrete are assumed to have strength of 3000 psi and 5000 psi respectively. Expansion joint hinges are not present along the spans, and longitudinal cable restrainers are not present. Each bent consists of three reinforced concrete columns of circular cross section. The columns have 30 inch lap splices at the bottom. All the columns are identical with 2'-6" diameter and 10 #11 longitudinal bars. The main reinforcing steel is lap spliced just above the footings, and the column transverse steel consists of #4 hoops at 12".

Abutments are seat type supported on 50-ton piles with approach retaining walls. They are oriented in parallel to bent caps with the skew angle of 34°57'. The superstructure is supported on elastomeric bearings, which are not explicitly modeled. All columns are supported on pile footings aligned parallel to the bent caps. A 5 pile design is used for middle columns while a 4 pile design is used for exterior columns (using standard pile spec sheet). Piles design load are 50 tons and are assumed to be fixed at the base of the footing. The reinforcing steel from the piles extends into the footing by 1'4" and can resist the seismic uplift capacity of the piles.

A field inspection of the bridge revealed some deterioration of the structure, which is not accounted for in the modeling.

1.2 Determination of Seismic Retrofit Category (SRC)

The seismic retrofit category is determined first, which is the basis for all decisions regarding bridge evaluation methods. Details about how to determine the seismic retrofit

category are given in Chapter 1 of the FHWA retrofit manual (FHWA, 2006) and Chapter 2 of the Utah guidelines (Wilson and Ryan, 2009). Step by step calculations and plotted response spectra are shown in Appendix 1A.

Because the bridge has a remaining service life of 33 years, the 500 year return period earthquake represents the Lower Level (LL) motion and the 2500 year return period earthquake represents the Upper Level (UL) motion. The bridge is in Anticipated Service Life Category 2 (ASL 2), and is assumed to be of standard importance; thus it will be evaluated against Performance Level 3 (PL3 = Fully Operational) for the LL motion and Performance Level 1 (PL1 = Life Safety) for the UL motion.

The Seismic Hazard Levels (SHL) for UL and LL motions are functions of the site response spectra. S_s and S_1 values are determined from the software included with the Retrofit Manual (FHWA, 2006). The site category is to be determined through harmonic mean of blow counts of soil layers in the top 100 ft (Table 2-2 of FHWA, 2006). Boring 1 is used to find the blow count number because it is the only one with a height of about 100 ft. The Site Class is D based on the boring data (Table 2-2 of FHWA, 2006), but because it is close to the limit it is considered to be Site Class E. The SHL is found to be Category IV for both UL and LL motions.

Based on the Performance Level and Seismic Hazard Levels the Seismic Retrofit Category (SRC) is C for both UL and LL motions.

1.3 Overview of Evaluation Methods

For the LL motion, the bridge will be evaluated using Analysis Method C. Method C computes demand/capacity ratios at a component level for the bridge. Because it does not recognize the redistribution of forces after an element yields, Method C can be inaccurate. As such, Method C is recommended for bridges that remain elastic or nearly so. The applicability of Method C should be evaluated based on the results of this example, recognizing that a 500 year return period motion is used rather than the 100 year return period motion typically recommended for LL evaluation.

Both the Retrofit Manual (FHWA, 2006) and the Utah Guidelines (Wilson and Ryan, 2009) recommend a step by step procedure for the LL evaluation that culminates in Method C. This example proceeds directly to Method C since the bridge is assumed to be likely to exhibit inelastic response to the LL motion. Method C requires a linear elastic analysis of the complete

bridge to determine the demands of individual components. The capacities of columns, footings, etc. are determined on an individual basis by hand calculations or software.

For the UL motion, the bridge should be evaluated by Method D1 (capacity spectrum method) or D2 (pushover analysis) in combination with an elastic demand analysis. This bridge fails to qualify for Method D1 because it has a skew of nearly 35°. Therefore, the capacity of the bridge is evaluated by pushover analysis of the individual bents, which is performed in LARSA.

A multi-modal linear response spectrum analysis of the complete bridge is performed in LARSA to assess the demand. As recommended by FHWA (2006), inelastic response is accounted for indirectly by iteration of the footing and abutment stiffnesses using an equivalent linear approach. The stiffness of each element is decreased as necessary until the force and moment capacities are not exceeded by more than 30%. This approach limits the forces transferred to the columns. The demand analysis is based on the assumption that the elastic displacement demands are representative of the true demands of the structure, which will actually respond inelastically. This well known "equal displacement rule" is considered to be reasonable for long period structures, and can be applied here because modeling the foundation with equivalent linear elements causes the structure to degrade into the nonlinear range (Buckle, 2007).

1.4 Creating a LARSA Model

Software is needed to carry out the demand analysis: response spectrum analysis (i.e. MM method) for both the LL and UL motions. As described above, the demand analysis for the UL motion is iterative to force the foundation forces to remain within the range of their capacities. The model in the first iteration for UL motion is the same as the model for the LL motion. The recommended complexity of the model is also determined by the geometry of the bridge. The bridge has been interpreted as irregular due to its skew angle of 34°57' in accordance with the criteria for application of Uniform Load Method and analysis method D1 (Table 5-3 of FHWA 2006). Therefore, the superstructure elements are recommended to be modeled individually rather than as one gross composite section (Sec. 7.3 of FHWA, 2006). Elastic beam-column elements are sufficient for modeling beams and columns in the bridge.

The geometric connectivity of columns, bent caps, and girders is accounted for using the approach recommended in Sec. 4.4.2(c) of Priestly et. al. (1996). A joint connecting two elements is located at the crossing point of center lines of the two elements. Joint link elements

are modeled with cracked or effective column properties to reflect the yield penetration into the joint region and increased flexibilities from joint shear distress. Based on this, the girder to bent cap connection has the details shown in Fig. 1.4.1, where *d* represents the depth and *b* the width of elements.

In addition to the geometry of the bridge, beam and column element cross sections and abutment and foundation elements must also be defined. As recommended by the Retrofit Manual (FHWA, 2006), the foundation elements are modeled using springs, with stiffnesses based on the pile group stiffness. LARSA allows general foundation springs formulated using 6x6 stiffness matrices.

The LARSA files included to demonstrate the modeling and analysis of this bridge are indicated in Table 1.4.1.

1.4.1 Superstructure Elements

1.4.1.1 Deck

In this example, the deck is not modeled directly and therefore, equivalent member properties for the beam elements need to be derived that represent the composite stiffness of the girders with deck overlay. The effective widths of the deck slab in the longitudinal and transverse directions were calculated for the side and middle girders and transverse beams in each span. The following relation was used, where L and b_0 are the length and width of concrete slab due to each element in the considered direction, and *Edge* is the slab extension at sides (see Fig. 1.4.2)

$$b_{effective} = \min\left\{\frac{L}{4}, b_0, \frac{b_0}{2} + Edge\right\}$$

Table 1.4.1 LARSA modeling and analysis files for bridge example 1

LaytonInt_Sections.lpsx	a Section Composer file containing all bridge sections
LaytonInt _LowerLevel.drs	a database file containing the design spectrum for the lower level motion
LaytonInt _UpperLevel.drs	a database file containing the design spectrum for the upper level motion
LaytonInt _TensionLL.lar	a LARSA file defining the tension model of the bridge and analysis to the lower level motion
LaytonInt _CompressionLL.lar	a LARSA file defining the compression model of the bridge and analysis to the lower level motion
LaytonInt _TensionUL.lar	a LARSA file defining the tension model of the bridge and analysis to the upper level motion
LaytonInt _CompressionUL.lar	a LARSA file defining the compression model of the bridge and analysis to the upper level motion
LaytonInt _PushoverParallelBent3.lar	a LARSA file modeling bents with nonlinear elements for pushover analysis parallel to the bent
LaytonInt _PushoverNormalBent3.lar	a LARSA file modeling bents with nonlinear elements for pushover analysis normal to the bent
LaytonInt _BaseIsoUL.lar	a LARSA file to model base-isolated bridge for the upper level motion
LaytonInt _BaseIsoUpperLevel.drs	a database file containing the design spectrum for the upper level motion for the isolated bridge
Foundation_Iter.xls	an Excel worksheet for the iterative procedure in demand analysis

1.4.1.2 Girders

The effective width of the deck acting with the girders leads to a composite sections. These elements should be modeled realistically, but in lieu of modeling details for prestressed elements, Sec. 4.4.2 of Priestley et al. (1996) proposes to use 50% and 100% of the flexural stiffness of the gross section for reinforced and prestressed concrete sections respectively, while the whole effective area may be considered for axial and shear rigidities.

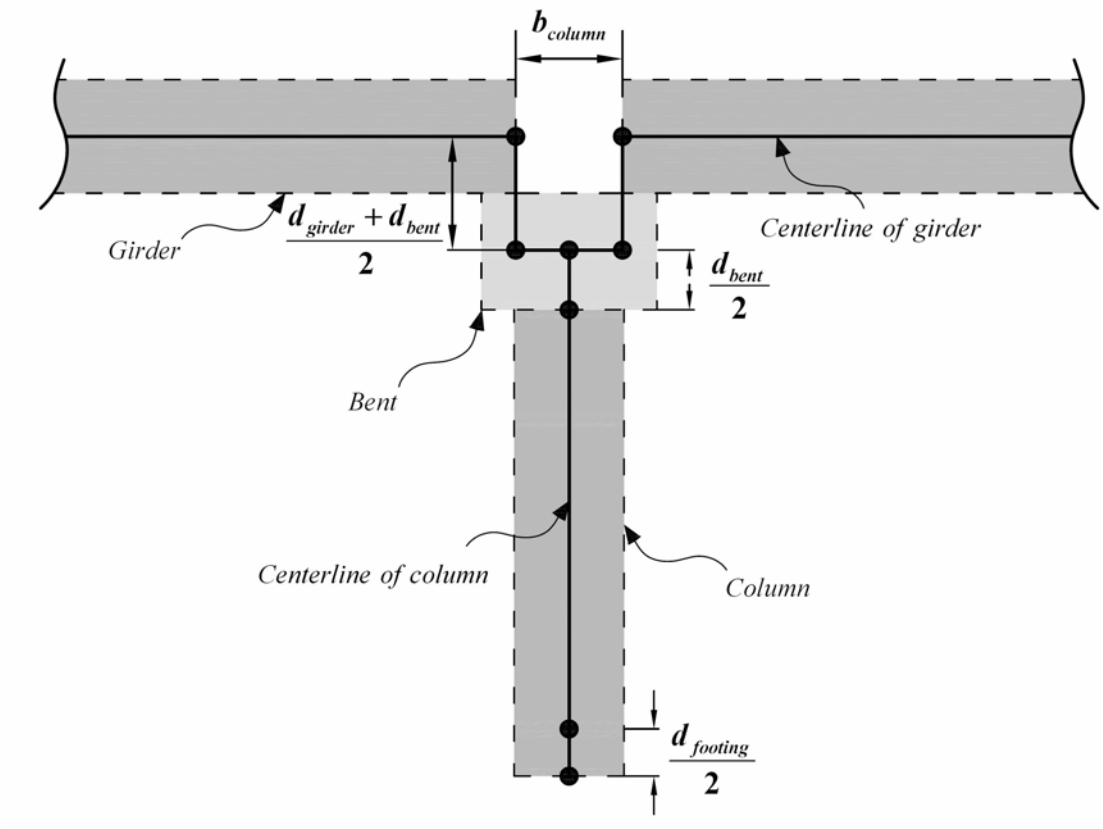

Figure 1.4.1. Girder-bent-column connection details.(solid lines show the model)

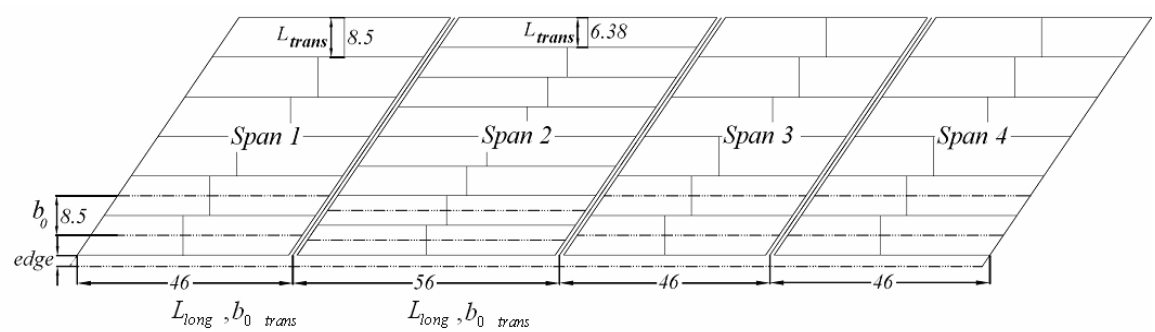

Figure 1.4.2. Definition of L, b_0, and *Edge* for longitudinal and transverse directions.

The procedure to model these elements is described for the middle girders in spans 1, 3, and 4. First, the two sections, AASHTO Type I, II, III, IV for prestressed section and a rectangle for the deck contribution, are defined in Section Composer and then attached to each other (LaytonInt_Sections.lpsx). Because gross section properties are used, bars are not considered. A typical composite section made up of a girder and the effective width of the deck acting with the girder is shown in Fig. 1.4.3. These two sections are made up of concrete with different

properties: $f_c^{'}$ is 5000 psi for the prestressed concrete girders and 3000 psi for the deck. Different materials can be assigned to parts of a composite section under the Section menu in Composite Materials. Pre-defined materials Fc_3 and Fc_5 are assigned to the deck and girder, respectively. Note that when the composite section is assigned to a member, the reference material specified in Section Composer should be selected as the material applied to the element in LARSA. The width b_o of the deck for the girders under consideration is 102 in; therefore $b_{eff} = 0.5 \times 102 = 51$ inches for the deck and LARSA computes $I = 1.9877e5 \;\; in^4$ as a composite value for the section.

The axial rigidity is based on the entire area of the composite section (A= 1317 in^2) as reported by Section Composer. These values of A and I must be entered manually in LARSA using *Input Data- Properties- Sections- Properties*. This is required to allow the effective properties to be modified from the values computed by Section Composer. Because the true dimensions of the deck are modeled as part of the section for the longitudinal girders elements and the axial rigidity of these elements are not altered, the models accurately account for the contribution of the superstructure mass.

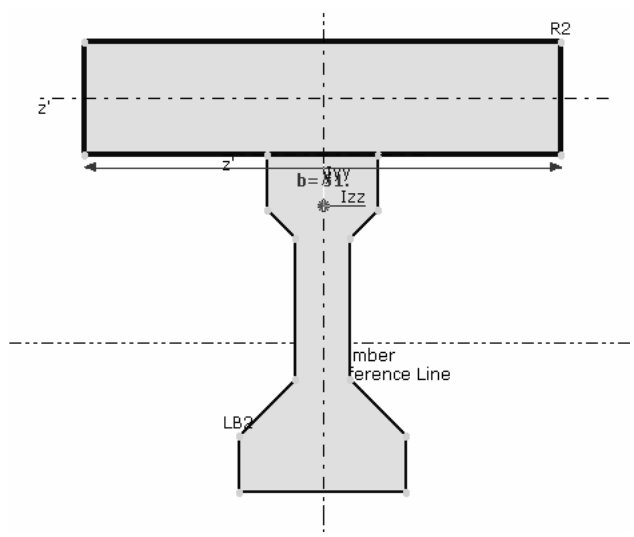

Figure 1.4.3. Composite section with girder and effective deck width

1.4.2 Substructure Elements

1.4.2.1 Bent Caps

Based on Table 7-1 of FHWA (2006), some changes should be applied to section properties of concrete elements in the substructure to account for cracking during excitation. For a linear elastic demand analysis, cracked section properties are generally used for columns and bent caps (Sec. 7.3.2.1 of FHWA, 2006). The flexural rigidities of the columns are modified to represent the behavior up to yield. Assuming that cracking but not hinging is expected in bent caps, which is usually the case, 50%, 40%, and 100% of flexural, shear, and axial rigidity of bent caps are applied for the demand model. These changes may be applied in section properties in LARSA accessible through *Input Data- Properties- Sections- Properties.*

1.4.2.2 Columns

The Retrofit Manual (Sec. 7.3 of FHWA, 2006) recommends to model tall columns with two or more elements due to some concerns regarding the distribution of mass along the column. In this example, columns are modeled by two beam elements.

Column flexural rigidity is derived from Eq. 7-2 of FHWA (2006)

$$E_c I_{eff} = M_n D' / 2\varepsilon_y$$

where M_n is the nominal yield moment, D' is the distance between outer layers of longitudinal reinforcement, and ε_y is the yield strain of steel reinforcement. The capacity M_n can be derived from charts or from section analysis using appropriate software; we performed moment curvature analysis of the composite section using Matlab. The capacity M_n depends on the column axial load, which is unknown without prior analysis. As a result, the bridge is analyzed with the elastic flexural rigidity of the column (0.5 E_cI_c) to determine the axial load and find the new value M_n. Because the axial load also depends on Mn, this process is iterative and is illustrated in Appendix 1C. Upon completion of this process, the new E_cI_{eff} is entered into LARSA. With initial column axial loads of approximately 200 kips, M_n = 7690.9 kip-in and I_{eff} = 23813 in^4. This I_{eff} is assigned to each column section in the bridge model. While flexural stiffness based on nominal moment capacity may not typically be applicable to Method C, it is used here because plastic hinging is expected in the columns.

1.4.3 Foundation Elements

The Retrofit Manual (FHWA, 2006) recommends modeling pile groups in one of two ways: a series of uncoupled springs or a fully coupled foundation stiffness matrix, as shown in Figure 1.4.4. The latter model is the most general and rigorous approach, and is used here. In summary, the translational, rotational, and cross coupling stiffness of a single pile are determined based on the bending inertia EI, and are looked up in charts located in the Retrofit Manual

(Figures 6-14 to 6-16 of FHWA, 2006). The stiffness of the pile group is calculated by assembling the stiffness matrices from each pile into a single stiffness matrix located at the geometric center of the pile group. Torsional and bending resistances are added to the pile group stiffness matrix as a result of the assembly process. Lateral footing stiffness is computed due to the passive pressure of soil on the sides of the footing, and the other stiffness components are computed from Tables 6-1 and 6-2 of FHWA (2006). The pile group and footing stiffness are assembled into a single matrix. Detailed calculations are shown in Appendix 1B. A footing stiffness matrix for the foundation elements can be input in LARSA by selecting *Input Data – Properties - Spring Properties*; selecting 6×6 *stiffness matrix* for *Type*; and selecting *Spring Properties - Edit stiffness matrix* to input the calculated stiffness matrix. To add the coupled spring elements to the LARSA model, enter the node numbers and select *Input Data –Geometry – springs*; for *Type* select *Linear*, and for *Direction* select the name of the footing stiffness matrix.

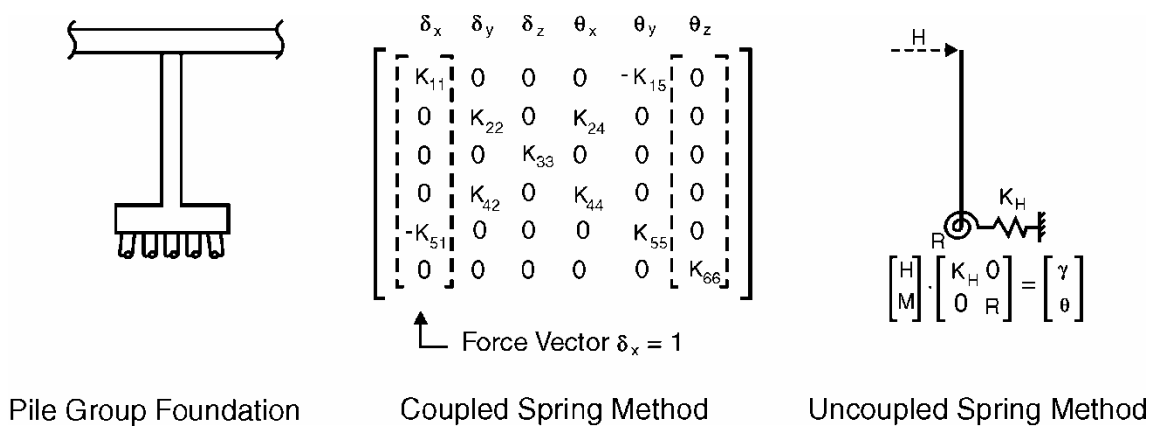

Figure 1.4.4. Methods to evaluate pile group stiffness (Figure 6-18 of FHWA, 2006)

1.4.4 Abutment Springs

Abutment walls and wingwalls can play a very beneficial role in the performance of the bridge during an earthquake, because the back fills behind these walls can resist large inertial loads and thus reduce ductility demands elsewhere in the bridge. All degrees of freedom of the abutment-pile system except longitudinal and transverse components are assumed to be fixed. Abutment stiffness is based directly on the passive pressure of the soil surrounding it. Default passive pressures are used according to Sec. 6.2.2.4 of (FHWA, 2006). Since the soil type for

this bridge is close to sand; 2H/3 is used for passive pressure. The effects of the piles beneath the abutment are also included in abutment stiffness, which leads to:

$$P_p = p_p.H.L + N_p.C_p$$

where P_p is the total lateral capacity of the abutment-pile system, p_p is the passive pressure, L is the width of the backwall, N_p is the number of piles, and C_p is the capacity of each pile (Fig. 1.4.5). The piles are assumed to yield when the soil reaches its passive pressure. The displacement at which soil reaches its passive pressure is called mobilization displacement, recommended to be 0.02H (FHWA, 2006). Thus, the effective stiffness is:

$$K_{eff1} = \frac{P_p}{0.02H}$$

As shown in Fig. 1.4.6, abutments are modeled by individual springs connected to end nodes transversely distributed over the end of the bridge. Individual springs are assigned to each node in both lateral and longitudinal directions. The value of passive pressure defined above is for the entire abutment, and should be distributed among the individual springs. The stiffness to each node is distributed proportional to the effective width adjacent to the node. For calculation details, see Appendix 2B.

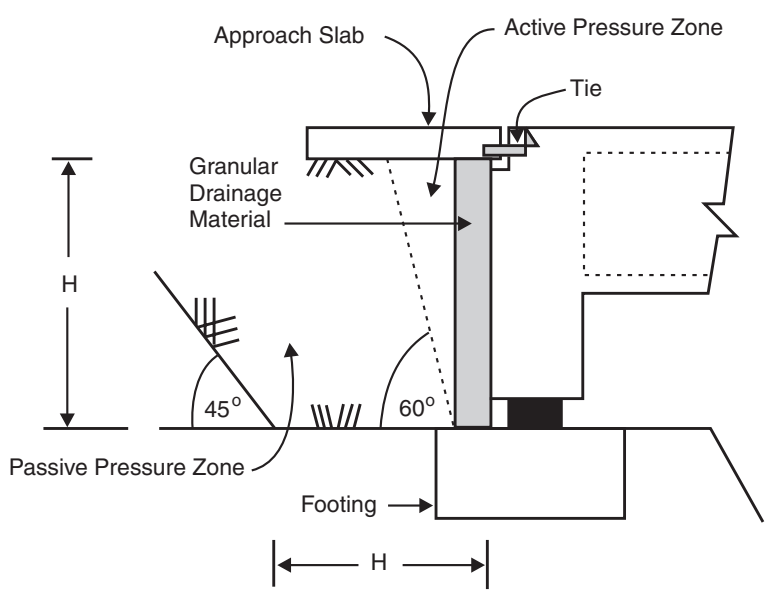

Figure 1.4.5. Calculation of abutment passive pressure (Figure 6-23 of FHWA, 2006)

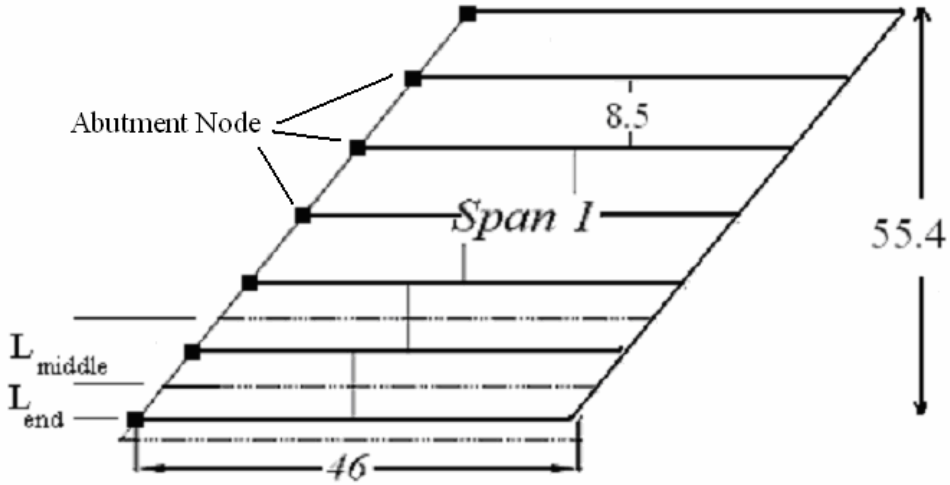

Figure 1.4.6. Geometry for abutment springs

1.4.5 Summary of the LARSA Bridge Model

3D and elevation renderings of the bridge model, created using the LARSA software, are shown in Figs. 1.4.7 and 1.4.8. The bridge skew can be observed in the elevation view, where the columns associated with a given pier are not aligned. The 3D rendering of the bridge does not depict the contribution of the deck to the composite sections. Recall that only section effective properties were entered into LARSA, and the values were not preserved.

The bridge is to be analyzed in two different conditions (Sec. 7.3.3 of FHWA, 2006). In the compression model, the hinges at the ends of the simple spans are closed, i.e, fixed against relative longitudinal displacements and can therefore transfer longitudinal forces (LaytonInt _CompressionLL.lar). In the tension model, the hinges are open, i.e. relative longitudinal displacements are allowed and longitudinal forces cannot be transferred (LaytonInt _TensionLL.lar). An eigenvalue analysis of the bridge is performed for both the tension and compression models, and the first twenty natural periods are shown in Table 1B.1 of Appendix 1B.

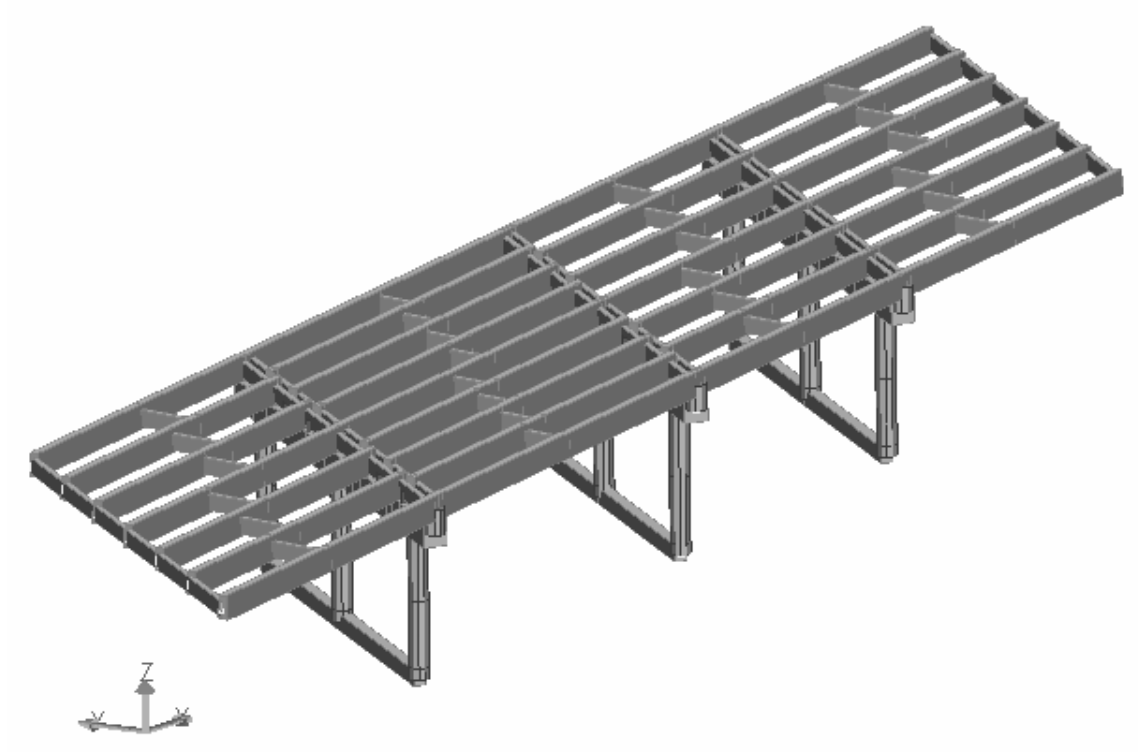

Figure 1.4.7. 3D rendering of LARSA bridge model excluding composite section geometry

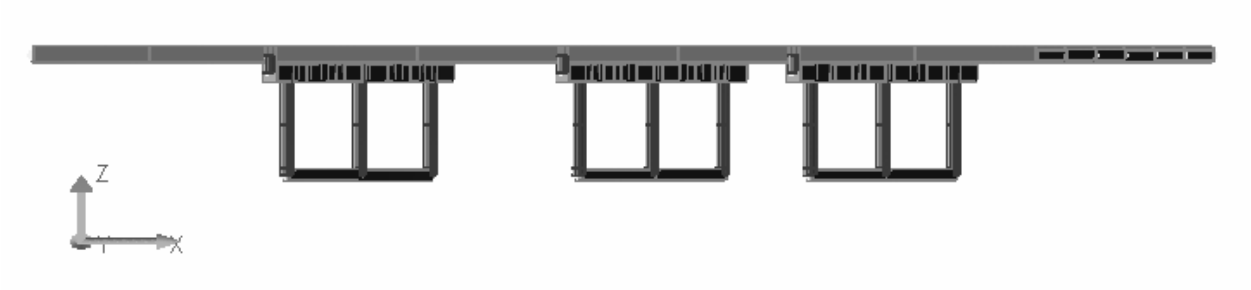

Figure 1.4.8. Elevation rendering of LARSA bridge model

1.5 Evaluation of the Bridge for the LL Ground Motion

As described in Sec. 1.3, the bridge is evaluated for the LL ground motion using Method C, which calculates capacity/demand ratios for bridge components that may be damaged during an earthquake. Ratios greater than one indicate sufficient capacity to resist the earthquake demand; ratios less than one indicate components in need of attention and possible retrofitting. Capacity/demand (C/D) ratios are therefore used to indicate the need for retrofitting and may also be used to assess the effectiveness of various retrofit strategies.

Components that should be evaluated vary with the Seismic Retrofit Category of the bridge, based on the assumption that certain components will respond fine in moderate shaking. Table 5-2 (FHWA, 2006) indicates components and failure modes that should be checked.

Appendix D of the Retrofit Manual provides detailed guidelines for evaluation of the C/D ratios, while Appendix E works through an example problem (FHWA, 2006). Evaluation of C/D ratios for various member and component limit states is based on a combination of analysis, testing, and engineering judgment.

Eleven ratios are defined in four categories as follows:

1. Support length and restrainer C/D ratios:

r_{ad} displacement C/D ratio for abutment

r_{bd} displacement C/D ratio for bearing seat or expansion joint

r_{bf} force C/D ratio for bearing or expansion joint restrainer

2. Column C/D ratios:

r_{ca} anchorage length C/D ratio for column longitudinal reinforcement

r_{cc} confinement C/D ratio for column transverse reinforcement

r_{cs} splice length C/D ratio for column longitudinal reinforcement

r_{cv} shear force C/D ratio for column

r_{ec} bending moment C/D ratio for column

3. Footing C/D ratios:

r_{ef} bending moment C/D ratio for footing

r_{fr} rotation C/D ratio for footing

4. Soil C/D ratio:

r_{sl} acceleration C/D ratio for liquefaction potential

The restrainer C/D ratio is essentially irrelevant for this bridge since there is no restrainer in the bridge in the evaluation stage. However, seat widths at bearings are checked against the minimum required values. Liquefaction is outside of the scope of this project. Therefore, the evaluation in this example focuses on column and footing C/D ratios. First, bending moment C/D ratios for columns (r_{ec}) and footings (r_{ef}) are evaluated. If these ratios are less than 1, column details are evaluated to assess the ability of the columns to form plastic hinges. Similarly, a rotation C/D ratio is developed for the footing as an overall assessment of its ductility.

1.5.1 Component Capacity Evaluation

Nominal moment capacities for the columns were already developed according to Section 1.4.2 and discussed in detail in Appendix 1C. The moment capacities of the pile-footing elements, or foundation springs, are determined next.

The pile capacities are difficult to determine; thus standard recommended values are used. In the longitudinal and transverse directions, the capacity of piles is assumed to be 40 kips (Sec. 20-4 of Caltrans, 1995). The design load capacity in the vertical direction is 100 kips, which is close to the recommended value of 90 kips in the Retrofit Manual (Sec. 6.2 of FHWA, 2006). Ultimate capacities in axial compression and tension are assumed to be 180 and 90 kips, respectively.

The moment capacity of the pile-footing system is determined from a static analysis of the pile-footing system, where each of the piles is assumed to be stressed to its capacity. Figure 6-19 of the Retrofit Manual (FHWA, 2006) illustrates the procedure. The moment capacity depends on the footing axial load. The procedure is illustrated in Appendix 1C for one of the pile-footing systems. Tables 1C.1-1C.3 show iterative calculations of the column moment capacities in addition to the pile-footing moment capacities for the last iteration.

1.5.2 Structure Demand Evaluation

The following load cases and load combinations are defined in LARSA for demand evaluation.

<u>Load Cases</u>

1. Self Weight (Dead Load)
2. Longitudinal Earthquake Loading
3. Transverse Earthquake Loading

<u>Load Combinations</u>

1. 1.0*Longitudinal + 0.3*Transverse
2. 0.3*Longitudinal + 1.0*Transverse

Note that the Retrofit Manual (FHWA, 2006) recommends that a 100% + 40% load combination be used in place of the 100% + 30% load combination used here. The elastic moment demands are calculated by combining the maximum moments of the columns (obtained from a load combination) about the principal (x and y) axes using a square root of sums (SRSS) combination rule. In most cases, Load Combination 1 leads to the highest demands. Moments due to the Self Weight load case are added to each component after applying the combination rule. Moments at the base of the footing are obtained by a free body analysis assuming the moment and shear at the top of the footing are known. The largest elastic demand moments for each column or footing for both the compression and tension models are listed in Tables 1D.1-1D.2.

In LARSA, load cases are defined under *Input Data, Load Groups and Stages, Load Cases.* For dead loads, the analysis type is static and the weight factor z is -1 because gravity acts up to down. For response spectrum analysis, first, an acceleration spectrum is defined in *Input Data, Edit Databases, New Database, New Response Spectra Curves Database.* Load cases for earthquakes are applied as described above, but setting the analysis type to Response Spectrum and the weight factor z to zero. To apply the response spectrum, Edit Loads is after right clicking the name of the earthquake analysis, and under RSA Loads tab, a previously defined response spectrum is assigned to the direction of interest.

Load combinations are defined through *Input Data, Load Groups and Stages, Load Combinations.* Under the Name tab, a name should be assigned to each load combination. *Edit Load Combination* is selected by right clicking on the load combination name. A new window will be appeared under which the load case name and participation factor can be assigned. To run the analysis, select *Analysis - Eigenvalue/Response Spectra Analysis*. The number of mode shapes determines the number of modes to be considered in modal analysis. Modal and spatial combination methods are chosen as CQC and SRSS methods respectively. In this example, 20 mode shapes are assigned for RSA, with modal damping ratios prescribed to the default values of 5%. The option *Linear Static + Eigenvalue + RSA* will automatically perform all analyses in one step. Results are available under *Results* menu. Nodal displacements and member forces in local coordinate system are accessible under *Results, Spreadsheets, Joint, Displacements* and *Results, Spreadsheets, Member, End Forces-Local.*

1.5.3 Evaluation of Capacity/Demand Ratios

The most critical combinations of the unfactored nominal ultimate moment capacities (M_u) and elastic moment demands are used to calculate r_{ec} (column bending moment capacity/demand ratio) and r_{ef} (footing bending moment capacity/demand ratio) at each bent. These values are summarized in Table 1E.1, and are in the range of 0.3 to 0.4.

When r_{ec} and r_{ef} C/D ratios are less than 1, further evaluation is required to assess the ability of the columns or footings to form plastic hinges. Regardless of the values of r_{ec} and r_{ef}, C/D ratios should be evaluated for anchorage of longitudinal reinforcement (r_{ca}), splice length in longitudinal reinforcement (r_{cs}), and column shear (r_{cv}). If plastic hinges may potentially form in the footing, C/D ratios should be evaluated for footing rotation (r_{fr}). If plastic hinges may potentially form at the base or tops of the columns, C/D ratios should be evaluated for column transverse confinement reinforcement (r_{cc}). Sample calculations for all these C/D ratios are

given in Appendix 1E, and Tables 1E.2 and 1E.3 summarize the results. The C/D ratios for anchorage and splice length are in the range of 0.2 to 0.3, and the C/D ratios for column shear are in the range of 0.3 to 0.4.

C/D ratios are also evaluated at the abutments based on assumed displacement capacities and the displacement demands calculated from the elastic demand analysis (Table 1E.4). These ratios are greater than 1, which indicates that abutment failure is not expected to be a problem.

Overall, the results suggest that the bridge certainly will not remain elastic or even nearly elastic under the LL ground motion, which is the premise of the component-based procedure. These results are not surprising given that the LL ground motion has been chosen as a 500 year return period earthquake, rather than the standard 100 year return period earthquake recommended by the Retrofit Manual. In this case, seismic deficiencies in the LL earthquake are likely to control the overall retrofit evaluation, and UDOT may wish to re-evaluate whether elastic response in a 500 year event is an appropriate goal.

Furthermore, the anchorage and splice length C/D ratios suggest a limited capacity for the columns to form plastic hinges. However, the component-based procedure may be overly conservative for bridges expected to deform largely into the inelastic range, and it is appropriate to make a comprehensive evaluation following analysis to the UL ground motion.

1.6 Evaluation of the Bridge for the UL Ground Motion

As explained before, method D2 (pushover analysis) is used for capacity assessment in combination with a linear elastic analysis for demand estimation to evaluate the bridge for the UL motion. In contrary to method C, which uses force capacity/demand ratios at the element level, method D2 uses displacement capacity/demand ratios at the global level (evaluated for each bent) to identify deficiencies in the bridge. The displacement-based method accounts for structure nonlinearities and the re-distribution of loads as certain members yield.

1.6.1 Capacity Evaluation

Pushover analysis is based on incrementally increasing lateral forces (for earthquake loads) in the presence of non-varying forces (dead loads). The aim is to find the ultimate deformation of a reference degree-of-freedom (in most cases the lateral displacement of the superstructure) that can be sustained. This displacement evaluation is applied to individual bents, and represents the maximum displacement that the whole bent can reach before it collapses. Therefore, bridge bents are modeled and evaluated by pushover analysis independently. A

complete pushover analysis determines the ultimate displacement and the load path taken to reach it, which is represented as a pushover curve – reference displacement plotted against lateral load. To properly account for P-Δ effects, the contributions of the superstructure dead load to column axial loads are modeled by vertical point forces on each column in the bent.

In a pushover analysis, the lateral loads are increased and analysis continues until one or more stopping criteria are reached. The stopping criteria are generally controlled by local element deformation limits, such as strain and curvature. These stopping criteria can be defined for both footings and columns, but here only column rotational deformation limits are used to assess each bent. Curvature limits have been shown to be appropriate criteria to represent the damage threshold. Several modes of failure must be considered, and the one which leads to the least plastic rotational capacity will govern the limiting state. Eight plastic curvature limit states considered in this example are as follows (Table 7-3 of FHWA, 2006):

1. Compression failure of unconfined concrete.
2. Compression failure of confined concrete.
3. Compression failure due to buckling of the longitudinal reinforcement.
4. Longitudinal tensile fracture of reinforcing bar.
5. Low cycle fatigue of the longitudinal reinforcement.
6. Failure in the lap-splice zone.
7. Shear failure of the member that limits ductile behavior.
8. Failure of the joint.

Detailed calculations for each of the limit states are shown in Appendix 1F.

1.6.2 Pushover Analysis with LARSA

Method D2 focuses on displacement capacity of each bent individually instead of looking at the whole structure. Therefore, the LARSA model for this type of analysis contains only one bent consisting of three columns, a bent cap, and three foundation elements. The analysis is done in two directions: parallel to the bent and normal to the bent. In the parallel case, the varying pushover loads are in parallel to the bent cap, while in the normal case pushover loads are normal to the bent (LaytonInt _PushoverParallelBent3.lar and LaytonInt _PushoverNormalBent3.lar). In pushover analysis, nonlinear behavior of structural elements is a key factor affecting final capacity. Bilinear spring and nonlinear hysteretic beam elements are used to model foundation springs and columns in each bent.

For spring elements, first, their properties are defined in *Input Data-Properties-Spring Properties.* After choosing a name for the spring, its type is selected which in this example it is *Curve: Translational* or *Curve: Rotational*. Then *Edit Curve* is selected from *Spring Properties-Edit Curve.* The defined spring elements are assigned to corresponding nodes in LARSA through *Input Data-Geometry-Springs.*

Nonlinear behavior of columns is modeled in LARSA using *Hysteretic Beam Elements*. Several ways can be applied to capture the nonlinearity for hysteretic type of elements. The one used in this example is through moment-curvatures. Using commercial software Xtract, moment curvature curves for a set of axial forces can be derived. Then through *Input Data-Properties-Spring Properties, Moment Curvature* is selected as the type of the spring and the data from Xtract are entered in *Spring Properties-Edit Curve.* Moment curvature curves defined above are assigned to column sections through *Properties-Sections-Properties*-Name of the Column Section-*Sections-(Moment Y Curvature* and *Moment Z Curvature)*.

To do pushover analysis in LARSA, following steps are followed:

- select all the elements in the model
- In the menu available on the left, select *Group*. A menu called *Structure Groups* appears. Select *Add Group* from the top bar.
- Again from the menu on the left, select *Stage* then *Add Stage*. Add *Group* and *Dead Load* to *Step 1*. Add another *Stage* and add pushover load to the new *Stage*. Right click on *Step 1* and from properties select *Plastic Pushover* in the *Analysis Type* menu.
- The analysis can be performed through *Analysis-Stage Construction Analysis*

Pushover analysis requires some deformation limits to stop the analysis when that limit is reached. These stopping criteria are expressed in terms of curvature limits in the Retrofit Manual (FHWA, 2006) but, the current version of LARSA only reports element displacements and nodal rotations. As a result, the computed curvature limits are converted to approximate displacement limits to be applied in LARSA. The procedure is illustrated in Figure 1.6.1. Through Eqs. (7-25) and (7-27) of the Retrofit Manual (FHWA, 2006), it is easy to find yield displacement Δ_y and plastic displacements Δ_p. The ultimate allowable column drift $\Delta_u = \Delta_y + \Delta_p$. In addition to column drift, footing displacement Δ_b and rotation $\theta_b h$ also contribute to the total column top displacement. LARSA reports total displacement Δ_{total}, footing rotation, and footing displacement at each pushover analysis step. Therefore, in the LARSA analysis Δ_u is estimated at

each load step by subtracting reported footing deformation, displacements due to lateral movement of footing and rotation at the base from the reported total displacement:

$$\Delta_u = \Delta_{total} - \Delta_b - \theta_b h$$

When Δ_u from LARSA exceeds the ultimate allowable column drift, the analysis is terminated and Δ_{total} represents the allowable displacement of the bent.

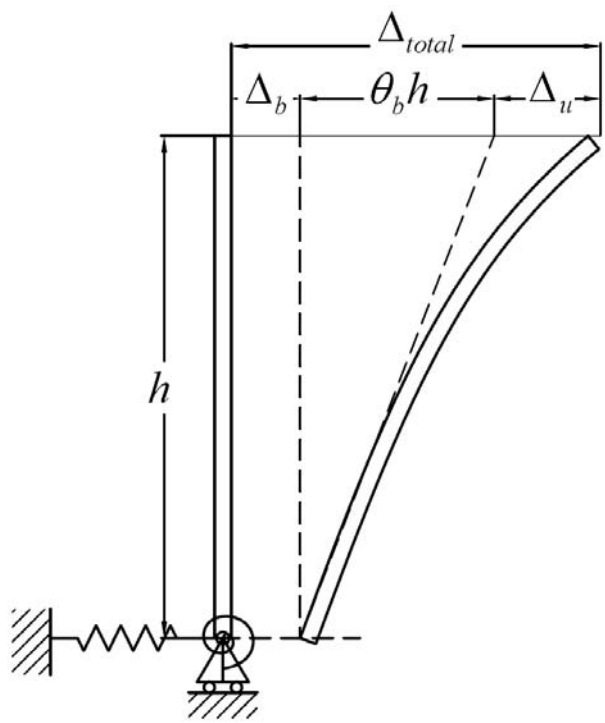

Figure 1.6.1. Sketch of column displaced shape and contributions to column displacement

1.6.3 Demand Evaluation

The demand evaluation in method D2 is based on a linear elastic model. Because the bridge capacity is found through nonlinear analysis, the model for demand should somehow reflect the nonlinear behavior of the structure. Since the pushover analysis is a displacement-based analysis, the equal displacement rule applies for bridges in the medium to long period range. That is, the displacement demand of the nonlinear bridge is equivalent to the corresponding displacement demand assuming the bridge remains elastic.

The Retrofit Manual implies that the stiffness of foundation elements (footings and abutments) should be scaled iteratively until the resultant forces in these elements are within 30% of their capacities (Sec. 6.2.2.4(c) of FHWA, 2006). We infer two possible reasons for

adjusting the stiffness: (1) adjusting the foundation stiffnesses prevents the foundation forces from being unreasonable high, and limits the total force input to the bridge to the forces that the foundation could reasonably transfer; (2) many bridges are initially in the short period range for which the equal displacement rule does not apply. Adjusting the foundation stiffness causes the bridge to degrade to a longer period range such that the equal displacement rule can be applied.

A Macro is written in Visual Basic to change the stiffness properties of foundations and abutments at each iteration (Foundation_Iter.xls). This worksheet can be used for bridges with different geometries. This worksheet is explained in Appendix 1G. The same LARSA model as for implementation of demand analysis for LL ground motion is used to start the iterative procedure (LaytonInt _TensionUL.lar and LaytonInt _CompressionUL.lar). The only difference is in the ground motion. In this part upper level ground motion found from SRC is used (LaytonInt _UpperLevel.drs).

1.6.4 Analysis Results and Discussion

The results of pushover analysis (Appendix 1F) and demand evaluation by response spectrum analysis (Appendix 1G) are summarized in Table 1.6.1. The demands represent the overall maximum determined from either of the tension or compression model. The demands exceed the capacities by large amounts in bents 2 and 3 in the longitudinal direction, and by a small amount for bent 2 in the transverse direction.

Table 1.6.1 Comparison of displacement capacities and demands in bent local directions

	Bent Longitudinal Direction (in)		Bent Transverse Direction (in)	
	Capacity	Demand	Capacity	Demand
Bent 2	8.72	14.54	11.33	11.96
Bent 3	8.56	11.19	10.52	9.82
Bent 4	8.56	7.56	10.38	6.72

Given the age of the bridge and the fact that it is being evaluated for a 2500 year return period event, the results are somewhat surprising. Worth noting, the displacement capacities in the bents determined from pushover analysis contain relative components of footing displacement and rotation, but only column displacement limits are considered. Footing displacement and rotation demands may be exceeded. However, the usual strategy is to limit foundation demands by designing the columns to yield prior to the foundations.

Compared to the pushover analysis, the component procedure applied for the LL ground motion is a more thorough procedure that considers many of the bridge details. However, both

analyses suggest that the key seismic deficiencies in the bridge lie in the column flexural capacities. Clearly, a substantial retrofit measure is needed to either enhance the bridge capacity or lower its demands.

1.7 Bridge Retrofit using Seismic Isolation

This bridge is considered to be a good candidate for seismic isolation because it uses expansion bearings for the bent to girder connections and at the abutments. The expansion bearings can simply be replaced with seismic isolation bearings. Seismic isolation bearings, which are very flexible, cause the effective stiffness of the bridge to be reduced and its natural period to be lengthened. The period lengthening in turn shifts the bridge into the lower acceleration region of the design spectrum, therefore substantially reducing the demands. In an effective seismic isolation retrofit, the bridge should be able to sustain the reduced demands elastically such that no further strengthening or ductility enhancement is required. In this example, an isolation system is designed and evaluated as the retrofit measure.

The following issues of practical concern deserve mention. First, low profile elastomeric bearings are used in the current bridge. Replacing these bearings with isolation bearings will require extra effort since additional space will need to be created between the bent and the girders to fit the taller isolation bearings. Second, the clearance between the abutment and the backwall is not sufficient to accommodate the expected displacement of the isolation system in the design level earthquake. The Retrofit Manual (FHWA, 2006) suggests that it may be acceptable and cost effective not to provide adequate clearance at the time of retrofit. In the event of a large earthquake, the backwall will be damaged due to collision of the isolators, but this damage can be repaired and adequate clearance provided for subsequent events.

The following steps are followed in this example to design isolation system (Priestly et. al. 1996; MCEER, 2006).

1. *Select the yield strength of the isolation system.* The strength of isolators should be less than the strength of the corresponding piers, to ensure that the isolators yield before the columns yield. For this purpose, the column shear capacity is defined as the shear force in the column when it reaches its ultimate moment capacity, based on the height of the column and fixity conditions at the ends. This assumes that plastic hinges will develop before the column fails in shear. The equivalent yield strength of the isolators in a bent should be less than 85% of the summed column shear capacities. To get a regular

response in the bridge, the shear strength of the weakest bent determines the yield strength of isolators.

2. *Select the natural period of vibration and damping coefficient for the isolation system based on the design spectrum.* The natural period and damping ratio are selected such that the provided force capacity of the isolation system equals the elastic spectral acceleration demand at that period and damping ratio. Assuming elastic-perfectly plastic behavior in the isolation system, the total lateral force is the sum of the yield strengths of all isolators in the bridge. The spectral acceleration given by the design spectrum, as a function of natural period and damping ratio, is equated with the lateral force capacity of the isolation system. The spectral displacement, which represents the global displacement the bridge incurs during design earthquake, is computed from the spectral acceleration.
3. *Evaluate resultant displacement demands in the bent and in the isolators corresponding to yielding in the isolators.* The sum of bent and isolator displacements equals the total bridge displacement evaluated from the design spectrum in Step 2.
4. *Evaluate effective damping ratios of the bridge according to an assumed maximum ductility for the isolators.* The global ductility of each foundation-pier-isolator system is computed.
5. *Evaluate effective stiffness of the isolators and develop the model of the isolation system for analysis.* The equivalent stiffness of each isolator equals the force capacity found in Step 1 divided by the effective isolator displacement found in Step 3. Because isolators act in parallel, the equivalent yield strength is the sum of yielding strength of all the isolators in the bent. As seismic forces are proportional to weight, in this example the equivalent yield strength is distributed to the bearings in proportion to the weight transferred through each bearing.
6. *Develop a model for the isolators and perform modal analysis of the bridge structure in LARSA to determine the natural vibration periods*. Isolators can be modeled as springs with linear or bilinear force-deformation characteristics. The disadvantage to this approach is that depending on the software, the springs are uncoupled in the two lateral and vertical directions. The vertical stiffness and lateral-vertical interaction is often ignored, unless buckling is a consideration as with slender elastomeric bearings. In this

example, equivalent beam elements are used to represent the resultant force-deformation characteristics of the isolators.

7. *Develop a hybrid design spectrum to reflect varied damping characteristics for different vibration modes of the bridge.* The effective damping ratios for the bridge computed in Step 4 reflect an overall increase in damping due to hysteretic energy dissipation of the isolation devices. In an approximate sense, the isolator deformations dominate the fundamental modes of vibration while higher vibration modes are dominated by structural participation. Therefore, the effective isolation damping ratio is used in the fundamental, or isolation modes and 5% damping ratio is used in the remaining modes. A hybrid design spectrum is required with different levels of damping for the structural and isolated modes of vibration. To get the hybrid spectrum, the 5% damped spectrum is modified at periods above 0.8 times the fundamental period by dividing by the damping modification factor B computed in Step 4.
8. *Iteratively analyze the bridge using response spectrum analysis until the computed displacement demands computed agree with the assumed values.* Response spectrum analysis determines the global displacement and displacement demands at each pier. If these responses are considerably different from the values assumed during the design phase, iteration is required for convergence. To iterate, new values of global and pier displacement are substituted for the assumed design values in Steps 2 and 3 and Steps 2-8 are repeated.

Appendix 1H demonstrates the above procedure. The isolation bearings were not designed in detail, but we assume that it is feasible to design bearings that satisfy the desired characteristics.

The converged analysis results from the iterative procedure are summarized below in Table 1.7.1. The displacements from analysis agree well with the design values. Bent and abutment displacements are larger than assumed for design due to additional flexibility in the foundation. Based on the close agreement of the results and the assumed values, the foundation flexibility can be ignored.

A comparison of bent displacements for the retrofitted bridge with the capacity limits of Table 1F.5 indicates that the retrofitted demand displacements are below the capacity limits for the UL ground motion. This analysis does not guarantee that the system will remain elastic in the LL ground motion, and the component capacity/demand analysis for the LL motion was not repeated. However, with seismic isolation, the forces transmitted from the superstructure to the

piers and foundations are substantially smaller, and it can be expected that the bridge will survive a LL earthquake event without substantial damage.

Table 1.7.1 Deformation response of the isolated bridge from response spectrum analysis

		Abut 1	Bent 2	Bent 3	Bent 4	Abut 5
Global displacement (in)	Long	18.15	18.15	18.15	18.15	18.15
	Trans	8.8	9.25	9.67	9.79	9.46
Bent/abutment displacement (in)	Long	0.04	3.22	2.82	2.54	0.04
	Trans	0.56	3.46	3.16	2.87	0.6

Appendix 1. Detailed Analysis for Clearfield Interchange Overpass

Appendix 1A. Determination of Seismic Retrofit Category

Bridge Importance:

Standard

Anticipated Service Life:

The bridge plans are approved on January 24, 1963, and the bridge is assumed to be constructed in 1964.

Bridge age: ~ 43 years

Anticipated Service Life: 75-43=32 years

Service life category: ASL2

Bridge Performance Level:

UL Motion: PL3

LL Motion: PL1

Site Class:

The site condition is determined through harmonic mean of blow counts of soil layers in the top 100 ft (Table 2-3 of FHWA, 2006). The plan of soil data is based on elevation, thus the elevation of the surface grade must be determined.

Elevation of the finished grade

Height from the finished grade in N.B.L. to the top of bent cap 3 (Bridge Plans, sheet 1: elevation): 16'7"=16.58 ft

Elevation at bottom of bent cap 3 in N.B.L (Bridge Plans, sheet 7, point E): 4546.83 ft

Height of bent cap (Bridge Plans, sheet 7): 3'11"=3.92 ft

Elevation of the finished grade= 4546.83+3.92-16.58=4534.17 ft

From Boring 1, N = 18.95

Site Class: D or E

Detailed calculations are presented in Table 1A.1

Spectral Accelerations and Soil Factors:

The bridge is located in the Layton to Hill Field interchange. The exact location is

Latitude: 41° 6'11.26"N

Longitude: 112° 0'15.03"W

Zip code: 84015

Summary of Definitions

Ss	0.2- second period spectral acceleration
S_1	1- second period spectral acceleration
F_a	Site coefficient for short period
F_v	Site coefficient for long period
$S_{DS}=F_a S_s$	Design earthquake response spectral acceleration at short period
$S_{D1}=F_v S_1$	Design earthquake response spectral acceleration at long period
SHL	Seismic hazard level

Determination of Seismic Hazard Level (SHL)

From Table 1-4 and 1-5 of (FHWA, 2006)

	S_s (g)	S_1 (g)	F_a	F_v	S_{DS} (g)	S_{D1} (g)	SHL
Lower Level: 500-year	0.469	0.16	1.8	3.32	0.844	0.531	IV
Upper Level: 2500-year	1.10	0.38	0.9	2.48	0.99	0.94	IV

Seismic Retrofit Category (SRC)

From Table 1-6 of (FHWA, 2006)

UL: **SRC = C**

LL: **SRC = D**

Table 1A.1 Blow count number of soil

Elevation	Thickness (d)	BC1	BC2	Average (BCa)	d/Bca
4534.17	2.47	19	28	23.5	0.105106
4531.7	2.7	21	26	23.5	0.114894
4529	8	5	8	6.5	1.230769
4521		16	37		
		22	42		
	12	34	45	32.6667	0.367347
4509		12	17		
		19	33		
	14	29	47	26.16667	0.535032
4495		56	91		
		12	48		
	16	33	37	46.16667	0.34657
4479		9	13		
		10	19		
		11	20		
		11	16		
		15	22		
	29	16	26	15.66667	1.851063
4450	4	30	48	39	0.102564
4446					
∑=	88.17			∑=	4.653345

Blow Count Number

18.94766

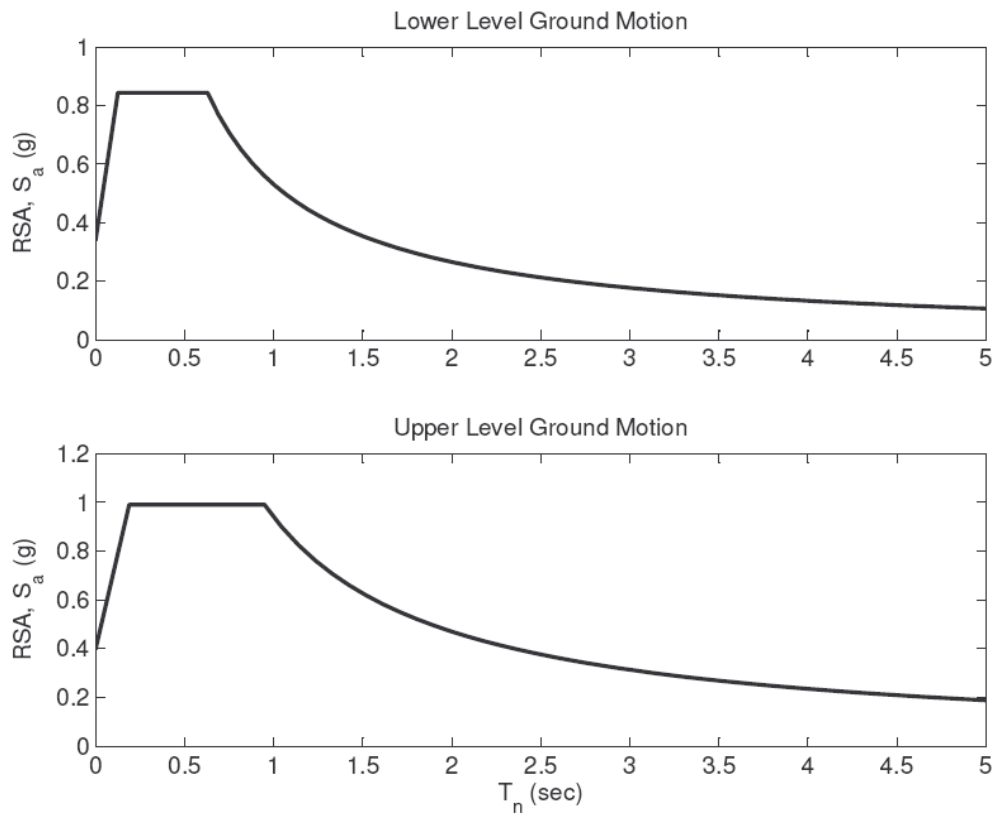

Figure 1A.1. Acceleration design spectra for LL and UL ground motions

Appendix 1B. Element Properties in LARSA Model

Pile Stiffness

Lpile: = 22 *ft*	Length of the pile
D: =1 *ft*	Diameter of the piles
H: = 3.0833 *ft*	Height of the footing
B: = 4 *ft*	Distance between two piles in the longitude direction
L: = 4 *ft*	Distance between two piles in the transverse direction
l: = 7 *ft*	Length of the footing
b: = 7 *ft*	Width of the footing
γ: = 50 lb/ft^3	Weight density of soil
G: = 14.39 *ksi*	Shear modulus
Z: = 7.42 *ft*	Embedment depth:

Elevation of the finished grade: 4534.17 *ft*

Elevation of the bottom of the footing: 4526.75 *ft*

Embedment depth: 4534.2-4526.75=7.42 *ft*

E: = 2.55e6 *psi*	Modulus of elasticity (Concrete type: FC-2)
I: = 1017.9 in^4	Moment of inertia of pile
EI=2.596e9 *psi*	Flexural stiffness of pile
$\varphi=32^\circ$	Internal friction angle of the soil (sand)
f=8 lb/in^3	Coefficient of variation in subgrade stiffness (Fig. 6-12 of FHWA, 2006)

Single pile stiffness

$K_{\delta x}= K_{\delta y}$=5e4 *lb/in*	Translational Stiffness - Fixed Head (Fig. 6-14 of FHWA, 2006)
$K_{\theta x}= K_{\theta y}$=1e8 *lb.in/rad*	Rotational Stiffness (Fig. 6-15 of FHWA, 2006)
$K_{\delta y\theta x}= -K_{\delta y\theta x}$=1.7e6 *lb*	Cross-Coupling Stiffness (Fig. 6-16 of FHWA, 2006)

The Retrofit Manual (FHWA, 2006) suggests that axial stiffness EA/L be factored by a coefficient α, where α can take a lower bound value of 1 for end-bearing piles on rock and an upper bound value of 2 for friction piles. The bridge structure was analyzed to both α=1 and α=2 to determine the sensitivity of the results to this parameter. It was observed that both deformations and forces were insensitive to α within a measure of precision expected from the analysis. Therefore, α=1 is used in this example.

α=1

$K_{\delta z}$=EA/L=1.3e6 *lb/in*

Substituting these values in the appropriate positions give the following stiffness matrix for one pile, with DOFs as indicated.

$$K_{pile} = \begin{array}{c} \\ \delta_x \\ \delta_y \\ \delta_z \\ \theta_x \\ \theta_y \\ \theta_z \end{array} \begin{array}{c} \begin{array}{cccccc} \delta_x & \delta_y & \delta_z & \theta_x & \theta_y & \theta_z \end{array} \\ \begin{bmatrix} 5\times10^4 & 0 & 0 & 0 & -1.7\times10^6 & 0 \\ 0 & 5\times10^4 & 0 & 1.7\times10^6 & 0 & 0 \\ 0 & 0 & 1.34\times10^6 & 0 & 0 & 0 \\ 0 & 1.7\times10^6 & 0 & 10^8 & 0 & 0 \\ -1.7\times10^6 & 0 & 0 & 0 & 10^8 & 0 \\ 0 & 0 & 0 & 0 & 0 & 0 \end{bmatrix} \end{array}$$

Pile Group Stiffness

As the next step, the individual pile stiffness matrices are assembled into a stiffness matrix for the pile group. Lateral and cross-coupling terms are simply added or multiplied by the number of piles. Rotational stiffnesses about the in-plane axes are modified by adding the summation of the vertical stiffness multiplied by the moment arm:

$$\left(k_{\theta\ x}\right)_{pilegroup} = \sum_i \left(k_{\theta\ x}\right)_{pile\ i} + \sum_i \left(k_z \frac{L^2}{4}\right)_{pile\ i}$$

$$\left(k_{\theta\ y}\right)_{pilegroup} = \sum_i \left(k_{\theta\ y}\right)_{pile\ i} + \sum_i \left(k_z \frac{B^2}{4}\right)_{pile\ i}$$

$$\left(k_{\theta\ x}\right)_{pilegroup} = 4\times1e8 + 4\times1.34e6\times\frac{(4\times12)^2}{4} = 3.48e9 \qquad lb.in/rad$$

$$\left(k_{\theta\ y}\right)_{pilegroup} = 4\times1e8 + 4\times1.34e6\times\frac{(4\times12)^2}{4} = 3.48e9 \qquad lb.in/rad$$

The torsional component of the stiffness matrix (the (6,6) entry) is zero for an individual pile but is determined from the summation of lateral stiffnesses multiplied by the appropriate moment arms. This is illustrated in Fig. 2B.1. For each pile the resistance against torsion is divided into two components: x and y. Taking the moment of these forces with respect to the centroid leads to:

$$k_{torsion} = \sum_i \left(k_\delta l\sin(\theta)\times l\sin(\theta) + k_\delta l\cos(\theta)\times l\cos(\theta)\right) = 4\times k_\delta \times l^2$$

$$k_{torsion} = 4 \times k_{\delta} \times \left(\frac{L}{2 \times \sin(\theta)} \right)^2$$

$$k_{torsion} = k_{\delta} \times \left(\frac{L}{\sin(\theta)} \right)^2$$

L = 4 *ft*

θ = 45°

$k_{torsion} = 5e4 \quad (4 \times 12)^2 \times 2 = 2.3e8 \quad lb.in/rad$

Thus, the pile group stiffness is

$$K_{pile\ group} = \begin{bmatrix} 2e5 & 0 & 0 & 0 & -6.8e6 & 0 \\ 0 & 2e5 & 0 & 6.8e6 & 0 & 0 \\ 0 & 0 & 5.34e6 & 0 & 0 & 0 \\ 0 & 6.8e6 & 0 & 3.48e9 & 0 & 0 \\ -6.8e6 & 0 & 0 & 0 & 3.48e9 & 0 \\ 0 & 0 & 0 & 0 & 0 & 2.3e8 \end{bmatrix}$$

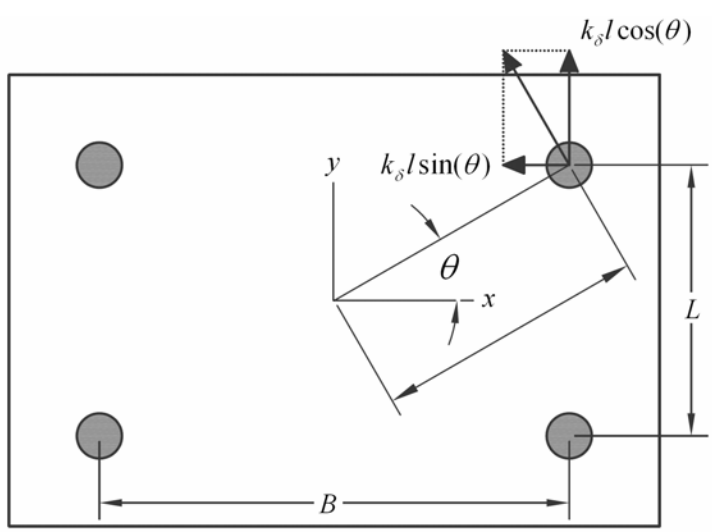

Figure 1B.1. Calculating rotational stiffness of pile group

Footing Stiffness

Shear modulus:

The shear modulus of the soil is developed using the relation proposed by Imai and Yoshimura:

$G = a.N^b.10^2 \quad kPa$

a=100 regression parameter

b=0.78 regression parameter

N=19 number of blow counts

G=2071.95 *ksf*

Poisson Ratio

ν = 0.4 FHWA Geotechnical Engineering Circular No.3 for sand and silty sand.

Stiffness components:

Given G, ν, B, and L, stiffness parameters are determined from Table 6-1 (FHWA, 2006). The derived stiffnesses are corrected for the embedment depth by factors *e* defined in Table 6-2 (FHWA, 2006). Contributions to the lateral soil stiffness from the footing's base and side shear are neglected in the case of a pile-footing foundation. Thus, the lateral stiffness of the footing is determined from the passive pressure on the sides (Figure 6-6 of FHWA, 2006).

K_p=3	
Z=7.42 ft	Depth to the bottom of footing
H=3'1"	
Z_m=Z-H/2=5.88 *ft*	Mid depth
$K_p.\gamma.Z_m$=882 *lb/ft*^{2}	Average passive pressure
L=7 *ft*	
F_c= 882×H×L=19.03 *kips*	Total force capacity on pile cap
Δ=0.02×Z=0.148 *ft*	Mobilization displacement of soil
k_{fx}= k_{fy}=19.03/0.148/12	
=10.69 kips/in	Lateral stiffness

Other stiffness components of the footing are found using the formulas in Tables 6-1 and 6-2 (FHWA, 2006).

k_z' =4.6e3 *kips/in*

e_z =3.11

k_z =1.42e4 *kips/in*

$k_{\theta x}'$ =6.4e6 *kips.in/rad*

$e_{\theta x}$ =3.28

$k_{\theta x}$ =2.09e7 *kips.in/rad*

$k_{\theta y}'$=3.72e6 *kips.in/rad*

$e_{\theta y}$= 3.80

$k_{\theta y}$ =9.06e6 *kips.in/rad*

R= 4 *ft*

$k_{\theta z}$ =7.05e6 *kips.in/rad*

Pile-Footing Stiffness

Finally, the stiffness matrices of the pile group and footing are assembled into a single matrix for the foundation stiffness.

$$K_{pile\ footing\ 4} = K_{piles\ 4} + K_{footing} = \begin{bmatrix} 2528.2 & 0 & 0 & 0 & -6800 & 0 \\ 0 & 2528.2 & 0 & 6800 & 0 & 0 \\ 0 & 0 & 2.35e5 & 0 & 0 & 0 \\ 0 & 6800 & 0 & 2.04e6 & 0 & 0 \\ -6800 & 0 & 0 & 0 & 2.17e6 & 0 \\ 0 & 0 & 0 & 0 & 0 & 6.06e5 \end{bmatrix}$$

The above stiffness matrix has the units of kips and feet. As mentioned before, the footings are aligned in the direction of the 34°57' bridge skew. This detail can be handled in one of two ways. The first option is to rotate the stiffness matrix from local coordinate to global coordinate system. The stiffness matrix in global coordination can be found by applying the transformation:

$$K_{global} = T' K_{local} T$$

where T is the rotation matrix given by

$$T = \begin{bmatrix} \cos(\theta) & -\sin(\theta) & 0 & 0 & 0 & 0 \\ \sin(\theta) & \cos(\theta) & 0 & 0 & 0 & 0 \\ 0 & 0 & 1 & 0 & 0 & 0 \\ 0 & 0 & 0 & \cos(\theta) & -\sin(\theta) & 0 \\ 0 & 0 & 0 & \sin(\theta) & \cos(\theta) & 0 \\ 0 & 0 & 0 & 0 & 0 & 1 \end{bmatrix}$$

The second option, conveniently allowed by LARSA, is to introduce a user defined local coordinate system and specify the nodes of the foundation elements using this alternate local Coordinate System. This allows the pile-footing stiffness matrix to be entered directly into LARSA without a transformation, and is the approach applied in this example.

Abutment Stiffness

$$L = (67 \times 12 + 3 + 1/16) \times 1/12 \times \cos(124.57 - 90) = 55.4 \quad ft$$

Width of the backwall based on Figure 1B.2

θ: = 34°57’ Skew angle

H: = 5.6 ft Height of the abutment

C_p: = 40 kips Capacity of the pile

The total capacity of the abutment-pile system in longitudinal direction is

$$P_p = p_p.H.L + N_p.C_p$$
$$= P_p = \frac{2}{3} \times 5.6^2 \times 55.4 + 7 \times 40 = 1438 \quad kips$$

For seat type abutments in the longitudinal direction, the soil passive pressure contributes to the overall abutment stiffness for compression. As mentioned previously, abutments are modeled through some nodes along the abutment axis. Thus, the total capacity for the whole abutment is decomposed to find the stiffness corresponding to each node. Therefore, the effective compression stiffness is given by:

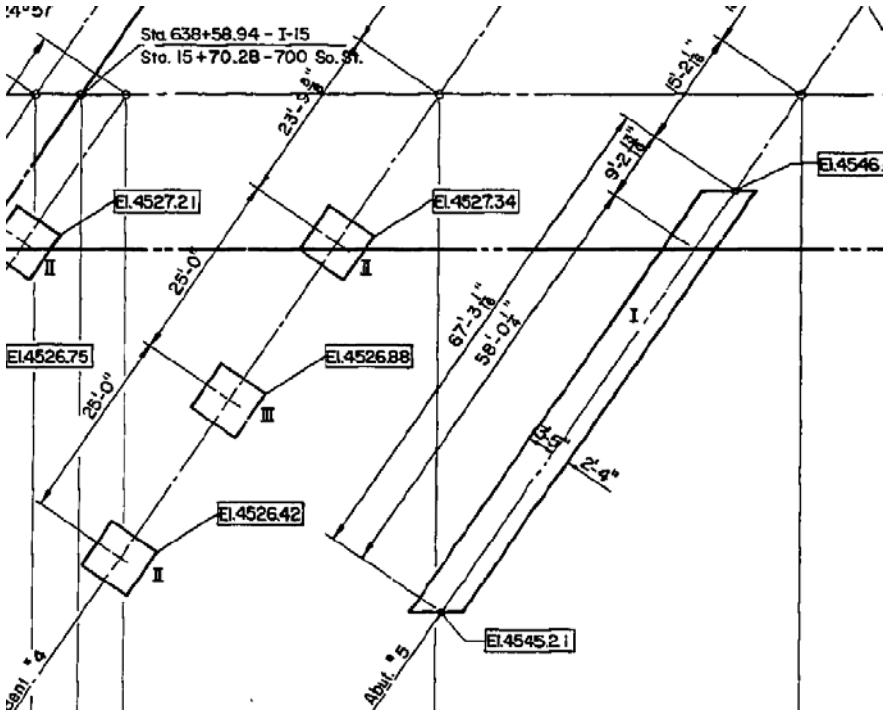

Figure 1B.2. Abutment plan

$$L_{end} = \frac{55.4 - 5 \times 8.5}{2} = 6.45 \quad ft$$

$$L_{middle} = 8.5 \quad ft$$

$$K_{eff \quad end(Comp,Long)} = \frac{P_p}{0.02H} \times \frac{L_{end}}{L} = \frac{1438}{0.02 \times 5.6} \times \frac{L_{end}}{55.4} = 1495 \quad kips / ft$$

$$K_{eff \quad middle(Comp,Long)} = \frac{P_p}{0.02H} \times \frac{L_{middle}}{L} = \frac{1438}{0.02 \times 5.6} \times \frac{L_{middle}}{55.4} = 1970 \quad kips / ft$$

In tension, only piles contribute to the stiffness:

$$P_{p \quad piles} = 7 \times 40 = 280 \quad kips$$

$$K_{eff \quad (Tension)} = \frac{P_p}{0.02H \times N_{Nodes}} = \frac{280}{7 \times 0.02 \times 5.6} = 357 \quad kips / ft$$

A similar procedure is applied in the transverse direction, but the transverse stiffness of the abutment is provided by wing walls. Sec. 4.4.2(e) of Priestley et al. (1996) proposes to take the

effective width as the length of the wing walls multiplied by a factor of 8/9 to account for differences in participation of both wing walls.

$$L = \frac{8}{9} \times \left(7 + \frac{7}{12} + 9 + \frac{3}{12}\right) \times \cos(124.57 - 90) = 12.3 \quad ft$$ Width of the wingwall

θ: = 34°57' Skew angle

H: = 5.6 ft Height of the abutment

C_p: = 40 kips Capacity of the pile

The total capacity of the abutment-pile system in the transverse direction is

$$P_{p\ \ wingwall} = \frac{2}{3} \times 5.6^2 \times 12.3 = 257 \quad kips$$

$$P_{p\ \ piles} = 7 \times 40 = 280 \quad kips$$

$$K_{eff\ \ end} = \frac{257/2 + 280/7}{0.02 \times 5.6} = 1505 \quad kips/ft$$

$$K_{eff\ \ middle} = \frac{280/7}{0.02 \times 5.6} = 357 \quad kips/ft$$

Nonlinear spring elements are used to model these springs. LARSA considers the compression stiffness in response spectrum analysis, therefore, one can model only compression stiffness using spring elements available through *Input Data-Geometry-Springs*.

For boundary conditions, the abutment is assumed to be fully constrained in the vertical direction and for rotation around the longitudinal axis, but can rotate freely around the transverse axis. The effective stiffness derived above is assigned to each bearing in the corresponding direction.

Table 1B.1 Natural periods of bridge in tension and compression model

Tension Model		Compression Model	
Mode	Period (sec)	Mode	Period (sec)
1	0.905	1	0.673
2	0.824	2	0.488
3	0.793	3	0.335
4	0.674	4	0.329
5	0.502	5	0.234
6	0.354	6	0.200
7	0.244	7	0.197
8	0.222	8	0.179
9	0.210	9	0.156
10	0.204	10	0.131
11	0.189	11	0.124
12	0.156	12	0.123
13	0.142	13	0.123
14	0.129	14	0.118
15	0.128	15	0.114
16	0.124	16	0.110
17	0.124	17	0.105
18	0.118	18	0.103
19	0.115	19	0.092
20	0.113	20	0.089

Appendix 1C. Column and Footing Moment Capacities

Column Moment Capacities

Ultimate moment capacities for the columns are obtained from the computer generated column interaction diagrams shown in Figure 1C.1. Because the elastic moment demands are primarily in the plane of the bent, moment capacities will be calculated for bending in this plane. This requires a consideration of the variation in axial load due to bent overturning as outlined in the iterative procedure presented in article 4.8.2 of Division I-A of the AASHTO Standard Specifications (AASHTO, 2002). The steps of this procedure are as follows.

Step 1. Overstrength Moment Capacities at Axial Load Corresponding to Dead Load

Table 1C.1 summarizes the overstrength column and footing moment capacities taken from the interaction diagrams.

Table 1C.1 Column and footing overstrength moments.

Bent	End	Axial Force (kip)	1.3 Mn (kip-ft)	
			Column	footing
B-2 (C-1)	top	194.5935211	833.2	
B-2 (C-1)	bottom	200.8360138	833.2	1362.4
B-2 (C-2)	top	272.7033386	886.8	
B-2 (C-2)	bottom	278.9458313	895.2	1404
B-2 (C-3)	top	241.322998	860.8	
B-2 (C-3)	bottom	247.565506	869.6	1242.8
B-3 (C-1)	top	231.8602295	860.8	
B-3 (C-1)	bottom	238.1027222	860.8	1263.6
B-3 (C-2)	top	265.1020813	878.3	
B-3 (C-2)	bottom	271.344574	886.8	1404
B-3 (C-3)	top	195.0166016	833.2	
B-3 (C-3)	bottom	201.2590942	833.2	1357.2
B-4 (C-1)	top	194.6977386	833.2	
B-4 (C-1)	bottom	200.9402313	833.2	1362.4
B-4 (C-2)	top	247.9158783	869.6	
B-4 (C-2)	bottom	254.158371	869.6	1404
B-4 (C-3)	top	193.0752106	823.6	
B-4 (C-3)	bottom	199.3177032	833.2	1362.4

Step 2. Axial Forces Due to Overturning in the Transverse Direction

Because the bents are symmetric, the axial forces in the middle columns due to seismic loading are zero. Satisfying equilibrium, the axial force due to overturning in side columns is

$$P = \frac{M_{T1} + M_{T2} + M_{T3}}{2L}$$

where M_{Ti} is the moment capacity at the top of the column i and L is the distance of the center to center of two adjacent columns in a bent.

Bent 2: Axial Force = (833.2+886.8+860.8) ÷(2×25)= +51.62 *kips*

Bent 3: Axial Force = (860.8+878.3+833.2) ÷(2×25)= +51.45 *kips*

Bent 4: Axial Force = (833.2+869.6+823.6) ÷(2×25)= +50.53 *kips*

Step 3. Revised Overstrength Moment Capacities

The axial loads due to overturning calculated in Step 2 are used to obtain new overstrength moment capacities from the interaction diagrams. Table 1C.2 summarizes these revised moment capacities. These moment capacities are used to calculate revised axial forces. These axial loads are used to recalculate the overstrength moments, which are summarized in Table 1C.3. The bent moments and axial forces are now within 10 percent of the previously calculated moments and forces and therefore no further iteration is needed.

Pile Footing Moment Capacities

The moment capacity of the footing also depends on the axial load that is transferred from the column. The converged axial load from the iterative procedure described before is used to find the moment capacity of footings. The results are presented in Table 1C.3 besides the moment capacity of columns.

The process of computing the footing capacity is illustrated here for one pile-footing. Suppose the axial load transferred to the footing is 200 kips. We must identify the configuration of axial loads in the piles that results in maximum moment and also satisfies vertical equilibrium (see Figure 1C.2). Since the axial load on the footing is large, the right piles are assumed to be at capacity in compression (2 x 180 kips), and the axial forces in the left piles are found through equilibrium

$P_2 = 360$ *kips* (compression)

$P_1 = P - P_2$

$= 200 - 2\times180 = -160$ *kips* (tension)

Dividing P_1 by 2 to find the axial force in each pile leads to:

$$P_{1\ pile} = \frac{-160}{2} = -80 > -90 \qquad kips$$

d = 4 ft Distance between piles

$$M_n = 2\times\frac{4}{2}\times180 + 2\times\frac{4}{2}\times80 = 1040 \qquad kips.ft$$

$1.3\ M_n = 1.3\times1040 = 1352$ *kips.ft*

This load pattern gives the maximum moment and satisfies both the equilibrium and capacity limits for axial loads.

Table 1C.2 Revised column and footing overstrength moments (iteration 1).

Bent	End	Axial Force (kip)	1.3 Mn (k-ft) Column
B-2 (C-1)	top	142.9779	783.6
B-2 (C-1)	top	246.2091	869.6
B-2 (C-1)	bottom	149.2204	793.9
B-2 (C-1)	bottom	252.4516	869.6
B-2 (C-2)	top	272.7033	886.8
B-2 (C-2)	top	272.7033	886.8
B-2 (C-2)	bottom	278.9458	895.2
B-2 (C-2)	bottom	278.9458	895.2
B-2 (C-3)	top	189.7074	823.6
B-2 (C-3)	top	292.9386	903.4
B-2 (C-3)	bottom	195.9499	833.2
B-2 (C-3)	bottom	299.1811	903.4
B-3 (C-1)	top	180.415	813.9
B-3 (C-1)	top	283.3054	895.2
B-3 (C-1)	bottom	186.6575	823.6
B-3 (C-1)	bottom	289.5479	895.2
B-3 (C-2)	top	265.1021	878.3
B-3 (C-2)	top	265.1021	878.3
B-3 (C-2)	bottom	271.3446	886.8
B-3 (C-2)	bottom	271.3446	886.8
B-3 (C-3)	top	143.5714	783.6
B-3 (C-3)	top	246.4618	869.6
B-3 (C-3)	bottom	149.8139	793.9
B-3 (C-3)	bottom	252.7043	869.6
B-4 (C-1)	top	144.1687	783.6
B-4 (C-1)	top	245.2267	869.6
B-4 (C-1)	bottom	150.4112	793.9
B-4 (C-1)	bottom	251.4692	869.6
B-4 (C-2)	top	247.9159	869.6
B-4 (C-2)	top	247.9159	869.6
B-4 (C-2)	bottom	254.1584	869.6
B-4 (C-2)	bottom	254.1584	869.6
B-4 (C-3)	top	142.5462	783.6
B-4 (C-3)	top	243.6042	869.6
B-4 (C-3)	bottom	148.7887	793.9
B-4 (C-3)	bottom	249.8467	869.6

Table 1C.3 Revised column and footing overstrength moments (iteration 2).

Bent	End	Axial Force	1.3 Mu	
			Column	footing
B-2 (C-1)	top	144.7117211	793.9	
B-2 (C-1)	top	247.7901211	869.6	
B-2 (C-1)	bottom	150.9542138	793.9	1336
B-2 (C-1)	bottom	254.0326138	869.6	1227
B-2 (C-2)	top	272.7033386	886.8	
B-2 (C-2)	top	272.7033386	886.8	
B-2 (C-2)	bottom	278.9458313	895.2	1404
B-2 (C-2)	bottom	278.9458313	895.2	1404
B-2 (C-3)	top	191.441198	823.6	
B-2 (C-3)	top	294.519598	903.4	
B-2 (C-3)	bottom	197.683706	833.2	1368
B-2 (C-3)	bottom	300.762106	903.4	1108
B-3 (C-1)	top	182.3434295	823.6	
B-3 (C-1)	top	284.7226295	895.2	
B-3 (C-1)	bottom	188.5859222	823.6	1394
B-3 (C-1)	bottom	290.9651222	903.4	1134
B-3 (C-2)	top	265.1020813	878.3	
B-3 (C-2)	top	265.1020813	878.3	
B-3 (C-2)	bottom	271.344574	886.8	1404
B-3 (C-2)	bottom	271.344574	886.8	1404
B-3 (C-3)	top	145.4998016	793.9	
B-3 (C-3)	top	247.8790016	869.6	
B-3 (C-3)	bottom	151.7422942	793.9	1336
B-3 (C-3)	bottom	254.1214942	869.6	1227
B-4 (C-1)	top	145.9603386	793.9	
B-4 (C-1)	top	246.8755386	869.6	
B-4 (C-1)	bottom	152.2028313	793.9	1342
B-4 (C-1)	bottom	253.1180313	869.6	1227
B-4 (C-2)	top	247.9158783	869.6	
B-4 (C-2)	top	247.9158783	869.6	
B-4 (C-2)	bottom	254.158371	869.6	1404
B-4 (C-2)	bottom	254.158371	869.6	1404
B-4 (C-3)	top	144.3378106	783.6	
B-4 (C-3)	top	245.2530106	869.6	
B-4 (C-3)	bottom	150.5803032	793.9	1336
B-4 (C-3)	bottom	251.4955032	869.6	1232

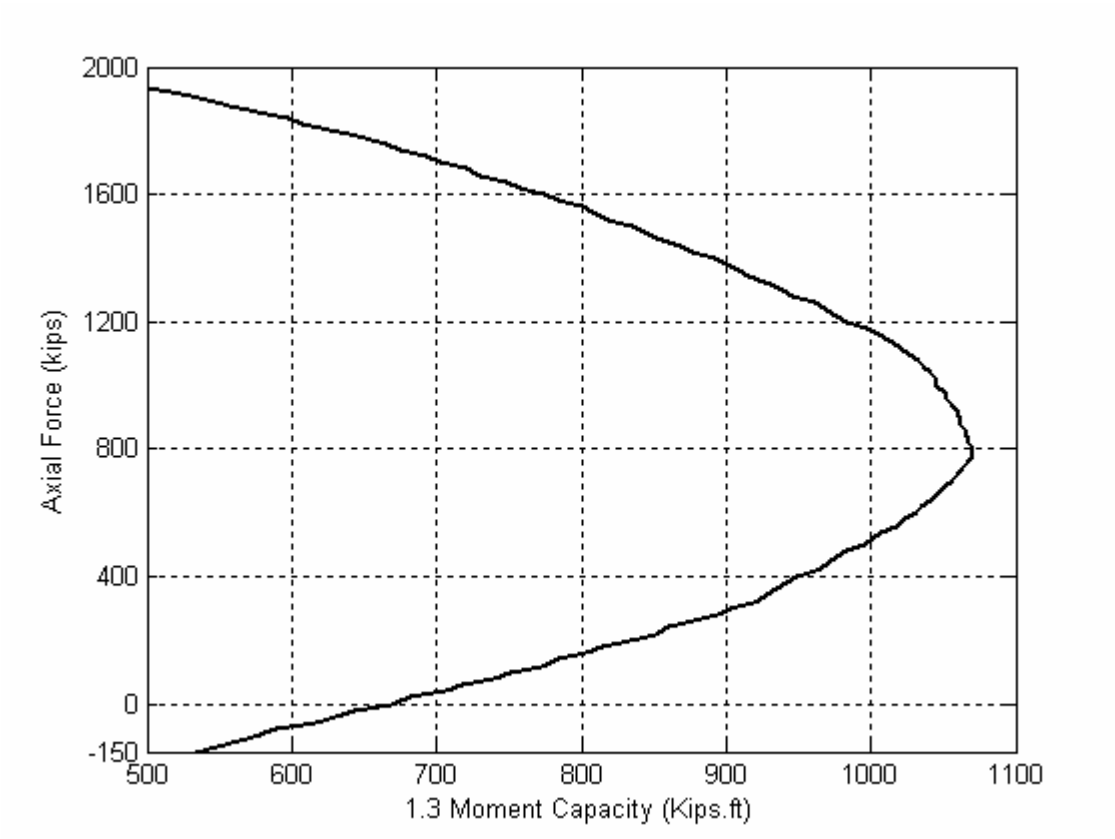

Figure 1C.1. Column interaction diagram

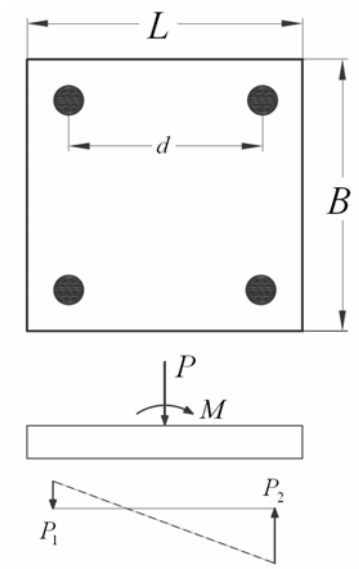

Figure 1C.2. Computing pile-footing moment capacity using statics (From FHWA, 2006)

Appendix 1D. Elastic Moment Demands for LL Evaluation

Table 1D.1 Maximum elastic moment demands for compression model

Location	Component	Axial Force (kip)	Fz	Fz	Trans. Moment My (k-ft)		Fy	Fy	Long. Moment Mz (k-ft)		Elastic Moment (k-ft)
		DL	DL	EQ	EQ	DL	DL	EQ	EQ	DL	Demand
B-2 (C-1) Top	Column	-195.72			1020.7	13.01			290.38	-13.54	1077.4583
B-2 (C-1) Bottom	Column	201.964	-1.084	127.2	1136.4	5.4707	-1.164	36.268	315.63	-6.284	1186.3659
B-2 (C-1) Bottom	Footing	201.964			1528.6	2.127			427.45	-9.872	1591.9738
B-2 (C-2) Top	Column	-271.63			1072.2	-2.072			290.98	-2.686	1113.6891
B-2 (C-2) Bottom	Column	277.874	0.1928	132.86	1181.3	-1.215	-0.228	36.08	311.93	-1.2	1223.2513
B-2 (C-2) Bottom	Footing	277.874			1590.9	-0.62			423.18	-1.904	1647.3351
B-2 (C-3) Top	Column	-241.18			1021.5	-8.515			290.46	2.1414	1070.7942
B-2 (C-3) Bottom	Column	247.418	0.7568	127.45	1139.8	-4.382	0.2066	36.247	315.07	1.3788	1187.106
B-2 (C-3) Bottom	Footing	247.418			1532.7	-2.049			426.83	2.0157	1593.5854
B-3(C-1) Top	Column	-231.92			1289.4	9.117			300.91	-3.55	1333.6995
B-3 (C-1) Bottom	Column	238.162	-0.804	160.82	1437.6	4.5923	-0.322	37.236	321.47	-1.938	1477.9972
B-3 (C-1) Bottom	Footing	238.162			1933.5	2.1119			436.29	-2.931	1984.7807
B-3 (C-2) Top	Column	-264.36			1341.9	0.7725			302.28	2.6105	1376.8965
B-3 (C-2) Bottom	Column	270.606	-0.08	166.32	1478.8	0.5864	2E-01	37.129	318.26	1.2422	1513.4553
B-3 (C-2) Bottom	Footing	270.606			1991.6	0.3406			432.75	1.9392	2038.8034
B-3 (C-3) Top	Column	-195.78			1281.9	-11.94			307.13	11.802	1332.5291
B-3 (C-3) Bottom	Column	202.025	0.999	159.69	1425.9	-5.081	1.0204	37.961	327.45	5.5873	1469.2532
B-3 (C-3) Bottom	Footing	202.025			1918.3	-2.001			444.5	8.7335	1973.0672
B-4 (C-1) Top	Column	-194.69			1019	9.5266			297.6	-6.871	1072.6276
B-4 (C-1) Bottom	Column	200.929	-0.835	129	1168.2	4.7089	-0.575	34.647	305.02	-2.936	1212.677
B-4 (C-1) Bottom	Footing	200.929			1566	2.1332			411.85	-4.71	1622.4763
B-4 (C-2) Top	Column	-247.81			1061.3	-0.787			282.43	-8E-02	1099.0536
B-4 (C-2) Bottom	Column	254.053	5.3E-02	133.3	1199.3	-0.123	-6.1E-04	34.948	305.54	0.07	1237.7243
B-4 (C-2) Bottom	Footing	254.053			1610.3	0.0419			413.3	0.0681	1662.5458
B-4 (C-3) Top	Column	-193.18			995.35	-9.118			334.89	5.3589	1060.5268
B-4 (C-3) Bottom	Column	199.421	0.7747	126.1	1142.7	-4.085	0.4607	36.017	316.35	2.4915	1190.2776
B-4 (C-3) Bottom	Footing	199.421			1531.5	-1.696			427.41	3.9119	1592.7162

Table 1D.2 Maximum elastic moment demands for tension model

Location	Component	Axial Force (kip)	Fz	Fz	Trans. Moment My (k-ft)		Fy	Fy	Long. Moment Mz (k-ft)		Elastic Moment (k-ft)
		DL	DL	EQ	EQ	DL	DL	EQ	EQ	DL	Demand
B-2 (C-1) Top	Column	-194.59			1058.4	0.5804			1206.1	13.486	1615.1868
B-2 (C-1) Bottom	Column	200.836	-1.15	130.5	1163.4	-0.58	-0.761	164.59	1592.3	6.1127	1977.4997
B-2 (C-1) Bottom	Footing	200.836			1565.8	-4.126			2099.8	3.766	2624.5709
B-2 (C-2) Top	Column	-272.7			1119.6	-1.594			1267.5	-2.397	1694.0278
B-2 (C-2) Bottom	Column	278.946	0.1965	137.54	1223.3	1.5936	0.1695	171.17	1643.2	-0.951	2051.2251
B-2 (C-2) Bottom	Footing	278.946			1647.4	2.1994			2170.9	-0.429	2727.959
B-2 (C-3) Top	Column	-241.32			1076.5	-3.694			1203.8	-9.354	1624.4038
B-2 (C-3) Bottom	Column	247.566	0.8045	133.41	1194.8	3.6944	0.5916	164.41	1591.4	-4.357	1996.5915
B-2 (C-3) Bottom	Footing	247.566			1606.1	6.1751			2098.3	-2.533	2649.0211
B-3(C-1) Top	Column	-231.86			1394.4	-6.623			1029.8	12.244	1746.047
B-3 (C-1) Bottom	Column	238.103	-1.108	172.37	1533.1	6.6226	-0.49	141.34	1372.6	6.6396	2065.038
B-3 (C-1) Bottom	Footing	238.103			2064.6	3.2061			1808.4	5.13	2750.3025
B-3 (C-2) Top	Column	-265.1			1406.6	-7.14			1087.9	1.752	1784.9294
B-3 (C-2) Bottom	Column	271.345	-0.173	173.28	1537.6	7.1398	-8E-02	147.57	1420.5	1.1958	2095.359
B-3 (C-2) Bottom	Footing	271.345			2071.8	6.6064			1875.5	0.9406	2796.4698
B-3 (C-3) Top	Column	-195.02			1299.9	-3.149			1043	-13.35	1677.3833
B-3 (C-3) Bottom	Column	201.259	1.1375	161.72	1447.3	3.1486	0.5724	142.69	1382.1	-6.037	2006.3615
B-3 (C-3) Bottom	Footing	201.259			1945.9	6.656			1822.1	-4.273	2669.642
B-4 (C-1) Top	Column	-194.7			1122.8	-6.451			803.11	9.5388	1391.2646
B-4 (C-1) Bottom	Column	200.94	-0.839	136.94	1213.3	6.4512	-0.482	120.29	1241.5	4.7517	1740.7959
B-4 (C-1) Bottom	Footing	200.94			1635.6	3.8656			1612.4	3.2666	2300.8133
B-4 (C-2) Top	Column	-247.92			1087.7	3.0007			848.66	-1E+00	1382.5449
B-4 (C-2) Bottom	Column	254.158	7.3E-02	132.23	1169.6	-3.001	6.4E-02	125.07	1278	-0.275	1733.0673
B-4 (C-2) Bottom	Footing	254.158			1577.3	-2.775			1663.6	-0.079	2293.129
B-4 (C-3) Top	Column	-193.08			966.13	1.2008			861.74	-9.997	1302.1736
B-4 (C-3) Bottom	Column	199.318	0.8752	118.08	1052.9	-1.201	0.4179	122.48	1252.3	-4.918	1640.9207
B-4 (C-3) Bottom	Footing	199.318			1417	1.4978			1629.9	-3.629	2163.8266

Table 1D.3 Maximum elastic moment demands

Location	Component	Moment Demand (k-ft)
B-2 (C-1) Top	Column	1615.1868
B-2 (C-1) Bottom	Column	1977.4997
B-2 (C-1) Bottom	Footing	2624.5709
B-2 (C-2) Top	Column	1694.0278
B-2 (C-2) Bottom	Column	2051.2251
B-2 (C-2) Bottom	Footing	2727.959
B-2 (C-3) Top	Column	1624.4038
B-2 (C-3) Bottom	Column	1996.5915
B-2 (C-3) Bottom	Footing	2649.0211
B-3(C-1) Top	Column	1746.047
B-3 (C-1) Bottom	Column	2065.038
B-3 (C-1) Bottom	Footing	2750.3025
B-3 (C-2) Top	Column	1784.9294
B-3 (C-2) Bottom	Column	2095.359
B-3 (C-2) Bottom	Footing	2796.4698
B-3 (C-3) Top	Column	1677.3833
B-3 (C-3) Bottom	Column	2006.3615
B-3 (C-3) Bottom	Footing	2669.642
B-4 (C-1) Top	Column	1391.2646
B-4 (C-1) Bottom	Column	1740.7959
B-4 (C-1) Bottom	Footing	2300.8133
B-4 (C-2) Top	Column	1382.5449
B-4 (C-2) Bottom	Column	1733.0673
B-4 (C-2) Bottom	Footing	2293.129
B-4 (C-3) Top	Column	1302.1736
B-4 (C-3) Bottom	Column	1640.9207
B-4 (C-3) Bottom	Footing	2163.8266

Appendix 1E. Capacity/Demand Ratios for LL Evaluation

The most critical combinations of the unfactored nominal ultimate moment capacities (M_u) and elastic moment demands are used to calculate r_{ec} and r_{ef} at each bent. Values of r_{ec} and r_{ef} are summarized in Table 1E.1, and provide the absolute maximum considering both the tension and the compression model.

Table 1E.1 Ultimate moment capacity/elastic moment demand ratios

Bent	End	Axial Force	Column			Footing		
			Demand (k-ft)	Capacity (k-ft)	r_{ec}	Demand (k-ft)	Capacity (k-ft)	r_{ef}
B-2 (C-1)	top	Min	1615.2	610.7	0.378			
B-2 (C-1)	top	Max	1615.2	668.9	0.414			
B-2 (C-1)	bottom	Min	1977.5	610.7	0.309	2624.6	1028	0.3917
B-2 (C-1)	bottom	Max	1977	668.9	0.338	2625	944	0.3597
B-2 (C-2)	top	Min	1694	682.2	0.403			
B-2 (C-2)	top	Max	1694	682.2	0.403			
B-2 (C-2)	bottom	Min	2051.2	688.6	0.336	2728	1080	0.3959
B-2 (C-2)	bottom	Max	2051.2	688.6	0.336	2728	1080	0.3959
B-2 (C-3)	top	Min	1624.4	633.6	0.39			
B-2 (C-3)	top	Max	1624.4	694.9	0.428			
B-2 (C-3)	bottom	Min	1996.6	640.9	0.321	2649	1052	0.3971
B-2 (C-3)	bottom	Max	1996.6	694.9	0.348	2649	852	0.3216
B-3 (C-1)	top	Min	1746	633.6	0.363			
B-3 (C-1)	top	Max	1746	688.6	0.394			
B-3 (C-1)	bottom	Min	2065	633.6	0.307	2750.3	1072	0.3898
B-3 (C-1)	bottom	Max	2065	694.9	0.337	2750	872	0.3171
B-3 (C-2)	top	Min	1784.9	675.6	0.379			
B-3 (C-2)	top	Max	1784.9	675.6	0.379			
B-3 (C-2)	bottom	Min	2095.4	682.2	0.326	2796.5	1080	0.3862
B-3 (C-2)	bottom	Max	2095.4	682.2	0.326	2796	1080	0.3862
B-3 (C-3)	top	Min	1677.4	610.7	0.364			
B-3 (C-3)	top	Max	1677.4	668.9	0.399			
B-3 (C-3)	bottom	Min	2006.4	610.7	0.304	2669.6	1028	0.3851
B-3 (C-3)	bottom	Max	2006.4	668.9	0.333	2670	944	0.3536
B-4 (C-1)	top	Min	1391.3	610.7	0.439			
B-4 (C-1)	top	Max	1391.3	668.9	0.481			
B-4 (C-1)	bottom	Min	1740.8	610.7	0.351	2300.8	1032	0.4485
B-4 (C-1)	bottom	Max	1740.8	668.9	0.384	2301	944	0.4103
B-4 (C-2)	top	Min	1382.5	668.9	0.484			
B-4 (C-2)	top	Max	1382.5	668.9	0.484			
B-4 (C-2)	bottom	Min	1733.1	668.9	0.386	2293.1	1080	0.471
B-4 (C-2)	bottom	Max	1733.1	668.9	0.386	2293	1080	0.471
B-4 (C-3)	top	Min	1302.2	602.8	0.463			
B-4 (C-3)	top	Max	1302.2	668.9	0.514			
B-4 (C-3)	bottom	Min	1640.9	610.7	0.372	2163.8	1028	0.4751
B-4 (C-3)	bottom	Max	1640.9	668.9	0.408	2164	948	0.4381

C/D Ratios for Plastic Hinging at the Bottoms of the Columns

The calculations shown follow the procedure of Appendix D.5 of FHWA (2006).

Bent 2 Column 1- Case VI (r_{ec} = 0.31 and r_{ef} = 0.39):

1. Anchorage (Appendix D.5.1 of FHWA, 2006) - Hooked anchorage

$L_a(c)$ = 22 in Effective anchorage length, capacity

The bars are #11 and the side cover is larger than 2.5 in, and the cover on the bar extension beyond the hook is larger than 2 inch, therefore k_m is 0.7.

$L_a(d) = 1200 k_m d_b \left(\frac{f_y}{60000\sqrt{f_c'}} \right) > 15 d_b$ Anchorage length, demand

d_b =1.41 *in* (#11) Nominal bar diameter

f_y = 36000 *psi*, Yield strength of reinforcement

f_c'=3000 *psi*, Concrete compression strength

$$L_a(d) = 1200 \times 0.7 \times 1.41 \times \left(\frac{36000}{60000 \times \sqrt{3000}} \right) = 12.97 \quad in < 15 \times 1.41 = 21.15 \quad in$$

$$L_a(d) = 21.15 \quad in$$

Therefore, Case B applies. Conditions of Detail 5 are satisfied, therefore:

r_{ca}= 1 C/D ratio for anchorage of column reinforcement

2. Splices (Appendix D.5.2 of FHWA, 2006)

Clear spacing between spliced bars $= \frac{\pi \times (30 - 2 \times 2)}{10 \times 2} - 1.41 = 2.67 \quad in < 4 \times 1.41 = 5.64 \quad in$

This indicates that $A_{tr}(c)$ is the area of transverse bars crossing the potential splitting crack along a row of spliced bars divided by the number of splices.

$$A_{tr}(c) = \frac{2 \times 0.2}{10/2} = \quad 0.08 \quad in^2$$

$$A_{tr}(d) = \frac{s f_y}{L_s f_{yt}} A_b = \frac{12 \times 36}{30 \times 36} \times 1.56 = 0.62 \quad in^2$$

Transverse reinforcement spacing, s = 12 inch > 6 inch, therefore Case A applies.

$$r_{cs} = \frac{A_{tr}(c)}{A_{tr}(d)}\left(\frac{\left(\frac{6}{s}\right)L_s}{\left(\frac{1860}{\sqrt{f_c^{'}}}\right)d_b}\right)r_{ec} = \frac{0.2}{0.62}\times\left(\frac{\frac{6}{12}\times 30}{\frac{1860}{\sqrt{3000}}\times 1.41}\right)\times 0.31 = 0.1\times 0.31 < 0.75\times 0.31$$

$$r_{cs} = 0.75\times 0.31 = 0.23$$

r_{cs} = 0.23 **C/D ratio for splices in column reinforcement**

3. Confinement (Appendix D.5.4 of FHWA, 2006)

$r_{cc} = \mu r_{ec}$

$$\mu = 2 + 4\left(\frac{k_1 + k_2}{2}\right)k_3$$ Ductility

$$k_1 = \frac{\rho(c)}{\rho(d)\left(0.5 + \frac{1.25P_c}{f_c^{'}A_g}\right)} \le 1$$

$$\rho(c) = \frac{0.2\times\pi\times 27}{\pi\times(30/2)^2\times 12} = 0.002$$ Volumetric ratio of existing transverse reinforcement

$$\rho(d) = 0.45\left(\frac{\pi\times(30/2)^2}{\pi\times(27/2)^2}\right)\times\frac{3}{36} = 0.0088$$ Required vol. ratio of transverse reinforcement

P_c = 194.6 *kips* Axial compressive load on column

f_c' = 3000 *psi* Compressive strength of concrete

$A_g = \pi\times 15^2\ in^2$ Gross area of column

$$\frac{P_c}{f_c^{'}A_g} = \frac{200.8}{3\times\pi\times(30/2)^2} = 0.095$$

$$k_1 = \frac{0.002}{0.0088(0.5 + 1.25\times 0.095)} = 0.368$$

s = 12 *in* Spacing of transverse steel

d_b = 1.41 *in* Diameter of longitudinal reinforcement

b_{min} = 30 *in* Minimum width of the column cross section

$$k_2 = \min(6d_b/s, 0.2b_{min}/s) = \min(6\times 1.41/12, 0.2\times 30/12) = 0.5$$

Because transverse steel is poorly anchored, an iterative solution for μ is required.

Try k_3 = 0.35 (corresponds to μ = 2.7)

$$\mu = 2 + 4\left(\frac{0.368 + 0.5}{2}\right) \times 0.35 = 2.61 \quad ok$$

r_{cc} = μr_{ec} = 2.61(0.31) = 0.81

r_{cc} = 0.81 C/D ratio for transverse confinement reinforcement

4. Footing Rotation (Appendix D.5.5 of FHWA, 2006)

Because C/D ratio of splice is less than 80% of r_{ef}, splice failures will prevent footing rotation. Therefore, footing rotation capacity/demand ratio need not be considered. The same procedure should be repeated for the other combination (r_{ec} = 0.34 and r_{ef} = 0.36).

C/D Ratios for Plastic Hinging at the Tops of the Columns

Bent 2 Column 1 (r_{ec} = 0.378)

1. Anchorage (Appendix D.5.1 of FHWA, 2006)

$L_a(c)$ = 28 in Effective anchorage length, capacity

$$L_a(d) = \frac{k_s d_b}{(1 + 2.5c/d_b + k_{tr})\sqrt{f_c'}} \geq 30d_b$$ Anchorage length, demand

$$k_s = \frac{(f_y - 11000)}{4.8} \; psi$$ Constant for reinforcing steel with yield stress of f_y

$$k_s = \frac{36000 - 11000}{4.8} = 5208.3 \quad psi$$

$$c = \min\left(\frac{\pi \times (30 - 2 \times 2)}{10} - 1.41, 2 + 0.5\right) = 2.5 \quad in$$

$$A_{tr}(c) = \frac{2 \times 0.2}{10/2} = 0.08$$

f_{yt}=36000 *psi* yield stress of transverse reinforcement

$$k_{tr} = \frac{A_{tr}(c) f_{yt}}{600 \times s \times d_b} = \frac{0.08 \times 36000}{600 \times 12 \times 1.41} = 0.284$$

$$L_a(d) = \frac{5208.3 \times 1.41}{(1 + 2.5 \times 2.5/1.41 + 0.284) \times \sqrt{3000}} = 23.45 \quad in < 30d_b = 42.3 \quad in$$

$L_a(d) = 42.3 \quad in$

$L_a(d) > L_a(c)$. Therefore Case A applies:

$$r_{ca} = \frac{L_a(c)}{L_a(d)} r_{ec} = \frac{28}{42.3} \times 0.378 = 0.25$$

r_{ca}= 0.25 C/D ratio for anchorage of column reinforcement

2. Splices - Does not apply

3. Confinement (Appendix D.5.4 of FHWA, 2006)

$r_{cc} = \mu r_{ec}$

$$\mu = 2 + 4\left(\frac{k_1 + k_2}{2}\right) k_3$$ Ductility

$$k_1 = \frac{\rho(c)}{\rho(d)\left(0.5 + \frac{1.25 P_c}{f_c' A_g}\right)} \leq 1$$

$$\rho(c) = \frac{0.2 \times \pi \times 27}{\pi \times (30/2)^2 \times 12} = 0.002$$ Volumetric ratio of existing transverse reinforcement

$$\rho(d) = 0.45\left(\frac{\pi \times (30/2)^2}{\pi \times (27/2)^2}\right) \times \frac{3}{36} = 0.0088$$ Required vol. ratio of transverse reinforcement

$P_c = 194.6$ *kips* Axial compressive load on column

$f_c' = 3000$ *psi* Compressive strength of concrete

$A_g = \pi \times 15^2$ in^2 Gross area of column

$$\frac{P_c}{f_c' A_g} = \frac{194.6}{3 \times \pi \times (30/2)^2} = 0.092$$

$$k_1 = \frac{0.002}{0.0088(0.5 + 1.25 \times 0.092)} = 0.37$$

$s = 12$ *in* Spacing of transverse steel

$d_b = 1.41$ *in* Diameter of longitudinal reinforcement

$b_{min} = 30$ *in* Minimum width of the column cross section

$$k_2 = \min(6d_b / s, 0.2 b_{min} / s) = \min(6 \times 1.41/12, 0.2 \times 30/12) = 0.5$$

Because transverse steel is poorly anchored, an iterative solution for μ is required. Try $k_3 = 0.35$ (corresponds to μ=2.7) where k_3 is the effectiveness of transverse bar anchorage.

$$\mu = 2 + 4\left(\frac{0.37 + 0.5}{2}\right) \times 0.35 = 2.61 \quad ok$$

$r_{cc} = \mu r_{ec} = 2.61(0.378) = 0.99$

r_{cc} = 0.99 C/D ratio for transverse confinement reinforcement

The same procedure should be followed for other columns. C/D ratios for all the columns are presented in Table 1E.2.

Table 1E.2 C/D ratios for columns and footings.

Bent	End	Axial Force	r_{ec}	r_{ef}	r_{ca}	r_{cs}	r_{cc}	r_{fr}
B-2 (C-1)	top	Min	0.378		0.25	N/A	0.986428	N/A
B-2 (C-1)	bottom	Min	0.309	0.3917	1	0.231618	0.805221	N/A
B-2 (C-1)	bottom	Max	0.338	0.3597	1	0.253709	0.88202	N/A
B-2 (C-2)	top	Min	0.403		0.267	N/A	1.043333	N/A
B-2 (C-2)	bottom	Min	0.336	0.3959	1	0.251776	0.869314	N/A
B-2 (C-2)	bottom	Max	0.336	0.3959	1	0.251776	0.869314	N/A
B-2 (C-3)	top	Min	0.39		0.258	N/A	1.01323	N/A
B-2 (C-3)	bottom	Min	0.321	0.3971	1	0.240751	0.833447	N/A
B-2 (C-3)	bottom	Max	0.348	0.3216	1	0.261032	0.90366	N/A
B-3 (C-1)	top	Min	0.363		0.24	N/A	0.943428	N/A
B-3 (C-1)	bottom	Min	0.307	0.3898	1	0.230106	0.797254	N/A
B-3 (C-1)	bottom	Max	0.337	0.3171	1	0.25238	0.87443	N/A
B-3 (C-2)	top	Min	0.379		0.251	N/A	0.981308	N/A
B-3 (C-2)	bottom	Min	0.326	0.3862	1	0.244174	0.843595	N/A
B-3 (C-2)	bottom	Max	0.326	0.3862	1	0.244174	0.843595	N/A
B-3 (C-3)	top	Min	0.364		0.241	N/A	0.949814	N/A
B-3 (C-3)	bottom	Min	0.304	0.3851	1	0.228286	0.793606	N/A
B-3 (C-3)	bottom	Max	0.333	0.3536	1	0.250059	0.869298	N/A
B-4 (C-1)	top	Min	0.439		0.291	N/A	1.145181	N/A
B-4 (C-1)	bottom	Min	0.351	0.4485	1	0.263112	0.914702	N/A
B-4 (C-1)	bottom	Max	0.384	0.4103	1	0.288207	1.001942	N/A
B-4 (C-2)	top	Min	0.484		0.32	N/A	1.256234	N/A
B-4 (C-2)	bottom	Min	0.386	0.471	1	0.289492	1.001615	N/A
B-4 (C-2)	bottom	Max	0.386	0.471	1	0.289492	1.001615	N/A
B-4 (C-3)	top	Min	0.463		0.306	N/A	1.207859	N/A
B-4 (C-3)	bottom	Min	0.372	0.4751	1	0.279127	0.970524	N/A
B-4 (C-3)	bottom	Max	0.408	0.4381	1	0.305749	1.063089	N/A

C/D Ratios for Column Shear

Following Appendix D.5.3 of FHWA (2006)

Bent 2 Column 1- Transverse bending - An anchorage failure at the top of the column and rotation of the footing at the bottom of the column will limit the maximum shear.

$V_u(d) = \frac{1.3\sum M_u}{L_c}$ Maximum column shear force with plastic hinging

$= \frac{793.9 + 1336}{17.4 + (3 + 1/12)} = 103.9 \quad kips$

$V_e(d) = 130.5$ kips Maximum calculated elastic shear force

$v_c = 2\sqrt{f_c^{'}}$ Yield stress in shear

d=30-2-0.5=27.5 *in* Depth to the outer layer of tension steel from the extreme compression fiber

b=30 *in* Width of column section

$V_i(c) = v_c db + \frac{A_{tr} f_{yt} d}{s}$ Initial shear resistance of undamaged column

$= 2 \times \sqrt{3000} \times 27.5 \times 30 + \frac{2 \times 0.2 \times 36000 \times 26.8}{12} = 120.2 \quad kips$

Because column axial stress may fall below $0.10f_c^{'}$ and transverse steel is ineffective:

$V_f(c) = 0$

Therefore, Case A applies; i.e.:

$r_{cv} = \frac{120.2}{130.5} = 0.92 > 0.338$

$r_{cv} = 0.338$

r_{cv} = 0.338 C/D ratio for column shear

Table 1E.3 C/D ratios for column shear

Bent	End	r_{ec}	$V_u(d)$ Top & Bottom	$V_u(d)$ Top & Footing	$V_c(d)$	$V_i(c)$	r_{cv}
B-2 (C-1)	top	0.378	175.1	180.3	130.5	120.2	0.338
B-2 (C-1)	bottom	0.309					
B-2 (C-1)	bottom	0.338					
B-2 (C-2)	top	0.403	182.33	187.9	137.5	120.2	0.336
B-2 (C-2)	bottom	0.336					
B-2 (C-2)	bottom	0.336					
B-2 (C-3)	top	0.39	176.54	181.8	133.4	120.2	0.348
B-2 (C-3)	bottom	0.321					
B-2 (C-3)	bottom	0.348					
B-3 (C-1)	top	0.363	185.1	190.7	172.4	120.2	0.337
B-3 (C-1)	bottom	0.307					
B-3 (C-1)	bottom	0.337					
B-3 (C-2)	top	0.379	188.33	194.2	173.3	120.2	0.326
B-3 (C-2)	bottom	0.326					
B-3 (C-2)	bottom	0.326					
B-3 (C-3)	top	0.364	179.12	184.5	161.7	120.2	0.333
B-3 (C-3)	bottom	0.304					
B-3 (C-3)	bottom	0.333					
B-4 (C-1)	top	0.439	152.97	157.3	136.9	120.2	0.384
B-4 (C-1)	bottom	0.351					
B-4 (C-1)	bottom	0.384					
B-4 (C-2)	top	0.484	152.2	156.6	133.3	120.2	0.386
B-4 (C-2)	bottom	0.386					
B-4 (C-2)	bottom	0.386					
B-4 (C-3)	top	0.463	143.84	147.7	126.1	120.2	0.408
B-4 (C-3)	bottom	0.372					
B-4 (C-3)	bottom	0.408					

Capacity/Demand Ratio for Abutments

Calculations based on Appendix D.6 of FHWA (2006). Abutment C/D ratios are based on the displacements from the analysis.

Transverse Displacement

D(c) = 0.2 *ft* = 2.4 *in* Based on Sec. 20-4 of Caltrans, 1995

Abutment 1:

D(d) = 0.86 *in* Transverse displacement demand

r_{ad} = (0.2×12)/0.86=2.79

Abutment 5:

D(d) = 0.85 *in*

r_{ad} = (0.2×12)/0.85=2.84

Longitudinal Displacement

D(c) = 0.2 *ft* = 2.4 *in* Based on Sec. 20-4 of Caltrans, 1995

Abutment 1:

D(d) = 0.93 *in* Longitudinal displacement demand

r_{ad} = (0.2×12)/0.93=2.58

Abutment 5:

D(d) = 0.95 *in*

r_{ad} =(0.2×12)/0.95=2.54

Table 1E.4 Capacity/demand ratios for abutments

	Longitudinal	Transverse
Abutment 1	2.58	2.79
Abutment 5	2.54	2.84

Table 1E.5 summarizes the C/D ratios for the bridge.

Table 1E.5 Capacity/demand ratios for the as-built bridge.

Bent	End	r_{ca}	r_{cs}	r_{cc}	r_{fr}	r_{cv}
B-2 (C-1)	top	0.250278	N/A	0.986428	N/A	0.338279
B-2 (C-1)	bottom	1	0.231618	0.805221	N/A	
B-2 (C-1)	bottom	1	0.253709	0.88202	N/A	
B-2 (C-2)	top	0.266559	N/A	1.043333	N/A	0.335702
B-2 (C-2)	bottom	1	0.251776	0.869314	N/A	
B-2 (C-2)	bottom	1	0.251776	0.869314	N/A	
B-2 (C-3)	top	0.258177	N/A	1.01323	N/A	0.348043
B-2 (C-3)	bottom	1	0.240751	0.833447	N/A	
B-2 (C-3)	bottom	1	0.261032	0.90366	N/A	
B-3 (C-1)	top	0.24019	N/A	0.943428	N/A	0.336507
B-3 (C-1)	bottom	1	0.230106	0.797254	N/A	
B-3 (C-1)	bottom	1	0.25238	0.87443	N/A	
B-3 (C-2)	top	0.250554	N/A	0.981308	N/A	0.325566
B-3 (C-2)	bottom	1	0.244174	0.843595	N/A	
B-3 (C-2)	bottom	1	0.244174	0.843595	N/A	
B-3 (C-3)	top	0.240998	N/A	0.949814	N/A	0.333413
B-3 (C-3)	bottom	1	0.228286	0.793606	N/A	
B-3 (C-3)	bottom	1	0.250059	0.869298	N/A	
B-4 (C-1)	top	0.29056	N/A	1.145181	N/A	0.384276
B-4 (C-1)	bottom	1	0.263112	0.914702	N/A	
B-4 (C-1)	bottom	1	0.288207	1.001942	N/A	
B-4 (C-2)	top	0.32028	N/A	1.256234	N/A	0.38599
B-4 (C-2)	bottom	1	0.289492	1.001615	N/A	
B-4 (C-2)	bottom	1	0.289492	1.001615	N/A	
B-4 (C-3)	top	0.306416	N/A	1.207859	N/A	0.407665
B-4 (C-3)	bottom	1	0.279127	0.970524	N/A	
B-4 (C-3)	bottom	1	0.305749	1.063089	N/A	

Appendix 1F. Deformation Capacity of Columns

Before evaluating the different failure criteria, we calculate two parameters commonly used in the limits.

Yield Curvature

$f_y = 36 \quad kips/in^2$ Steel yield force

$E_s = 29000 \quad kips/in$ Steel elastic modulus

Concrete cover $= 2 \quad in$

$d_{stirrup} = 0.5 \quad in$ Transverse bar diameter

$D' = 30 - 2 \times 2 - 2 \times 0.5 = 25 \quad in$ Distance between the outer layers of longitudinal steel

$$\phi_y = \frac{2\varepsilon_y}{D'} = \frac{2f_y}{E_s D'} = \frac{2 \times 36}{29000 \times 25} = 9.93103\text{E-}05 \quad \text{rad/in}$$

Depth to Neutral Axis

$$\frac{c}{D} = \frac{1}{\beta}\left[\frac{\frac{P_e}{f_c^{'}A_g} + 0.5\rho_t \frac{f_y}{f_c^{'}}\left(\frac{1-2c/D}{1-2d'/D}\right)}{1.32\,\alpha}\right]^{0.725}$$

The above parameters are defined in Sec. 7.8.3 of the Retrofit Manual (FHWA, 2006).

D=30 *in* Column diameter

P_e= Axial load on the section

$f_{ce}^{'} = 1.3 f_c' = 1.3 \times 3 = 3.9 \quad kips/in^2$ Ultimate expected compressive strength of concrete

$f_{ye}' = 1.2 f_y' = 43.2 \quad kips/in^2$

$A_g = \pi \times D^2/4 = 706.86 \; in^2$ Gross cross section of the column

d′= 2+0.5+1.41/2=3.205 *in* Distance from the extreme compression fiber to the center of the nearest compression reinforcing bars (= Concrete cover + Transverse bar diameter + 0.5×Longitudinal bar diameter)

$\rho_t = \frac{A_{st}}{A_g} = \frac{10 \times 1.56}{\pi \times 15^2} = 0.0221$ Volumetric ratio of the longitudinal reinforcement

Two parameters, α and β, are related to concrete stress block and defined in Sec. 7.7.1.2 of the Retrofit Manual (FHWA, 2006).

$\alpha = 0.85 + 0.12(K-1)^{0.4}$ Ratio of average concrete stress in compression zone to confined concrete strength

$\beta = 0.85 + 0.13(K-1)^{0.6}$ Stress block factor

$K = 2.254\sqrt{1 + 7.94\frac{f'_\ell}{f'_c}} - 2\frac{f'_\ell}{f'_c} - 1.254$ Strength enhancement factor

$f'_l = \frac{1}{2}k_e \rho_s f_{yh}$ Lateral stress supplied by the transverse reinforcement at yield

$\rho_s = \frac{4\,A_{bh}}{s\,D''}$ Volumetric ratio of spirals or circular hoops to the core concrete

s=12 *in* Spacing of spirals or hoops

$D'' = 30 - 2\times 2 - 0.5 = 25.5 \quad in$ Diameter of transverse hoop or spiral

$A_{bh} = A_{hoop} = 0.2 \quad in^2$ Area of one spiral or hoop bar

$$\rho_s = \frac{4\times 0.2}{12\times 25.5} = 0.002614$$

$k_e = \frac{(1 - \chi\ s/D'')}{(1 - \rho_{cc})}$ Confinement effectiveness coefficient

Columns have hoops as transverse reinforcement. Therefore

$$\chi = 1$$

$$\rho_{cc} = \rho_s = 0.002614$$

$$k_e = \frac{1 - 1\times 12/25.5}{1 - 0.002614} = 0.530799$$

$$f'_l = \frac{1}{2}\times 0.530799\times 0.002614\times 36 = 0.02498 \quad \text{kips/in}^2$$

$$K = 2.254\times\sqrt{1 + 7.94\times\frac{0.02498}{3\times 1.3}} - 2\times\frac{0.02498}{3\times 1.3} - 1.254 = 1.04379$$

$$\alpha = 0.85 + 0.12(1.04379 - 1)^{0.4} = 0.884$$

$$\beta = 0.85 + 0.13(1.04379 - 1)^{0.6} = 0.870$$

The procedure to find the depth of the neutral axis is iterative. Neutral axis depths for all the columns are presented in Table 1F.1.

Table 1F.1 Neutral axis depth in columns

Column No.	Axial Dead Load (kips)	Depth to Neutral Axis (in)
1	201.4	7.74
2	280.7	8.49
3	246.0	8.16
4	237.6	8.1
5	272.8	8.43
6	200.2	7.71
7	198.7	7.71
8	257.2	8.28
9	199.5	7.71

Failure Modes

1. Compression Failure of Confined Concrete

$$\phi_p = \frac{\varepsilon_{cu}}{(c - d'')} - \phi_y$$ Plastic curvature

$$\varepsilon_{cu} = 0.005 + \frac{1.4\,\rho_s\, f_{yh}\, \varepsilon_{su}}{f'_{cc}}$$ Ultimate compression strain of the confined core concrete

$$f'_{cc} = K \times f'_{ce}$$
$$= 1.04379 \times 1.3 \times 3 = 4.07 \quad kips/in^2$$ Confined concrete strength

$$\rho_s = \frac{4 \times 0.2}{12 \times 25.5} = 0.002614$$ Volumetric ratio of transverse steel

$$f_{yh} = 36 \quad kips/in^2$$ Yield stress of the transverse steel

$$\varepsilon_{su} = 0.16$$

$$\varepsilon_{cu} = 0.005 + \frac{1.4 \times 0.002614 \times 36 \times 0.16}{4.07} = 0.0101789$$

$d'' = 2 + 0.5/2 = 2.25 \quad in$ Distance from the extreme compression fiber of the cover concrete to the centerline of the perimeter hoop

c=7.74 *in* Depth to neutral axis

$$\phi_p = \frac{0.0101789}{7.74 - 2.25} - 0.0000993 = 0.0017548$$

2. Buckling of Longitudinal Bars

$$\phi_p = \frac{\varepsilon_b}{c - d'} - \phi_y$$

$d' = 2 + 0.5 + 1.41/2 = 3.205 \quad in$ Distance from the extreme compression fiber to the center of the nearest compression reinforcing bars

If $6d_b < s < 30d_b$, the buckling strain may be taken as twice the yield strain of the longitudinal steel. As shown, the inequality holds.

$$6d_b = 8.46\ in\ \le s = 12\ in\ \le\ 30d_b = 42.3\ in$$

$$\varepsilon_b = \frac{2f_y}{E_s} = \frac{2 \times 36}{29000} = 0.0024828$$

$$\phi_p = \frac{0.0024828}{7.74 - 3.205} - 0.0000993 = 0.0004482$$

3. Fracture of the Longitudinal Reinforcement

$$\phi_p = \frac{\varepsilon_{s\ \max}}{(d - c)} - \phi_y$$

$\varepsilon_{s\ \max} = 0.1$ Tensile strain

$d = 30 - 2 - 0.5 = 27.5 \quad in$ Depth to the outer layer of tension steel from the extreme compression fiber

$$\phi_p = \frac{0.1}{(27.5 - 7.74)} - 0.0000993 = 0.0049614$$

4. Low Cycle Fatigue of Longitudinal Reinforcement

This failure mode is evaluated in both the longitudinal and transverse direction.

$$\phi_p = \frac{2\varepsilon_{ap}}{(d - d')} = \frac{2\varepsilon_{ap}}{D'}$$

$D' = 30 - 2 \times 2 - 0.5 \times 2 = 25 \quad in$ Pitch circle diameter of the longitudinal reinforcement

$T_{n\ long} = 1.3 \quad \text{sec}$ Natural period of vibration in longitudinal direction

$N_{f\ long} = 3.5 \times \left(T_{n\ long}\right)^{-1/3} = 3.21$ Effective number of equal-amplitude cycles of loading that lead to fracture

$\varepsilon_{ap\ long} = 0.08\left(2N_{f\ long}\right)^{-0.5} = 0.0316$ Plastic strain amplitude

$$\phi_{p\ long} = \frac{2 \times 0.0316}{25} = 0.002528$$

$T_{n\ trans} = 0.8$ sec Natural period in the transverse direction

$$N_{f\ trans} = 3.5 \times \left(T_{n\ trans}\right)^{-1/3} = 3.77$$

$$\varepsilon_{ap\ trans} = 0.08\left(2N_{f\ trans}\right)^{-0.5} = 0.0291$$

$$\phi_{p\ trans} = \frac{2 \times 0.0291}{25} = 0.002328$$

5. Failure in the Lap-splice Zone

$l_s = 0.032 \dfrac{f_{ye}}{\sqrt{f'_{ce}}} d_b = 0.032 \times \dfrac{1.2 \times 36000}{\sqrt{1.3 \times 3000}} \times 1.41 = 31.21 \quad in$ Required lap-splice length

$l_{lap} = 30\ in\ <\ l_s \quad \Rightarrow$ The lap-splice is short $\quad \Rightarrow L_p = L_{lap} = 30\ \ in$

$M_s < M_e \quad \Rightarrow \quad \mu_{lap\ \phi} = 0$

$$\phi_p = \left(\mu_{lap\ \phi} + 7\right)\phi_y = 7 \times 0.0000993 = 0.0006952$$

6. Shear Failure

$$A_g = \pi \times D^2 / 4 = 706.86 \quad in^2$$

$$\frac{P_e}{f'_{ce} A_g} = \frac{201.4}{1.3 \times 3 \times 706.86} = 0.0731$$

$$\rho_t = \frac{A_{st}}{A_g} = \frac{10 \times 1.56}{\pi \times 15^2} = 0.0221$$

$$\frac{P_t}{f'_{ce} A_g} = -\rho_t \frac{f_{ye}}{f'_{ce}} = -0.0221 \times \frac{1.2 \times 36}{1.3 \times 3} = -0.2445$$

$f'_{ce} = 1.3 \times 3 = 3.9 \quad ksi < 4.3 \quad ksi \quad \Rightarrow \quad \beta_1 = 0.85$

$$\frac{P_b}{f'_{ce} A_g} = 0.425\beta_1 = 0.36125$$

$$D' = 0.8D = 0.8 \times 30 = 24 \quad in$$

$K_{shape} = 0.32$

$\kappa_0 = 0.6$

$$\frac{M_b}{f'_{ce}A_g D} = \left(K_{shape}\rho_t \frac{f_{ye}}{f'_{ce}}\frac{D'}{D} + \frac{P_b}{f'_{ce}A_g}\frac{1-\kappa_0}{2} \right)$$

$$= 0.32 \times 0.0221 \times \frac{1.2 \times 36}{1.3 \times 3} \times 0.8 + 0.0731 \times \frac{1-0.6}{2} = 0.13483$$

$$\frac{M_e}{f'_c A_g D} = \left(\frac{M_b}{f'_c\ A_g D} \right) \left[1 - \left(\frac{\frac{P_e}{f'_c\ A_g} - \frac{P_b}{f'_c\ A_g}}{\frac{P_t}{f'_c\ A_g} - \frac{P_b}{f'_c\ A_g}} \right)^2 \right]$$

$$= 0.13483 \times \left[1 - \left(\frac{0.0731 - 0.36125}{-0.2445 - 0.36125} \right)^2 \right] = 0.1043093$$

$M_e = 0.1043093 \times 1.3 \times 3 \times 706.86 \times 30/12 = 718.89$ kips.ft

$$V_{m\ long} = \frac{M_e}{L} = \frac{622.01}{17.4} = 35.75 \quad kips$$

$$V_{m\ trans} = \frac{M_e}{L/2} = \frac{622.01}{17.4/2} = 71.5 \quad kips$$

$V_{m\ long} < V_f = 98.9 \quad kips \quad \Rightarrow$ The rotational capacity is not limited by shear.

$V_{m\ trans} < V_f = 98.9 \quad kips \quad \Rightarrow$ The rotational capacity is not limited by shear.

7. Joint or Connection Failure

$h_b = 3.5 \quad ft$ Bent thickness

$V_{jh} = \frac{M_e}{h_b} = \frac{622.01}{3.5} = 177.72 \quad kips$ Horizontal shear in the joint

$A_{jh} = \pi \times D^2/4 = 706.86 \quad in^2$ Column area

$f_v = \frac{-P}{A_{jh}} = \frac{-201.4}{706.86} = -0.285 \quad kips/in^2$ Average axial stress on the joint

$f_h = 0 \quad kips/in^2$ Average horizontal stress on the joint

$$p_{t\,i} = 0.42\sqrt{f'_{ce}} \quad MPa$$
$$= 0.42 \times \sqrt{\frac{1.3 \times 3}{0.145038}} \times 0.145038 = 0.31588 \quad kips$$

Initial major principle tension stress

$$p_{t\,f} = 0.29\sqrt{f'_{ce}} \quad MPa$$
$$= 0.29 \times \sqrt{\frac{1.3 \times 3}{0.145038}} \times 0.145038 = 0.21811 \quad kips$$

Final major principle tension stress

$$v_{j\,i} = \sqrt{p_{t\,i}^{\;2} - p_{t\,i}\left(f_v + f_h\right) + 2 f_v f_h} = 0.436 \quad kips/in^2$$

Initial average joint shear stress

$$v_{j\,f} = \sqrt{p_{t\,f}^{\;2} - p_{t\,f}\left(f_v + f_h\right) + 2 f_v f_h} = 0.331 \quad kips/in^2$$

Final average joint shear stress

$$V_{j\,i} = v_{j\,i} A_{jh} = 307.94 \quad kips$$

Initial shear strength

$$V_{j\,f} = v_{j\,f} A_{jh} = 234.14 \quad kips$$

Final shear strength

$V_{j\,h} < V_{j\,f} \quad \Rightarrow$ The rotational capacity is not limited by joint shear.

Failure curvature for all the columns can be found from the same procedure described above. These values are presented in Table 1F.2.

Plastic hinge length

Based on the Retrofit Manual (Sec. 7.8.1.1 of FHWA, 2006), the plastic hinge length is

$$L_p = 0.08L + 4400\varepsilon_y d_b$$

where L is the shear span and d_b is the diameter of the longitudinal tension reinforcement.

$$L_{long} = 17.4 \quad ft$$

$$L_{trans} = 17.4/2 = 8.7 \quad ft$$

$$L_{p\;\;long} = 0.08 \times 17.4 \times 12 + 4400 \times \frac{36}{29000} \times 1.41 = 24.41 \quad in$$

$$L_{p\;\;trans} = 0.08 \times \frac{17.4 \times 12}{2} + 4400 \times \frac{36}{29000} \times 1.41 = 16.05 \quad in$$

Because the lap-splice length is less than the required length l_s, we verify that the plastic hinge lengths found above are less than or equal to the lap-splice length. The plastic rotation capacity is simply the plastic curvature capacity times the plastic hinge length.

$$\theta_{p\;\;long} = \phi_{p\;\;long} L_{p\;\;long} = 0.000448 \times 24.41 = 0.01094 \quad rad$$

$$\theta_{p\ \ trans} = \phi_{p\ \ trans} L_{p\ \ trans} = 0.000448 \times 16.05 = 0.007194 \quad rad$$

The yield rotation is given as

$$\theta_{y\ \ long} = \frac{1}{3}\phi_y L = \frac{1}{3} \times 9.93 \times 10^{-5} \times 17.4 \times 12 = 0.006912 \quad rad$$

$$\theta_{y\ \ trans} = \frac{1}{3}\phi_y L = \frac{1}{3} \times 9.93 \times 10^{-5} \times \frac{17.4}{2} \times 12 = 0.003456 \quad rad$$

The total rotational capacity of a column is the sum of the plastic rotational capacity and the yield rotation.

$$\theta_{u\ \ long} = \theta_{p\ \ long} + \theta_{y\ \ long} = 0.01094 + 0.006912 = 0.017849 \quad rad$$

$$\theta_{u\ \ trans} = \theta_{p\ \ trans} + \theta_{y\ \ trans} = 0.007194 + 0.003456 = 0.01065 \quad rad$$

These values for all of the columns are presented in Table 1F.3.

Table 1F.2 Plastic curvature capacity of columns.

Column No.	Compression Failure of Confined Concrete	Buckling of Longitudinal Bars	Fracture of the Longitudinal Reinforcement	Low Cycle Fatigue of Longitudinal Reinforcement (long)	Low Cycle Fatigue of Longitudinal Reinforcement (trans)	Failure in the Lap-splice Zone	Shear Failure	Joint or Connection Failure	Min Curvature (long)	Min Curvature (trans)
1	0.001755	0.000448	0.004961	0.002527	0.002331	0.000695	N/A	N/A	0.000448	0.000448
2	0.001532	0.000370	0.005161	0.002527	0.002331	0.000695	N/A	N/A	0.000370	0.000370
3	0.001623	0.000402	0.005071	0.002527	0.002331	0.000695	N/A	N/A	0.000402	0.000402
4	0.001641	0.000408	0.005055	0.002527	0.002331	0.000695	N/A	N/A	0.000408	0.000408
5	0.001548	0.000376	0.005145	0.002527	0.002331	0.000695	N/A	N/A	0.000376	0.000376
6	0.001765	0.000452	0.004954	0.002527	0.002331	0.000695	N/A	N/A	0.000452	0.000452
7	0.001765	0.000452	0.004954	0.002527	0.002331	0.000695	N/A	N/A	0.000452	0.000452
8	0.001589	0.000390	0.005104	0.002527	0.002331	0.000695	N/A	N/A	0.000390	0.000390
9	0.001765	0.000452	0.004954	0.002527	0.002331	0.000695	N/A	N/A	0.000452	0.000452

Table 1F.3 Total rotational capacity of columns.

Column No.	$\theta_{p\ \ long}$	$\theta_{p\ \ trans}$	$\theta_{u\ \ long}$	$\theta_{u\ \ trans}$
1	0.01094	0.00719	0.01785	0.01065
2	0.00904	0.00595	0.01595	0.00940
3	0.00980	0.00645	0.01672	0.00991
4	0.00995	0.00655	0.01687	0.01000
5	0.00917	0.00603	0.01609	0.00949
6	0.01103	0.00725	0.01794	0.01071
7	0.01103	0.00725	0.01794	0.01071
8	0.00952	0.00626	0.01643	0.00972
9	0.01103	0.00725	0.01794	0.01071

Ultimate Allowable Bent Drift

As explained before, the stopping criteria for pushover analysis is the column allowable drift Δ_u. This drift consists of two components: elastic deformation until yielding Δ_y and plastic displacement Δ_p.

$\phi_y = 9.931 \times 10^{-5}$ *Yield Curvature*

L=17.4 *ft* *Column length*

$$\Delta_y = \frac{1}{3}\phi_y L^2 = \frac{1}{3} \times 9.931 \times 10^{-5} \times (17.4 \times 12)^2$$

The displacement due to plastic hinge deformation depends on the plastic curvature. Each bent has three columns with different plastic curvature. Because a mechanism does not occur until all columns fail in both the longitudinal and transverse directions, the maximum plastic curvature of all the columns in a bent in each direction is used to find the corresponding displacement.

L_p=24.41 *ft* Plastic hinge length in longitudinal direction

$\phi_p = 4.48 \times 10^{-4}$ Maximum longitudinal plastic curvature in bent 2

$$\Delta_p = \phi_p L_p (L - 0.5 L_p) = 4.48 \times 10^{-4} \times 24.41 \times (17.4 \times 12 - 0.5 \times 24.41) = 2.15 \quad in$$

$$\Delta_u = \Delta_y + \Delta_p = 3.59 \quad in$$

The ultimate allowable drifts for each bent in each direction are given in Table 1F.4.

Table 1F.4 Allowable drift in each bent

	Δ_u (*longitudinal*) (in)	Δ_u (*transverse*) (in)
Bent 2	2.11	3.59
Bent 3	2.12	3.61
Bent 4	2.12	3.61

Since the stopping criterion in LARSA must be specified in terms of a nodal displacement or rotation rather than column drift, we first push the bridge past its stopping criteria and then back calculate the column drift at each step. The column drift is evaluated from:

$$\Delta_u = \Delta_{total} - \Delta_b - \theta_b h$$

where Δ_{total} (total displacement), Δ_b (footing displacement) and θ_b (footing rotation) are reported by LARSA. The bent reaches its capacity when Δ_u based on LARSA analysis exceeds the limiting values in Table 1F.4. Following the above procedure, the results presented in Table 1F.5 were obtained.

Table 1F.5 Allowable drift in each bent

	Δ_{total} (*longitudinal*) (in)	Δ_{total} (*transverse*) (in)
Bent 2	8.72	11.33
Bent 3	8.56	10.52
Bent 4	8.56	10.38

Appendix 1G. Excel Worksheet for Iterative Demand Analysis

For convenience, an Excel Worksheet is provided to systematically calculate modifications to the foundation spring stiffnesses. Inputs to the worksheet consist of two parts: general information about the bridge (e.g. number of nodes and component capacities), and response quantities calculated at each iteration (e.g. support reaction and nodes deformation). Use of the worksheet is demonstrated using data for the Clearfield Overpass bridge.

In the general information section as shown in Figure 1G.1, the following information must be entered by the user.

B1: Current number of iterations. When starting the demand analysis this value is 1, and automatically increases by the number of iterations done in the worksheet.

B2: Total number of nodes in the bridge

B4: Number of columns of the bridge

B5: Number of nodes in the first abutment

B6: Number of nodes in the second abutment

B7: Number of footings in the bridge

D5 to J5: IDs of the nodes in the first abutment. The cell group can be extended or shortened based on the number of nodes in the abutment. For example, if the first abutment has 9 nodes (B5=9), then user fills out D5 to L5 with nodes IDs.

D6 to J6: IDs of the nodes in the second abutment.

D7 to L7: IDs of the nodes of footings. Adjust cell group size as needed.

D8 to L8: Corresponding footing capacity in the local longitudinal direction.

D9 to L9: Corresponding footing capacity in the local transverse direction.

D10 to L10: Corresponding footing capacity in vertical direction.

D11 to L11: Moment capacity of footing around its local longitudinal axis

D12 to L12: Moment capacity of footing around its local transverse axis

B13 & B14: Capacities of abutments in longitudinal direction

D13 & D14: Capacities of abutments in transverse direction

	A	B	C	D	E	F	G	H	I	J	K	L
1	Iteration No	1										
2	Total Nodes No.	258										
3												
4	no of cols	9										
5	Abutment 1 Nodes no	7	Abutment 1 Nodes	1	5	10	15	20	25	30		
6	Abutment 2 Nodes no	7	Abutment 2 Nodes	122	126	130	134	138	142	145		
7	Footings Nodes no	9	Footings Nodes	224	227	232	237	240	245	250	253	258
8			Footing Capacity Long.	186.5	226.5	186.5	186.5	226.5	186.5	186.5	226.5	186.5
9			Footing Capacity Trans.	186.5	226.5	186.5	186.5	226.5	186.5	186.5	226.5	186.5
10			Footing Capacity Vert. (Comp.)	720	900	720	720	900	720	720	900	720
11			Footing Capacity M X	1048	1080	956	972	1080	1044	1048	1080	1048
12			Footing Capacity M Y	1048	1080	956	972	1080	1044	1048	1080	1048
13	Abutment 1 Capacity Long.	1438	Abutment 1 Capacity Trans.	537								
14	Abutment 2 Capacity Long.	1438	Abutment 2 Capacity Trans.	537								
15												

Figure 1G.1. General bridge information for spreadsheet utility

Capacities of foundations and abutments mentioned above are based on the properties derived in Appendices 1B and 1C.

Longitudinal Capacity of Foundations

Two parts contribute to the capacity of the foundation: pile cap and piles.

$F_{pile\ cap}$=19.03 kips, (F_c in footing stiffness, Appendix 1B)

$F_{piles\ 4}$=4×40=160 kips, for foundations with 4 piles

$F_{piles\ 5}$=5×40=200 kips, for foundations with 5 piles

$F_{foundation\ 4}$=19.03+160=179.03 kips, longitudinal capacity of foundations with 4 piles

$F_{foundation\ 5}$=19.03+200=219.03 kips, longitudinal capacity of foundations with 5 piles

Transverse Capacity of Foundations

Because foundations are symmetric, they have the same capacity in transverse direction as in longitudinal direction.

Vertical Capacity of Foundations

Only the capacity of piles is considered here.

$F_{vertical\ 4}$=4×180=720 kips, vertical capacity of foundations with 4 piles

$F_{vertical\ 5}$=5×180=900 kips, vertical capacity of foundations with 5 piles

Moment Capacity of Foundations around Longitudinal and Transverse Axes

Explained in detail in Appendix 1C: *Pile Footing Moment Capacities*.

Longitudinal and Transverse Capacities of Abutments

(Explained in Appendix 1B: *Abutment Stiffness*)

$F_{abutment\ long}$ =1438 kips

$F_{abutment\ trans}$ =$F_{wing\ walls}$+F_{piles}=257+280=537 kips

Support reactions are copied from LARSA into the worksheet named "Support Reaction". These data are available in *Results-Spreadsheets-Joint-Reactions*. Deformation responses are copied from LARSA into the worksheet named "Nodes Deformation". These data are available in *Results-Spreadsheets-Joint-Displacements.* It should be noted that absolute maximum values for each quantity are needed for the worksheet. These are obtained by checking the option "Envelope Selected Result Cases" in the top left side of the window in LARSA and then choosing the desired results (e.g. "Translation X"), with "Max Only" and "ABS" options. The same procedure explained above should be followed for each response quantity.

To use the worksheet as a guide for iterative analysis, follow this procedure. In the first step, rename the bridge model "DC2.lar" and perform an "Eigenvalue Response Spectra Analysis". Copy the support reactions and nodes deformations into the corresponding worksheets as explained above. Select "Alt+F8" to execute the macro and complete the first iteration. Two new LARSA files will be created "DC3.lar" and "DC4.lar" where "DC3.lar" is a backup file for "DC2.lar". "DC2.lar" and "DC3.lar" are deleted and "DC4.lar" is renamed to "DC2.lar". Worksheet automatically calculates new component stiffnesses and copy the changes into the LARSA input file. Repeat analysis for the new "DC2.lar" to obtain a modified bridge response, and copy support reactions and nodes responses from LARSA into the corresponding worksheets.

19																			
20	Iteration	1																	
21			Force X	Force Y	K X	K Y													
22	Abutmer	1	1535.71	388.302															
23	Abutmer	2	1573.77	379.74															
24																			
25			Force X	Force Y	Force Z	M X	M Y	M Z	1.3 MX Ca	1.3 MY Ca	K X	K Y	K Teta X	K Teta Y	K Z	K Teta Z	K X Teta Y	K Y Teta X	
26	Footing	1	73.5	132.7	47.5	1303.7	988.7	293.7	1362.4	1362.4	2528.2	2528.2	2035249.3	2171671.3	235081.0	606402.7	-6800.0	6800.0	
27	Footing	2	86.1	163.5	9.5	1295.3	956.5	60.3	1404.0	1404.0	3128.2	3128.2	2107780.8	2244202.7	251130.5	611202.7	-8500.0	8500.0	
28	Footing	3	74.7	132.6	72.0	1301.8	986.6	298.4	1242.8	1242.8	2528.2	2528.2	1240995.4	2171671.3	235081.0	606402.7	-6800.0	5151.5	
29	Footing	4	95.1	167.0	80.6	1628.3	1245.6	263.0	1263.6	1263.6	2528.2	2528.2	1006137.1	2171671.3	235081.0	606402.7	-6800.0	4499.1	
30	Footing	5	106.3	205.7	14.0	1624.5	1204.7	84.4	1404.0	1404.0	3128.2	3128.2	1117563.5	2244202.7	251130.5	611202.7	-8500.0	5890.4	
31	Footing	6	91.5	166.9	60.5	1632.7	1247.7	311.7	1357.2	1357.2	2528.2	2528.2	1083087.0	2171671.3	235081.0	606402.7	-6800.0	4723.7	
32	Footing	7	70.6	137.0	45.2	1282.1	1043.4	212.7	1362.4	1362.4	2528.2	2528.2	2035249.3	2171671.3	235081.0	606402.7	-6800.0	6800.0	
33	Footing	8	78.6	168.7	2.2	1277.8	1012.4	127.1	1404.0	1404.0	3128.2	3128.2	2107780.8	2244202.7	251130.5	611202.7	-8500.0	8500.0	
34	Footing	9	63.5	136.9	45.2	1288.1	1041.2	332.5	1362.4	1362.4	2528.2	2528.2	2035249.3	2171671.3	235081.0	606402.7	-6800.0	6800.0	
35																			
36																			

Figure 1G.2. Results in the first iteration for compression model.

56																			
57																			
58	Iteration	3																	
59			Force X	Force Y	K X	K Y													
60	Abutmer	1	1536.72	389.739															
61	Abutmer	2	1574.8	381.285															
62																			
63			Force X	Force Y	Force Z	M X	M Y	M Z	1.3 MX Ca	1.3 MY Ca	K X	K Y	K Teta X	K Teta Y	K Z	K Teta Z	K X Teta Y	K Y Teta X	
64	Footing	1	73.7133	132.807	47.7564	1309.81	998.245	2.93E+02	1.36E+03	1.36E+03	2.53E+03	2.53E+03	2.04E+06	2.17E+06	2.35E+05	6.06E+05	-6.80E+03	6.80E+03	
65	Footing	2	86.3201	163.567	8.69516	1297.63	955.894	6.04E+01	1.40E+03	1.40E+03	3.13E+03	3.13E+03	2.11E+06	2.24E+06	2.51E+05	6.11E+05	-8.50E+03	8.50E+03	
66	Footing	3	74.8024	131.453	73.4152	1.28E+03	9.18E+02	300.978	1242.8	1242.8	2528.24	2528.24	950425.5	2171671	235081	606403	-6800	4485.14	
67	Footing	4	96.0353	163.107	83.7658	1.58E+03	1.10E+03	262.497	1.26E+03	1.26E+03	2.53E+03	2.53E+03	6.69E+05	2.17E+06	2.35E+05	6.06E+05	-6.80E+03	3.63E+03	
68	Footing	5	107.271	201.601	13.9487	1.53E+03	1.10E+03	86.688	1.40E+03	1.40E+03	3.13E+03	3.13E+03	8.05E+05	2.24E+06	2.51E+05	6.11E+05	-8.50E+03	4.96E+03	
69	Footing	6	92.2897	163.172	63.4698	1.60E+03	1.13E+03	314.607	1.36E+03	1.36E+03	2.53E+03	2.53E+03	7.55E+05	2.17E+06	2.35E+05	6.06E+05	-6.80E+03	3.91E+03	
70	Footing	7	71.0024	138.076	45.777	1.29E+03	1.05E+03	2.12E+02	1.36E+03	1.36E+03	2.53E+03	2.53E+03	2.04E+06	2.17E+06	2.35E+05	6.06E+05	-6.80E+03	6.80E+03	
71	Footing	8	79.0232	170.077	2.17357	1.29E+03	1.02E+03	130.315	1404	1404	3128.24	3128.24	2107781	2244203	251131	611203	-8500	8500	
72	Footing	9	63.756	137.996	45.6207	1296.13	105							E+06	2.35E+05	6.06E+05	-6.80E+03	6.80E+03	
73																			
74																			
75																			
76																			
77	Iteration	4																	
78			Force X	Force Y	K X	K Y													
79	Abutmer	1	1536.88	389.962															
80	Abutmer	2	1574.97	381.574															
81																			
82			Force X	Force Y	Force Z	M X	M Y	M Z	1.3 MX Ca	1.3 MY Ca	K X	K Y	K Teta X	K Teta Y	K Z	K Teta Z	K X Teta Y	K Y Teta X	
83	Footing	1	73.749	132.822	47.7939	1.31E+03	999.828	2.93E+02	1.36E+03	1.36E+03	2.53E+03	2.53E+03	2.04E+06	2.17E+06	2.35E+05	6.06E+05	-6.80E+03	6.80E+03	
84	Footing	2	86.3496	163.583	8.56479	1.30E+03	955.86	6.05E+01	1.40E+03	1.40E+03	3.13E+03	3.13E+03	2.11E+06	2.24E+06	2.51E+05	6.11E+05	-8.50E+03	8.50E+03	
85	Footing	3	74.8141	131.281	73.6494	1273.31	907.001	3.01E+02	1.24E+03	1.24E+03	2.53E+03	2.53E+03	9.16E+05	2.17E+06	2.35E+05	6.06E+05	-6.80E+03	4.40E+03	
86	Footing	4	96.2021	162.381	84.3232	1562.03	1092.39	262.422	1.26E+03	1.26E+03	2.53E+03	2.53E+03	3.35E+05	2.17E+06	2.35E+05	6.06E+05	-6.80E+03	2.17E-02	
87	Footing	5	107.445	200.882	13.9249	1501.91	1103.47	87.0873	1.40E+03	1.40E+03	3.13E+03	3.13E+03	7.71E+05	2.24E+06	2.51E+05	6.11E+05	-8.50E+03	4.85E+03	
88	Footing	6	92.4313	162.485	63.9745	1588.67	1105.69	3.15E+02	1.36E+03	1.36E+03	2.53E+03	2.53E+03	3.78E+05	2.17E+06	2.35E+05	6.06E+05	-6.80E+03	2.07E-02	
89	Footing	7	71.0846	138.273	45.8852	1291.36	1054.43	2.12E+02	1.36E+03	1.36E+03	2.53E+03	2.53E+03	2.04E+06	2.17E+06	2.35E+05	6.06E+05	-6.80E+03	6.80E+03	
90	Footing	8	79.0926	170.321	2.16473	1287.09	1023.05	1.31E+02	1.40E+03	1.40E+03	3.13E+03	3.13E+03	2.11E+06	2.24E+06	2.51E+05	6.11E+05	-8.50E+03	8.50E+03	
91	Footing	9	63.7968	138.195	45.6935	1297.6	1052.2	336.352	1.36E+03	1.36E+03	2.53E+03	2.53E+03	2.04E+06	2.17E+06	2.35E+05	6.06E+05	-6.80E+03	6.80E+03	
92																			
93																			

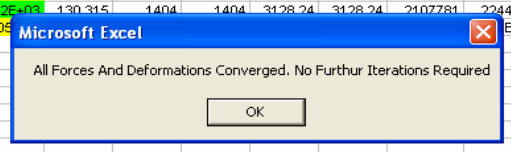

Figure 1G.3. Results of the last iteration for compression model.

209																			
210	Iteration No.	11																	
211			Force X	Force Y	K X	K Y													
212	Abutment	1	754.9	478.3															
213	Abutment	2	159.7	304.7															
214																			
215			Force X	Force Y	Force Z	M X	M Y	M Z	1.3 MX C	1.3 MY C	K X	K Y	K Teta X	K Teta Y	K Z	K Teta Z	K X Teta	K Y Teta X	
216	Footing	1	154.0	230.0	360.6	655.1	1832.9	554.6	1362.4	1362.4	1774.1	1249.3	502026.6	291.9	235081.0	606402.7	-26.9	2154.8	
217	Footing	2	169.3	252.2	26.7	595.3	1684.5	150.8	1404.0	1404.0	2150.1	1357.1	508048.7	300.8	251130.5	611202.7	-33.0	2535.4	
218	Footing	3	154.8	230.8	273.8	632.3	1767.1	322.3	1242.8	1242.8	1778.0	1243.4	425922.4	266.2	235081.0	606402.7	-25.1	1942.2	
219	Footing	4	84.7	215.5	166.9	696.1	1840.9	236.1	1263.6	1263.6	2528.2	1837.7	2035249.3	717.3	235081.0	606402.7	-53.7	5724.5	
220	Footing	5	87.4	235.2	75.7	681.2	1803.1	468.8	1404.0	1404.0	3128.2	2092.6	2107780.8	797.2	251130.5	611202.7	-71.2	6813.8	
221	Footing	6	78.5	198.4	185.1	695.1	1837.0	666.4	1357.2	1357.2	2528.2	1799.1	2035249.3	770.9	235081.0	606402.7	-56.9	5654.2	
222	Footing	7	47.7	172.8	131.4	550.2	1538.6	494.3	1362.4	1362.4	2528.2	2528.2	2035249.3	3280.5	235081.0	606402.7	-150.0	6800.0	
223	Footing	8	48.1	196.5	23.8	504.5	1532.3	756.9	1404.0	1404.0	3128.2	3128.2	2107780.8	13528.1	251130.5	611202.7	-421.2	8500.0	
224	Footing	9	46.5	157.8	145.2	552.5	1536.3	907.5	1362.4	1362.4	2528.2	2528.2	2035249.3	3283.5	235081.0	606402.7	-150.2	6800.0	
225																			
226																			

Figure 1G.4. Results of the last iteration for tension model.

The results computed at the first iteration of the spreadsheet macro for the compression model of the bridge are shown in Figure 1G.2. Note the cells indicated in green, yellow, and red. If the element force is less than its capacity, the cell is colored green. If the element force ranges from 1.0 to 1.3 times its capacity, the cell is colored yellow. When the element force exceeds 1.3 times its capacity, the cell is colored red. The macro modifies the stiffness of elements with force demands exceeding 1.3 times the corresponding capacity, according to the element deformation. The iterative LARSA/spreadsheet analysis is considered converged when changes in forces and deformations are less than 10% and 20% respectively, compared to the results of the previous iteration. The user is notified when these criteria satisfied. The user can pursue further iterations, but small incremental changes are expected beyond this point and it may not always be possible to bring the foundation spring demands to below 1.3 times their capacities.

The results of the last iteration for compression and tension models are presented in Figure 1G.3 and Figure 1G.4 respectively. Demands in only a small number of elements exceed 1.3 times capacity (shown in red). Bent deformations are presented in Table 1G.1.

Table 1G.1 Bent deformations in global X and Y-directions

	Bridge X (Longitudinal) direction (in)		Bridge Y (Transverse) direction (in)	
	Comp.	Tension	Comp.	Tension
Bent 2	1.41	14.57	4.10	4.49
Bent 3	1.42	10.24	5.19	4.87
Bent 4	1.38	6.77	4.21	3.5

The bent deformations in the demand analysis are in the bridge global X and Y-directions while the capacities determined from pushover analysis are in the bent local directions – normal and parallel to the bent. Therefore, a transformation is required to evaluate demands in the bent local directions (Table 1G.2). The transformation assumes the components of longitudinal or transverse deformation computed from global X and Y-deformations combine positively, because the displacements could be acting in either direction.

Table 1G.2 Bent deformations in bent longitudinal and transverse directions

	Bent Longitudinal Direction (in)		Bent Transverse Direction (in)	
	Comp.	Tension	Comp.	Tension
Bent 2	3.49	14.54	4.18	11.96
Bent 3	4.11	11.19	5.08	9.82
Bent 4	3.53	7.56	4.25	6.72

These values are compared to maximum allowable deformations derived in Appendix 1F (Table 1F.5). Longitudinal displacements in Bent 2 and Bent 3 exceed their capacity substantially.

Appendix 1H. Design and Evaluation of Isolation Systems

Detailed calculations are shown for the steps mentioned in Section 1.7.

Step1. Yield strength of isolators

As mentioned before, the yield strength of isolators is based on the moment capacity of piers. The moment capacities of columns are found from P-M interaction diagrams, as described in Appendix 1C. Because the bridge uses fixed-pinned (cantilever) columns in the longitudinal direction and fixed-fixed columns in the transverse direction, the shear length of the columns is different in the two directions.

$L_{shear\ long}$=Height of the column

$L_{shear\ trans}$=Height of the column/2

Shear forces derived above should not be larger than the final shear capacity of columns. The shear capacities of all the columns in a bent are added to give the shear capacity of the bent. To induce regular response in the bridge, the minimum shear capacity of all the bents controls the yield strength of isolators. The sum of yield strength of isolators at abutments is assumed to be half of the minimum shear capacity of bents, to limit the forces transferred to the abutments. These results are presented in Table1H.1.

Table 1H.1 Design shear forces for isolators

Column	Paxial	Mn	$V_{m\ long}$	$V_{m\ trans}$	V_f	$V_{m\ long}$	$V_{m\ trans}$	$V_{m\ long}$*0.85	V m trans*0.85
1	200.8	833.2	47.9	95.8	98.9	47.9	95.8	40.7	81.4
2	279	895.2	51.4	102.9	98.9	51.4	98.9	43.7	84.1
3	247.6	869.6	50	100	98.9	50	98.9	42.5	84.1
							sum	126.9	249.5
4	238.1	860.8	49.5	98.9	98.9	49.5	98.9	42	84.1
5	271.3	886.8	51	101.9	98.9	51	98.9	43.3	84.1
6	201.3	833.2	47.9	95.8	98.9	47.9	95.8	40.7	81.4
							sum	126.1	249.5
7	200.9	833.2	47.9	95.8	98.9	47.9	95.8	40.7	81.4
8	254.2	869.6	50	100	98.9	50	98.9	42.5	84.1
9	199.3	833.2	47.9	95.8	98.9	47.9	95.8	40.7	81.4
							sum	123.9	246.9
						Min factored Bent Force		123.9	246.9
						Min Abut Force		61.9	123.4
							Total	495.5	987.5

Step 2. Total lateral force and resulting dynamic properties (natural period and damping ratio)

The total force acting on the bridge superstructure is the sum of yield strength of all of the isolators in the bridge. As shown in Table 1H.1, the total force in longitudinal direction is 495.5 kips and in transverse direction is 987.5 kips.

Design acceleration spectra for the UL ground motion are used to find the natural period and damping ratio. The design spectral acceleration for a one second period, S_{D1} = 0.94 g (Appendix1A) and the acceleration in the long period range is $S_a = 0.94/T_n$. Because isolation systems provide damping well beyond that observed in typical structural configurations, this spectral acceleration is modified for increased damping according to:

$$S_a = \frac{S_{D1}}{T_n B}$$

where B is a modification factor for long periods (Table 5-4 of FHWA, 2006):

$$B = \left(\frac{\xi_{eff}}{0.05} \right)^{0.3}$$

The spectral acceleration corresponding to the force capacity calculated in the previous step is found by dividing by the superstructure weight W:

$$S_a = \frac{F_{total}}{W}$$

Equating the two relations for S_a, the natural vibration period is

$$T_n = \frac{W.S_{D1}}{F_{total}.\left(\frac{\xi_{eff}}{0.05}\right)^{0.3}}$$

Assuming ξ_{eff}, we can find the corresponding T_n. Effective damping ratios within the range of 15% to 30% are appropriate for bridge isolation. Different damping ratios can be assumed for longitudinal and transverse directions. In this example, damping ratios of 20% and 30% are assumed for the longitudinal and transverse directions, respectively, for the first iteration.

W=2533 kips	Total weight of superstructure.
S_{D1}=0.94 g	Spectral acceleration for time period of one second for the ULGM.
$F_{total\ long}$=495.5 kips	Total force acting on the superstructure in longitudinal direction.
$F_{total\ trans}$=987.5 kips	Total force acting on the superstructure in transverse direction.
$\xi_{eff\ long}$=20%	Equivalent damping for the isolated modes in longitudinal direction
$\xi_{eff\ trans}$=30%	Equivalent damping for the isolated modes in transverse direction
$T_{n\ long}$=3.2 sec	Calculated effective period in the longitudinal direction
$T_{n\ trans}$=1.41 sec	Calculated effective period in the transverse direction

The spectral displacement is given by:

$$S_d = \frac{S_a.T_n^{\ 2}}{4\pi^2}$$

$$S_{d\ long} = \frac{495.5 \times 3.2^2}{4 \times \pi^2} = 19.22 \quad in$$

$$S_{d\ trans} = \frac{987.5 \times 1.41^2}{4 \times \pi^2} = 7.56 \quad in$$

Step 3. Bent displacement and effective isolator displacement

Because bents and isolators are in series, they have the same force demand. Bent stiffness is evaluated using cracked section properties of columns, and hence displacement is evaluated. In the design phase, the effects of foundation flexibility are ignored.

E=3122 kips/in^2	Elastic modulus of concrete
I=23813 in^4	Cracked moment of inertia
h=17.4 ft	Column height

$$K_{bent\ long} = \frac{3EI}{h^3} \times 3 = 882 \quad kips/ft$$

$$K_{bent\ trans} = \frac{12EI}{h^3} \times 3 = 3528 \quad kips/ft$$

Bent displacements when isolators yield are

$$\Delta_{py\ long} = \frac{F_{bent\ long}}{K_{bent\ long}} = \frac{123.9}{882} \times 12 = 1.69 \quad in$$

$$\Delta_{py\ trans} = \frac{F_{bent\ trans}}{K_{bent\ trans}} = \frac{246.9}{3528} \times 12 = 0.84 \quad in$$

The effective displacements in isolators = total displacement - bent displacement.

$$\Delta_{DEb\ long} = S_{d\ long} - \Delta_{py\ long} = 19.22 - 1.69 = 17.79 \quad in$$

$$\Delta_{DEb\ trans} = S_{d\ trans} - \Delta_{py\ trans} = 7.56 - 0.84 = 6.85 \quad in$$

The effective displacements of isolators in abutments = total displacement

Abutment stiffness is assumed to be very large.

$$\Delta_{DEa\ long} = S_{d\ long} = 19.22 \quad in$$

$$\Delta_{DEa\ trans} = S_{d\ trans} = 7.56 \quad in$$

Step 4. Equivalent damping of the bridge

To find the yield displacement of isolators, a ductility factor of 4 is assumed (μ=4). The yield displacements of isolators are

$$\Delta_{Dyb\ long} = \frac{\Delta_{DEb\ long}}{\mu} = \frac{17.79}{4} = 4.45 \quad in$$

$$\Delta_{Dyb\ trans} = \frac{\Delta_{DEb\ trans}}{\mu} = \frac{6.85}{4} = 1.71 \quad in$$

$$\Delta_{Dya\ long} = \frac{\Delta_{DEa\ long}}{\mu} = \frac{19.22}{4} = 4.81 \quad in$$

$$\Delta_{Dyb\ trans} = \frac{\Delta_{DEb\ trans}}{\mu} = \frac{7.56}{4} = 1.89 \quad in$$

The total ductility of the pier-isolator system can be found: (Eq. 6.14 of Priestly et. al., 1996)

$$\mu_G = 1 + (\mu - 1)\frac{\Delta_{Dy}}{\Delta_S + \Delta_{Dy}} = \frac{S_d}{\Delta_{py} + \Delta_{Dy}}$$

$$\mu_{G\ b\ long} = \frac{19.22}{1.69 + 4.45} = 3.13$$

$$\mu_{G\ b\ trans} = \frac{7.56}{0.84 + 1.71} = 2.96$$

$$\mu_{G\ a\ long} = \frac{19.22}{0 + 4.81} = 4$$

$$\mu_{G\ a\ trans} = \frac{7.56}{0 + 1.89} = 4$$

The equivalent ductility of the isolation system is (Eq 6.13 of Priestly et. al., 1996)

$$\xi_{DE} = \frac{2e_f(1 - 1/\mu)}{\pi}$$

where e_f is the efficiency factor to take into account the smaller area of the typical cycle in force-deformation response compared to the ideal elastic-perfectly plastic case.

$$\xi_{DE\ b\ long} = \frac{2 \times 0.7(1 - 1/3.13)}{\pi} = 0.30$$

$$\xi_{DE\ b\ trans} = \frac{2 \times 0.7(1 - 1/2.96)}{\pi} = 0.30$$

$$\xi_{DE\ a\ long} = \frac{2 \times 0.7(1 - 1/4)}{\pi} = 0.33$$

$$\xi_{DE\ b\ trans} = \frac{2 \times 0.7(1 - 1/4)}{\pi} = 0.33$$

The effective damping ratio for the bridge is (Eq 6.20 of Priestly et. al., 1996)

$$\xi_b = \frac{\sum \xi_i M_i}{M_{superstructure}} = \frac{\xi_{DE\ b} M_b + \xi_{DE\ a} M_a}{M_b + M_a}$$

W_b=2042.5 kips Total weight on bents

W_a=490.7 kips Total weight on abutments

$$\xi_{b\ long} = \frac{0.3 \times 2042.5 + 0.33 \times 490.7}{2533} = 0.31$$

$$\xi_{b\ trans} = \frac{0.3 \times 2042.5 + 0.33 \times 490.7}{2533} = 0.31$$

The corresponding damping modification factors are

$$B_{long} = \left(\frac{0.31}{0.05}\right)^{0.3} = 1.72$$

$$B_{trans} = \left(\frac{0.31}{0.05}\right)^{0.3} = 1.72$$

Step 5. Modeling of isolators for structural analysis

Although the isolation system is nonlinear, the equivalent linear properties of the isolation system will be used for analysis. The effective damping ratios for bridge response have already been computed based on deformations from the design spectrum, and their application in modal analysis will be discussed. The effective stiffness of the isolation system also depends on the displacement demand across the isolators, which was computed in Step 3:

$$k_{e\ isolator} = \frac{F_{y\ isolator}}{\Delta_{DE}}$$

F_y for a single isolator is the fraction of the minimum factored bent or abutment force transmitted to the bearing and Δ_{DE} is the effective displacement of the bearing.

Example: Bent 2, Longitudinal direction

Minimum factored bent force: F_y= 123.9 kips

The yield force in a single isolator is proportional to the axial load transferred to that isolator from the supported girder. Seven isolators are needed to support the seven girders spanning in from the left and nine isolators are needed to support the nine girders spanning from the right. This configuration is needed since the girders are not continuous across the bent and the spacing is different on each side. Assuming *w* is the weight of the superstructure per square foot, the axial loads in isolators supporting the left and right girders in bent 2 are

$$p_{bent2\ left} = \frac{L.w}{2N_{girders}} = \frac{46 \times w}{2 \times 7} = 3.29w$$

$$p_{bent2\ right} = \frac{L.w}{2N_{girders}} = \frac{56 \times w}{2 \times 9} = 3.11w$$

The total axial force in bent 2 is

$$p_{total} = \sum p_{bent1} = 7 \times 3.29w + 9 \times 3.11w = 51.02w$$

Thus, the axial loads in individual isolators supporting the left girders and the right girders are:

$$F_{y\ bent2\ left} = \frac{3.29w}{51.02w} \times 123.9 = 8.0 \quad kips$$

$$F_{y\ bent2\ right} = \frac{3.11w}{51.02w} \times 123.9 = 7.6 \quad kips$$

The effective stiffness of each isolator is

$$k_{e\ isolator\ bent2\ left} = \frac{8.0}{17.97} = 0.45 \quad kips/in$$

$$k_{e\ isolator\ bent2\ right} = \frac{7.6}{17.97} = 0.42 \quad kips/in$$

Step 6. Isolator modeling and modal analysis to find natural vibration periods

A beam element linking the girder to the bent is used to represent the effective stiffness of the isolator. The effective stiffness of a beam element depends on the boundary condition and is:

$$k_e = \begin{cases} \dfrac{3EI}{h^3} & \text{for a cantilever column} \\ \dfrac{12EI}{h^3} & \text{for a fixed-fixed column} \end{cases}$$

The cantilever column assumption is appropriate for friction isolators, which do not transfer moment through the isolator while the fixed-fixed column assumption is appropriate for elastomeric bearings, which are generally bolted top and bottom and can transfer moment. Although the specific isolators have not been chosen, the cantilever column boundary conditions are assumed. Thus, the equivalent moment of inertia that should be assigned to the isolator element is:

$$I = \frac{k_e h^3}{3E_c}$$

k_e = 0.45 ksi Effective stiffness of bearing

h = 3.25 ft Height of the link element

E_c = 3122 ksi Elastic modulus of concrete (any material could be selected)

$$I_{e\ bent2\ long\ left} = \frac{k_e h^3}{3E_c} = \frac{0.45 \times (3.25 \times 12)^3}{3 \times 3.122 \times 10^3} = 2.84 \quad in^4$$

$$I_{e\ bent2\ long\ right} = \frac{k_e h^3}{3E_c} = \frac{0.42 \times (3.25 \times 12)^3}{3 \times 3.122 \times 10^3} = 2.69 \quad in^4$$

This procedure is followed for each bent and abutment. The results are presented in Table 1H.2.

Table 1H.2 Equivalent moment of inertia for isolators

		Seismic Force (kips)		Isolator displacement (in)		Isolator ke (kips/in)		Moment of Inertia (in^4)	
	side	Long	Trans	Long.	Trans.	Long.	Trans.	Long.	Trans.
abut 1	-	8.84	17.69	19.22	7.56	0.46	2.34	2.91	14.81
bent 2	left	7.99	15.98	17.79	6.85	0.45	2.33	2.84	14.77
	right	7.55	15.11	17.79	6.85	0.42	2.21	2.69	13.97
bent 3	left	7.55	15.11	17.79	6.85	0.42	2.21	2.69	13.97
	right	7.99	15.98	17.79	6.85	0.45	2.33	2.84	14.77
bent 4	left	8.85	17.70	17.79	6.85	0.50	2.58	3.15	16.37
	right	8.85	17.70	17.79	6.85	0.50	2.58	3.15	16.37
abut 5	-	8.84	17.69	19.22	7.56	0.46	2.34	2.91	14.81

It is not economical to design too many different isolators for a bridge. Therefore, the same isolators will be used everywhere, characterized by the minimum yield force in any isolator (from Table 1H.2). These results are shown in Table 1H.3.

Table 1H.3 Equivalent moments of inertia selected for economy of design

		Seismic Force (kips)		Isolator Disp. (in)		Isolator ke (kips/in)		Moment of Inertia (in^4)	
	side	Long	Trans	Long.	Trans.	Long.	Trans.	Long.	Trans.
abut 1	-	7.55	15.11	19.22	7.56	0.39	2.00	2.49	12.65
bent 2	left	7.55	15.11	17.79	6.85	0.42	2.21	2.69	13.97
	right	7.55	15.11	17.79	6.85	0.42	2.21	2.69	13.97
bent 3	left	7.55	15.11	17.79	6.85	0.42	2.21	2.69	13.97
	right	7.55	15.11	17.79	6.85	0.42	2.21	2.69	13.97
bent 4	left	7.55	15.11	17.79	6.85	0.42	2.21	2.69	13.97
	right	7.55	15.11	17.79	6.85	0.42	2.21	2.69	13.97
abut 5	-	7.55	15.11	19.22	7.56	0.39	2.00	2.49	12.65

The model of the retrofitted structure is identical to the model described in Section 1.4, except that the girder-to-bent link elements are replaced by cantilever beam elements representing the effective stiffness of the isolator elements. Modeling isolators according to moments of inertia given in Table 1H.3 and performing modal analysis, the following natural vibration periods were obtained from LARSA.

T_{long} =3.37 sec

T_{trans}=1.66 sec

Step 7. Hybrid response spectrum for the analysis

The hybrid response spectrum is based on the fundamental period of the bridge with isolation. This spectrum uses 5% damping for periods smaller than $0.8T_e$ and the effective isolation damping for periods larger than $0.8T_e$. The fundamental vibration periods in the two translational directions are found by performing modal analysis on the bridge model.

0.8 T_{long} =2.7 sec

0.8 T_{trans}=1.33 sec

B=1 for 5% structural damping

B_{long}=1.72 for 31% effective damping for the isolated modes in longitudinal direction

B_{trans}=1.72 for 31% effective damping for the isolated modes in transverse direction

Because the bridge has significantly different natural periods in longitudinal and transverse directions, two hybrid spectrums are developed and assigned to each direction. The hybrid design spectra are shown in Figure 1H.1.

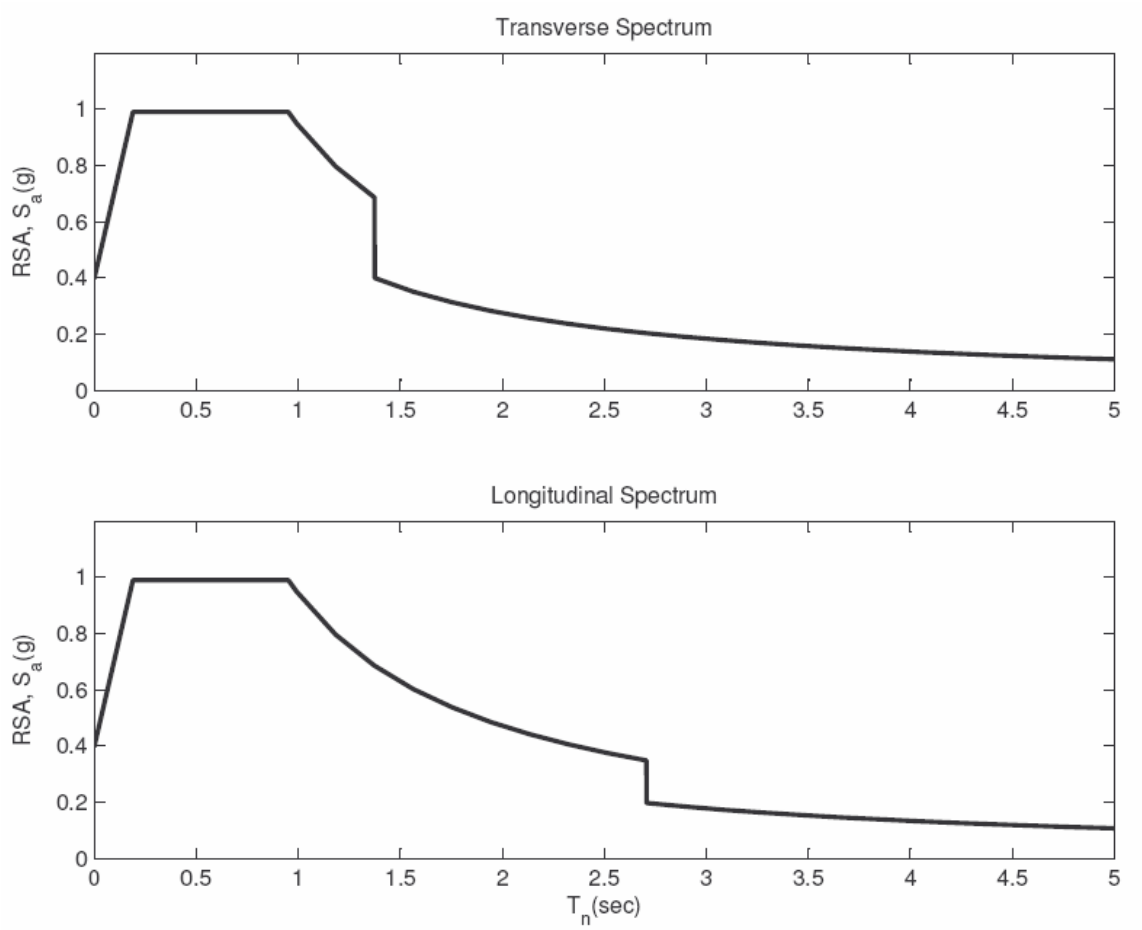

Figure 1H.1. Hybrid design spectrum for the first iteration

Step 8. Response spectrum analysis

The multi-mode response spectrum method is used in the analysis of the retrofitted bridge. Satisfactory agreement between the assumed and computed demands was achieved in one iteration. The results are presented in Section 1.7.

THIS PAGE INTENTIONALLY LEFT BLANK

2. Church Street Underpass, So. Layton to Hill Field Interchange

2.1 Existing Structure

The bridge is a 4-span continuous reinforced concrete bridge located on the I-15 corridor. It passes over I-15 Northbound and Southbound in the middle two spans. The bridge was designed in 1966 and estimated to be constructed in 1967. The exterior spans are 35', while the interior spans are 80'-6", and the bridge has a horizontal skew of 30°36'. The superstructure consists of an 7.5" thick (49'-61/4" wide) reinforced concrete slab supported on four rectangle reinforced concrete girders spaced at 10'- 8". The superstructure is fixed in the transverse direction and contains hinges in the longitudinal direction at each of the four piers. The superstructure contains cold hinges at interior locations of Spans 2 and 3; the abutments are integral. All piers are multi-column bents with three identical 2'-6" diameter circular reinforced concrete columns. Each column is supported on a pile footing; four 12" diameter circular reinforced concrete piles with a 3'-1'' pile cap. Existing bridge geometry is shown in Figure 2.1.1.

2.2 Determination of Seismic Retrofit Category (SRC)

The seismic retrofit category is determined first, which is the basis for all decisions regarding bridge evaluation methods. Details about how to determine the seismic retrofit category are given in Chapter 1 of the retrofit manual (FHWA, 2006) and Chapter 2 of the Utah guidelines (Wilson and Ryan, 2009). Step by step calculations and plotted response spectra are shown in Appendix 2A.

Because the bridge has a remaining service life of 35 years, the 500 year return period earthquake represents the Lower Level (LL) motion and the 2500 year return period earthquake represents the Upper Level (UL) motion. The bridge is in Anticipated Service Life Category 2 (ASL 2), and is assumed to be of standard importance; thus it will be evaluated against Performance Level 3 (PL3 = Fully Operational) for the LL motion and Performance Level 1 (PL1 = Life Safety) for the UL Motion.

The Seismic Hazard Levels (SHL) for UL and LL motions are functions of the site response spectra. S_s and S_1 values are determined from the software included with the Retrofit Manual (FHWA, 2006). The site category is to be determined through harmonic mean of blow counts of soil layers in the top 100 ft (Table 2-2 of FHWA, 2006); however, the greatest boring

depth is 65 ft in Boring 2, which is used to find the blow count number. Based on the boring data the Site Class is borderline D or E. Therefore, the Site Class is taken to be E except for the coefficient F_a for the UL motion, where it is more conservative to use Site Class D. The SHL is found to be Category IV for both UL and LL motions.

Based on the Performance Level and Seismic Hazard Levels the Seismic Retrofit Category (SRC) is C for both UL and LL motions.

2.3 Overview of Evaluation Methods

For the LL motion, the bridge will be evaluated using Analysis Method C. Method C computes demand/capacity ratios at a component level for the bridge. Because it does not recognize the redistribution of forces after an element yields, Method C can be inaccurate. As such, Method C is recommended for bridges that remain elastic or nearly so. The applicability of Method C should be evaluated based on the results of this example, recognizing that a 500 year return period motion is used rather than the 100 year return period motion typically recommended for LL evaluation.

Both the Retrofit Manual (FHWA, 2006) and the Utah guidelines (Wilson and Ryan, 2009) recommend a step by step procedure for the LL evaluation that culminates in Method C. This example proceeds directly to Method C since the bridge is assumed to be likely to exhibit inelastic response to the LL motion. Method C requires a linear elastic analysis of the complete bridge to determine the demands of individual components. The capacities of columns, footings, etc. are determined on an individual basis by hand calculations or software.

For the UL motion, the bridge should be evaluated by Method D1 (capacity spectrum method) or D2 (pushover analysis) in combination with an elastic demand analysis. Restrictions on the use of Method D1 are given (Sec. 5.5.6 of FHWA, 2006). This bridge does not strictly qualify for Method D1, because (1) the skew angle 30°36' slightly exceeds the recommended maximum of 30°, and (2) the ratio of the longest to shortest span lengths = 2.29 exceeds the recommended maximum of 1.5. However, the bridge does not seem to be highly irregular, and is thus evaluated by Method D1 for demonstration and in contrast to Example 1 which used Method D2. Method D1 is always used in combination with the Uniform Load Method for elastic demand analysis. The bridge capacity curve is evaluated by hand calculations.

2.4 Creating a LARSA Model

Software is needed to carry out the demand analysis: response spectrum analysis (i.e. Multi-Mode method) for the LL motion and the Uniform Load Method for the UL motion. Although the analyses use different loading, a single bridge model suffices. The recommended complexity of the model is also determined by the geometry of the bridge. The bridge is nearly regular and due to its in-plane rigidity can be assumed to move as a rigid body under seismic loads. Therefore, a "spine" model is used; that is, the bridge superstructure is modeled single beam elements – representative of the composite stiffness of the cross section – that span between bents or internal hinges. Beam elements are also used to model the bent caps and columns in the bridge. A joint connecting two elements is located at the crossing point of centerlines of the two elements. There are several ways of applying geometric connectivity of columns, bent caps, and girders. Priestly et. al. (1996) recommends using link elements that penetrate the joint regions. In this example, member end offsets are used. This option is provided in LARSA and is available under *Input Data- Geometry- Members- Member end offsets*. The relative positions of the end nodes of the elements with respect to the reference nodes are entered.

While simpler programs such as SEISAB can create spine models very easily, LARSA has some features that are very helpful for this bridge. For instance, LARSA's parametric sections allow the change in depth of the girders over the span to be modeled accurately. As recommended by the Retrofit Manual (FHWA, 2006), the foundation elements are modeled using springs, with stiffnesses based on the pile group stiffness. LARSA allows general foundation springs formulated using 6x6 stiffness matrices.

The LARSA files included to demonstrate the modeling and analysis of this bridge are indicated in Table 2.4.1:

Table 2.4.1 LARSA modeling and analysis files for bridge example 2

ChurchSt_Sections.lpsx	a Section Composer file containing all bridge sections
ChurchSt_LowerLevel.drs	a database file containing the design spectrum for the lower level motion
ChurchSt_TensionLL.lar	a LARSA file defining the tension model of the bridge and analysis to the lower level motion
ChurchSt_CompressionLL.lar	a LARSA file defining the compression model of the bridge and analysis to the lower level motion
ChurchSt_TensionULD1.lar	a LARSA file defining the tension model of the bridge and determination of the bridge stiffness via the uniform load method to be used with method D1
ChurchSt_CompressionULD1.lar	a LARSA file defining the compression model of the bridge and determination of the bridge stiffness via the uniform load method to be used with method D1
ChurchsSt_SuperstructureMass.lar	a LARSA file to determine the superstructure self weight to be used with method D1

2.4.1 Superstructure Elements

One element is used for each of the exterior spans while three elements are used for the interior spans (the elements span between the cold hinges). The superstructure elements are modeled with composite sections, including the deck and girders, using LARSA Section Composer. Section Composer takes into account the geometry of the composite section and the longitudinal reinforcement. Section Composer computes the element stiffness and mass based on material properties and geometry. Moment releases are applied about the transverse direction at the in-span hinges located in the middle two spans of the deck.

LARSA Section Composer can account for the nonprismatic variation of the girders in the section properties of the composite superstructure elements. Knowing the approximate variation of the section, we fit a curve to the depth as a function of longitudinal position. Because the section is a custom shape, equations are input for the section points that vary along the length. For this example, the equations can be viewed in the Section Composer file ChurchSt_Sections.lpsx, section name top(1), top(2) or top(3). Under *Points* on the bottom right window, quadratic equations have been input for the y-coordinates as a function of x (longitudinal position). The variation of the section depth with longitudinal position can then be viewed by selecting *Section – Nonprismatic Variation – Section Diagram* in Section Composer. Note that the position of reinforcing steel cannot easily be changed using nonparametric variation.

2.4.2 Substructure Elements

Based on the Retrofit Manual (Table 7-1 of FHWA, 2006), some changes are applied to section properties of concrete elements in the substructure to account for cracking during excitation. For a linear elastic demand analysis, cracked section properties are generally used for columns and bent caps (Sec. 7.3.2.1 of FHWA, 2006). The flexural rigidity of the columns are modified to represent the behavior up to yield.

2.4.2.1 Bent Caps

Based on Table 7-1 of the Retrofit Manual (FHWA, 2006), assuming that cracking but not hinging is expected in bent caps which is usually the case, 50%, 40%, and 100% of flexural, shear, and axial rigidity of bent caps are applied for the demand model. The section properties computed by Section Composer in LARSA can be modified through *Input Data – Properties – Sections - Properties.*

2.4.2.2 Columns

Each circular reinforced concrete column with reinforcement is modeled as a single element, with elastic section properties determined by section composer. It is worth noting that the Retrofit Manual recommends that tall columns be modeled with two or more elements due to some concerns regarding the distribution of mass along the column; however this was not done here. The column flexural rigidity is derived from

$$E_c I_{eff} = \frac{M_n D'}{2\varepsilon_y}$$

where M_n is the nominal yield moment, D' is the distance between outer layers of longitudinal reinforcement, and ε_y is the yield strain of steel reinforcement. The capacity M_n can be derived from charts or from section analysis using appropriate software; we performed moment curvature analysis of the composite section using Matlab. The capacity M_n depends on the column axial load, which is unknown without prior analysis. As a result, the bridge is analyzed with the elastic flexural rigidity of the column (0.5 $E_c I_c$) to determine the axial load and find the new value M_n. Because the axial load also depends on Mn, this process is iterative and is illustrated in Appendix 2C. Upon completion of this process, the new $E_c I_{eff}$ is entered into LARSA. While flexural stiffness based on nominal moment capacity may not typically be applicable to Method C, it is used here because plastic hinging is expected in the columns.

2.4.3 Foundation Elements

The Retrofit Manual (FHWA, 2006) recommends modeling pile groups in one of two ways: a series of uncoupled springs or a fully coupled foundation stiffness matrix, as shown in Figure 2.4.1. The latter model is the most general and rigorous approach, and is used here. In summary, the translational, rotational, and cross coupling stiffness of a single pile are determined based on the bending inertia EI, and are looked up in charts located in the Retrofit Manual (Figures 6-14 to 6-16 of FHWA, 2006). The stiffness of the pile group is calculated by assembling the stiffness matrices from each pile into a single stiffness matrix located at the geometric center of the pile group. Torsional and bending resistances are added to the pile group stiffness matrix as a result of the assembly process. Lateral footing stiffness is computed due to the passive pressure of soil on the sides of the footing, and the other stiffness components are computed from Tables 6-1 and 6-2 of FHWA (2006). The pile group and footing stiffness are assembled into a single matrix. Detailed calculations are shown in Appendix 2B. A footing stiffness matrix for the foundation elements can be input in LARSA by selecting *Input Data – Properties - Spring Properties*; selecting 6×6 *stiffness matrix* for *Type*; and selecting *Spring Properties - Edit stiffness matrix* to input the calculated stiffness matrix. To add the coupled spring elements to the LARSA model, enter the node numbers and select *Input Data –Geometry – springs*; for *Type* select *Linear*, and for *Direction* select the name of the footing stiffness matrix.

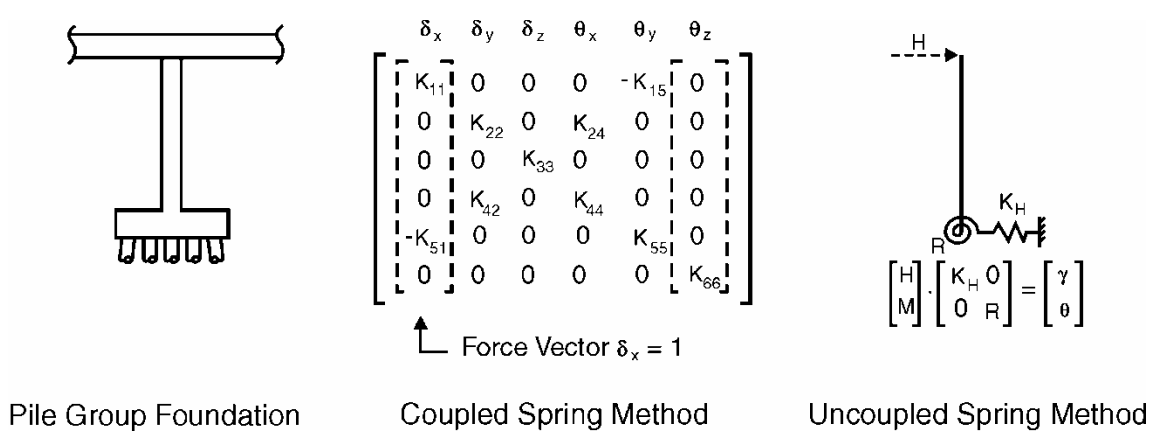

Figure 2.4.1. Methods to evaluate pile group stiffness (Figure 6-18 of FHWA, 2006)

2.4.4 Abutment Springs

Abutment walls and wingwalls can play a very beneficial role in the performance of the bridge during an earthquake, because the backfills behind these walls can resist large inertial loads and thus reduce ductility demands elsewhere in the bridge. Abutment stiffness is based directly on the passive pressure of the soil surrounding it. Default passive pressures are used according to Sec. 6.2.2.4 of (FHWA, 2006). Since the soil type for this bridge is close to sand; 2H/3 is used for passive pressure. The effects of the piles beneath the abutment are also included in abutment stiffness, which leads to:

$$P_p = p_p.H.L + N_p.C_p$$

where P_p is the total lateral capacity of the abutment-pile system, p_p is the passive pressure, L is the width of the backwall, N_p is the number of piles, and C_p is the capacity of each pile. The piles are assumed to yield when the soil reaches its passive pressure. The displacement at which soil reaches to its passive pressure is called mobilization displacement, recommended to be 0.02H (FHWA, 2006). Thus, the effective stiffness is:

$$K_{eff1} = \frac{P_p}{0.02H}$$

The composite abutment stiffnesses in the lateral transverse and orthogonal direction and for rotation about the vertical axis are computed in Appendix 2B. These are implemented in LARSA as uncoupled spring elements. The implementation of the springs is similar to that described for the footing elements, but uses uniaxial springs rather than a spring stiffness matrix. The longitudinal and rotational spring stiffnesses differ for compression and tension; thus these springs are defined as nonlinear springs with separate stiffness for tension and compression.

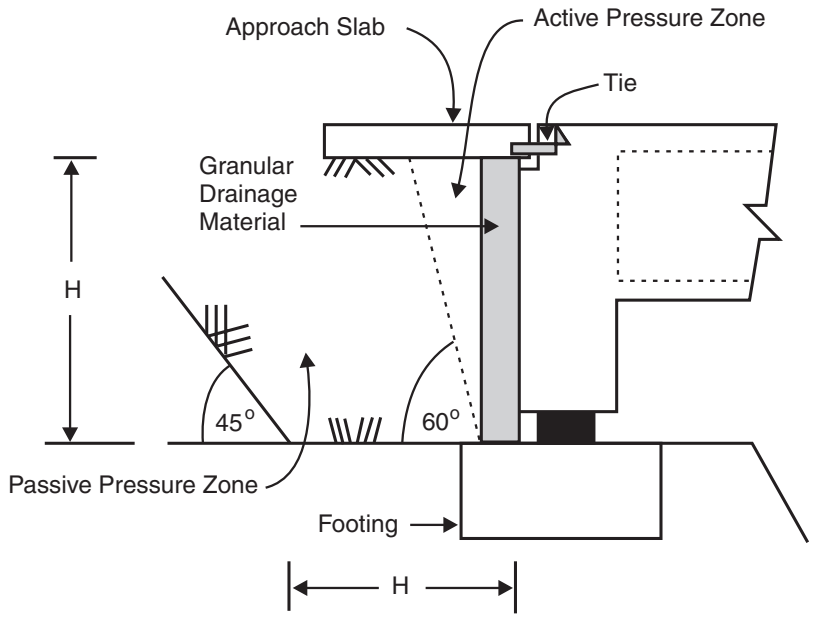

Figure 2.4.2. Calculation of abutment passive pressure (Figure 6-23 of FHWA, 2006)

2.4.5 Summary of the LARSA Bridge Model

Several renderings of the bridge model, created using the LARSA software, are shown in Figs. 2.4.3-2.4.5. The skeleton rendering in Fig. 2.4.5 indicates the numbering scheme for most nodes and elements. The rendering of the abutment and foundation springs can be difficult to make out. The bridge skew can be observed in the elevation view, where the columns associated with a given pier are not aligned.

Due to the presence of in-span cold hinges, the bridge is analyzed in two different conditions. In the compression model, the hinges are closed, i.e, fixed against relative longitudinal displacements but can transfer longitudinal forces. In the tension model, the hinges are open, i.e. relative longitudinal displacements are allowed but longitudinal forces cannot be transferred. An eigenvalue analysis of the bridge is performed for both the tension and compression models, and the first twenty natural periods are shown in Table 2B.1 of Appendix 2B.

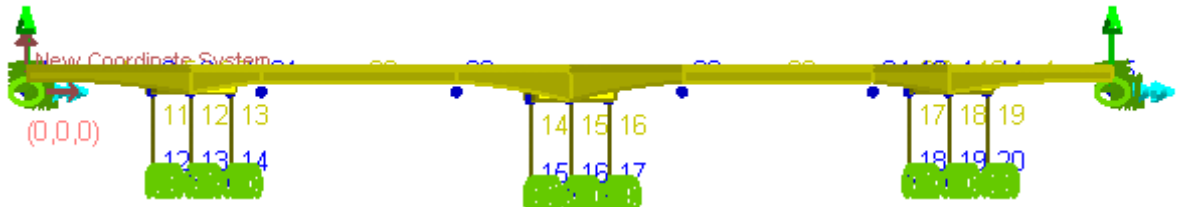

Figure 2.4.3. Elevation rendering of LARSA bridge model

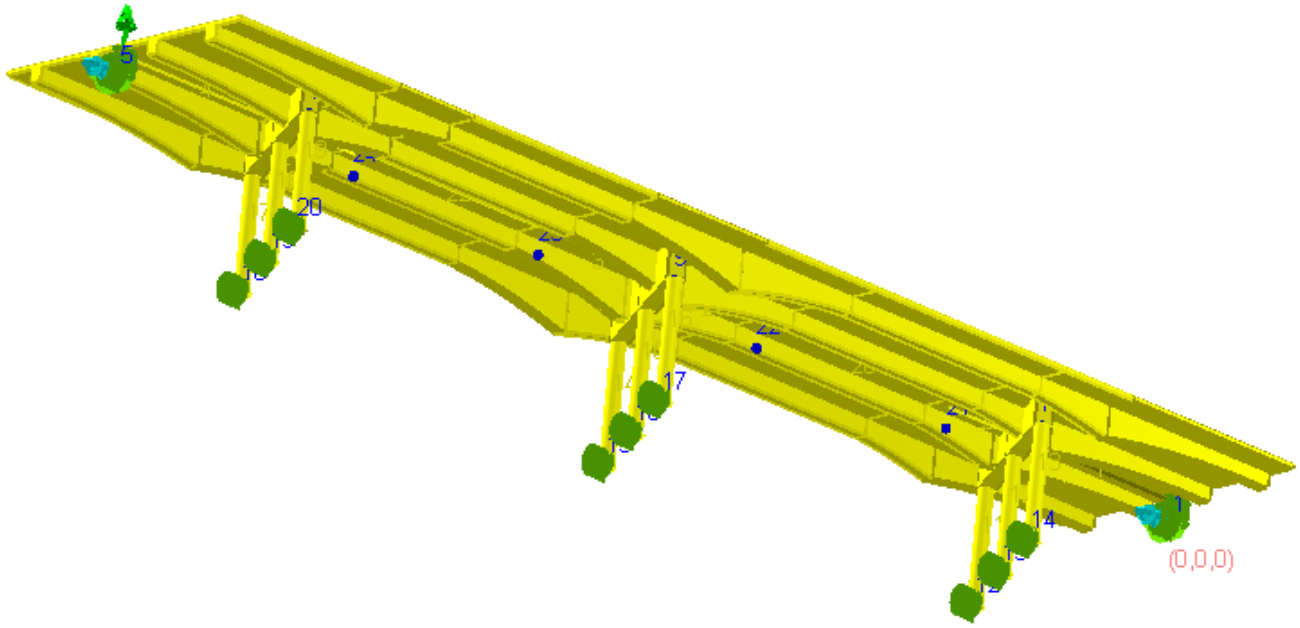

Figure 2.4.4. 3D rendering of LARSA bridge model

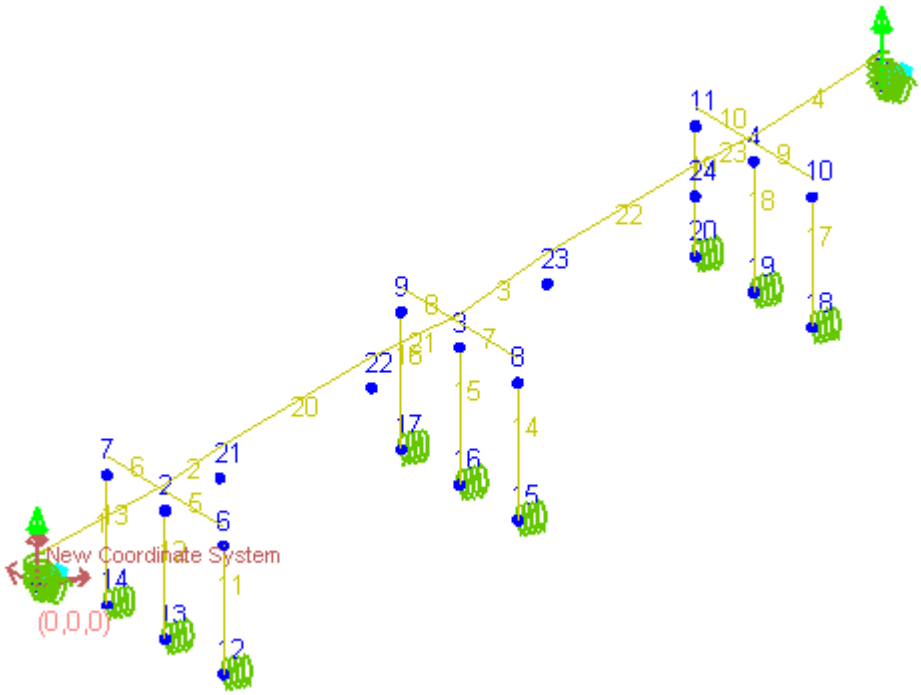

Figure 2.4.5. Skeleton rendering of LARSA bridge model indicating nodes and elements

2.5 Evaluation of the Bridge for the LL Ground Motion

As described in Sec. 2.3, the bridge is evaluated for the LL ground motion using Method C, which calculates capacity/demand ratios for bridge components that may be damaged during an earthquake. Ratios greater than one indicate sufficient capacity to resist the earthquake demand; ratios less than one indicate components in need of attention and possible retrofitting. Capacity/demand (C/D) ratios are therefore used to indicate the need for retrofitting and may also be used to assess the effectiveness of various retrofit strategies.

Components that should be evaluated vary with the Seismic Retrofit Category of the bridge, based on the assumption that certain components will respond fine in moderate shaking. Table 5-2 (FHWA, 2006) indicates components and failure modes that should be checked. Appendix D of the Retrofit Manual provides detailed guidelines for evaluation of the C/D ratios, while Appendix E works through an example problem (FHWA, 2006). Evaluation of C/D ratios for various member and component limit states is based on a combination of analysis, testing, and engineering judgment.

Eleven ratios are defined in four categories as follows:

1. Support length and restrainer C/D ratios:

r_{ad} displacement C/D ratio for abutment

r_{bd} displacement C/D ratio for bearing seat or expansion joint

r_{bf} force C/D ratio for bearing or expansion joint restrainer

2. Column C/D ratios:

r_{ca} anchorage length C/D ratio for column longitudinal reinforcement

r_{cc} confinement C/D ratio for column transverse reinforcement

r_{cs} splice length C/D ratio for column longitudinal reinforcement

r_{cv} shear force C/D ratio for column

r_{ec} bending moment C/D ratio for column

3. Footing C/D ratios:

r_{ef} bending moment C/D ratio for footing

r_{fr} rotation C/D ratio for footing

4. Soil C/D ratio:

r_{sl} acceleration C/D ratio for liquefaction potential

The superstructure support length and restrainer C/D ratios are essentially irrelevant for this bridge since the connections are integral at the columns and at the abutments. Insufficient detail is provided in the bridge plans to be able to evaluate the cold hinges. Liquefaction is outside of the scope of this project. Therefore, the evaluation in this example focuses on column and footing C/D ratios. First, bending moment C/D ratios for columns (r_{ec}) and footings (r_{ef}) are evaluated. If these ratios are less than 1, column details are evaluated to assess the ability of the columns to form plastic hinges. Similarly, a rotation C/D ratio is developed for the footing as an overall assessment of its ductility.

2.5.1 Component Capacity Evaluation

Nominal moment capacities for the columns were already developed according to Section 2.4.2 and discussed in detail in Appendix 2C. The moment capacities of the pile-footing elements, or foundation springs, are determined next.

The pile capacities are difficult to determine; thus standard recommended values are used. In the longitudinal and transverse directions, the capacity of piles is assumed to be 40 kips (Sec. 20-4 of Caltrans, 1995). The design load capacity in the vertical direction is 100 kips, which is close to the recommended value of 90 kips in the Retrofit Manual (Sec. 6.2.2.2 of

FHWA, 2006). Ultimate capacities in axial compression and tension are assumed to be 180 and 90 kips, respectively.

The moment capacity of the pile-footing system is determined from a static analysis of the pile-footing system, where each of the piles is assumed to be stressed to its capacity. Figure 6-19 of FHWA (2006) illustrates the procedure. The moment capacity depends on the footing axial load. The procedure is illustrated in Appendix 2B for one of the pile-footing systems. Because the moment capacity of the pile-footing also depends on the axial load, these capacities are developed iteratively as they were for the column. As a result, Tables 2C.1-2C.3 show iterative calculations of the pile-footing moment capacities in addition to the column moment capacities.

2.5.2 Structure Demand Evaluation

The following load cases and load combinations are defined in LARSA for demand evaluation.

<u>Load Cases</u>

4. Self Weight (Dead Load)
5. Longitudinal Earthquake Loading
6. Transverse Earthquake Loading

<u>Load Combinations</u>

3. 1.0*Longitudinal + 0.3*Transverse
4. 0.3*Longitudinal + 1.0*Transverse

Note that the Retrofit Manual (FHWA, 2006) recommends that a 100% + 40% load combination be used in place of the 100% + 30% load combination used here. The elastic moment demands are calculated by combining the maximum moments of the columns (obtained from a load combination) about the principal (x and y) axes using a square root of sums (SRSS) combination rule. In most cases, Load Combination 1 leads to the highest demands. Moments due to the Self Weight load case are added to each component prior to applying the combination rule. The Self Weight load case is added by hand, rather than factored into the load combination so that the results do not become direction dependent. Moments at the base of the footing are obtained by a free body analysis assuming the moment and shear at the top of the footing are known.

In LARSA, load cases are defined under *Input Data, Load Groups and Stages, Load Cases.* Load combinations are defined through *Input Data, Load Groups and Stages, Load Combinations.* A name should be assigned to each load case or load combination as it is defined. For dead loads, the Analysis Type is 'Static' and a weight factor of -1 is applied in the z-direction. For response spectrum analysis, the Analysis Type is 'Response Spectrum' and the weight factor is zero. First, an acceleration spectrum is defined in *Input Data, Edit Databases, New Database, New Response Spectra Curves Database.* The earthquake loading is then applied by right clicking the name of the load case, selecting *Edit Loads - RSA Loads*, and assigning a previously defined spectrum curve to the direction of interest.

Load combinations are created by right clicking the name of the load combination, selecting *Edit Load Combination*, and selecting the load cases and participation factors to be assigned. To run the analysis, select *Analysis - Eigenvalue / Response Spectra Analysis*. The number of mode shapes used in a linear response spectrum analysis can be specifed; 20 mode shapes are assigned for RSA in this example. Modal and spatial combination rules can be defined as CQC or SRSS. The modal damping ratio is 5% by default, unless changed by the user. An option for *Linear Static + Eigenvalue + RSA* will automatically perform the analyses sequentially. Results can be viewed from the *Results* menu. Nodal displacements and member forces in local coordinate system are accessible under *Results – Spreadsheets – Joint - Displacements* and *Results – Spreadsheets – Member - End Forces - Local.* For this example, the largest elastic demand moments for each column or footing for both the compression and tension models are listed in Tables 2D.1 and 2D.2.

2.5.3 Evaluation of Capacity/Demand Ratios

The most critical combinations of the unfactored nominal ultimate moment capacities (M_u) and elastic moment demands are used to calculate r_{ec} (column bending moment capacity/demand ratio) and r_{ef} (footing bending moment capacity/demand ratio) at each bent. These values are summarized in Table 2E.1-2E.2. The column values r_{ec} range from 0.7 to 1.0 and the footing values r_{ef} range from 0.25 to 0.5.

When r_{ec} and r_{ef} C/D ratios are less than 1, further evaluation is required to assess the ability of the columns or footings to form plastic hinges. C/D ratios should be evaluated for anchorage of longitudinal reinforcement (r_{ca}), splices in longitudinal reinforcement (r_{cs}), and column shear (r_{cv}). If plastic hinges may potentially form in the footing, C/D ratios should be

evaluated for footing rotation (r_{fr}). If plastic hinges may potentially form at the base or tops of the columns, C/D ratios should be evaluated for column transverse confinement reinforcement (r_{cc}). Sample calculations for all these C/D ratios are given in Appendix 2E, and the results are summarized in Tables 2E.3 – 2E.9. Only the C/D ratios for splice length are consistently below 1.0, and these values range from 0.3 to 0.5.

C/D ratios are also evaluated at the abutments based on assumed displacement capacities and the displacement demands calculated from the elastic demand analysis (Appendix 2E). These values are also greater than 1.0.

Like the first bridge example, this analysis suggests that the bridge will not remain elastic to the LL ground motion. However, checks of the detailing do not indicate the same concerns in the ability of the bridge to form plastic hinges. Only the splice length C/D ratio was well below 1.0. Therefore, we assume that the retrofit measures taken to address the deficiencies of the bridge in the UL motion will also be adequate to improve the response in the LL motion.

2.6 Evaluation of the Bridge for the UL Ground Motion

As described in Sec. 2.3, the bridge is evaluated for the UL ground motion using Method D1. The estimated inelasticity of the bridge is included in both the capacity analysis, through the evaluation of approximate displacement limit states, such as bearing failure and unseated beams, and the demand analysis, through an equivalent linear approximation of the nonlinear hysteretic behavior. The method considers the bridge as a single-degree-of-freedom (SDOF) system, and as such, is intended to be applied to bridges that satisfy certain assumptions, such as regular geometry and uniform distribution of weight and stiffness. While the bridge considered here does not strictly qualify for the method, it is a relatively simple highway bridge and appears to be a good candidate for the method according to our engineering judgment.

2.6.1 Bridge Capacity Evaluation

The capacity of a bridge to resist lateral loads may be expressed by a pushover curve. A pushover curve shows the total lateral load acting on the bridge plotted against the deflection of a reference degree of freedom, which assumes the bridge responds as a SDOF system. The response depends on the lateral load distribution, and a uniform distribution is usually assumed, wherein the design forces are proportional to the inertial forces that would be generated by ground acceleration. This distribution is expected to induce a response that is close to the first

mode response. The reference point is typically the center of mass of the bridge, or the degree of freedom where the displacement is maximized. A pushover curve is developed independently for the longitudinal and transverse directions. In most highway bridges, the center of mass is located within the superstructure. Limit states corresponding to specified failure modes are described as specific points on the bridge pushover curve.

The Retrofit Manual (FHWA, 2006) recommends using a simple bilinear curve characterized by initial stiffness, strength, and postyield stiffness for the capacity curve (Figure 2.6.1).

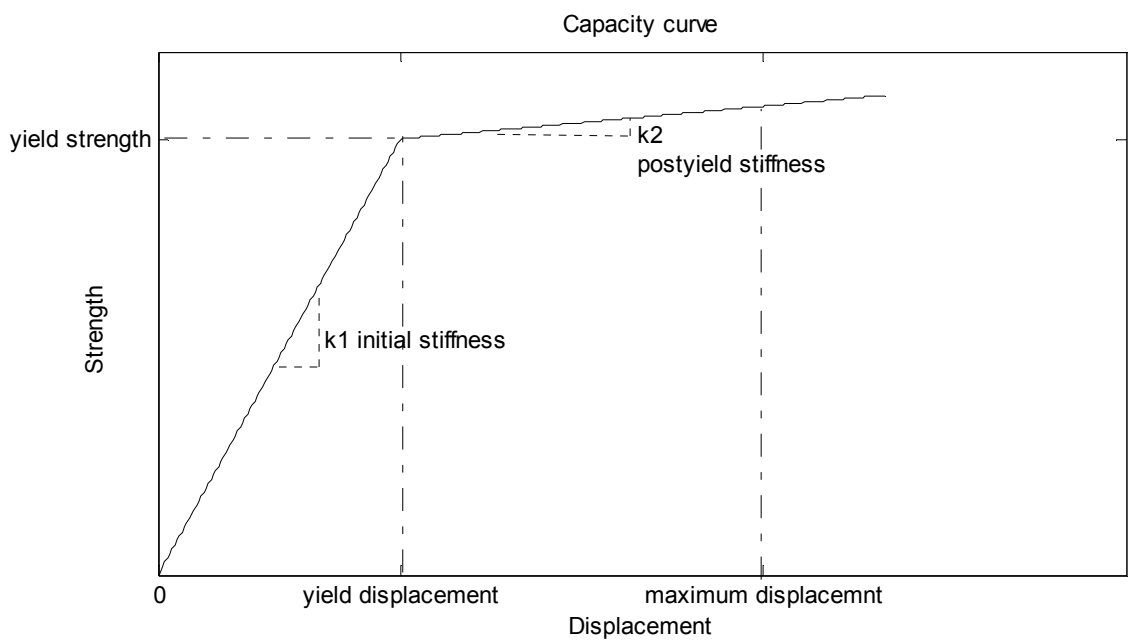

Figure 2.6.1. Capacity curve to be used in capacity spectrum method

2.6.1.1. Initial stiffness (k_1):

The uniform load method is used to calculate the initial stiffness. A uniform load is applied in the direction under consideration, and the induced response is used to estimate the stiffness in the fundamental degree of freedom. The equivalent stiffness is calculated using the maximum displacement that occurs when an arbitrary uniform lateral load is applied to the bridge. As before, the bridge is analyzed with closed hinges (compression model) and open hinges (tension model).

The following load cases and load combinations are defined in LARSA for the uniform load method.

Load Cases

7. Self Weight (Dead Load)
8. Longitudinal Uniform Loading
9. Transverse Uniform Loading

Load Combinations

5. 1.0* Dead Load + 1.0* Longitudinal Uniform Loading
6. 1.0* Dead Load + 1.0* Transverse Uniform Loading

Section 2.5.2 describes how to enter load cases and load combinations in LARSA. In this case, a uniform load is entered as *Analysis Type – Static*. In this case, a uniform load is entered by selecting *Edit load - Member loads*, entering the element number(s) of the superstructure over which the load is applied, a Magnitude (=10 kips), a type (=Uniform Force), and a direction (=global X for longitudinal and global Y for transverse) (Figure 2.6.2-2.6.3). The maximum displacement of the superstructure node of interest in the longitudinal or transverse direction is obtained under *Results – Spreadsheets – Joint - Displacements*.

Calculations of initial stiffness are described in Appendix 2F, and the result is summarized in Table 2F.1.

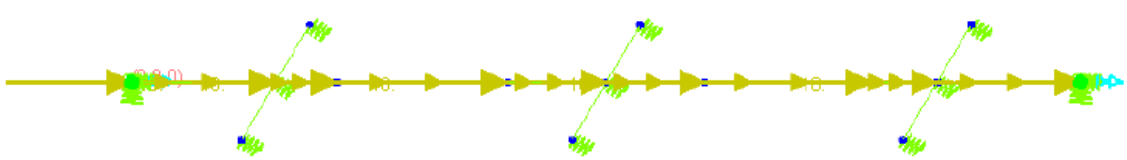

Figure 2.6.2. Longitudinal uniform loading of LARSA bridge model

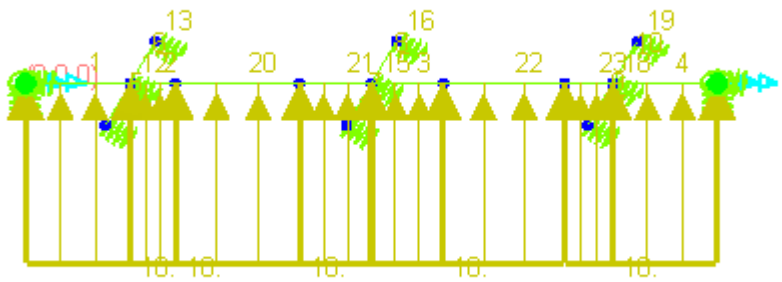

Figure 2.6.3. Transverse uniform loading of LARSA bridge model

2.6.1.2. Yield strength (F_y):

The yield strength F_y is calculated from the sum of the individual column lateral strengths (V_{ui}) in the direction under consideration, where

$$F_y = \sum V_{ui} = \sum \left(\frac{M_n}{H} \right)_i$$

where M_n is the column's nominal yield moment calculated from a moment interaction curve for column i, using column axial loads, dimensions and reinforcement details, and H is the clear height of column i. This summation is made over all of the columns supporting the superstructure (excluding abutments), and should include moment capacities at both the tops and bottom of the columns. For this bridge, the moment capacity at the tops of the column is zero in the longitudinal direction due to hinges. The column axial loads may be taken equal to the gravity load values when calculating M_n. Calculations of yield strength are described in Appendix 2F and summarized in Table 2F.3.

2.6.1.3. Post yield stiffness (k_2):

The post yield stiffnes k_2 is linearized to approximate actual behavior in this part of the capacity curve. In the absence of rigorous analysis, k_2 may be taken equal to five percent of the elastic stiffness, i.e., $k_2 = 0.05\ k_1$ (FHWA 2006). Calculations of post yield stiffness are described in Appendix 2F and summarized in Table 2F.1.

2.6.1.4. Limit states:

Limit states are identified as points along the capacity curve that characterize the behavior of the bridge under increasing load or deformation. A limit state may represent a particular deficiency that should be addressed by a retrofit procedure. A demand analysis

determines whether each limit state is reached. The following maximum displacement limit states Δ_{max} are identified in the Retrofit Manual (FHWA, 2006). The maximum capacity of the bridge is set to the lesser of the following three displacement limit states (Fig. 2.6.1).

1. Plastic hinge rotation

$$\Delta_{max} < \theta_p H$$

where $\theta_p = 0.035$ for reinforced concrete columns, and H is the clear height of the column in inches.

2. P-delta (P-Δ)

$$\Delta_{max} < 0.25\ C_c\ W'\ (H/P)$$

where W' is the seismic weight per column, and P is the axial load on the column due to gravity loads

3. Seat length

$$\Delta_{max} < N_0$$

where N_0 is the existing seat width at an abutment or pier cap.

For this bridge the plastic hinge rotation is the controlling limit state, and with a clear column height of 20', the displacement capacity $\Delta_{max} = 8.4$ inches. This limit state represents collapse due to insufficient column ductility. Because the bridge uses integral connections, the seat length limit state need not be considered.

2.6.2 Bridge Demand Evaluation

Because the bridge is assumed to be a SDOF system, the earthquake demand may be represented by a response spectrum. The resultant spectral acceleration, when scaled by seismic mass, gives the seismic forces acting through the center of mass of the bridge. In the capacity spectrum method, the response spectrum is reformatted so that it can be depicted graphically on the same plot as the capacity curve. A response spectrum is typically plotted as spectral acceleration vs. natural period (Figure 2.6.4); however, from this information the spectral displacement can also be determined, and thus the response spectrum can be plotted as spectral acceleration vs. spectral displacement. In this format, lines of constant period can be drawn extending from the origin (Figure 2.6.5).

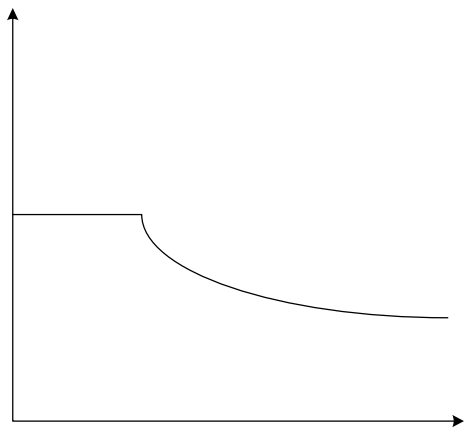

Figure 2.6.4. Response spectrum in spectral acceleration vs. natural period format

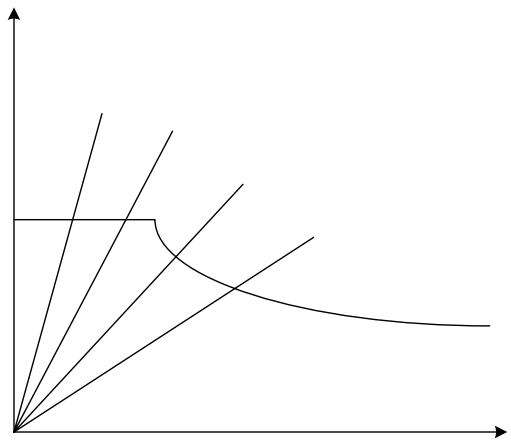

Figure 2.6.5. Response spectrum in spectral acceleration vs. spectral displacement format

Although the demand analysis is linear, in reality the bridge yields once it reaches its yield strength F_y. This yielding is accounted for by assuming equivalent, or effective linear properties in the demand analysis. The effective period is based on the secant stiffness, or period of the bridge (the slope of a line drawn from the origin to the current position on the capacity curve), and the effective damping is based on the hysteretic energy dissipated by the bridge as it yields. Given an effective damping ratio, the linear demand spectrum, typically defined for 5% damping, must be modified for damping ratios other than five percent. Two damping factors, B_S and B_L, are introduced to modify the spectrum in the short period (constant acceleration) and

long period (constant velocity) regions, respectively. A procedure for calculating the effective damping ratio ξ_{eff} and damping factors B_S and B_L is given in Table 5-4 (FHWA, 2006). The effective damping ratio depends on the displacement ductility factor μ, defined as follows:

$$\mu = \frac{\Delta}{\Delta_y},$$

where Δ is the current estimate of displacement, and Δ_y is the yield displacement. The theoretically calculated effective damping ratios used in original applications of the capacity spectrum method led to unconservative results, therefore, in this revision, the estimates of damping are entirely empirical.

At the start of the analysis, the final effective linear properties, and hence the intersection of the demand and capacity curves, are unknown. Iteration is required to determine the state of the bridge. An initial estimate for displacement is based on the elastic demand (assuming no yielding) and iteration is applied until the assumed value and the calculated value are in agreement. At each step of iteration, the displacement demand is computed from the demand spectrum, and the intersecting point on the capacity curve is determined. From this intersection point new estimates of ductility, effective period, and effective damping are calculated, which leads to a modified demand spectrum. The first few iterative steps are illustrated in Figure 2.6.6. This procedure can be completed by simple calculations with a spread sheet, and does not require LARSA analysis beyond determining the initial stiffness of the bridge. Basic steps in the method are listed below (Part C of Method D1, FHWA, 2006).

Step1. Start iteration by setting Δ equal to the displacement of the bridge assuming elastic behavior (see Table 2F.4 of Appendix 2F) and calculate ductility factor μ;

Step2. Calculate the appropriate damping factor using Table 5-4 (FHWA, 2006). This determines the effective damping ratio.

- B_L for $T > T_S$ (long period bridges), and
- B_S for $T < T_S$ (short period bridges)

Note that FHWA (2006) gives a separate procedure for long and short period bridges. At each iteration the period of the bridge should be re-assessed to determine if the effective period has shifted from the short period to the long period, or vice versa.

Step 3. Calculate the capacity coefficient C_c. This determines the effective period.

Step 4. Calculate spectral displacement demand S_d.

Step 5. Compare S_d with the assumed Δ (Step 1) and if in agreement, the procedure terminates. Otherwise set $\Delta = S_d$, recalculate μ, and repeat from Step 2.

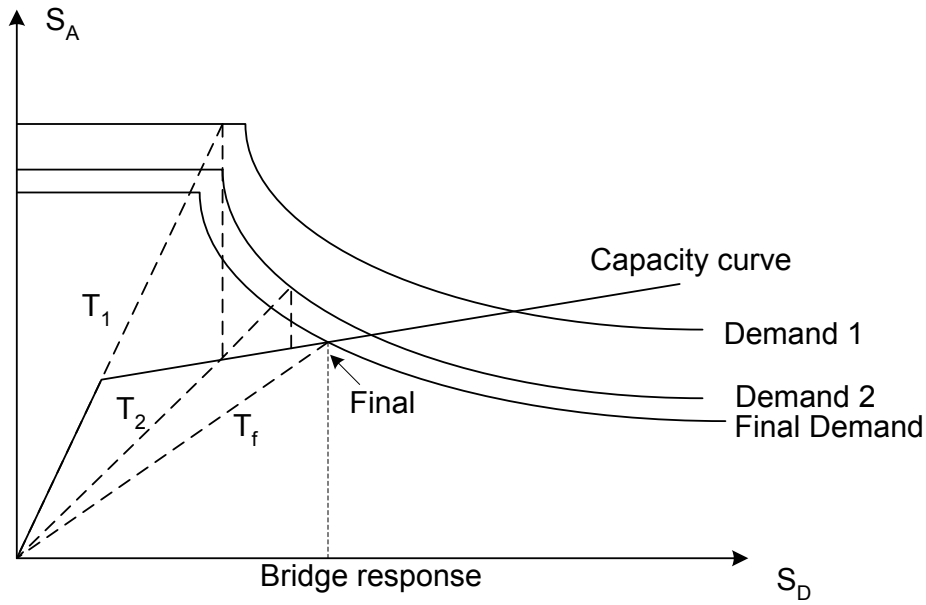

Figure 2.6.6. Illustration of iterative procedure

An initialization procedure (Part A) and capacity/demand ratio checks (Part B) are also described as part of the capacity spectrum method. Part A simply formalizes the steps needed to calculate the initial stiffness via the uniform load method, the elastic period of the structure, the initial elastic demand, and the capacity curve as characterized by yield strength and post-yield stiffness. This initialization procedure is followed step by step in Appendix 2F.

Part B evaluates the demands corresponding to limit points along the capacity curve. This part of the procedure is seen as redundant, and is not completed here. Our primary desire is to know the actual demand of the bridge under the upper level ground motion, and the iterative procedure in Part C is the best approach to determine this.

The results of the calculations from Appendix 2F are summarized in Table 2.6.1. Recall that the bridge capacity was estimated to be 8.4 inches. Therefore, for both tension and compression models, longitudinal and transverse directions, the displacement demand of the bridge during the UL ground motion is greater than the maximum displacement of capacity of

the bridge. Retrofit measures are needed to increase the capacity of the bridge. Retrofit measures will attempt to remedy the deficiencies found in both the UL and LL ground motions.

Table 2.6.1 Displacement response of bridge

model	Direction	Δ (in)
Tension	Transverse	11.32
	Longitude	14.74
Compression	Transverse	11.32
	Longitude	14.31

2.7 Proposed Retrofit Measures and Evaluation

The desired behavior of the bridge under the LL ground motion is elastic. Because capacity/demand ratios for column moments (r_{ec}) and footing moments (r_{ef}) are both less than 1, the bridge is not expected to remain elastic if the LL motion occurs. However, a footing retrofit is deemed to be impractical and achieving elastic response in the columns is also thought to be impractical. Inadequate splice length in the columns ($r_{cs} < 1$) is a deficiency that should be remedied.

Analysis to the UL ground motion indicated that the global demand exceeds the capacity determined by a plastic hinge rotation limit state (θp=0.035 for reinforced concrete columns). In our judgment, the preferred approach is to increase the ductility and overall displacement capacity of the columns. This can be done by applying a partial steel jacket. A steel jacket increases the volumetric ratio of transverse reinforcement, increasing the ultimate compression strain and allowing for a larger rotation capacity.

Adding a steel jacket will also address the inadequate splice length detected in the LL analysis. Additional confinement protects the flexural integrity of the lap splices by providing adequate clamping pressure at the splice location (Priestly et. al., 1996). As an indirect effect of providing a steel shell, column strength and stiffness will also be increased. However, this increase is not expected to be sufficient to keep the bridge elastic under the LL motion.

The steel jacket is the most widely used method for passive confinement and is the preferred method used by Caltrans for the seismic retrofits of bridge columns (Caltrans, 1995).

Section 9.2.1.3(a) of FHWA (2006) describes the construction and fabrication process. Application of the steel shell to circular columns is shown in Figure 2.7.1.

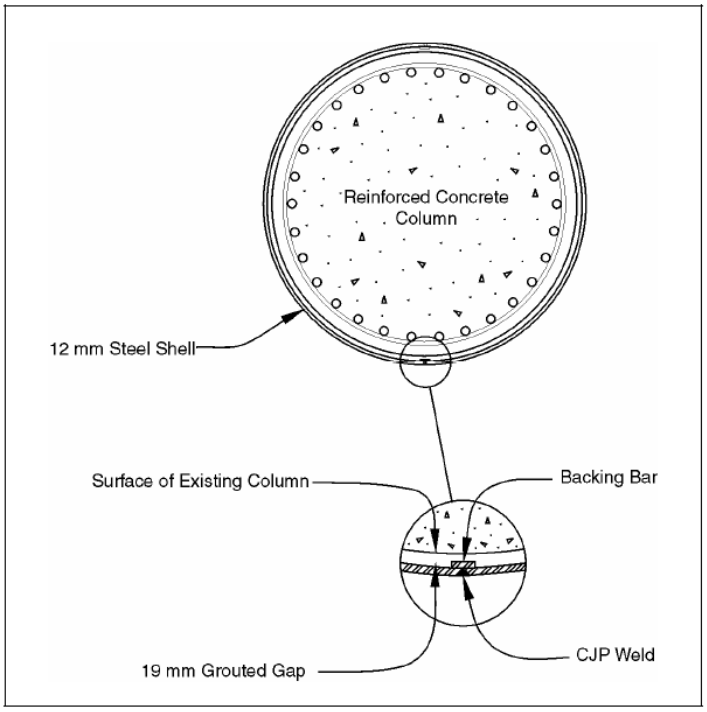

Figure 2.7.1. Typical steel shell retrofit of round column (Figure 9-9 of FHWA, 2006)

To design the steel shell, we need to determine the thickness of the steel shell (Priestly et. al., 1996) to meet the following conditions:

(1) develop adequate ductility or plastic rotation capacity;

(2) provide sufficient confinement to prevent lap splice failure.

The minimum shell thickness needed to provide the additional ductility capacity was found to be 6 mm, and calculations are presented in Appendix 2G. This shell thickness was also calculated to provide adequate splice length. According to FHWA (2006) and Caltrans (1995), practical constraints due to construction and fabrication procedures require that steel jackets have a minimum thickness of 10 mm (0.375 in). Therefore, if a 10 mm thick jacket is provided, the bridge will have about 50% reserve capacity relative to the displacement demands computed for the UL motion. The minimum length of the jacket needed to develop this flexural capacity was computed to be 32 inches. The jacket should be applied over both the top and bottom of the columns to develop the flexural strength and ductility capacity at each location.

Appendix 2. Detailed Analysis for Church Street Underpass

Appendix 2A. Determination of Seismic Retrofit Category

Bridge Importance:

Standard

Anticipated Service Life:

The bridge plans are approved on April 18, 1966, and the bridge is assumed to be constructed in 1967.

Bridge age: ~ 40 years

Anticipated Service Life: 75-40=35 years

Service life category: ASL2

Bridge Performance Level:

UL Motion: PL1

LL Motion: PL3

Site Class:

From Boring 1, N = 16.4

Site Class: D or E

Spectral Accelerations and Soil Factors:

The bridge is located in the Layton to Hill Field interchange. The exact location is

Latitude: 41° 03'48.58"N

Longitude: 111° 58'01.33"W

Summary of Definitions

Ss	0.2- second period spectral acceleration
S_1	1- second period spectral acceleration
F_a	Site coefficient for short period
F_v	Site coefficient for long period
$S_{DS}=F_a S_s$	Design earthquake response spectral acceleration at short period
$S_{D1}=F_v S_1$	Design earthquake response spectral acceleration at long period
SHL	Seismic hazard level

Determination of Seismic Hazard Level (SHL)

From Table 1-4 and 1-5 of (FHWA, 2006)

	S_s (g)	S_1 (g)	F_a	F_v	S_{DS} (g)	S_{D1} (g)	SHL
Lower Level: 500-year	0.5287	0.1805	1.6426	3.2585	0.868	0.588	IV
Upper Level: 2500-year	1.217	0.484	1.0132	2.4	1.233	1.162	IV

Seismic Retrofit Category (SRC)

From Table 1-6 of (FHWA, 2006)

UL: **SRC = C**

LL: **SRC = C**

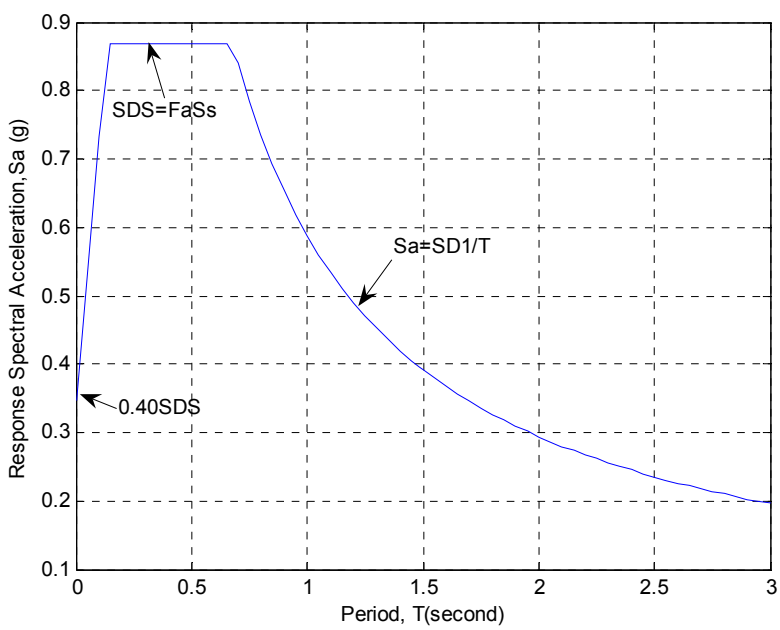

Figure 2A.1. The seismic design response spectrum (Lower Level ground motion)

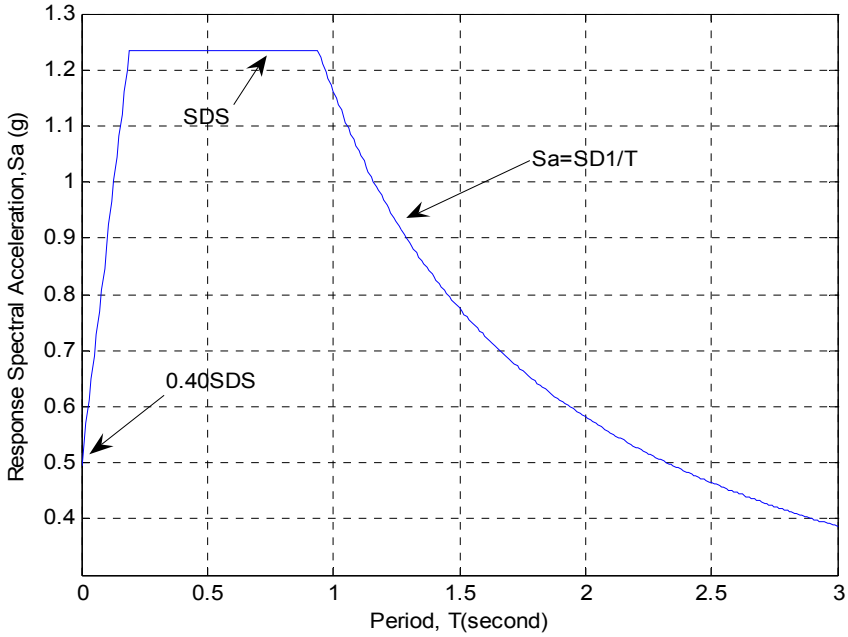

Figure 2A.2. The seismic design response spectrum (Upper Level ground motion)

Appendix 2B. Element Properties in LARSA Model

Pile Stiffness

Lpile: = 22 *ft*	Length of the pile
D: =1 *ft*	Diameter of the piles
H: = 3.0833 *ft*	Height of the footing
B: = 3 *ft*	Distance between two piles in the longitude direction
L: = 3 *ft*	Distance between two piles in the transverse direction
l: = 6 *ft*	Length of the footing
b: = 6 *ft*	Width of the footing
γ: = 50 lb/ft^3	Weight density of soil
G: = 12.85 *ksi*	Shear modulus
Z: = 5.53 *ft*	Embedment depth:
A=113.10 in^2	Area of pile

Elevation of the finished grade: 4352.87 *ft*

Elevation of the bottom of the footing: 4347.34 *ft*

Embedment depth: 4352.87-4347.34=5.53 *ft*

E: = 2.55e6 *psi*	Modulus of elasticity (Concrete type: FC-2)
I: = 1017.9 in^4	Moment of inertia of pile
EI=2.596e9 *psi*	Flexural stiffness of pile
φ=32°	Internal friction angle of the soil (sand)
f=8 lb/in^3	Coefficient of variation in subgrade stiffness (Fig. 6-12 of FHWA, 2006)

Single pile stiffness

K_δ=5e4 *lb/in*	Translational Stiffness - Fixed Head (Fig. 6-14 of FHWA, 2006)
K_θ=1e8 *lb.in/rad*	Rotational Stiffness (Fig. 6-15 of FHWA, 2006)
$K_{\delta\theta}$=1.7e6 *lb*	Cross-Coupling Stiffness (Fig. 6-16 of FHWA, 2006)
K_z= EA/Lpile	
$= 1.09\times10^6$ *lb/in*	Axial Stiffness

The Retrofit Manual (FHWA, 2006) suggests that axial stiffness EA/L be factored by a coefficient α, where α can take a lower bound value of 1 for an end-bearing pile on rock and an upper bound value of 2 for friction piles; α=1 is used in this example. Substituting these values in the appropriate positions give the following stiffness matrix for one pile. The DOFs corresponding to each column are indicated.

$$K_{pile} = \begin{array}{c} \begin{array}{cccccc} \delta_x & \delta_y & \delta_z & \theta_x & \theta_y & \theta_z \end{array} \\ \begin{bmatrix} 5\times10^4 & 0 & 0 & 0 & -1.7\times10^6 & 0 \\ 0 & 5\times10^4 & 0 & 1.7\times10^6 & 0 & 0 \\ 0 & 0 & 1.09\times10^6 & 0 & 0 & 0 \\ 0 & 1.7\times10^6 & 0 & 10^8 & 0 & 0 \\ -1.7\times10^6 & 0 & 0 & 0 & 10^8 & 0 \\ 0 & 0 & 0 & 0 & 0 & 0 \end{bmatrix} \end{array}$$

Pile Group Stiffness

As the next step, the individual pile stiffness matrices are assembled into a stiffness matrix for the pile group. Lateral and cross-coupling terms are simply added or multiplied by the number of piles. Rotational stiffnesses about the in-plane axes are modified by adding the summation of the vertical stiffness multiplied by the moment arm:

$$\left(k_{\theta\ xx}\right)_{pilegroup} = \sum_i \left(k_{\theta\ xx}\right)_{pile\ i} + \frac{L}{2}\sum_i \left(k_z\right)_{pile\ i}$$

$$\left(k_{\theta\ yy}\right)_{pilegroup} = \sum_i \left(k_{\theta\ yy}\right)_{pile\ i} + \frac{B}{2}\sum_i \left(k_z\right)_{pile\ i}$$

$$\left(k_{\theta\ xx}\right)_{pilegroup} = 4\times 1e8 + \frac{3}{2}\times 4\times 1.09e6 = 4e8 \qquad kip\text{-}in/rad$$

$$\left(k_{\theta\ yy}\right)_{pilegroup} = 4\times 1e8 + \frac{3}{2}\times 4\times 1.09e6 = 4e8 \qquad kip\text{-}in/rad$$

The torsional component of the stiffness matrix (the (6,6) entry) is zero for an individual pile but is determined from the summation of lateral stiffnesses multiplied by the appropriate moment arms. This is illustrated in Fig. 2B.1. For each pile the resistance against torsion is divided into two components: x and y. Taking the moment of these forces with respect to the centroid leads to:

$$k_{torsion} = \sum_i \left(k_\delta l\sin(\theta)\times l\sin(\theta) + k_\delta l\cos(\theta)\times l\cos(\theta)\right) = 4\times k_\delta \times l^2$$

$$k_{torsion} = 4\times k_\delta \times \left(\frac{L}{2\times\sin(\theta)}\right)^2$$

$$k_{torsion} = k_\delta \times \left(\frac{L}{\sin(\theta)}\right)^2$$

L = 3 *ft*

θ = 45°

$$k_{torsion} = 5e4 \quad (3\times 12)^2 \times 2 = 1.3e8 \quad kips.in$$

Thus, the pile group stiffness is

$$K_{pile\ group} = \begin{bmatrix} 2e5 & 0 & 0 & 0 & -6.8e6 & 0 \\ 0 & 2e5 & 0 & 6.8e6 & 0 & 0 \\ 0 & 0 & 5.35e6 & 0 & 0 & 0 \\ 0 & 6.8e6 & 0 & 2.14e9 & 0 & 0 \\ -6.8e6 & 0 & 0 & 0 & 2.14e9 & 0 \\ 0 & 0 & 0 & 0 & 0 & 1.3e8 \end{bmatrix}$$

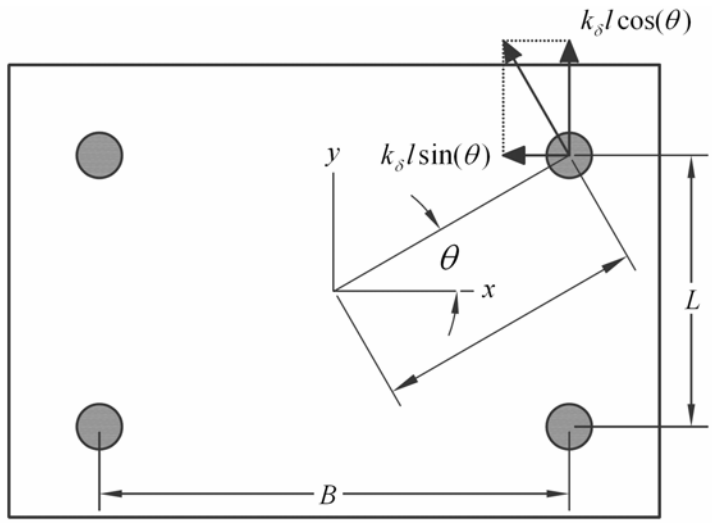

Figure 2B.1. Calculating rotational stiffness of pile group

Footing Stiffness

Shear modulus:

The shear modulus of the soil is developed using the relation proposed by Imai and Yoshimura:

$G = a.N^b.10^2 \quad kPa$

a=100 regression parameter

b=0.78 regression parameter

N=16.4 number of blow counts

G=1903.18 *ksf*

Poisson Ratio

ν = 0.4 FHWA Geotechnical Engineering Circular No.3 for sand and silty sand.

Stiffness components:

Given G, ν, B, and L, stiffness parameters are determined from Table 6-1 (FHWA, 2006). The derived stiffnesses are corrected for embedment by factors *e* defined in Table 6-2 (FHWA, 2006). Contributions to the lateral soil stiffness from the footing's base and side shear are neglected in the case of a pile-footing foundation. Thus, the lateral stiffness of the footing is determined from the passive pressure on the sides (Figure 6-6 of FHWA, 2006).

K_p=3

Z=5.53 ft Depth to the bottom of footing

Z_m=Z-H/2=3.99 *ft*	Mid depth
$K_p.\gamma.Z_m$=4.1545 *psi*	Average passive pressure
H=3'1"	
β=120.6-90=30.6	
L = 6 ft	
F_c= 4.1545×144×H×L=1.516 *kips*	Total force capacity on pile cap
Δ=0.02×Z=0.1106 ft=1.3272 *in*	Mobilization displacement of soil
$k_{footing}$=76.32717043/1.3272/12	
=4.79 *kips/in*	Lateral stiffness

Other stiffness components of the footing are found using the formulas in Tables 6-1 and 6-2 (FHWA, 2006).

k_z' =3.5e4 *kips/in*
e_z =2.948
k_z =1.51e4 *kips/in*

$k_{\theta x}'$ =3.6e6 *kip-in/rad*
$e_{\theta x}$ =3.79
$k_{\theta x}$ =2.11e7 *kip-in/rad*

$k_{\theta y}'$=3.72e6 *kip-in/rad*
$e_{\theta y}$= 3.80
$k_{\theta y}$ =9.06e6 *kip-in/rad*

R= 3.95 *ft*
$k_{\theta z}$ =7.05e6 *kips/rad*

Pile-Footing Stiffness

Finally, the stiffness matrices of the pile group and footing are assembled into a single matrix for the foundation stiffness.

$$K_{pile\ footing} = \begin{bmatrix} 2458 & 0 & 0 & 0 & -6800 & 0 \\ 0 & 2458 & 0 & 6800 & 0 & 0 \\ 0 & 0 & 64320 & 0 & 0 & 0 \\ 0 & 6800 & 0 & 1.38e7 & 0 & 0 \\ -6800 & 0 & 0 & 0 & 1.43e7 & 0 \\ 0 & 0 & 0 & 0 & 0 & 10800 \end{bmatrix}$$

The above stiffness matrix has the units of kips and feet. The footings are aligned in the direction of skew; thus the stiffness matrix should be applied in the local x-y coordinate system of the pile-footing foundation.

Abutment Stiffness

L: = $49 \times 12 + 6 + 1/4 = 594.25$ in	Width of the backwall
θ: = $30^{o}36'$	Skew angle
H: = 5.125 ft	Height of the abutment
C_p: = 40 kips	Capacity of the pile
D_g: = 0	Gap width

For cohesionless, non-plastic backfill (fines content less than 30 percent), the passive pressure, p_p, may be assumed equal to H/10 MPa (H in meters) or 2H/3 ksf (H in feet). Because the bridge has the $30^{o}36'$ skew angle, the total capacity of the abutment-pile system is

$$P_p = p_p.H.L + N_p.C_p$$

$$= \frac{2}{3} \times 5.125 \times 5.125 \times 594.25/12 \times \cos(30.6) + 4 \times 40 = 906.4\ kips$$

For integral or diaphragm abutments, an initial secant stiffness, K_{eff1} may be calculated as follows:

$$K_{eff\quad compression(longitude)} = \frac{P_p}{0.02H} = \frac{906.4}{0.02 \times 5.125} = 8842.7 kips/ft$$

In tension only piles contribute to the stiffness:

$$P_{p\quad tension} = 4 \times 40 = 160 \qquad kips$$

$$K_{eff\quad tension(longitude)} = \frac{P_p}{0.02H} = \frac{160}{0.02 \times 5.125} = 1560.98 \quad kips/ft$$

A similar procedure is applied in the transverse direction, but the transverse stiffness of the abutment is provided by wing walls. Priestley et al. (1996) proposed to take the effective width as the length of the wing walls multiplied by a factor of 8/9 to account for differences in participation of both wing walls.

$L = 9 + 2/12 + 9 + 7/12 = 18.75 \ ft$	Width of the wingwall
θ: = $30^o36'$	Skew angle
H: = 5.125 ft	Height of the abutment
C_p: = 40 kips	Capacity of the pile
D_g: = 0	Gap widths

Because the bridge has the $30^o36'$ skew angle,

$$P_{p \quad wingwall} = \frac{2}{3} \times 5.125^2 \times 18.75 \times \cos(30.6) = 245.62 \quad kips$$

$$P_{p \quad piles} = 4 \times 40 = 160 \quad kips$$

$$K_{eff \quad transverse} = \frac{245.62 + 160}{0.02 \times 5.125} = 3957.2 \quad kips / ft$$

Table 2B.1 Natural periods of bridge in tension and compression model

Tension Model		Compression Model	
Mode	Period (sec)	Mode	Period (sec)
1	1.4629	1	0.5647
2	0.5444	2	0.5153
3	0.5128	3	0.4015
4	0.3348	4	0.3342
5	0.3317	5	0.2024
6	0.3242	6	0.1927
7	0.1945	7	0.1914
8	0.1923	8	0.1338
9	0.1850	9	0.1009
10	0.1337	10	0.0996
11	0.1009	11	0.0829
12	0.0984	12	0.0808
13	0.0810	13	0.0804
14	0.0804	14	0.0788
15	0.0789	15	0.0733
16	0.0778	16	0.0707
17	0.0706	17	0.0683
18	0.0689	18	0.0560
19	0.0682	19	0.0528
20	0.0559	20	0.0455

The resistance of the backwall leads to torsional resistance about the vertical axis. In summary, the abutment stiffnesses, represented in their global coordinate system, are:

$K_{x,compression}$=8842.7 *kips/ft*

$K_{x,tension}$= 1560.2 *kips/ft*

K_y=3957.2 *kips/ft*

$K_{\theta z}= K_x \times \frac{l^2}{12}$

$K_{\theta z,tension}$=2.3607e5 *kips.ft/rad*

$K_{\theta z,compression}$=1.3373e6 *kips.ft/rad*

For boundary conditions, the abutment is assumed to be fully constrained in the vertical direction and for rotation around the longitudinal axis, but can rotate freely around the transverse axis.

Appendix 2C. Column and Footing Moment Capacities

Column Moment Capacities

Ultimate moment capacities for the columns are obtained from computer generated column interaction diagrams. Moment capacities depend on axial loads while axial loads in turn depend on moment capacities. Initially, the axial force due to dead load is distributed to the columns, with 40% to the middle column and 30% to each side column. This assumption is necessary because the spine model does not accurately distribute the dead loads to the columns. Because the elastic moment demands are primarily in the plane of the bent, moment capacities will be calculated for bending in this plane. This requires a consideration of the variation in axial load due to bent overturning as outlined in the iterative procedure presented in article 4.8.2 of Division I-A of the AASHTO Standard Specifications (AASHTO, 2002). The steps of this procedure are as follows.

Step 1. Overstrength Moment Capacities at Axial Load Corresponding to Dead Load

Table 2C.1 summarizes the overstrength column and footing moment capacities taken from the interaction diagrams.

Step 2. Axial Forces Due to Overturning in the Transverse Direction

Because the bents are symmetric, the axial forces in the middle columns due to overturning are zero. The axial loads due to overturning are calculated with the assistance Figs. 2C.1 and 2C.2. First, based on column equilibrium (Fig. 2C.1), the shear force sustained by each column is given by:

$$V_1 = \frac{M_{B1} + M_{T1}}{H}$$

$$V_2 = \frac{M_{B2} + M_{T2}}{H}$$

$$V_3 = \frac{M_{B3} + M_{T3}}{H}$$

where M_{Ti} and M_{Bi} are the overstrength moment capacities (i.e. 1.3Mn) at the top and bottom of the columns, and H is the column height. The overstrength capacities are used for conservatism, assuming that the column is acting in the negative slope region of the axial-moment interaction diagram (Fig. 2C.3). Next, based on equilibrium of the entire bent with the column shears viewed as applied loads, P is calculated by:

Table 2C.1 Column and footing overstrength moments

member	END	Axial force due to dead load (kip)	1.3Mn(kips-ft)	
			Column	Footing
B-2(C_1)	Top	204.253901	1137.6	
B-2(C_1)	Bottom	212.82469	1143.8	988.99185
B-2(C_2)	Top	272.338535	1171.8	
B-2(C_2)	Bottom	283.76626	1175.8	850.655799
B-2(C_3)	Top	204.253901	1137.6	
B-2(C_ 3)	Bottom	212.82469	1143.8	988.99185
B-3(C_1)	Top	305.052095	1179.1	
B-3(C_1)	Bottom	311.64564	1179.1	796.291001
B-3(C_2)	Top	406.736127	1195.9	
B-3(C_2)	Bottom	415.52752	1195.9	593.721335
B-3(C_3)	Top	305.052095	1179.1	
B-3(C_ 3)	Bottom	311.64564	1179.1	796.291001
B-4C_1)	Top	208.312088	1143.8	
B-4(C_1)	Bottom	216.88288	1143.8	981.078385
B-4(C_2)	Top	277.749451	1171.8	
B-4(C_2)	Bottom	289.17717	1175.8	840.104513
B-4(C_3)	Top	208.312088	1143.8	
B-4(C_ 3)	Bottom	216.88288	1143.8	981.078385

$$P = \frac{M_{T1} + M_{T2} + M_{T3}}{2L}$$

where L is the center to center distance of two adjacent columns in a bent. Based on this formula, the axial load P is computed as follows. In iteration 2, the moments computed from maximum and minimum axial load are averaged. However, the best approach would be to use the larger value for conservatism.

Iteration 1:

Bent 2: P= (1137.6+1171.8+1137.6)/(2*16.25)=106.06 kips

Bent 3: P= (1179.1+1195.9+1179.1)/(2*16.25)=109.36kips

Bent 4: P= (1143.8+1171.8+1143.8)/(2*16.25)=106.44kips

Iteration 2:

Bent 2: P= [(1082.7+1179.1)/2+(1082.7+1179.1)/2+(1179.1+1179.1)/2]/(2*16.25)=105.87 kips

Bent 3: P= [(1131.3+1197.6)/2+(1131.3+1195.9)/2+(1197.6+1195.9)/2]/(2*16.25)=108.46 kips

Bent 4: P= [(1082.7+1179.1)/2+(1082.7+1181.5)/2+(1179.1+1181.5)/2]/(2*16.25)=105.95 kips

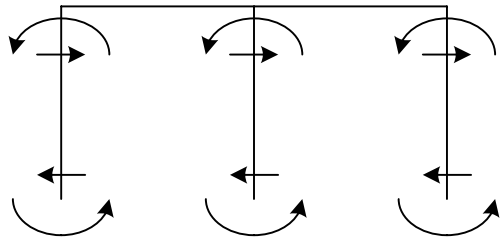

Figure 2C.1. Column moment and shear to satisfy equilibrium

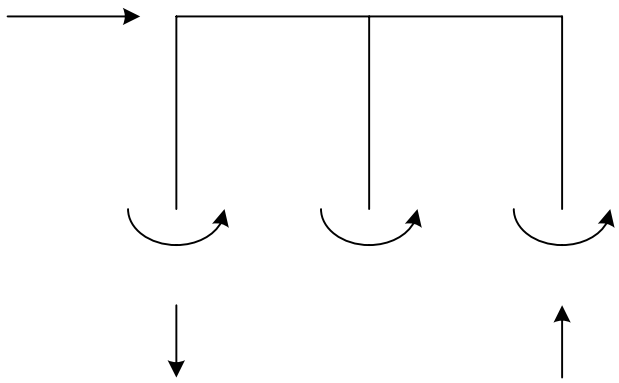

Figure 2C.2. Bent equilibrium to determine axial force due to overturning

Step 3. Revised Overstrength Moment Capacities

The axial loads due to overturning calculated in Step 2 are used to obtain new overstrength moment capacities from the interaction diagrams. Table 2C.2 summarizes these revised moment capacities. These moment capacities are used to calculate revised axial forces. These axial loads are used to recalculate the overstrength moments, which are summarized in Table 2C.3. The bent moments and axial forces are now within 10 percent of the previously calculated moments and forces, and no further iteration is needed.

Table 2C.2 Revised column and footing overstrength moments (iteration 1).

member	Axial load	END	Axial force due to dead load+overturning	1.3Mn(kips-ft) Column
B-2(C_1)	Min.	Top	98.1923624	1082.7
B-2(C_1)	Max.	Top	310.315439	1179.1
B-2(C_1)	Min.	Bottom	106.763154	1082.7
B-2(C_1)	Max.	Bottom	318.886231	1181.5
B-2(C_2)		Top	272.338535	1179.1
B-2(C_2)		Bottom	283.766257	1179.1
B-2(C_3)	Min.	Top	98.1923624	1082.7
B-2(C_ 3)	Max.	Top	310.315439	1179.1
B-2(C_3)	Min.	Bottom	106.763154	1082.7
B-2(C_ 3)	Max.	Bottom	318.886231	1181.5
B-3(C_1)	Min.	Top	195.695172	1131.3
B-3(C_1)	Max.	Top	414.409018	1195.9
B-3(C_1)	Min.	Bottom	202.288717	1137.6
B-3(C_1)	Max.	Bottom	421.002564	1197.6
B-3(C_2)		Top	406.736127	1197.6
B-3C_2)		Bottom	415.527521	1197.6
B-3(C_3)	Min.	Top	195.695172	1131.3
B-3(C_ 3)	Max.	Top	414.409018	1195.9
B-3(C_3)	Min.	Bottom	202.288717	1137.6
B-3(C_ 3)	Max.	Bottom	421.002564	1197.6
B-4(C_1)	Min.	Top	101.869011	1082.7
B-4(C_1)	Max.	Top	314.755165	1181.5
B-4(C_1)	Min.	Bottom	110.439803	1090.1
B-4(C_1)	Max.	Bottom	323.325957	1181.5
B-4(C_2)		Top	277.749451	1179.1
B-4(C_2)		Bottom	289.177173	1179.1
B-4(C_3)	Min.	Top	101.869011	1082.7
B-4(C_ 3)	Max.	Top	314.755165	1181.5
B-4(C_3)	Min.	Bottom	110.439803	1090.1
B-4(C_ 3)	Max.	Bottom	323.325957	1181.5

Table 2C.3 Revised column and footing overstrength moments (iteration 2)

member	Axial load	END	Axial force due to dead load+overturning	1.3Mn(kips-ft) Column
B-2(C_1)	Min.	Top	98.3800548	1082.7
B-2(C_1)	Max.	Top	310.127747	1179.1
B-2(C_1)	Min.	Bottom	106.950846	1082.7
B-2(C_1)	Max.	Bottom	318.698539	1181.5
B-2(C_2)		Top	272.338535	1179.1
B-2(C_2)		Bottom	283.766257	1179.1
B-2(C_3)	Min.	Top	98.3800548	1082.7
B-2(C_ 3)	Max.	Top	310.127747	1179.1
B-2(C_3)	Min.	Bottom	106.950846	1082.7
B-2(C_ 3)	Max.	Bottom	318.698539	1181.5
B-3(C_1)	Min.	Top	196.59671	1131.3
B-3(C_1)	Max.	Top	413.50748	1195.9
B-3(C_1)	Min.	Bottom	203.190256	1137.6
B-3(C_1)	Max.	Bottom	420.101025	1197.6
B-3(C_2)		Top	406.736127	1197.6
B-3C_2)		Bottom	415.527521	1197.6
B-3(C_3)	Min.	Top	196.59671	1131.3
B-3(C_ 3)	Max.	Top	413.50748	1195.9
B-3(C_3)	Min.	Bottom	203.190256	1137.6
B-3(C_ 3)	Max.	Bottom	420.101025	1197.6
B-4(C_1)	Min.	Top	102.364396	1082.7
B-4(C_1)	Max.	Top	314.25978	1181.5
B-4(C_1)	Min.	Bottom	110.935187	1090.1
B-4(C_1)	Max.	Bottom	322.830572	1181.5
B-4(C_2)		Top	277.749451	1179.1
B-4(C_2)		Bottom	289.177173	1179.1
B-4(C_3)	Min.	Top	102.364396	1082.7
B-4(C_ 3)	Max.	Top	314.25978	1181.5
B-4(C_3)	Min.	Bottom	110.935187	1090.1
B-4(C_ 3)	Max.	Bottom	322.830572	1181.5

Pile Footing Moment Capacities

The moment capacity of the footing also depends on the axial load that is transferred from the column. The converged axial load from the iterative procedure described before is used to find the moment capacity of footings. The results of the iterative calculations for the footings are also presented in Tables 2C.1-2C.3.

The process of computing the footing capacity is illustrated here for one pile-footing. Suppose the axial load transferred to the footing is 200 kips. We must identify the configuration

of axial loads in the piles that results in maximum moment and also satisfies vertical equilibrium (see Figure 2C.4). Since the axial load on the footing is large, half the piles are assumed to be at capacity in compression (2 x 180 kips), and the axial force in the remaining piles is found through equilibrium.

$P_2 = 360$ *kips* (compression)

$P_1 = P - P_2$

$= 200 - 360 = -160$ *kips* (tension)

Dividing P_1 by 2 to find the axial force in each pile leads to:

$$P_{1\ pile} = \frac{-160}{2} = -80 > -90 \qquad kips \text{ (okay)}$$

d = 3 ft Distance between piles

$$M = \frac{3}{2} \times 2 \times 180 + \frac{3}{2} \times 2 \times 80 = 780 \qquad kips.ft$$

This load pattern gives the maximum moment and satisfies both the equilibrium and capacity limits for axial loads. For the four pile configuration used in this bridge, the following equations can be used in general to find the ultimate moment capacity.

Axial load	Moment capacity
N ≥ 180 kips	(720- N)*d/2
N < 180 kips	(360+N)*d/2

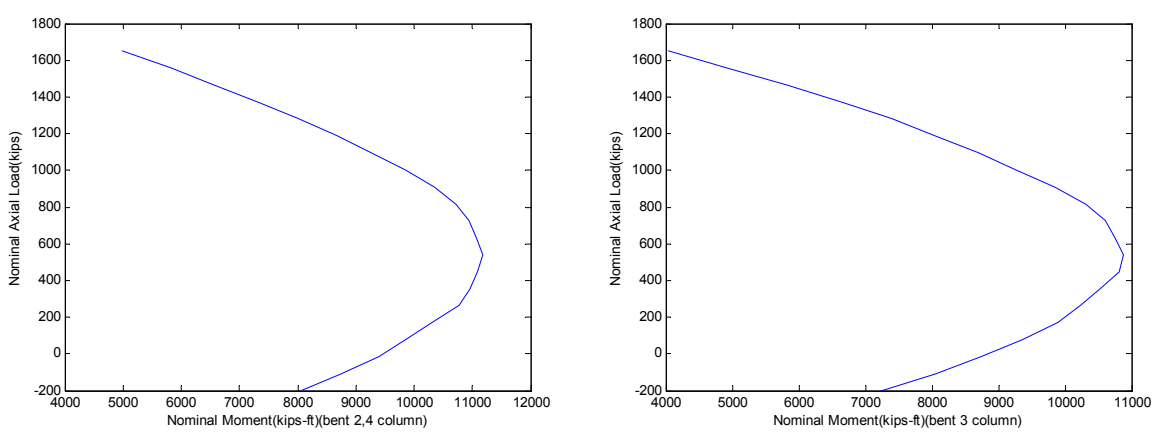

Figure 2C.3. Column interaction diagrams

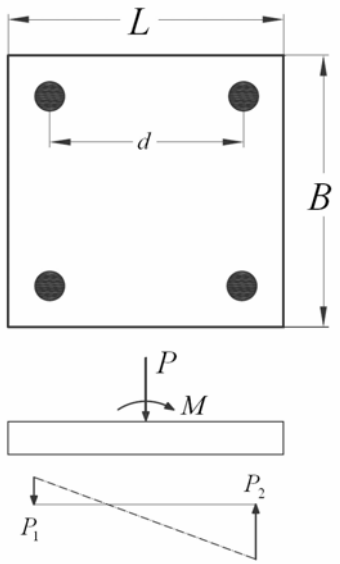

Figure 2C.4. Computing pile-footing moment capacity using statics

Appendix 2D. Elastic Moment Demands for LL Evaluation

Table 2D.1 Maximum elastic moment demands for compression model

Member		Moment Y (kips-ft)		Moment Z (kips-ft)		Elastic moment demand (kips-ft)
		EQ	DL	EQ	DL	
B-2(C_1)	Top	0	0	1064.34021	-33.771263	1098.11147
B-2(C_1)	Bottom	201.233932	9.54668617	1028.8739	-14.089016	1064.04893
B-2(C_1)	Footing	233.889964	11.0959292	1368.44993	-21.855816	1411.72524
B-2(C_2)	Top	0	0	1201.55347	-2.6843886	1204.23786
B-2(C_2	Bottom	186.978302	7.24805784	1117.76013	-2.8506444	1137.31807
B-2(C_2)	Footing	217.321272	8.42427776	1494.13866	-3.7488734	1514.80299
B-2(C_3)	Top	0	0	1099.00842	117.166237	1216.17466
B-2(C_3)	Bottom	179.307968	-3.3438151	1069.39551	39.6499977	1123.98559
B-2(C_3)	Footing	208.406191	-3.8864517	1421.19666	65.0982452	1501.3796
B-3(C_1)	Top	0	0	1319.44202	-89.290474	1408.73249
B-3(C_1)	Bottom	221.246979	8.80755424	1195.54321	-33.855293	1250.73809
B-3(C_1)	Footing	255.355889	10.1653856	1547.34437	-52.840265	1622.06424
B-3(C_2)	Top	0	0	1338.7644	1.12270176	1339.88711
B-3(C_2)	Bottom	245.994247	-0.1690946	1250.02747	1.18239248	1275.19508
B-3(C_2)	Footing	283.918363	-0.1430259	1649.11946	1.53776118	1674.92093
B-3(C_3)	Top	0	0	1327.09253	85.6146622	1412.70719
B-3(C_3)	Bottom	220.46701	-8.6384602	1203.28259	33.8855057	1258.20277
B-3(C_3)	Footing	254.455675	-9.9702227	1592.53418	52.3084485	1665.96169
B-4(C_1)	Top	0	0	1179.38367	-117.67763	1297.06129
B-4(C_1)	Bottom	177.260513	5.67428303	1148.95447	-38.196392	1201.1629
B-4(C_1)	Footing	206.026472	4.75345638	1526.76682	-63.491737	1604.1666
B-4(C_2)	Top	0	0	1299.255	5.59436989	1304.84937
B-4(C_2)	Bottom	186.780457	-4.9807386	1208.48584	5.63779068	1229.17393
B-4(C_2)	Footing	217.09132	-5.7890164	1615.44256	7.46055368	1638.13618
B-4(C_3)	Top	2.1083E-30	-7.889E-31	273.866699	99.1922302	373.058929
B-4(C_2)	Bottom	811.634888	9.98898983	242.597778	27.7769413	864.967216
B-4(C_2)	Footing	943.347564	11.61001	326.304114	48.3815879	1025.833

Table 2D.2 Maximum elastic moment demands for tension model

Member		Moment Y (kips-ft)		Moment Z (kips-ft)		elastic moment demand(kips-ft)
		EQ	DL	EQ	DL	
B-2(C_1)	Top	0	0	1036.97595	-33.771263	1070.74722
B-2(C_1)	Bottom	174.758179	9.54668617	999.04657	-14.089016	1029.76308
B-2(C_1)	Footing	203.117754	11.0959292	1329.41652	-21.855816	1368.14635
B-2(C_2)	Top	0	0	1163.96509	-2.6843886	1166.64948
B-2(C_2	Bottom	113.915604	7.24805784	1082.68909	-2.8506444	1092.28071
B-2(C_2)	Footing	132.401908	8.42427776	1447.2774	-3.7488734	1457.84404
B-2(C_3)	Top	0	0	1075.41357	117.166237	1192.57981
B-2(C_3)	Bottom	122.796371	-3.3438151	1039.5426	39.6499977	1086.53947
B-2(C_3)	Footing	142.723853	-3.8864517	1382.71947	65.0982452	1455.22188
B-3(C_1)	Top	0	0	1249.70679	-89.290474	1338.99726
B-3(C_1)	Bottom	873.362183	8.80755424	1169.90576	-33.855293	1492.40213
B-3(C_1)	Footing	1008.00552	10.1653856	1513.08263	-52.840265	1867.82936
B-3(C_2)	Top	0	0	1297.09277	1.12270176	1298.21548
B-3(C_2)	Bottom	873.404419	-0.1690946	1211.67065	1.18239248	1494.70505
B-3(C_2)	Footing	1008.05426	-0.1430259	1598.43447	1.53776118	1891.13006
B-3(C_3)	Top	0	0	1257.35291	85.6146622	1342.96757
B-3(C_3)	Bottom	865.02594	-8.6384602	1177.44556	33.8855057	1493.52349
B-3(C_3)	Footing	998.384094	-9.9702227	1552.39766	52.3084485	1895.22033
B-4(C_1)	Top	0	0	1151.85657	-117.67763	1269.53419
B-4(C_1)	Bottom	119.640495	5.67428303	1115.21326	-38.196392	1160.19723
B-4(C_1)	Footing	139.055839	4.75345638	1483.06295	-63.491737	1553.22649
B-4(C_2)	Top	0	0	1258.07605	5.59436989	1263.67042
B-4(C_2)	Bottom	100.873314	-4.9807386	1170.11194	5.63779068	1180.50519
B-4(C_2)	Footing	117.243107	-5.7890164	1564.15974	7.46055368	1576.42863
B-4(C_3)	Top	3.7532E-30	-7.889E-31	217.165787	99.1922302	316.358017
B-4(C_2)	Bottom	786.527344	9.98898983	179.986938	27.7769413	823.167115
B-4(C_2)	Footing	914.165539	11.61001	244.430374	48.3815879	970.978482

Appendix 2E. Capacity/Demand Ratios for LL Evaluation

Table 2E.1 Ultimate moment capacity/demand ratios for compression model

member	END	Axial load	Axial force due to dead load+overturning (k-ft)	Column			Footing		
				Demand (k-ft)	Capacity (k-ft)	r_{ec}	Demand (k-ft)	Capacity (k-ft)	r_{ef}
B-2(C_1)	Top	Min.	98.38	1098.111473	832.8462	0.758435			
		Max.	310.13	1098.111473	907	0.825964			
	Bottom	Min.	106.95	1064.048926	832.8462	0.782714	1411.725	700.4263	0.496149
		Max.	318.70	1064.048926	908.8462	0.854139	1411.725	601.9522	0.426395
B-2(C_2)	Top		272.34	1204.237855	907	0.753173			
	Bottom		283.77	1137.318069	907	0.79749	1514.803	654.3506	0.431971
B-2(C_3)	Top	Min.	98.38	1216.17466	832.8462	0.684808			
		Max.	310.13	1216.17466	907	0.745781			
	Bottom	Min.	106.95	1123.98559	832.8462	0.740976	1501.38	700.4263	0.466522
		Max.	318.70	1123.98559	908.8462	0.808592	1501.38	601.9522	0.400933
B-3(C_1)	Top	Min.	196.60	1408.732491	870.2308	0.61774			
		Max.	413.51	1408.732491	919.9231	0.653015			
	Bottom	Min.	203.19	1250.738092	875.0769	0.699648	1622.064	775.2146	0.477919
		Max.	420.10	1250.738092	921.2308	0.73655	1622.064	449.8485	0.277331
B-3(C_2)	Top		406.74	1339.887106	921.2308	0.687544			
	Bottom		415.53	1275.195083	921.2308	0.722423	1674.921	456.7087	0.272675
B-3(C_3)	Top	Min.	196.60	1412.707191	870.2308	0.616002			
		Max.	413.51	1412.707191	919.9231	0.651177			
	Bottom	Min.	203.19	1258.202774	875.0769	0.695498	1665.962	775.2146	0.465326
		Max.	420.10	1258.202774	921.2308	0.73218	1665.962	449.8485	0.270023
B-4(C_1)	Top	Min.	102.36	1297.061295	832.8462	0.642102			
		Max.	314.26	1297.061295	908.8462	0.700696			
	Bottom	Min.	110.94	1201.162896	838.5385	0.698106	1604.167	706.4028	0.440355
		Max.	322.83	1201.162896	908.8462	0.756639	1604.167	595.7541	0.371379
B-4(C_2)	Top		277.75	1304.849375	907	0.695099			
	Bottom		289.18	1229.173928	907	0.737894	1638.136	646.2342	0.394494
B-4(C_3)	Top	Min.	102.36	373.0589294	832.8462	2.232479			
		Max.	314.26	373.0589294	908.8462	2.4362			
	Bottom	Min.	110.94	864.9672162	838.5385	0.969445	1025.833	706.4028	0.688614
		Max.	322.83	864.9672162	908.8462	1.050729	1025.833	595.7541	0.580752

Table 2E.2 Ultimate moment capacity/demand ratios for tension model

member	END	Axial load	Axial force due to dead load+overturning	Column			Footing		
				Demand	Capacity	r_{ec}	Demand	Capacity	r_{ef}
B-2(C_1)	Top	Min.	98.38005476	1070.747215	832.8462	0.77781			
		Max.	310.1277471	1070.747215	907	0.84707			
	Bottom	Min.	106.9508464	1029.763079	832.8462	0.80877	1368.14	700.4263	0.5119
		Max.	318.6985387	1029.763079	908.8462	0.88257	1368.14	601.9522	0.4399
B-2(C_2)	Top		272.3385345	1166.649477	907	0.77744			
	Bottom		283.7662567	1092.280706	907	0.83037	1457.84	654.3506	0.4488
B-2(C_3)	Top	Min.	98.38005476	1192.579811	832.8462	0.69835			
		Max.	310.1277471	1192.579811	907	0.76053			
	Bottom	Min.	106.9508464	1086.539468	832.8462	0.76651	1455.22	700.4263	0.4813
		Max.	318.6985387	1086.539468	908.8462	0.83645	1455.22	601.9522	0.4136
B-3(C_1)	Top	Min.	196.5967104	1338.997261	870.2308	0.64991			
		Max.	413.5074796	1338.997261	919.9231	0.68702			
	Bottom	Min.	203.1902559	1492.402132	875.0769	0.58635	1867.82	775.2146	0.4150
		Max.	420.1010252	1492.402132	921.2308	0.61728	1867.82	449.8485	0.2408
B-3(C_2)	Top		406.7361267	1298.215475	921.2308	0.70961			
	Bottom		415.5275208	1494.705053	921.2308	0.61632	1891.13	456.7087	0.2415
B-3(C_3)	Top	Min.	196.5967104	1342.967567	870.2308	0.64799			
		Max.	413.5074796	1342.967567	919.9231	0.68499			
	Bottom	Min.	203.1902559	1493.523494	875.0769	0.58591	1895.22	775.2146	0.4090
		Max.	420.1010252	1493.523494	921.2308	0.61681	1895.22	449.8485	0.2373
B-4(C_1)	Top	Min.	102.3643957	1269.534195	832.8462	0.65602			
		Max.	314.2597803	1269.534195	908.8462	0.71588			
	Bottom	Min.	110.9351873	1160.19723	838.5385	0.72275	1553.22	706.4028	0.4547
		Max.	322.8305719	1160.19723	908.8462	0.78335	1553.22	595.7541	0.3835
B-4(C_2)	Top		277.7494507	1263.67042	907	0.71775			
	Bottom		289.1771729	1180.505191	907	0.76831	1576.42	646.2342	0.4099
B-4(C_3)	Top	Min.	102.3643957	316.358017	832.8462	2.63260			
		Max.	314.2597803	316.358017	908.8462	2.87284			
	Bottom	Min.	110.9351873	823.1671151	838.5385	1.01867	970.978	706.4028	0.7275
		Max.	322.8305719	823.1671151	908.8462	1.10408	970.978	595.7541	0.6135

C/D Ratios for Plastic Hinging at the Bottoms of the Columns

The calculations shown follow the procedure of Appendix D.5 of FHWA (2006).

Bent 2, Column 1

Because the compression model has the smallest C/D ratio

$r_{ec} = 0.7827$ and $r_{ef} = 0.426$ (Compression model)

Because r_{ec} exceeds 0.8 for both tension and compression model, the column falls under Case II of Figure D-3 (FHWA, 2006), and does not have to be evaluated for transverse reinforcement confinement.

1. Anchorage (Appendix D.5.1 of FHWA, 2006) - 90° standard hook

$L_a(c) = 22$ in Effective anchorage length, capacity

$L_a(d) = 1200 k_m d_b \left(\frac{f_y}{60000\sqrt{f_c'}} \right) > 15d_b$ Anchorage length, demand

$k_m = 0.7$ Given

$f_y = 36000$ *psi*, Yield strength of reinforcement

$f_c' = 2000$ *psi*, Concrete compression strength

$d_b = 1.375$ *in* (#11) Nominal bar diameter

$$L_a(d) = 1200 \times 0.7 \times 1.375 \times \left(\frac{36000}{60000 \times \sqrt{2000}} \right) = 15.5 \ in$$

$15d_b = 20.625$ in

$L_a(d) = 20.625$ in

$L_a(d) < L_a(c)$

Since the effective development length is sufficient, the C/D ratio depends on the reinforcing details at the anchorage. The large cover (20 in) in the footing has a confining effect equal to transverse steel with equivalent tensile strength. This capacity is sufficient to resist the weight of the overburden. Detail 5 is chosen.

r_{ca}= 1 C/D ratio for anchorage of column reinforcement

2. Splices (Appendix D.5.2 of FHWA, 2006)

$\frac{30 - 1.5 \times 2}{16 \times 2} \times 1.375 = 1.16 \ in < 4(1.375) \ in$ Clear spacing between splices

This indicates that $A_{tr}(c)$ is the area of transverse bars crossing the potential splitting crack along a row of spliced bars divided by the number of splices.

$s = 12$ *in* Spacing of transverse reinforcement

$L_s = 30$ *in* Splice length

$Ls < 1860 d_b / \sqrt{f_c'} = 1860 \times 1.375 / \sqrt{2000} = 64.88 \ in$

$f_{yt} = 36000$ psi Yield strength of transverse reinforcement

The splice length is inadequate.

$r_{cs}=\frac{L_S}{(1860/\sqrt{f_c'})d_b}r_{ec}=\frac{30}{(1860/\sqrt{2000})\times 1.375}r_{ec}$ =0.5246 r_{ec}

r_{cs}=0.5246*0.7827=0.4481 (compression model)

r_{cs} = 0.4102 C/D ratio for splices in column reinforcement

3. Footing Rotation (Appendix D.5.5 of FHWA, 2006)

Because anchorage or splice failures will not prevent footing rotation, the minimum C/D ratio for the footing is given by

$r_{fr} = \mu r_{ef}$ = 4(0.44) = 1.76 (tension model)

$r_{fr} = \mu r_{ef}$ = 4(0.426) = 1.704 (compression model)

where μ is a ductility factor, which is taken to be 4.

r_{fr} = 1.704 C/D ratio for footing rotation

Table 2E.3 C/D ratios for plastic hinging at column base (compression model)

member	END	Axial load	r_{ec}	r_{ef}	case	r_{ca}	r_{cs}	r_{fr}
B-2(C_1)	Bottom	Min.	0.782714	0.496149	2	1	0.41022	1.984597
B-2(C_1)	Bottom	Max.	0.854139	0.426395	2	1	0.447654	1.705579
B-2(C_2)	Bottom		0.79749	0.431971	2	1	0.417965	1.727883
B-2(C_3)	Bottom	Min.	0.740976	0.466522	2	1	0.388345	1.866087
B-2(C_3)	Bottom	Max.	0.808592	0.400933	2	1	0.423783	1.603731
B-3(C_1)	Bottom	Min.	0.699648	0.477919	2	1	0.366686	1.911674
B-3(C_1)	Bottom	Max.	0.73655	0.277331	2	1	0.386026	1.109323
B-3(C_2)	Bottom		0.722423	0.272675	2	1	0.378622	1.090699
B-3(C_3)	Bottom	Min.	0.695498	0.465326	2	1	0.36451	1.861302
B-3(C_3)	Bottom	Max.	0.73218	0.270023	2	1	0.383735	1.080093
B-4(C_1)	Bottom	Min.	0.698106	0.440355	2	1	0.365877	1.76142
B-4(C_1)	Bottom	Max.	0.756639	0.371379	2	1	0.396554	1.485517
B-4(C_2)	Bottom		0.737894	0.394494	2	1	0.38673	1.577974
B-4(C_3)	Bottom	Min.	0.969445	0.688614	2	1	0.508086	2.754455
B-4(C_3)	Bottom	Max.	1.050729	0.580752	2	1	0.550687	2.323006

Table 2E.4 C/D ratios for plastic hinging at the column base (tension model)

member	END	Axial load	r_{ec}	r_{ef}	case	r_{ca}	r_{cs}	r_{fr}
B-2(C_1)	Bottom	Min.	0.808775	0.511953	2	1	0.423879	2.047811
B-2(C_1)	Bottom	Max.	0.882578	0.439976	2	1	0.462559	1.759906
B-2(C_2)	Bottom		0.830373	0.448848	2	1	0.435198	1.795393
B-2(C_3)	Bottom	Min.	0.766513	0.481319	2	1	0.401729	1.925277
B-2(C_3)	Bottom	Max.	0.836459	0.41365	2	1	0.438388	1.654599
B-3(C_1)	Bottom	Min.	0.586355	0.415035	2	1	0.307308	1.66014
B-3(C_1)	Bottom	Max.	0.617281	0.24084	2	1	0.323517	0.963361
B-3(C_2)	Bottom		0.616329	0.2415	2	1	0.323018	0.966002
B-3(C_3)	Bottom	Min.	0.585914	0.409037	2	1	0.307078	1.636147
B-3(C_3)	Bottom	Max.	0.616817	0.237359	2	1	0.323274	0.949438
B-4(C_1)	Bottom	Min.	0.722755	0.454797	2	1	0.378796	1.819188
B-4(C_1)	Bottom	Max.	0.783355	0.383559	2	1	0.410556	1.534236
B-4(C_2)	Bottom		0.768315	0.409936	2	1	0.402674	1.639742
B-4(C_3)	Bottom	Min.	1.018673	0.727516	2	1	0.533887	2.910066
B-4(C_3)	Bottom	Max.	1.104085	0.613561	2	1	0.578651	2.454242

C/D Ratios for Plastic Hinging at the Tops of the Columns

Bent 2, Column 1

(r_{ec} = 0.7778) (Tension model)

(r_{ec} = 0.7584) (Compression model)

The top of the column need only be evaluated for column C/D ratios consistent with Case III of Figure D-3 (FHWA, 2006).

1. Anchorage (appendix D.5.1 of FHWA, 2006) – Straight anchorage

$L_a(c)$ = 45 in Effective anchorage length, capacity

$$L_a(d) = \frac{k_s d_b}{\left(1 + 2.5c/d_b + k_{tr}\right)\sqrt{f_c'}} \geq 30d_b$$ Anchorage length, demand

$$k_s = \frac{\left(f_y - 11000\right)}{4.8}\ psi$$ Constant for reinforcing steel with yield stress of f_y

$$= \frac{\left(36000 - 11000\right)}{4.8} = 5208.333\ psi$$

d_b = 1.375 *in* Nominal bar diameter

$A_{tr}(c)$ =2(1.56)/(32/2)= 0.195 in^2

$$k_{tr} = \frac{A_{tr}(c) f_{yt}}{600 s d_b} = \frac{0.195 \times 36000}{600 \times 12 \times 1.375} = 0.7091$$ Transverse reinforcement index

c = 1.5 *in* Lesser of clear cover or half clear spacing between adjacent bars

$$L_a(d) = \frac{5208.333 \times 1.375}{(1 + 2.5 \times 1.5 / 1.375 + 0.7091)\sqrt{2000}} = 42.96 \text{ in} > 30 d_b = 41.25 \text{ in}$$

$L_a(d)$ = 42.96 *in*

$L_a(d) < L_a(c)$

Since the effective development length is sufficient, the C/D ratio depends on the reinforcing details at the anchorage. The anchorage is in a bent cap, so the C/D ratios for anchorage should also be taken as 1.0. Detail 6 is chosen.

r_{ca}= 1 C/D ratio for anchorage of column reinforcement

2. Splices (Appendix D.5.2 of FHWA, 2006)

Because the clear spacing between splices = $\frac{30 - 1.5 \times 2}{16 \times 2} \times 1.375 = 1.16$ in < 4(1.375) in

L_s=30 in < $1860 d_b / \sqrt{f_c'} = 1860 \times 1.375 / \sqrt{2000} = 64.88 in$

The splice length is inadequate.

$$r_{cs} = \frac{L_S}{(1860/\sqrt{f_c'})d_b} r_{ec} = \frac{30}{(1860/\sqrt{2000}) \times 1.375} r_{ec} = 0.5246\ r_{ec}$$

r_{cs}=0.5246*0.7584=0.3979 (compression model)

r_{cs} = 0.3979 C/D ratio for splices in column reinforcement

3. Confinement (Appendix D.5.4 of FHWA, 2006)

$r_{cc} = \mu r_{ec}$

$$\mu = 2 + 4\left(\frac{k_1 + k_2}{2}\right) k_3$$ Ductility

$$k_1 = \frac{\rho(c)}{\rho(d)\left(0.5 + \frac{1.25P_c}{f_c' A_g}\right)} \leq 1$$

$$\rho(c) = \frac{0.2 \times 27}{15^2 \times 12} = 0.002$$ Volumetric ratio of existing transverse reinforcement

$$\rho(d) = 0.45\left(\frac{15^2}{13.5^2} - 1\right)\frac{2000}{36000} = 0.005864$$ Required vol. ratio of transverse reinforcement

$P_c = 98.38$ *kips* Axial compressive load on column

$f_c' = 2000$ *psi* Compressive strength of concrete

$A_g = \pi 15^2$ in^2 Gross area of column

$$\frac{P_c}{f_c' A_g} = \frac{98.38 \times 1000}{2000 \times \pi \times 15^2} = 0.06959$$

$$k_1 = \frac{0.002}{0.005864(0.5 + 1.25 \times 0.06959)} = 0.581$$

$s = 12$ *in* Spacing of transverse steel

$d_b = 1.375$ *in* Diameter of longitudinal reinforcement

$b_{min} = 30$ *in* Minimum width of the column cross section

$k_2 = 6d_b / s = 6 \times 1.375 / 12 = 0.685$ OR

$k_2 = 0.2b_{min} / s = 0.2 \times 30 / 12 = 0.5$

Choosing the smaller, k_2=0.5

k_3 =0.35 Effectiveness of transverse bar anchorage

Because transverse steel is poorly anchored, an iterative solution for μ may be required. The value chosen corresponds to μ = 2.7. (Figure D-4 of FHWA, 2006)

$$\mu = 2 + 4\left(\frac{0.581 + 0.5}{2}\right)0.35 = 2.757$$ (The value is assumed to be converged.)

$r_{cc} = \mu r_{ec}$ = 2.757(0.778)=2.144 (tension)

$r_{cc} = \mu r_{ec}$ = 2.757(0.758)=2.091 (compression)

r_{cc} = 2.091 C/D ratio for transverse confinement reinforcement

Table 2E.5 C/D ratios for plastic hinging at the column top (tension model)

member	END	Axial load	**Axial force due to dead load+overturning(kips)**	r_{ec}	$\mathbf{r_{cc}}$	r_{ca}	r_{cs}
B-2(C_1)	Top	Min.	98.38	0.777818	2.144222	1	0.583363
B-2(C_1)	Top	Max.	310.1277471	0.847072	2.251823	1	0.635304
B-2(C_2)	Top		272.3385345	0.77744	2.077529	1	0.58308
B-2(C_3)	Top	Min.	98.38	0.698357	1.925171	1	0.523768
B-2(C_3)	Top	Max.	310.1277471	0.760536	2.021779	1	0.570402
B-3(C_1)	Top	Min.	196.5967104	0.649912	1.757557	1	0.487434
B-3(C_1)	Top	Max.	413.5074796	0.687024	1.803986	1	0.515268
B-3(C_2)	Top		406.7361267	0.709613	1.864664	1	0.53221
B-3(C_3)	Top	Min.	196.5967104	0.647991	1.752361	1	0.485993
B-3(C_3)	Top	Max.	413.5074796	0.684993	1.798653	1	0.513745
B-4(C_1)	Top	Min.	102.3643957	0.656025	1.806883	1	0.492019
B-4(C_1)	Top	Max.	314.2597803	0.715889	1.902056	1	0.536917
B-4(C_2)	Top		277.7494507	0.71775	1.916538	1	0.538313
B-4(C_3)	Top	Min.	102.3643957	2.632606	7.25096	1	1.974455
B-4(C_3)	Top	Max.	314.2597803	2.872841	7.632886	1	2.15463

Table 2E.6 C/D ratios for plastic hinging at column top (compression model)

member	END	Axial load	Axial force due to dead load+overturning(kips)	r_{ec}	$\mathbf{r_{cc}}$	r_{ca}	r_{cs}
B-2(C_1)	Top	Min.	98.38	0.758435	2.09079	1	0.568826
B-2(C_1)	Top	Max.	310.1277471	0.825964	2.195709	1	0.619473
B-2(C_2)	Top		272.3385345	0.753173	2.012682	1	0.56488
B-2(C_3)	Top	Min.	98.38	0.684808	1.887821	1	0.513606
B-2(C_3)	Top	Max.	310.1277471	0.745781	1.982555	1	0.559336
B-3(C_1)	Top	Min.	196.5967104	0.61774	1.670554	1	0.463305
B-3(C_1)	Top	Max.	413.5074796	0.653015	1.714685	1	0.489761
B-3(C_2)	Top		406.7361267	0.687544	1.806671	1	0.515658
B-3(C_3)	Top	Min.	196.5967104	0.616002	1.665854	1	0.462002
B-3(C_3)	Top	Max.	413.5074796	0.651177	1.709861	1	0.488383
B-4(C_1)	Top	Min.	102.3643957	0.642102	1.768536	1	0.481577
B-4(C_1)	Top	Max.	314.2597803	0.700696	1.861689	1	0.525522
B-4(C_2)	Top		277.7494507	0.695099	1.856055	1	0.521325
B-4(C_3)	Top	Min.	102.3643957	2.232479	6.148892	1	1.674359
B-4(C_3)	Top	Max.	314.2597803	2.4362	6.47277	1	1.82715

C/D Ratios for Column Shear

Following Appendix D.5.3 of FHWA (2006)

Bent 2, Column 1

$V_u(d) = \frac{1.3\sum M_u}{L_c}$ Maximum column shear force with plastic hinging

$= \frac{1181.5 + 782.5378496}{22.0833} = 88.94\ kips$

$V_e(d)$=107.147 *kips* Maximum calculated elastic shear force

$V_i(c) = v_c db + \frac{A_{tr} f_{yt} d}{s}$ Initial shear resistance of undamaged column

(Article 8.16.6 of Division I, AASHTO, 2002)

$v_c = 2\sqrt{f_c'} = 2\sqrt{2000} = 89.44\ psi$ Allowable shear stress

d=28.5 *in* Distance from the extreme compression fiber to the centroid of the longitudinal tension reinforcement

b=30 in Column diameter

f_{ty}=36000 *psi* Yield stress of transverse reinforcement

s=12 *in* Spacing of transverse reinforcement

A_{tr}=0.2 in^2 Area of transverse reinforcement

$V_i(c) = 89.44 \times 28.5 \times 30 + \frac{0.2 \times 36000 \times 28.5}{12} = 110.67\ kips$

Because column axial stress is greater than $0.10f_c$', an allowable shear stress of $2\sqrt{f_c'}\ psi$ may be assumed for the core of the concrete column.

$V_f(c) = 89.44 \times 28.5 \times 30 / 1000 = 76.47\ kips$ Final shear resistance of damaged column

Since $V_i(c) > V_u(d) > V_f(c)$, Case B applies

$r_{cv} = \mu r_{ec}$

L_c = 22.08 *ft* Height of the column

b_c = 30 *in* Width of the column in the direction of shear

$$\mu = 2 + \left(0.75\frac{L_c}{b_c}\right)\left(\frac{V_i(c) - V_u(d)}{V_i(c) - V_f(c)}\right)$$

$$= 2 + (0.75*4)\left(\frac{110.67 - 88.94}{110.67 - 76.47}\right) = 3.906$$

Note that the column height-to-width ratio in the above formula was revised to the maximum allowed value of 4.

r_{cv}=3.906*0.854139=3.336

r_{cv} = 3.336 C/D ratio for column shear

Table 2E.7 C/D ratios for column shear (compression model)

member	shear (kips)	$V_e(d)$	$V_u(d)$	V_i	$\mathbf{r_{ec}}$	case	μ	r_{cv}
B-2(C_1)	110.1327667	110.1328	88.9377	110.6735	0.854139	B	3.906652	3.336825
B-2(C_2)	122.0687103	122.0687	91.91361	110.6735	0.79749	B	3.645607	2.907336
B-2(C_3)	114.0976715	114.0977	88.9377	110.6735	0.808592	B	3.906652	3.158889
B-3(C_1)	125.4754105	125.4754	77.21613	110.6735	0.73655	B	4.93486	3.634769
B-3(C_2)	129.4352417	129.4352	77.60248	110.6735	0.722423	B	4.900969	3.540575
B-3(C_3)	126.2437592	126.2438	77.21613	110.6735	0.73218	B	4.93486	3.613205
B-4(C_1)	122.5337372	122.5337	88.57283	110.6735	0.756639	B	3.938657	2.98014
B-4(C_2)	131.9859619	131.986	91.43581	110.6735	0.737894	B	3.687518	2.720998
B-4(C_3)	42.71762466	42.71762	88.57283	110.6735	1.050729	B	3.938657	4.138462

Table 2E.8 C/D ratios for column shear (tension model)

member	shear (kips)	$V_e(d)$	$V_u(d)$	V_i	$\mathbf{r_{ec}}$	case	μ	r_{cv}
B-2(C_1)	107.1470108	107.147	88.9377	110.6735	0.882578	B	3.906652	3.447924
B-2(C_2)	118.2448578	118.2449	91.91361	110.6735	0.830373	B	3.645607	3.027212
B-2(C_3)	111.3006058	111.3006	88.9377	110.6735	0.836459	B	3.906652	3.267755
B-3(C_1)	120.8454056	120.8454	77.21613	110.6735	0.617281	B	4.93486	3.046193
B-3(C_2)	125.4369125	125.4369	77.60248	110.6735	0.616329	B	4.900969	3.020611
B-3(C_3)	121.6060867	121.6061	77.21613	110.6735	0.616817	B	4.93486	3.043906
B-4(C_1)	119.3026047	119.3026	88.57283	110.6735	0.783355	B	3.938657	3.085366
B-4(C_2)	127.7992859	127.7993	91.43581	110.6735	0.768315	B	3.687518	2.833176
B-4(C_3)	41.39617157	41.39617	88.57283	110.6735	1.104085	B	3.938657	4.348611

Capacity/Demand Ratio for Abutments

Calculations based on Appendix D.6 of FHWA (2006)

Abutment C/D ratios are based on the displacements from the analysis.

Transverse Displacement

D(c) = 75 *mm* = 3 *in* Assumed transverse displacement capacity

Abutment 1:

D(d) = 1.7041 *in* (tension model) Transverse displacement demand

D(d) = 1.7588 *in* (compression model)

r_{ad} = 3/1.7588=1.71

Abutment 5:

D(d) = 1.9245 *in* (tension model)

D(d) = 1.9871 *in* (compression model)

r_{ad} = 3/1.9871=1.51

Longitudinal Displacement

D(c) = 150 *mm* = 6 *in* Assumed longitudinal displacement capacity

Abutment 1:

D(d) = 0.8493 *in* (tension model) Longitudinal displacement demand

d(d) = 1.2617 *in* (compression model)

r_{ad} = 6/1.2617=4.76

Abutment 5:

D(d) = 0.8128 *in* (tension model)

d(d) = 1.2601 in (compression model)

r_{ad} = 6/1.2601=4.76

Table 2E.9 C/D ratios for abutment displacement

Abutment	Direction	r_{ad}
1	Transverse	1.71
	Longitudinal	4.76
5	Transverse	1.51
	Longitudinal	4.76

Table 2E.10 Summary minimum C/D ratios for the bridge from tension or compression model

Member	End	r_{ca}	r_{cs}	r_{cc}	r_{fr}	r_{cv}
B-2 (C-1)	top	1	0.568826	2.09079		
B-2 (C-1)	bottom	1	0.41022		1.705579	3.336825
B-2 (C-2)	top	1	0.56488	2.012682		
B-2 (C-2)	bottom	1	0.417965		1.727883	2.907336
B-2 (C-3)	top	1	0.513606	1.887821		
B-2 (C-3)	bottom	1	0.388345		1.603731	3.158889
B-3 (C-1)	top	1	0.463305	1.670554		
B-3 (C-1)	bottom	1	0.366686		0.963361	3.634769
B-3 (C-2)	top	1	0.515658	1.806671		
B-3 (C-2)	bottom	1	0.378622		0.966002	3.540575
B-3 (C-3)	top	1	0.462002	1.665854		
B-3 (C-3)	bottom	1	0.36451		0.949438	3.613205
B-4 (C-1)	top	1	0.481577	1.768536		
B-4 (C-1)	bottom	1	0.365877		1.485517	2.98014
B-4 (C-2)	top	1	0.521325	1.856055		
B-4 (C-2)	bottom	1	0.38673		1.577974	2.720998
B-4 (C-3)	top	1	1.674359	6.148892		
B-4 (C-3)	bottom	1	0.508086		2.323006	4.138462

From these tables, we find that the C/D ratios of footing rotation during the middle bent are less than 1.0, but close to 1(in 5% range), so they are acceptable. Only the C/D ratios of splices are well less than 1.0.

Appendix 2F. Capacity Spectrum Evaluation for Upper Level Ground Motion (Method D1)

Part A: Initialization and Calculation of Bridge Capacity (FHWA, 2006)

Step A1

Recall from Appendix 2A:

S_{D1} = 1.161g

S_{DS} = 1.233g

Step A2

$$T_s = \frac{S_{D1}}{S_{DS}} = \frac{1.1616}{1.233} = 0.9421 \quad \text{sec}$$

Step A3

Initial stiffness k1

The weight of seismic mass, taken as the weight of the superstructure, is determined from LARSA file "ChurchSt_SuperstructureMass.lar"

W= 2573.238 kips

In the transverse direction, assumed uniform load P_0=10 kips/ft.

$V_{s,\,max}$=2.5240 in (tension model)

$V_{s,\,max}$= 2.5231 in (compression model)

L= 231 ft

$$K_{transverse} = \frac{P_0 L}{V_{s,\max}} = \frac{10 \times 231 \times 12}{2.524} = 10982.57 \text{ kips/ft (tension model)}$$

$$K_{transverse} = \frac{P_0 L}{V_{s,\max}} = \frac{10 \times 231 \times 12}{2.5231} = 10986.48 \text{ kips/ft (compression model)}$$

In the longitudinal direction, assumed uniform load P_0=10 kips/ft.

$V_{s,\,max}$=9.8544 in (tension model)

$V_{s,\,max}$= 5.1447 in (compression model)

L= 231 ft

$$K_{longitude} = \frac{P_0 L}{V_{s,\max}} = \frac{10 \times 231 \times 12}{9.8544} = 2812.957 \text{ kips/ft (tension model)}$$

$$K_{longitude} = \frac{P_0 L}{V_{s,\max}} = \frac{10 \times 231 \times 12}{5.1447} = 5388.069 \text{ kips/ft (compression model)}$$

Step A4

Calculate the elastic period of the bridge T:

K_2=0.05 K_1 post-yield stiffness

$$T=2\pi\sqrt{\frac{W}{gK_1}}$$ natural period

Table 2F.1 Stiffness and natural period of the bridge

model	Direction	Stiffness K_1 (kips/ft)	post-yield stiffness K_2 (kips/ft)	Period (T)
Tension	Transverse	10982.57	549.1285	0.535969
	Longitude	2812.957	140.6479	1.059035
Compression	Transverse	10986.48	549.324	0.535874
	Longitude	5388.069	269.4035	0.765201

Compare with T_S (=0.942 sec) and determine whether bridge falls in the short or long period portion of the spectrum, in both directions.

Step A5

$F_{el}= F_aS_sW$ (for short period)

$F_{el}= F_vS_1W/T$ (for long period)

$\Delta_{el}= F_{el}/K$

Table 2F.2 Elastic bridge response

model	Direction	Period	F_{el} (kips)	Δ_{el} (in)
Tension	Transverse	short	3172.968171	3.466913304
	Longitude	long	2989.073261	12.7513073
Compression	Transverse	short	3172.968171	3.465679458
	Longitude	short	3172.968171	7.066653758

Step A6

$$C_C=\frac{F}{W}$$ Seismic capacity coefficient

$$F_y=\Sigma V_{ui}=\Sigma\left(\frac{M_n}{H}\right)_i$$ yield force

Table 2F.3 Nominal yield moment of the columns

member	END	Height of column(ft)	Axial force due to dead load (kip)	M_n (kips-ft)	V_{ui} (kips)
B-2(C_1)	Top	19	204.253901	875.0769231	46.05668016
	Bottom		212.82469	879.8461538	46.30769231
B-2(C_2)	Top	19	272.338535	901.3846154	47.44129555
	Bottom		283.76626	904.4615385	45.22307692
B-2(C_3)	Top	19	204.253901	875.0769231	43.75384615
	Bottom		212.82469	879.8461538	43.99230769
B-3(C_1)	Top	20	305.052095	907	47.73684211
	Bottom		311.64564	907	47.73684211
B-3(C_2)	Top	20	406.736127	919.9230769	48.41700405
	Bottom		415.52752	919.9230769	48.41700405
B-3(C_3)	Top	20	305.052095	907	47.73684211
	Bottom		311.64564	907	47.73684211
B-4C_1)	Top	19	208.312088	879.8461538	46.30769231
	Bottom		216.88288	879.8461538	46.30769231
B-4(C_2)	Top	19	277.749451	901.3846154	47.44129555
	Bottom		289.17717	904.4615385	47.60323887
B-4(C_3)	Top	19	208.312088	879.8461538	46.30769231
	Bottom		216.88288	879.8461538	46.30769231

The yield force in the transverse direction is a summation of moments at the top and bottom while the yield force in the longitudinal direction considers only the nominal moments of the bottom of columns due to the hinges at the top.

F_y = 840.83 kips (in the transverse direction)

F_y = 420.42 kips (in the longitudinal direction)

<u>Step A7</u>

model	Direction	F_y (kips)	Δ_y (in)	Δel (in)
Tension	Transverse	840.83	0.918725	3.466913304
	Longitude	420.42	1.793501	12.7513073
Compression	Transverse	840.83	0.918398	3.465679458
	Longitude	420.42	0.936335	7.066653758

<u>Step A8</u>

$\Delta_{el} > \Delta_{y,}$ indicating that the bridge yields, and iteration is needed to determine the bridge response.

Part C: Bridge Response

The iterative procedure described in Part C, with steps listed in Section FHWA (2006) and in Section 2.6.2 is applied here for tension and compression models, longitudinal and transverse directions (Table 2F.4). The following equations are used in the calculations.

$$T_{eff} = 2\pi\sqrt{\frac{W}{K_{eff}\,g}} = 2\pi\sqrt{\frac{W}{g\times(F/\Delta)}} = 2\pi\sqrt{\frac{W\times\Delta}{g\times F}} = 2\pi\sqrt{\frac{\Delta}{g\times Cc}}$$ Effective period of bridge

$$\mu = \frac{\Delta}{\Delta_y}$$ Displacement ductility factor

$$B_s = \left[\xi_{eff}/0.05\right]^{0.5}$$ Damping factor (for short periods)

$$B_L = \left[\xi_{eff}/0.05\right]^{0.3}$$ Damping factor (for long periods)

$$\xi_{eff} = 0.05 + 0.16(1 - 1/\mu)$$ Effective viscous damping ratio (for nonductile, conventionally-designed columns)

$$S_d = \sqrt{\left[\frac{\Delta g}{Cc}\right]\left[\frac{F_v S_1}{2\pi B_L}\right]^2}$$ Spectral displacement (for long period bridge)

$$S_d = \left(\frac{\Delta}{Cc}\right)\left(\frac{F_a S_S}{B_S}\right)$$ Spectral displacement (for short period bridge)

Table 2F.4 Summary of iterations to calculate spectral displacement

Iter	model	Dir	Δ (in)	CC	Ts	Teff (calc)	μ	effective viscous damping ratios	BL	Bs	Sd (short period)	Sd (long period)	Sd(in)
1	T	Trans	3.47	0.37	0.94	0.98	3.77	0.17	1.44	1.83	6.28	7.71	7.71
2			7.71	0.45	1.20	1.33	8.39	0.19	1.49	1.95	10.87	10.09	10.09
3			10.09	0.49	1.23	1.45	10.98	0.20	1.51	1.98	12.84	10.95	10.95
4			10.95	0.51	1.24	1.49	11.92	0.20	1.51	1.98	13.48	11.22	11.22
5			11.22	0.51	1.24	1.50	12.21	0.20	1.51	1.98	13.67	11.29	11.29
6			11.29	0.51	1.24	1.50	12.29	0.20	1.51	1.98	13.72	11.31	11.31
7			11.31	0.51	1.24	1.50	12.31	0.20	1.51	1.98	13.74	11.32	11.32
8			11.32	0.51	1.24	1.50	12.32	0.20	1.51	1.99	13.74	11.32	11.32

Iter	model	Dir	Δ (in)	CC	Ts	Teff (calc)	μ	effective viscous damping ratios	BL	Bs	Sd (short period)	Sd (long period)	Sd(in)
1	T	Long	12.75	0.22	0.94	2.45	13.88	0.20	1.51	1.99	36.32	18.40	18.40
2			18.40	0.41	1.24	2.15	20.03	0.20	1.52	2.01	27.78	16.08	16.08
3			16.08	0.40	1.25	2.04	17.50	0.20	1.52	2.00	24.99	15.25	15.25
4			15.25	0.39	1.24	1.99	16.60	0.20	1.52	2.00	23.97	14.94	14.94
5			14.94	0.39	1.24	1.98	16.26	0.20	1.52	2.00	23.57	14.82	14.82
6			14.82	0.39	1.24	1.97	16.13	0.20	1.52	2.00	23.41	14.77	14.77
7			14.77	0.39	1.24	1.97	16.07	0.20	1.52	2.00	23.35	14.75	14.75
8			14.75	0.39	1.24	1.97	16.05	0.20	1.52	2.00	23.33	14.74	14.74
9			14.74	0.39	1.24	1.97	16.04	0.20	1.52	2.00	23.32	14.74	14.74

Iter	model	Dir	Δ (in)	CC	Ts	Teff (calc)	μ	effective viscous damping ratios	BL	Bs	Sd (short period)	Sd (long period)	Sd(in)
1	C	Trans	3.47	0.37	0.94	0.98	3.77	0.17	1.44	1.83	6.27	7.71	7.71
2			7.71	0.45	1.20	1.33	8.39	0.19	1.49	1.95	10.87	10.09	10.09
3			10.09	0.49	1.23	1.45	10.98	0.20	1.51	1.98	12.84	10.95	10.95
4			10.95	0.51	1.24	1.49	11.92	0.20	1.51	1.98	13.48	11.21	11.21
5			11.21	0.51	1.24	1.50	12.21	0.20	1.51	1.98	13.67	11.29	11.29
6			11.29	0.51	1.24	1.50	12.29	0.20	1.51	1.98	13.72	11.31	11.31
7			11.31	0.51	1.24	1.50	12.31	0.20	1.51	1.98	13.73	11.32	11.32
8			11.32	0.51	1.24	1.50	12.32	0.20	1.51	1.99	13.74	11.32	11.32

Iter	model	Dir	Δ (in)	CC	Ts	Teff (calc)	μ	effective viscous damping ratios	BL	Bs	Sd (short period)	Sd (long period)	Sd(in)
1	C	Long	7.07	0.27	0.94	1.63	7.69	0.19	1.49	1.95	16.42	12.40	12.40
2			12.40	0.37	1.23	1.86	13.50	0.20	1.51	1.99	20.89	13.96	13.96
3			13.96	0.40	1.24	1.90	15.19	0.20	1.51	2.00	21.80	14.25	14.25
4			14.25	0.40	1.24	1.91	15.51	0.20	1.51	2.00	21.95	14.30	14.30
5			14.30	0.40	1.24	1.91	15.56	0.20	1.52	2.00	21.98	14.31	14.31
6			14.31	0.40	1.24	1.91	15.57	0.20	1.52	2.00	21.98	14.31	14.31

Appendix 2G. Design of Steel Shell for Retrofitting

Plastic rotation capacity for shell thickness 10mm

The procedure is described in Section 9.2.1.3(a) and Section 7.8.2. (FHWA 2006)

t=10 mm shell thickness

D=32 in overall depth of section

Assume 1 in added to column for cement grout

Ag=706.858 in^2	gross cross-section area
d_b= 1.41 in	diameter of the longitudinal reinforcement (No.11)
f_y= 36000 psi	yield strength of longitudinal reinforcement (A36)
f_c'=2000 psi	concrete strength
Es=29000000 psi	elastic modulus of reinforcement
f_l= 300 psi	confinement stress
f_s=36000 psi	steel strength (A36)
Lp= 2 in	the clear gap between the edge of the shell and the bottom of the beam cap or top of the footing
f_{ys}=36000 psi	the yield stress in the shell steel
$\varepsilon_y = \frac{f_y}{E_s} = 0.00124$	strain of the longitudinal reinforcement

The equivalent plastic hinge length (after jacketing):

$$L_p = L_{gap} + 8800\varepsilon_y d_b = 17.403 \quad in$$

Determining ultimate strains in the concrete based on the ultimate achievable strains in the confining steel:

$\varepsilon_{su} = 0.10$	ultimate strain in the shell steel (A36 steel)
$f'_{cc} = f'_c\left(-1.254 + 2.254\sqrt{1+\frac{15.88tf_s}{Df'_c}} - \frac{4tf_s}{Df'_c}\right) = 5332.165 \quad psi$	related to the lateral confinement stress
$\varepsilon_{cu} = 0.004 + \frac{5.6tf_{ys}\varepsilon_{su}}{Df'_{cc}}$ =0.0533	ultimate strain in the concrete

The plastic rotational capacity of a member (θp) is based on the governing limit state for that member. After adding the steel shell, the ultimate compression strain of the confined core concrete is improved, and compression failure of the confined concrete controls the limit state.

$\phi_p = \frac{\varepsilon_{cu}}{(c-d'')} - \phi_y$	plastic curvature (FHWA, 2006)
$\theta_p = L_P\phi_P$	plastic hinge rotation
d''=1.75 in	distance from the extreme compression fiber of the cover

	concrete to the centerline of the perimeter hoop
D'=25.6 in	pitch circle diameter of the reinforcement
d'=2.705 in	depth from the extreme compression fiber to the center of the compression reinforcement
$\phi_y = \frac{2\varepsilon_y}{D'}$ =0.0001	the nominal yield curvature

For circular sections, the neutral axis depth ratio is given by:

$$\frac{c}{D} = \frac{1}{\beta}\left[\frac{\frac{P_e}{f'_c A_g} + 0.5\rho_t \frac{f_y}{f'_c}\left(\frac{1-2c/D}{1-2d'/D}\right)}{1.32\alpha}\right]^{0.725}$$

Table 2G.1 Values of plastic curvature and plastic rotation capacity (t= 10 mm)

	Pe(kips)	ρ_t	c (in)	Φp	θp
B-1(C_1)	212.82	0.0353	7.413	0.00929	0.161782
B-1(C_2)	283.76	0.0353	8.076	0.00831	0.144638
B-1(C_3)	212.82	0.0353	7.413	0.00929	0.161782
B-2(C_1)	311.64	0.0265	8.33	0.00798	0.138985
B-2(C_2)	415.52	0.0265	11.71	0.00524	0.091208
B-2(C_ 3)	311.64	0.0265	8.33	0.00798	0.138985
B-3(C_1)	216.88	0.0353	7.453	0.00923	0.160635
B-3(C_2)	289.17	0.0353	8.102	0.00827	0.144038
B-3(C_3)	216.88	0.0353	7.453	0.00923	0.160635

From this table, the minimum value of θp is 0.0912.

So when t= 0.4 in (10mm), θp = 0.0912 (plastic rotation capacity)

Minimum shell thickness

From the evaluation (method D1), the response of the bridge during the upper level ground motion is given in Table 2G.2:

Table 2G.2 Plastic rotation demand

model	Direction	Δ (in)	θp
Tension	Transverse	11.32	0.047898123
	Longitude	14.74	0.062898123
Compression	Transverse	11.32	0.047898123
	Longitude	14.31	0.061012158

θp=0.0629

After adding steel jacket, the columns will be stiffer, and the displacement demand along with the plastic rotation demands are expected to decrease. However, since the bridge shows sufficient capacity under a steel shell retrofit without a modification to the demand, we will not recalculate the strength of the column and determine a new demand.

0.0629 < 0.0912 ok

Based on approximate analysis, the retrofitted column can accommodate 50% larger than the plastic rotation demand that would be imposed on it during the design earthquake. The shell thickness could be reduced if constructability were not an issue. The following analysis shows that a shell thickness of 6 mm (0.236 in) is sufficient to resist the plastic rotation demands.

Table 2G.3 Values of plastic curvature and plastic rotation capacity (t= 6 mm)

	Pe(kips)	ρ_t	c (in)	Φp	θp
B-1(C_1)	212.82	0.0353	7.413	0.006851	0.119237
B-1(C_2)	283.76	0.035	8.076	0.006122	0.106552
B-1(C_3)	212.82	0.0353	7.413	0.006851	0.119237
B-2(C_1)	311.64	0.0265	8.33	0.005882	0.102369
B-2(C_2)	415.52	0.0265	11.71	0.003850	0.067018
B-2(C_ 3)	311.64	0.0265	8.33	0.005882	0.102369
B-3(C_1)	216.88	0.0353	7.453	0.006802	0.118388
B-3(C_2)	289.17	0.035	8.102	0.006097	0.106108
B-3(C_3)	216.88	0.035	7.453	0.006802	0.118388

The minimum plastic rotation capacity when t= 0.236 in (6 mm) is θp = 0.067, which is sufficient to meet the demand.

Length of the Steel Jacket

The minimum length for the jacket is greater of the D and 0.25La for the top of the columns, D or 0.25Lb for the bottom of the columns when the following criteria are met (Priestly et. al, 1996), where La and Lb are the distances from the top and bottom of column to zero moment location on the column.

$$\frac{P_e}{f'_{ce} A_g} = 0.29 < 0.3$$

D=32 in Column depth

La=Lb = 120 in

Thus, the minimum length for the extent of jacket is 32 in, and the jacket should be applied over both the top and bottom of the columns to develop the flexural strength and ductility capacity at each location.

Evaluation of Splice Length (Priestly et. al. 1996)

A_b= 1.56 in^2	area of the a lapped bar
ls = 30 in	the splice length
D'=25.6 in	pitch circle diameter of the reinforcement
d_b= 1.41 in	diameter of the longitudinal reinforcement (No.11)
c=1.5 in	clear cover
f_{yl}= 36000 psi	yield strength of longitudinal reinforcement (A36)
f_{yj}= 36000 psi	yield strength of steel shell
n=16 (bents 2 and 4)	number of longitudinal bars
n=12 (bent 3)	

$$p = \frac{\pi D'}{2n} + 2(d_b + c) \le 2\sqrt{2}(c + d_b)$$ perimeter of the characteristic block

p=8.23 in

$$\rho_{sj} = \frac{2.42 A_b f_{yl}}{p l_s (0.0015 E_{sj})}$$ effective volumetric ratio of confining steel

no less than $\frac{2.42 A_b f_{yl}}{p l_s f_{yj}}$

$$\rho_{sj} = 0.0153$$

$$\rho_s = \frac{4t_j}{D}$$

t_j=3.10 mm

Because the thickness of steel shell for the lap splice is less than 6 mm, we still choose 6 mm as the thickness of the steel shell.

3. B-Ramp Over I-215 and I-80

3.1 Introduction

This detailed retrofit evaluation examines an 8-span curved steel girder bridge with several in-span pin and hanger joints, which are provided for thermal expansion. This bridge belongs to a class of US bridges designed in the 1980's and before that utilize pin-hanger assemblies in some of the spans. However, pin-hanger assemblies are no longer permitted due to several deficiencies that have been observed in the connections.

A pin-hanger joint typically consists of an upper pin, a lower pin and two hangers that together connect the web of a suspended beam to the web of a cantilever beam. A typical configuration of a pin-hanger connection is shown in Fig. 3.1.1. The basic idea behind pin-hanger joints is to provide free rotation by the loose fit of pins into the web of girders. Under typical thermal expansion and contraction cycles, the hangers rotate around the upper and lower pins and torsional stresses are not induced in either the pins or the hangers.

Upon installation, the pin and hanger are assumed to be free of torsion. However, after years of exposure to atmosphere, deicing salts, and load variations; corrosion and wearing increase friction between mating surfaces, which tends to produce at least a partially fixed connection in rotation (El-Khoury et. al., 1996; South et. al, 1992). This change in the connection behavior imposes considerable unforeseen stresses on pins and hangers even in normal operating conditions. Eventually, these forces interfere with the normal operation of the connection and locking occurs. When the connection becomes fixed, the torsion introduces bending stresses in the hangers which are not considered in design, and can lead to development and growth of internal and external defects, flaws and discontinuities in the pin or the hanger. The initiation and growth of a crack in a fracture critical detail such as a pin or a link eyebar can lead to catastrophic failure. Also, corrosion and wear of a pin may produce large tensile stresses in the pin. These stresses may cause yielding of the pin or push the hanger off the pin.

A number of bridges with pin-hanger connections have failed due to aforementioned deficiencies in the connections. As an example, several pins failed in a bridge on I-55 in St. Louis, Missouri in 1987. The 24 year old Mianus River Bridge on I-95 in Greenwich, Connecticut collapsed in 1983 due to pin failure (South et. al, 1992).

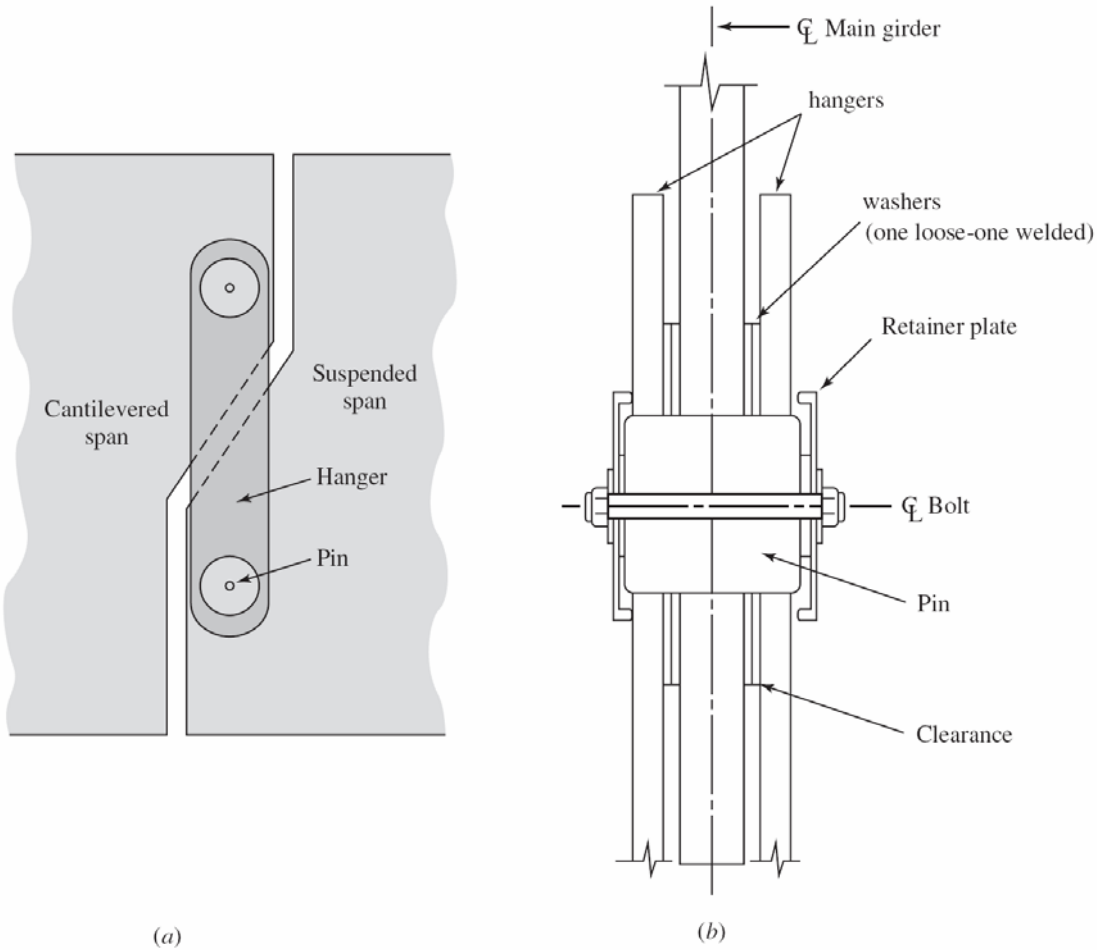

Figure 3.1.1. Typical pin-hanger joint details

The seismic performance of bridges with pin-hanger connections is an additional consideration. The large longitudinal forces applied to the bridge deck induce column deformations and may lead to differential motion of the spans separated by pin-hanger connections. Since the seismic gaps in pin-hanger joints are usually small the differential motion is likely to induce pounding of spans during earthquakes. Impact forces cause local damage at the point of contact. Furthermore, the seismic provisions of the 1980's are unconservative compared with recent codes, and pin-hanger joints are susceptible to failure because of the large stresses induced in the transverse direction during earthquakes (Lai, 1997). If the pin-hanger joints fail, partial or full collapse of the bridge is possible since the adjacent spans are cantilevered or suspended. If the abutment does not provide full fixity, the span adjacent to the abutment is most likely to collapse.

Only one previous study on the seismic response of bridges with pin-hanger joints was discovered in the literature review (Lai, 1997), and no previous studies were found that examined the seismic response of curved girder bridges with pin and hanger joints. The curved girder bridge examined in this study is representative of several similar bridges in the state of Utah. While other potential safety risks have been discussed, this study is restricted to seismic vulnerability assessment and exploration of retrofit strategies for the curved girder bridge assuming that the pin-hanger joints rotate freely as designed. The evaluation of bridges with pin-hanger assemblies for failures due to corrosion and fixity is not considered here.

3.2 Existing Bridge Structure

An eight span highway overcrossing curved bridge located on the way to Redwood Road in Salt Lake City crossing over I-215 and I-80 is considered for seismic retrofitting. The bridge was constructed in the mid 1980's. The bridge path is a sector of a circle with the radius of 1432 ft and the length of 1430.5 ft. The bridge passes over two parallel streets in the middle two spans.

The cross section of the superstructure is of constant width, 22.5' normal to the bridge path. The superstructure in all the spans consists of 4 welded I-section steel girders and a reinforced concrete deck. Pin-hanger joints are located in four of the spans. Girders are continuous between the pin-hanger joints and constrained to rotate with the column ends. Moreover, the longitudinal displacements of the girders and columns are restrained together in even numbered bents, and longitudinal forces can be transferred at those locations. The depth of the superstructure varies along the length of the bridge. No longitudinal cable restrainers are in place.

Abutments are seat type supported on 300-ton piles with approach retaining walls. They are oriented normal to the bridge path. The superstructure is directly seated on bearings over the abutments.

Each bent cap supports one reinforced concrete column of circular cross section on a pile footing. All the columns are 7' diameter; bents #4 and 5 are reinforced with 44 #10 bars and the rest with 50 #14 bars. The main reinforcing steel is lap spliced just above the footings, and the column transverse steel consists of #4 hoops at 3".

Pile caps are of identical size and are aligned parallel to the bent caps. Pile caps supporting bents #4 and 5 are settled on 14 piles, and the remaining pile caps are settled on 17 piles. Piles are designed for a vertical load of 300 tons.

3.3 Overview of Evaluation Methods

The following key considerations are expected to be important in evaluating the seismic susceptibility of the bridge:

- Excessive straining in the hangers due to longitudinal separation of the spans may lead to failure of the pin-hanger assembly.
- Pounding of the adjacent spans separated by pin-hanger assemblies may have adverse effects on the overall dynamic response of the bridge.
- Plastic hinge formation and excessive plastic hinge rotation in the columns is possible, regardless of the pin-hanger assemblies, because the bridge was designed to much smaller seismic forces in the 1980's.

Pounding is a dynamic effect that can only be captured properly through a time history analysis. The impact forces due to pounding are likely to have a significant influence also on the column response and the susceptibility of columns to forming plastic hinges or undergoing large column rotations. Therefore, we have concluded that inelastic time history analysis is essential for accurate evaluation of the vulnerability of this bridge.

The FHWA retrofit manual (FHWA, 2006) recommends evaluation procedures for bridges considering both upper level (UL) and lower level (LL) ground motions. This bridge is determined to be in Seismic Retrofit Category (SRC) C for the UL ground motion (Appendix 3A), whereby procedures to derive the SRC are summarized in Examples 1 and 2. For SRC C, the retrofit manual recommends that the bridge be analyzed by an elastic method (uniform load method or modal analysis) for demand assessment and one of several static methods, such as pushover analysis, for capacity assessment. Only for irregular or complex bridges in SRC D (or locations requiring site specific ground motions) does the manual suggest that inelastic time history analysis be considered.

Although this bridge is not in SRC D, the special considerations described above have led to the conclusion that an inelastic time history analysis is appropriate here. Furthermore, because the seismic hazard level (SHL) has the maximum category of IV, the bridge could be considered

SRC D if the bridge importance factor is interpreted as *Essential* rather than *Standard*. (Only essential bridges with more than 50 years of remaining service life (ASL 3) are considered to have an operational performance objective (PL 2) for the UL ground motions). Since this long span bridge is a viaduct connection two major freeways: I-215 northbound to I-80 westbound, it could be considered a major lifeline. If the bridge is interpreted as SRC D, selection of inelastic time history as the predominant evaluation method is appropriate due to its irregular characteristics.

Although the retrofit manual also recommends a separate evaluation for the LL ground motion using a static method, a LL evaluation is not performed here because the static evaluation is not expected to be sufficiently accurate.

3.3.1 Selection of Ground Motions for Response History Analysis

Guidelines for selecting ground motions given in the Retrofit Manual (FHWA, 2006) have been followed here. In general, ground motions should be selected that represent both the seismic environment and local site characteristics. Seismic environment includes the tectonic environment (shallow crustal faults versus subduction zone), earthquake magnitude, type of faulting, and source to site conditions. Due to a lack of recorded data, it is not always possible to find motions that represent the faulting and local soil characteristics.

Two main procedures are mentioned (Section 2.8.2 of FHWA 2006) for matching representative histories to the design spectrum. The scaling procedure involves scaling time histories by a constant factor so that the response spectrum of the ground motion approximately matches the design spectrum over the structural period range of significance. The spectrum matching procedure involves modifying the frequency content of the scaled recorded time history so that the modified response spectrum is a close match to the design spectrum over the structural period range of significance. Because spectrum matching is more involved, somewhat controversial, and best left to seismologists; recorded ground motions are selected and scaled according to the scaling procedure.

The seismic hazard deaggregation plot for this bridge location is shown in Figure 3.3.1. The major contribution to total hazard comes from earthquakes ranging in magnitude from 6.25 to 7.5 Mw and faults ranging from 0 to 7.5 km hypocentral distance from the bridge. The bridge is located on site class E soil with shear wave velocity less than 180 m/s. The Pacific Earthquake

Engineering Research Center NGA database (PEER, 2009), which contains over 10,000 motions from 173 earthquakes, was searched for motions satisfying these criteria. About 10 potential motions were identified; the number was limited due to the lack of available recorded motions in site class E.

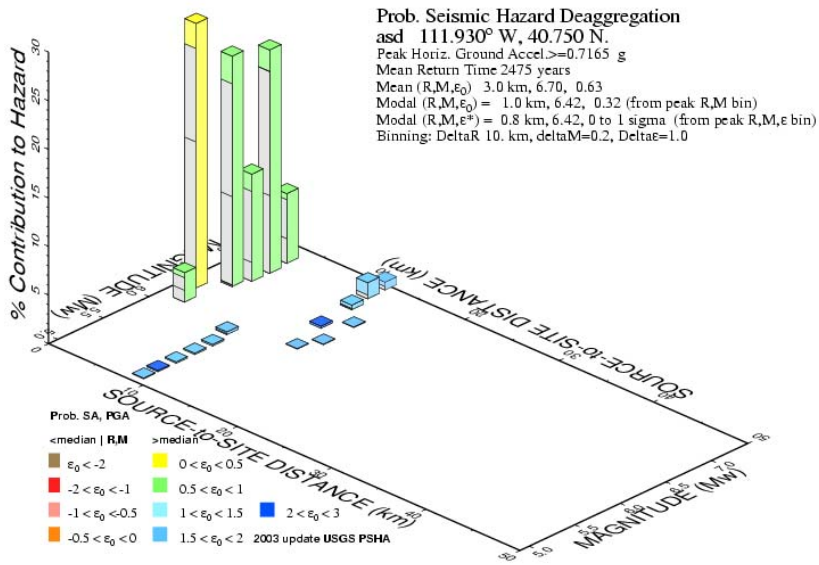

Figure 3.3.1. Seismic hazard deaggregation for 2475 year event at the bridge location

Scaling factors were identified for each pair of motions in the set of 10 using a least squares fit of the response spectrum to the target design spectrum. The same scaling factor was applied to the two lateral orthogonal time history components to preserve the relationship between the components. Seven of the ground motions with the scaling factors closest to 1.0 were selected for nonlinear response history analyses. As recommended by the design codes, the average of each response quantity over 7 ground motions shall be considered in evaluation. Table 3.3.1 summarizes the ground motions used in the response history analyses.

Table 3.3.1 Properties of ground motions used in the study

GM#	Earthquake	Station	CompX/CompY	Mw	Closest Distance (km)	PGA (g)	Scale Factor
1	Dinar, Turkey 1995	ERD 99999 Dinar	DIN090/DIN180	6.40	3.36	0.303	2.14
2	Chi-Chi Taiwan 1999	CWB 99999 TCU110	TCU110-E/TCU110-N	7.62	11.6	0.183	2.37
3	Imperial Valley 1979	CDMG 1336 EC Meloland Overpass FF	EMO000/EMO270	6.53	0.07	0.309	2.40
4	Imperial Valley 1940	USGS 117 El Centro Array #9	ELC180/ELC270	6.95	6.09	0.258	3.08
5	Superstition Hills 1987	USGS 9400 Poe Road (temp)	POE270/POE360	6.54	11.16	0.363	2.56
6	Imperial Valley 1979	USGS 5057 El Centro Array #3	E03140/E03230	6.53	12.85	0.255	3.22
7	Loma Prieta 1989	CDMG 57382 Gilroy Array #4	G0400/G04090	6.93	14.34	0.304	2.55

The median response spectrum of the scaled ground motions is shown in Figs. 3.3.2.

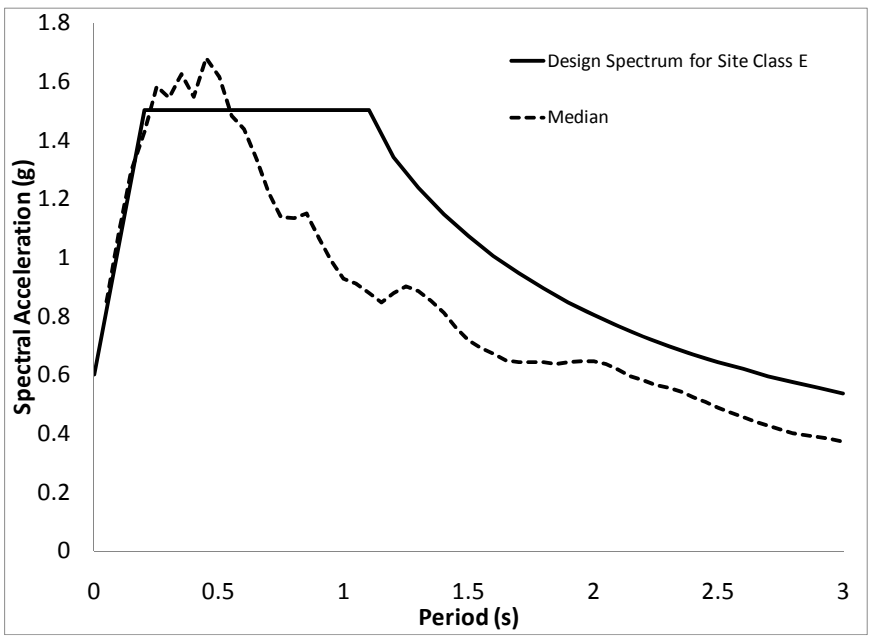

Figure 3.3.2. Median response spectra of the ground motions along with the design spectrum

3.4 Development and Verification of Pin/Hanger Element

In normal operating conditions, the pins undergo shear and bending stresses. Shear stress in the pin is due to the forces transferred from the hangers to the pin and from pin to the web. The lines of action of the loads on the pin are not acting at the same location. This offset distance induces bending stresses in the pin. The stress in hangers is most likely to be tension which is

induced by axial tension forces and bending moments in the transverse direction. The calculated minimum and maximum seismic gap opening/closing at the pin-hanger assemblies are required to be checked against the hanger length and design gap respectively. If the calculated minimum gap is larger than the existing gap, pounding of the adjacent girder segments at the pin-hanger assemblies is likely to happen. On the other hand, if the calculated maximum gap is larger than the hanger length, the hanger plates may become active as restrainers and experience unforeseen large tension stresses.

To model pin-hanger assemblies, two rigid links representing webs of the adjacent girders as shown in Fig. 3.4.1 connect the hanger to the girders. The connections of rigid links to the web of girders are fixed while the connections of rigid links to the hanger are free in rotation around the strong axis of the girder and fixed in all other degrees of freedom. A compression-only gap spring is added to represent pounding of the adjacent spans when the gap closes. The spring stiffness is calculated based on the axial stiffness of the adjacent spans acting in series. Viscous damping is applied based on calculated energy dissipation for an assumed coefficient of restitution (Jankowski et. al., 1998). The damping is proportional to the tangent stiffness, and thus only engages when the gap closes.

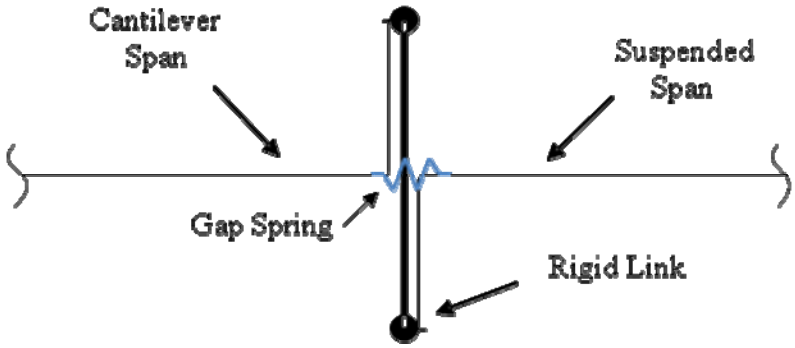

Figure 3.4.1. The pin-hanger joint model

Numerical models of the pin-hanger element (without the gap spring) were created both in LARSA 4D and OpenSees (McKenna and Fenves, 2001) and compared against analytical solutions for different configurations and loading conditions. The standalone pin-hanger element was assessed in 2D and 3D. Then the pin-hanger element modeled together with two adjacent frame elements, representing the model of a bridge girder containing a pin-hanger joint, was assessed in 2D. These comparison studies are described in detail in Appendix 3C. The

OpenSees and LARSA models were shown to deviate in dynamic load cases when geometric nonlinearity was assumed in the elements. In some cases we encountered difficulties satisfying equilibrium in LARSA. Therefore, we have elected to use OpenSees for the comprehensive bridge evaluation and response history analysis.

3.5 Evaluation of the Unretrofitted Bridge

3.5.1 Model Description

A complete model of the bridge has been implemented in both LARSA and OpenSees. The graphical user interface for LARSA is helpful for verification and visualization of the model, but as described in Section 3.4, OpenSees was selected for the nonlinear time history analysis due to observed convergence problems in LARSA. A script has been written to extract material properties, bridge geometry, etc. from LARSA and generate an input file for the bridge model to be executed with OpenSees. Therefore, changes made to the LARSA model can be automatically extended to the OpenSees model. The LARSA and OpenSees model definitions are essentially identical with discrepancies noted.

The superstructure is represented by elastic beam elements with composite sections to represent combined flexural action of the steel girders and concrete deck. A single composite section was developed to represent the combined stiffness of the girders and deck. As described earlier, the steel girders are built up wide flange sections whose flange depths vary unsystematically across the four bridge girders and over the length of the bridge. LARSA features a tool that accounts for parametric variation of section properties over the length of the bridge, but this model would be difficult to extend to OpenSees. Alternatively, a single section has been developed that represents the average superstructure section properties. The section is depicted graphically in Figure 3.5.1. The material properties used are E = 2133 ksi for concrete and E = 29000 ksi for steel; yield strengths are ignored because the section is assumed to remain elastic. Gross section properties are used and rebar in the deck is not considered. The composite section flexural stiffness is EI = 1.496E10 kip.in^2 and axial stiffness is EA = 1.66E7 kips, a determined through section analysis in Xtract.

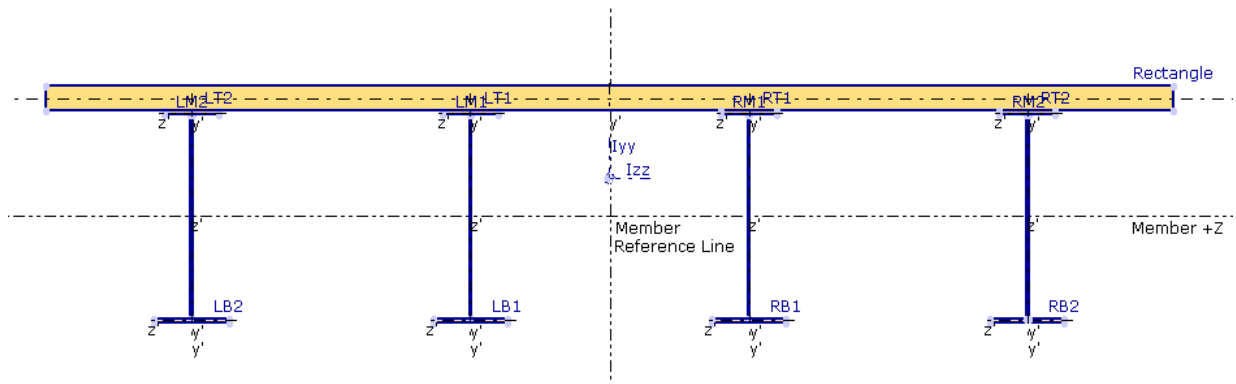

Figure 3.5.1. The cross section of deck.

For the purposes of modeling, the curvature of the bridge was idealized as an arc or segment of a perfect circle. In LARSA, an alternate Bridge Path coordinate system is defined to represent the path of the bridge along the ground. The bridge path is defined by selecting *CoorSystem* in *Model Data* and adding a *Bridge Path*. To define an arc, required input values to LARSA include the radius of curvature and the angle θ over which the arc is defined. From the bridge design drawings, the radius of curvature is r = 1432 *ft*, the total length of the bridge is L = 1428 *ft*, and θ is estimated as L/r =57.13˚. Elastic beam elements were constructed between adjacent nodes described on the bridge path. The spans are continuous, i.e. moment connections are assumed along the entire length of the bridge except at pin-hanger locations. As mentioned previously, pin-hanger assemblies are represented by a combination link element to represent hanger rotation and strain and gap element to represent pounding of the decks of adjacent spans.

Columns were modeled in OpenSees using the beamWithHinges element, which, when defined using resultant section properties, behaves as a concentrated plasticity element. A distributed plasticity element (nonlinearBeamColumn with a fiber section) was initially considered, but the concentrated plasticity approach was ultimately selected to decrease the complexity of the analysis and to stabilize the convergence of the model by decreasing the sensitivity to analysis properties. Input data for the beamWithHinges includes resultant section properties EI (for integration over the elastic interior) and EA, a nonlinear moment-curvature relationship, and a plastic hinge length. The section properties and moment-curvature relationship were derived through section analysis. The plastic hinge length was taken to be one sixth of the element length, which enforces a one-to-one relation between the rotation □ and the curvature κ when using modified Gauss-Radau integration (Scott and Fenves 2006). This plastic

hinge length was selected to control the element behavior only and is not meant to be a reflection of the true plastic hinge region of the member.

To perform the section analysis, a fiber section with a circular concrete core and radially distributed reinforcement is built in OpenSees using the patch command. The concrete was defined using a Mander model with f'_c = -1.4 ksi, and the reinforcement was defined using Steel02, which is essentially a bilinear stress-strain relation. The parameters used in the section analysis are outlined in Appendix 3C.

Since the axial loads in columns with the same cross section are closely matched, two sets of moment-curvature analyses (one for columns in bents 4 and 5 and one for the rest) were performed to derive the section resultant moment-curvature relations. A bilinear curve was fit to each moment curvature relation to estimate the nominal yield moment M_n and the postyield to initial stiffness ratio. Representative moment-curvature curves from section analysis along with their bilinear fits are given in Fig. 3.5.2. The allowable plastic rotation limits (θ_p) are found based on the procedures outlined in the Retrofit Manual (FHWA 2006) which were explained in detail for bridge example 1. Table 3.5.1 summarizes the height, axial load, and strength and plastic rotation capacity of each bent.

Table 3.5.1 Summary of bent element properties

Bent #	*Height*	*Axial Load*	*Mn*	Θ_p	*Hardening α (%)*
	(ft)	*(kip)*	*(kip-ft)*	*(rad)*	
2	40	1217.7	1.10E+05	0.0100	0.3
3	37	1179.8	1.10E+05	0.0096	0.3
4	16.25	1033.8	7.76E+04	0.0070	-1.2
5	23	1113.8	7.76E+04	0.0078	-1.2
6	46	1224.5	1.10E+05	0.0107	0.3
7	38	1207.4	1.10E+05	0.0097	0.3
8	36.5	1183.5	1.10E+05	0.0095	0.3

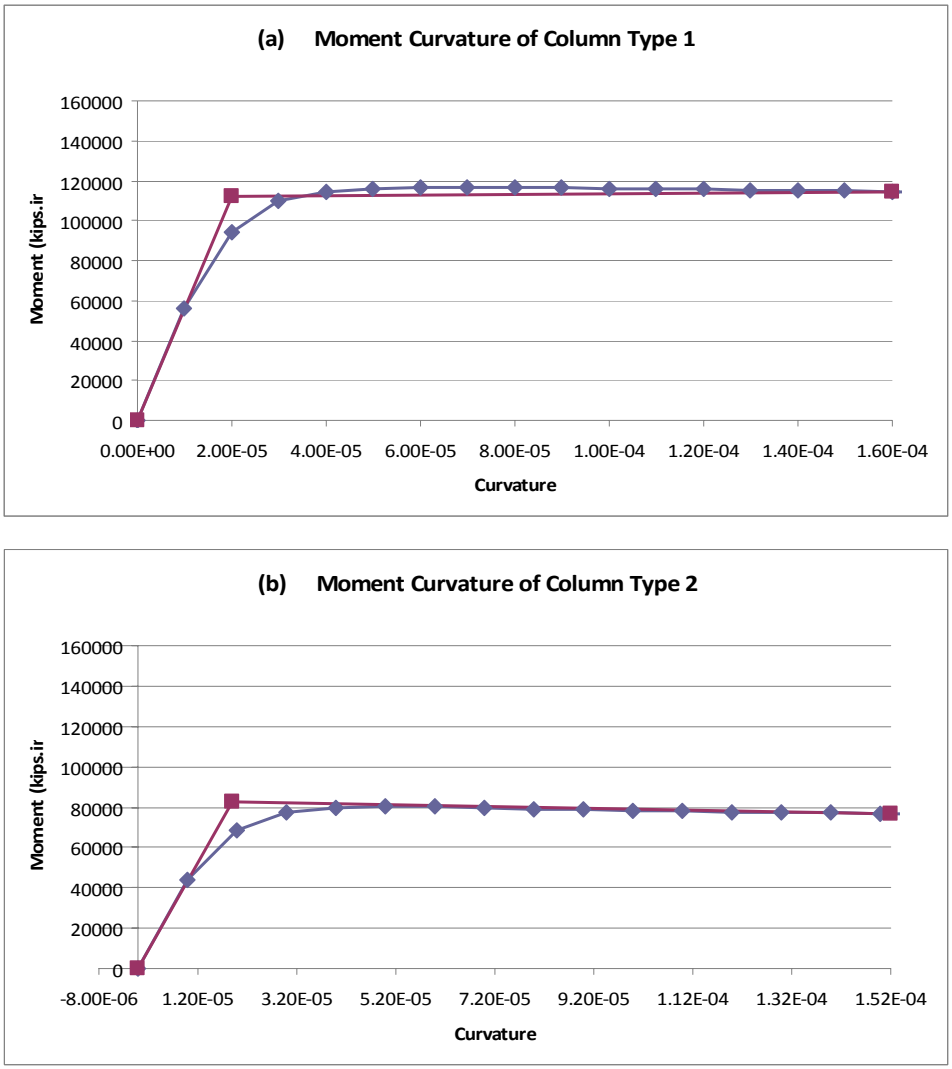

Figure 3.5.2. Moment-curvature curves of the two typical columns.

Each column was modeled with two elements to allow for distribution of mass along the column (Sec. 7.3 of FHWA, 2006). Because the bents widen at the top, a part of the column at the top of the length 4.375 ft was substituted with an essentially rigid element. This forces plastic hinging to occur away from the top of the column. Foundation elements were not modeled below the columns since from the previous two examples it was observed that the contribution of the foundation deformation to the top column translational displacement was not significant. The columns were fixed to the base and attached to the superstructure by a moment connection.

The flexibility of the abutments is modeled by inelastic springs in the transverse and longitudinal directions, where the longitudinal springs have different properties in tension and

compression. The abutment stiffness and strength is based directly on the passive pressure of the surrounding soil, and the theoretical calculation of these parameters has been well documented in the previous two examples. A transformation is required to convert the abutment stiffnesses and strengths from the longitudinal and transverse coordinates to the global x and y-directions. A single spring is provided for the abutment stiffness in the global x and y-directions, and for rotation about the vertical axis. The details of the abutment strength and stiffness calculations are tabulated in Appendix 3C.

A rendering of the LARSA bridge model showing node and element locations is given in Fig. 3.5.3.

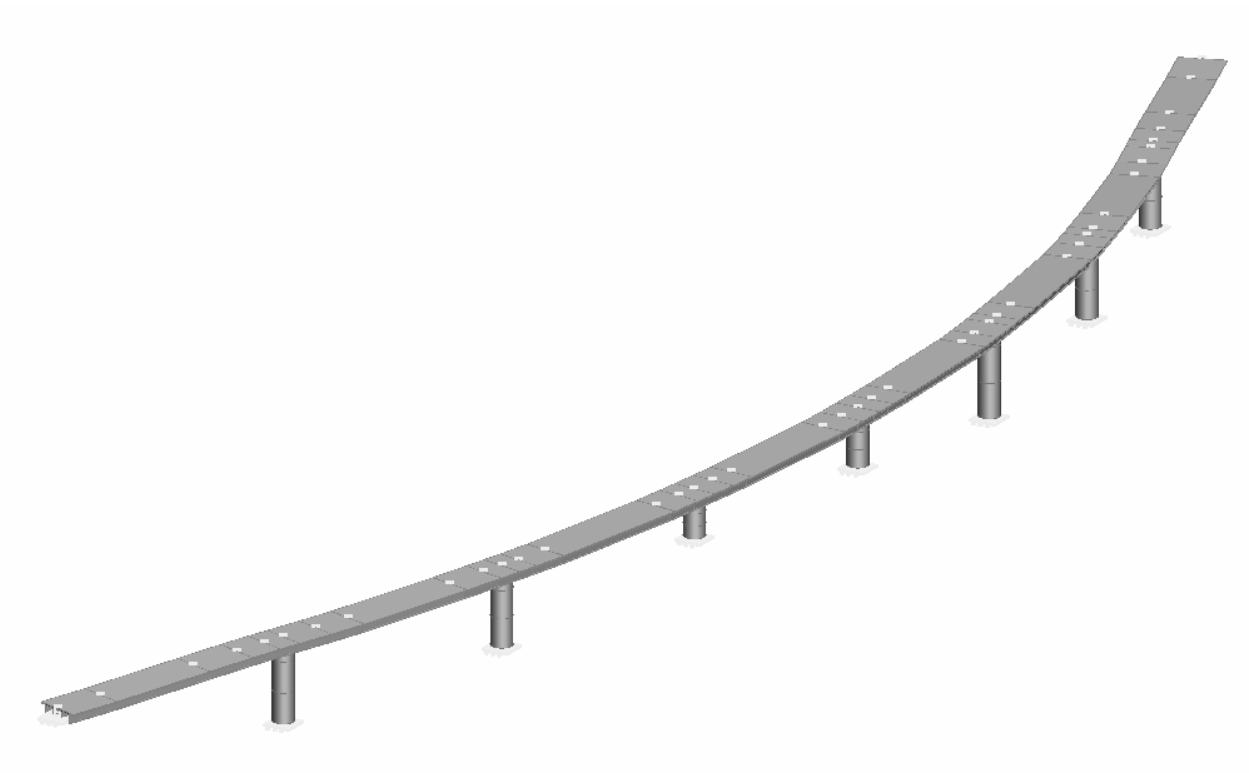

Figure 3.5.3. 3D view of the bridge model in LARSA.

The first few natural frequencies and mode shapes of the bridge given its linear elastic properties were computed in both LARSA and OpenSees, wherein a close match between the two models is observed. The graphical representation of the first few mode shapes is given in Appendix 3C.

3.5.2 Analysis Results

Nonlinear response history analysis of the unretrofitted bridge model to the seven ground motions selected earlier was performed in OpenSees. These simulation results are used to evaluate the bridge performance. The mean pounding forces computed over 7 ground motions are summarized in Table 3.5.2. These impact forces are on the order of the weight in the spans, and do not seem excessively large, but it is still desirable to reduce them. Maximum column plastic hinge rotations are presented along with the allowable rotations in Table 3.5.3. As seen, hinge rotations exceed the allowable limits by large amounts in four of the columns. Furthermore, the allowable plastic hinge rotations for columns are not favorable mainly due to very low concrete strength. Obtained results reveal the necessity for retrofit strategies that will not only reduce the deformation demands on the columns but also increase the plastic deformation capacity of the columns. Mean hanger longitudinal deformation demands versus the yield deformation are given in Table 3.5.4. It is seen that all the hangers remain elastic. Thus, addressing the excessive plastic rotation demands in the columns appears to be the most critical issue.

Table 3.5.2 Mean pounding force at each gap

Gap#	Pounding Force (kips)
1	2112.6
2	1985.7
3	1347.1
4	2062.2

Table 3.5.3 Columns deformation response

		Plastic Hinge Rotation		
	Axial Load	Demand	Capacity	Demand Capacity Ratio
Col1	1217.7	0.019	0.010	1.90
Col2	1179.8	0.025	0.010	2.56
Col3	1033.8	0.037	0.007	5.28
Col4	1113.8	0.043	0.008	5.58
Col5	1224.5	0.031	0.011	2.89
Col6	1207.4	0.038	0.010	3.95
Col7	1183.5	0.026	0.010	2.71

Table 3.5.4 Hanger longitudinal strains

	Yield Strain	Strain
Hanger 1		0.00039
Hanger 2		0.00014
Hanger 3		0.00010
Hanger 4	0.00069	0.00043

3.6 Proposed Retrofit Solutions

3.6.1 Fixing All the Hanger Joints

The first strategy that we considered is fixing or locking all of the pin-hanger joints (Figure 3.6.1a) This strategy addresses three major concerns about the bridge. First, the first and the last spans of the bridge in this study are of suspension type and therefore are statically determinate or non-redundant. Failure of the pin-hanger joints at the ends would clearly lead to major failure of the spans. Second, fixing the joints eliminates the possibility of pounding, and eliminates the possibility of failure of the pin-hanger joint due to excessive demands on the hanger in both the longitudinal and transverse direction. Locking the joint includes grouting the existing connection and installing pre-stressed cable restrainers that provide a compressive force across the connection (Priestly et. al. 1996). The existing pin-hanger joints can be left in place and need not be removed.

3.6.2 Partial Joint Fixity and Column Isolation

Since the bridge in this study is 1400 ft long and the pin-hanger joints were originally designed for movement, locking all the pin-hanger joints along the bridge is likely to produce excessive stress on bridge components due to thermal expansion. However, two points worth considering are: (1) in older bridges, all creep and shrinkage can reasonably be assumed to already taken have taken place at the time of the retrofit, and only thermal expansion need be considered (Priestly et. al., 1996), and (2) older bridges often have more movement joints than needed (Priestly et. al., 1996).

Thus, an alternative strategy is to lock the first and fourth pin-hanger joints, but to leave the second and third joints intact. Locking the first and fourth joints adds redundancy to the first and the last spans, which are in the greatest danger of collapse due to joint failure. However, leaving the second and third joints intact allows for some thermal expansion. The proposed bridge is thus partitioned into three freely moving segments in the longitudinal direction

connected by two pin-hanger joints (Figure 3.6.1b). Since the length of the new first and third segments is about equal to the length of the existing middle segment, it is reasonable to expect that the thermal expansion can be accommodated.

The second part of the strategy is to retrofit each of the bent caps with seismic isolation bearings to eliminate the pounding between the adjacent segments. While isolation bearings are generally used to modify the overall dynamic properties of the bridge, in this case they are proposed to modify the relative dynamic properties of the three segments such that the segments move together in phase. The isolated segments will be designed to have the same natural period, and the likelihood of pounding of adjacent spans and large transverse forces in pin-hanger joints will decrease substantially. As an additional benefit, implementation of isolation bearings will reduce force and ductility demands on piers by energy dissipation and elongation of the natural period of the bridge, and may eliminate the need for additional ductility enhancement of the columns.

For a linear system, it can be proven that, the properties of the isolators can be optimized to force the three segments of the bridge to move "in phase" preventing the pounding in the gaps. However, nonlinearities associated with the bridge behavior can result in shifts in the fundamental periods of the bridge segments. As such, the in-phase movement of the bridge segments may be interrupted and the bridge may become vulnerable to potential pounding. Hence, a series of numerical analyses will be conducted to evaluate the effectiveness of this retrofit scheme.

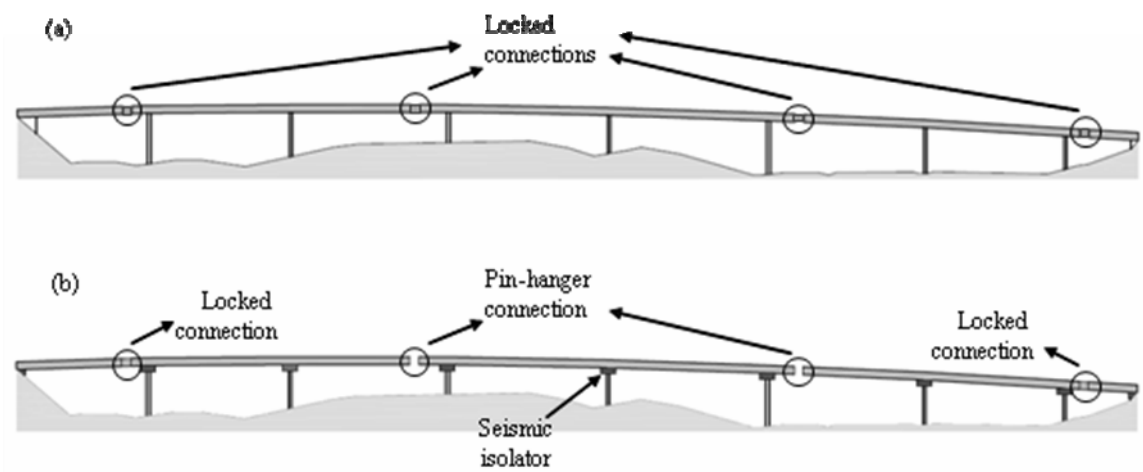

Figure 3.6.1. (a) Locking all pin-hanger joints, and (b) selectively locking pin-hanger joints with seismic isolation.

3.6.2.1 Isolation System Design

In order to match the periods of the segments, the original periods of the segments were determined. Free vibration analysis was conducted on the three segments of the bridge with first and fourth pin-hanger joints locked. Free vibration analysis was used instead of eigenvalue analysis to indirectly account for the nonlinear behavior of the bridge. A short duration impulse acceleration with a magnitude of 0.1g and a duration of 0.5 seconds was applied to the system and the resulting free vibration response was observed over 4.5 seconds. The analysis was repeated with the impulse applied in the negative direction. The results of the free vibration analysis are depicted in Figure 3.6.2.

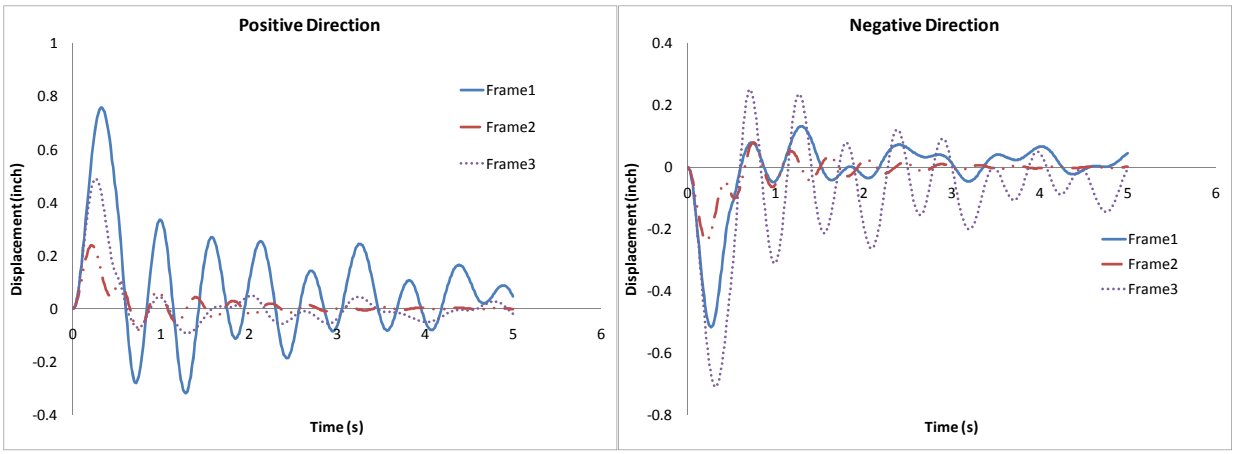

Figure 3.6.2. Free vibration analysis of bridge segments for positive and negative impulses

The resulting free vibration analysis illustrates that the behavior of the end segments (frame 1 and 3 in Figure 3.6.2) are very different in the positive and negative directions. When the acceleration is applied in the positive direction, the abutment at the end of frame 1 initially goes into tension while the abutment at the end of frame 3 initially goes into compression. The compressive stiffness of the abutment was computed to be around 3.5 times the tensile stiffness. Since the column stiffnesses and total mass of these two frames are very similar, the asymmetric abutment stiffness accounts for the observed difference in period and overall response between the first and third frames. When the acceleration is applied in the negative direction, the response of frames 3 and 1 are mirror images of the response of frames 1 and 3 due to a positive acceleration impulse. Furthermore, the end segments (frames 1 and 3) tend to exhibit free

vibration response about a shifted equilibrium position. Accounting for both the positive and negative free vibration responses, the period of the end segments was computed to be about 0.55 seconds, and the period of the middle segment was computed to be about 0.36 seconds.

Because the end segments already have essentially the same period, isolation is not needed to align the vibration periods of the segments. Furthermore, the end segments are more likely to move in phase if the effect of the abutment stiffness asymmetry can be minimized. Keeping the columns stiff relative to the abutments will help to minimize this effect. Therefore, we concluded that only the second segment should be isolated to make its period identical to the first and third segment.

The calculations to determine the isolator properties are summarized in Table 3.6.1. To estimate the total column stiffness, the deck is assumed to be completely rigid. Also, because the columns have essentially the same cross section properties and therefore the same *EI*, the total stiffness is assumed to be distributed to the columns in proportional to the inverse of the column height cubed. As such, 62.4% of the stiffness is distributed to Column 3, 31.3% of the stiffness is distributed to Column 4, and 6.4% of the stiffness is distributed to Column 5, where the columns are numbered according to their overall placement in the bridge. To attain a vibration period of 0.55 seconds, the target stiffness of the frame is reduced from 2658 kips/in to 1139 kips/in. Since Column 5 stiffness is already small (169.2 kip/in) relative to the overall desired stiffness, we elected to isolate only Columns 3 and 4. Both columns were assigned an identical target stiffness of 485.9 kips/in. The stiffness of an isolator/column assembly is given by:

$$\frac{1}{k} = \frac{1}{k_{col}} + \frac{1}{k_{iso}}$$

where k_{col} is the stiffness of the column and k_{iso} is the stiffness of the isolator. This equation assumes that the isolator and the column act in series. From the target k and known kcol values, the required isolator stiffness was computed to be 685.4 kips/in for Column 3 and 1163.1 kips/in for Column 4. Spring elements that represent the linear isolators were implemented in the OpenSEES model and the free vibration analysis was repeated to evaluate the effectiveness of the isolation scheme in matching the periods of each of the frames. The resulting free vibration analysis results are depicted in Figure 3.6.3, which suggests that the proposed isolation system is effective in matching the vibration periods of the three frames prior to yielding of the columns.

However, the discrepancy in amplitude of the vibration may still prevent the elimination of pounding.

Table 3.6.1 Calculations to determine isolator properties.

	Original Frame 2 (Observed Values)	Modified Frame 2 (Target Values)
Segment Natural Period	$T = 0.36$ sec	$T = 0.55$ sec
Mass	$M = 8.73$ kips/g	$M = 8.73$ kips/g
Total Column Stiffness	$K = M\left(\frac{2\pi}{T}\right)^2$ =2658 kips/in	$K = M\left(\frac{2\pi}{T}\right)^2$ =1139 kips/in
Stiffness Column 3	$K_{3c} = 1657.8$ kip/in	$K_3 = 485.9$ kip/in
Stiffness Column 4	$K_{4c} = 831.5$ kip/in	$K_4 = 485.9$ kip/in
Stiffness Column 5	$K_{5c} = 169.2$ kip/in	$K_5 = 169.2$ kip/in
Target Isolation Stiffness, Column 3		$K_{3i} = \frac{K_{3c}K_3}{(K_{3c} - K_3)}$ =684.5 k/in
Target Isolation Stiffness, Column 4		$K_{4i} = \frac{K_{4c}K_4}{(K_{4c} - K_4)}$ =1163.1 k/in

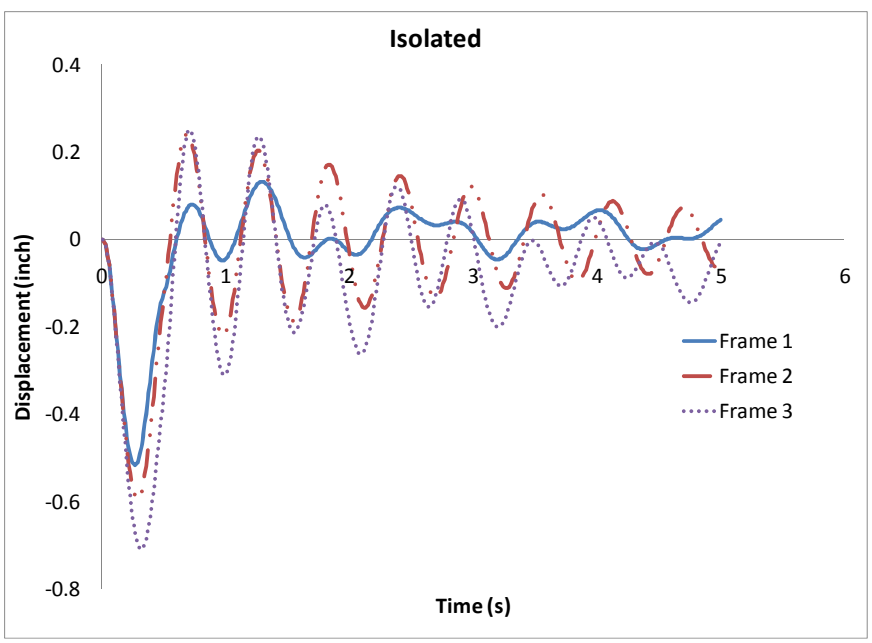

Figure 3.6.3. Free vibration analysis on the isolated bridge

3.6.3 Column Jacketing

A third retrofit strategy, which may be used in combination with the other two proposed strategies, is jacketing of the columns. For circular columns, steel jacketing is a very efficient method that increases both the flexural capacity and ductility of reinforced concrete columns (FHWA, 2006). As was shown previously, the columns lack sufficient ductility to survive strong ground motions (Table 3.5.3).

The compressive strength of concrete was specified as 1.4 ksi in the design drawings, which is low compared to the modern specifications. Applying a steel jacket that covers the original concrete column increases the confinement of concrete but does not significantly increase the stiffness of the columns. Increasing the stiffness of the columns would help to eliminate pounding simply by reducing the overall displacement demands and hence the relative displacement demands between bridge segments. Hence, we opted to increase the overall stiffness of the columns by adding an additional layer of higher strength concrete between the original column and the steel jacket. The extra layer of concrete has a thickness of 1 ft and an assumed compressive strength of 4 ksi. Thus the final column diameter is increased from 7 ft to 8 ft. The thickness of the steel jacket is assumed to be 0.4 in, which is the minimum limit for workmanship (FHWA, 2006).

Table 3.6.2 summarizes the plastic hinge rotation capacities of the jacketed columns, and Figure 3.6.4 depicts the moment curvature relationship of the jacketed columns. Note that jacketing the columns leads to an approximate 400% increase in the plastic rotation capacity of the columns.

Table 3.6.2 Summary of jacketed column properties

Bent #	*Height* (*ft*)	*Axial Load* (*kip*)	Θ_p (*rad*)
2	40	1217.7	0.048
3	37	1179.8	0.048
4	16.25	1033.8	0.025
5	23	1113.8	0.032
6	46	1224.5	0.054
7	38	1207.4	0.046
8	36.5	1183.5	0.045

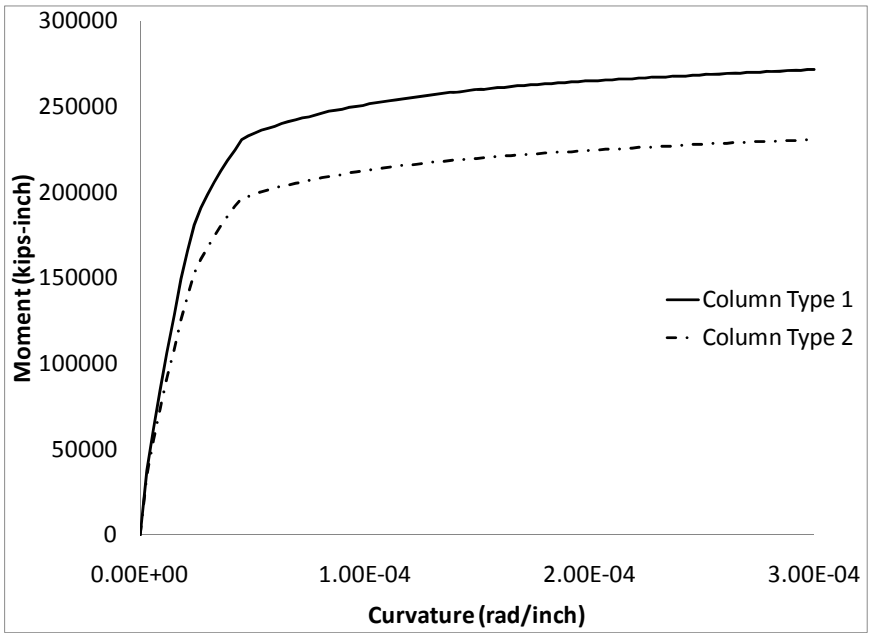

Figure 3.6.4. Moment – curvature diagram of jacketed columns

3.7 Evaluation of Retrofit Solutions

The three retrofit strategies described above are evaluated through nonlinear response history analysis of the retrofitted bridge to the seven ground motions, wherein a modified model of the bridge was created to represent each retrofit strategy. Comparative results are reported below for locking all pin-hanger joints (Strategy 1), partial isolation of columns 4 and 5 to match the periods of the three bridge segments (Strategy 2), and jacketing all columns with a combination concrete layer and steel shell (Strategy 3). In Strategies 2 and 3, pin-hanger joints 1 and 4 are locked, because these joints are close to the end and also experienced the largest pounding forces during analysis of the original bridge.

Figure 3.7.1 presents the average pounding forces recorded at each gap for Strategies 2 and 3 along with the forces in the original bridge. The partial isolation strategy, specifically designed to address the pounding at the gaps, was ineffective in preventing pounding at the second and third joints. The pounding force in joint 3 actually increased compared to the original analysis. In hindsight, the isolation approach failed because it could not address the asymmetry in abutment stiffnesses that caused segments 1 and 3 to have larger movement in one direction than the other. Jacketing the columns only resulted in a slight decrease in the pounding force demands at both joints.

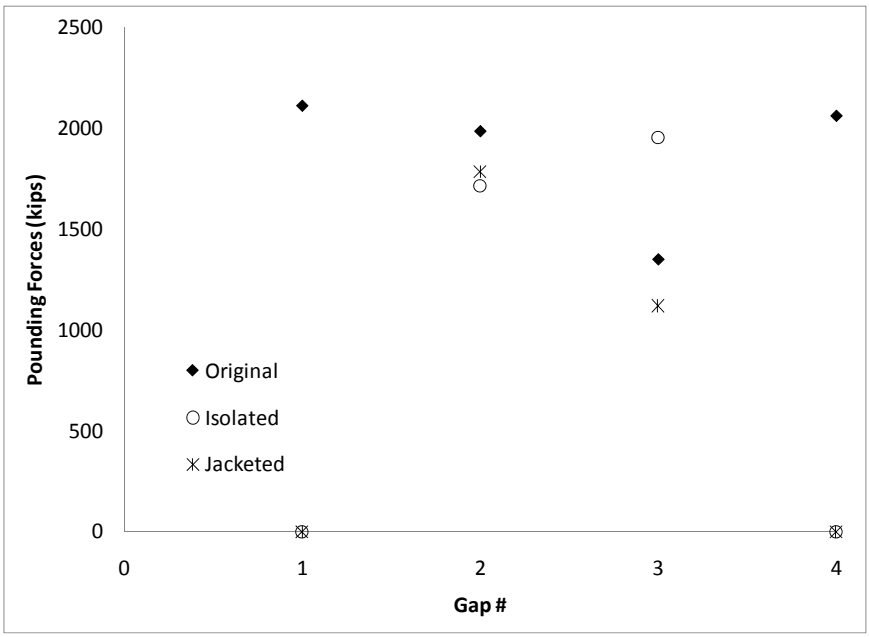

Figure 3.7.1. Average pounding forces in the gaps.

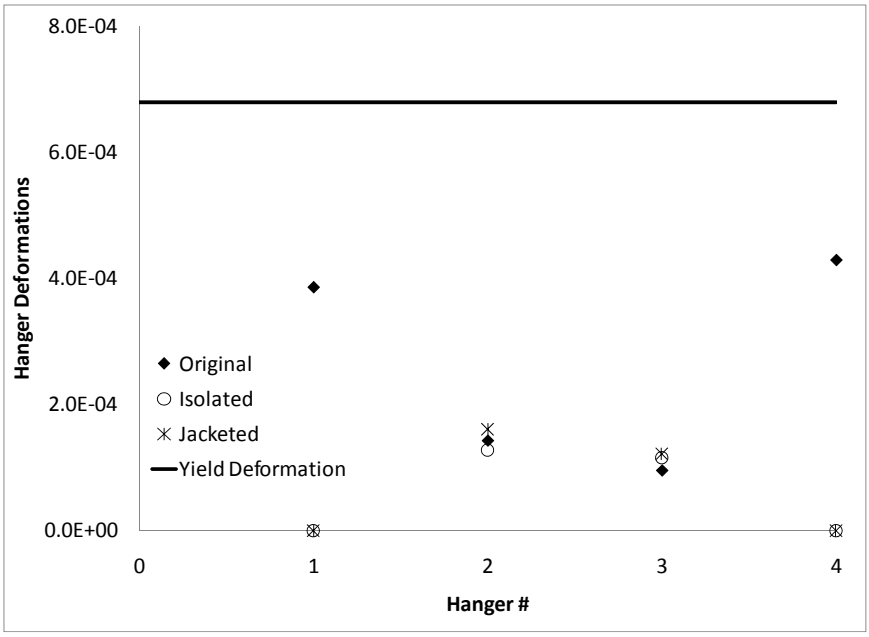

Figure 3.7.2. Average deformation demands in the hangers.

Figure 3.7.2 depicts the average deformation demands in the hangers for the original bridge and the proposed retrofit schemes. The deformation demands in the hangers did not exceed yield – indicated by a solid horizontal line across the graph – for any of the bridge

designs considered. The largest hanger deformation demands were observed in joints 1 and 4 in the original bridge. Since these joints were locked for retrofit strategies 2 and 3, the maximum deformation demand in any hanger decreased by more than a factor of 2, which would imply that retrofitting provides additional safety factor against hanger failure.

The ratio of the average plastic hinge rotation demands to the respective plastic rotation capacities (DCR) are depicted in Figure 3.7.3. Note that the column plastic rotation capacities for Strategies 1 (locking the joints) and 2 (partial isolation) are the same as those of the original bridge. While Strategies 1 and 2 lead to some improvement in the column rotation demands, the DCR are still predicted to be much larger than 1 for several of the columns. Jacketing the columns, which led to a marked increase in the rotation capacities, is effective in reducing the DCR to well below 1 for all columns.

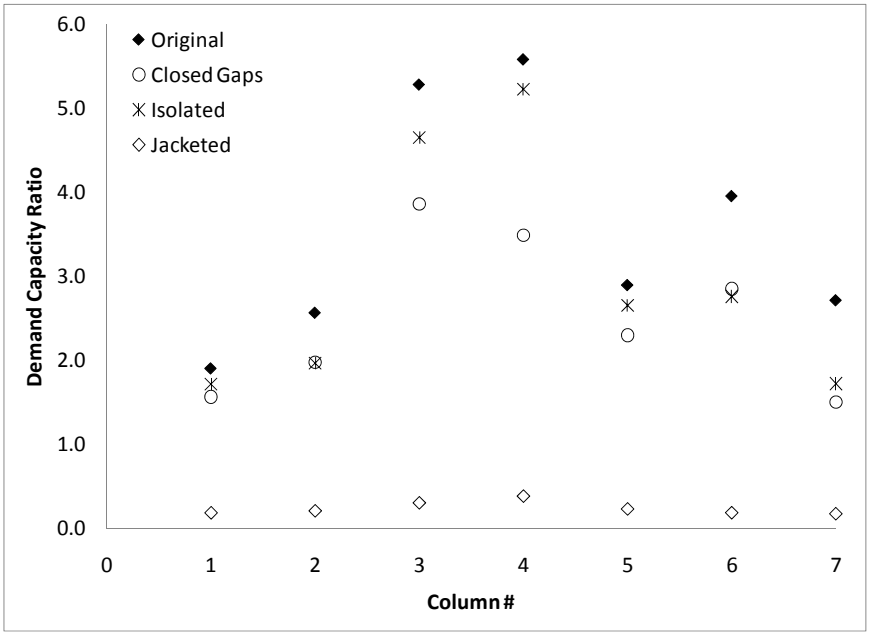

Figure 3.7.3. Average plastic rotation DCR's for all bridges

The average demands for the critical parameters investigated in this study presented in Figures 3.7.1 to 3.7.3 show that all retrofit schemes produce very similar results as far as pounding force and hanger deformation demands are concerned. However, only jacketing the columns leads to the substantial decrease in column rotation demand to capacity ratios as needed to prevent column collapse under the specified hazard level. Assuming the model is completely accurate, Strategy 3 is effective in alleviating the seismic deficiencies of the bridge. However,

the model cannot exactly account for damage due to pounding at the joints, and some uncertainty exists regarding how much pounding can be accommodated without adversely affecting the hangers or causing other unforeseen damage. Although the joints are predicted to have acceptable response based on the dynamic analysis that we have performed so far, developing a backup plan is advisable.

3.8 Design of Cable Restrainers

Cable restrainers are proposed across joints 2 and 3 as an optional additional measure of protection against failure of the pin-hanger joints. Cable restrainers are used across typical expansion joints, sometimes in combination with seat extenders, to prevent unseating of bridge spans. Caltrans implemented a widespread retrofit program in the 1970's using cable restrainers as a low cost means of preventing this type of failure (FHWA, 2006). Some early restrainer retrofits failed in the 1989 Loma Prieta and 1994 Northridge Earthquakes, which indicated design flaws in restrainers and in their connections. Restrainers must be sufficiently stiff and strong to prevent the expansion joint from pulling apart, and the bridge elements must be strong enough to resist additional forces that are transferred through the restrainers (FHWA, 2006).

The application of cable restrainers across the pin-hanger joints in this bridge is similar to their application across typical expansion joints, in that the goal in both cases is to limit the opening of the joint. Limiting joint opening in this curved girder bridge will further reduce the possibility that the pin-hanger connections could fail. Two types of restrainers have been used by Caltrans: cables and high strength bars (FHWA, 2006). Cables are more flexible and more economical to install. Bars have a higher ductility capacity, but the ductility is not utilized since the restrainers are designed to remain elastic. The reduced flexibility of bars means they must be longer to accommodate an equivalent displacement demand. We recommend the use of cable restrainers for this curved girder bridge.

Simplified restrainer design methods for restrainers in in-span expansion joints in a continuous superstructure were developed by DesRoches and Fenves (1998). Simplified methods are based on static analysis using a response spectrum to determine the seismic displacement demand across the hinge. The selection of a method depends on the ratio of substructure periods of the adjacent span segments, calculated from eigenvalue analysis of each bridge segment between hinges or at the ends of the bridge. A single-step static analysis may be

used for period ratios $T_i/T_j > 0.6$. An iterative static analysis may be used for period ratios T_i/T_j from 0.3 to 0.6. A full dynamic analysis is recommended if the period ratio is less than 0.3, because the vibration phases of the adjacent span segments will not be correlated. The periods of the segments following the retrofit were calculated through free vibration analysis of the bridge in the longitudinal direction: $T_1 = 0.53$ sec (left segment), $T_2 = 0.36$ sec (middle segment), and $T_3 = 0.50$ sec (right segment). Thus, the period ratios are $T_2/T_1 = 0.68$ and $T_2/T_3 = 0.72$, and the single step static method can be used.

The restrainer design method for a traditional expansion joint is based on available seat width D_{as}, or displacement that can be accommodated across the joint before the span becomes unseated, and the unrestrained joint displacement D_{eq0} as determined from a single-degree-of-freedom response spectrum analysis. Note that D_{as} is a measure of capacity while D_{eq0} is a measure of demand. For the bridge under consideration, we take D_{as} as the lateral displacement across the joint when the hangers start to yield and D_{eq0} as the average lateral displacement across the joint as determined from response history analysis to the seven representative motions. The hanger yield force (considering two hangers per girder acting over four girders) is 2560 kip. Computed from a static analysis (like that shown in Figure 3B.4), the positive lateral deformation across the hinge when each hinge starts to yield is 1.23 inches. However, this statically generated force deformation assumes the force across the hanger in the vertical direction to be zero. In reality, the hanger carries a force in the vertical direction that represents the transfer of gravity loads from the cantilevered span to the suspended span, and this force varies during dynamic analysis as a result of vertical vibration. As a result, the lateral deformation across the gap and the axial force in the hanger are not closely correlated. To illustrate, peak lateral deformation across the gap vs. peak axial force in the hanger for the seven response histories is plotted in Figure 3.8.1. As can be observed, lateral deformations across the gap ranges from 1 to 7 inches, but peak axial forces range from 300 to 1000 kips, which is only 2/5 of the yield force at the maximum. A great deal of scatter is observed, and the peak lateral deformations do not correlate with the peak axial forces. We interpret these results to indicate that a significant component of rigid rotation (vertical shortening) of the hanger accompanies the lateral deformation or widening of the gap, which is why the lateral deformation can be much larger than that which occurs at yield. Also, the peak axial force reported in Figure 3.8.1 could be representative of hanger movement in the opposite direction, or gap closing, since the axial force

in the hanger is positive in both directions. Larger hanger forces – up to yield - were observed in the analysis of the unretrofitted bridge, but these were correlated with much larger pounding forces and deformations, and were most likely observed in the negative direction. In short, the lateral displacement capacity across the hanger cannot be predicted.

For the purpose of cable restrainer design, we will design the restrainers so they are fully engaged at the current gap demand displacement of the bridge. Thus, we take D_{eq0} = 2.36 inches (the average positive gap displacement from the response history analyses), and D_{as} = 3.54 inches, such that $D_{eq0} = (2/3)D_{as}$. The restrainers are designed based on these assumptions, and calculations are summarized in Appendix 3D. Based on the design calculations, 8 restrainer bars are needed across each remaining pin-hanger connection, and each bar has a length of 8.75 ft.

To anchor the cables to the bridge, the cable restrainers can be assembled into four groups of two restrainers and bolted to the bottom flanges of the existing girders. A schematic of the connection is provided in Figure 3.8.2, based on a similar detail shown in Priestly et. al. (1996). A triangular anchor plate is used, wherein the bottom plate is bolted to the flange and the cable is passed through and anchored to the side plate. The connections should be designed for 125% of the nominal breaking force of the restrainers (FHWA, 2006).

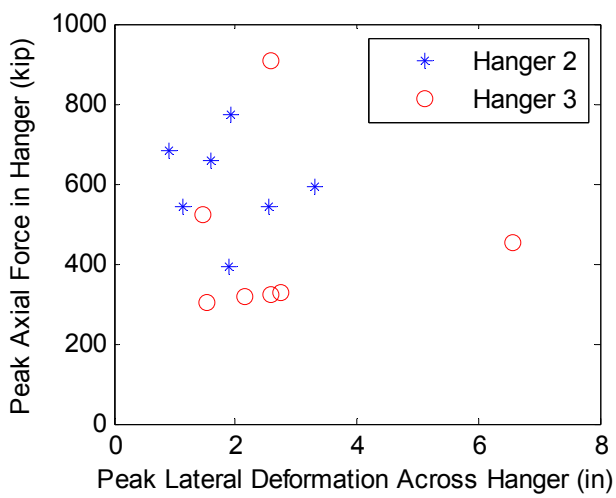

Figure 3.8.1. Peak axial force and positive lateral deformation in hangers observed from response history analysis of the retrofitted bridge

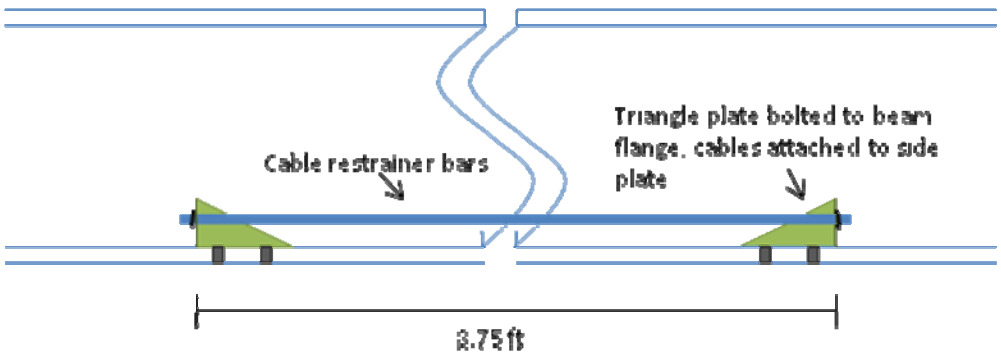

Figure 3.8.2. Schematic of cable restrainers connected to beam flanges spanning the pin-hanger connection.

Appendix 3. Detailed Analysis for B-Bent Over I-215 and I-80

Appendix 3A. Determination of Seismic Retrofit Category

Bridge Importance:

Standard

Anticipated Service Life:

The bridge plans are approved in 1984, and the bridge is assumed to be constructed in 1985.

Bridge age: ~ 23 years

Anticipated Service Life: 75-23=52 years

Service life category: ASL3

Bridge Performance Level:

UL Motion: PL1

LL Motion: PL3

Site Class:

The site condition is determined through harmonic mean of blow counts of soil layers in the top 100 ft (Table 2-3 of FHWA, 2006). The plan of soil data is based on elevation, thus the elevation of the surface grade must be determined.

From Borings, N ≈ 5

Site Class: E

Detailed calculations are presented in Table 3A.1

Spectral Accelerations and Soil Factors:

The bridge is located in the Layton to Hill Field interchange. The exact location is

Latitude: 40° 45' 53.18" N

Longitude: 111° 56' 59.66" W

Zip code: 84104

Summary of Definitions

Ss	0.2- second period spectral acceleration
S_1	1- second period spectral acceleration
F_a	Site coefficient for short period

F_v	Site coefficient for long period
$S_{DS}=F_a S_s$	Design earthquake response spectral acceleration at short period
$S_{D1}=F_v S_1$	Design earthquake response spectral acceleration at long period
SHL	Seismic hazard level

Determination of Seismic Hazard Level (SHL)

From Table 1-4 and 1-5 of (FHWA, 2006)

	S_s (g)	S_1 (g)	F_a	F_v	S_{DS} (g)	S_{D1}(g)	SHL
Lower Level: 500-year	0.632	0.213	1.44	3.15	0.91	0.67	IV
Upper Level: 2500-year	1.50	0.633	0.90	2.40	1.35	1.52	IV

Seismic Retrofit Category (SRC)

From Table 1-6 of (FHWA, 2006)

UL: **SRC = C**

LL: **SRC = D**

Table 3A.1 Blow count number of soil

Elevation	Thickness (d)	BC1	BC2	Average (BCa)	d/Bca
4534.17	2.47	19	28	23.5	0.105106
4531.7	2.7	21	26	23.5	0.114894
4529	8	5	8	6.5	1.230769
4521		16	37		
		22	42		
	12	34	45	32.6667	0.367347
4509		12	17		
		19	33		
	14	29	47	26.16667	0.535032
4495		56	91		
		12	48		
	16	33	37	46.16667	0.34657
4479		9	13		
		10	19		
		11	20		
		11	16		
		15	22		
	29	16	26	15.66667	1.851063
4450	4	30	48	39	0.102564
4446					

Blow Count Number

∑= 88.17 ∑= 4.653345 18.94766

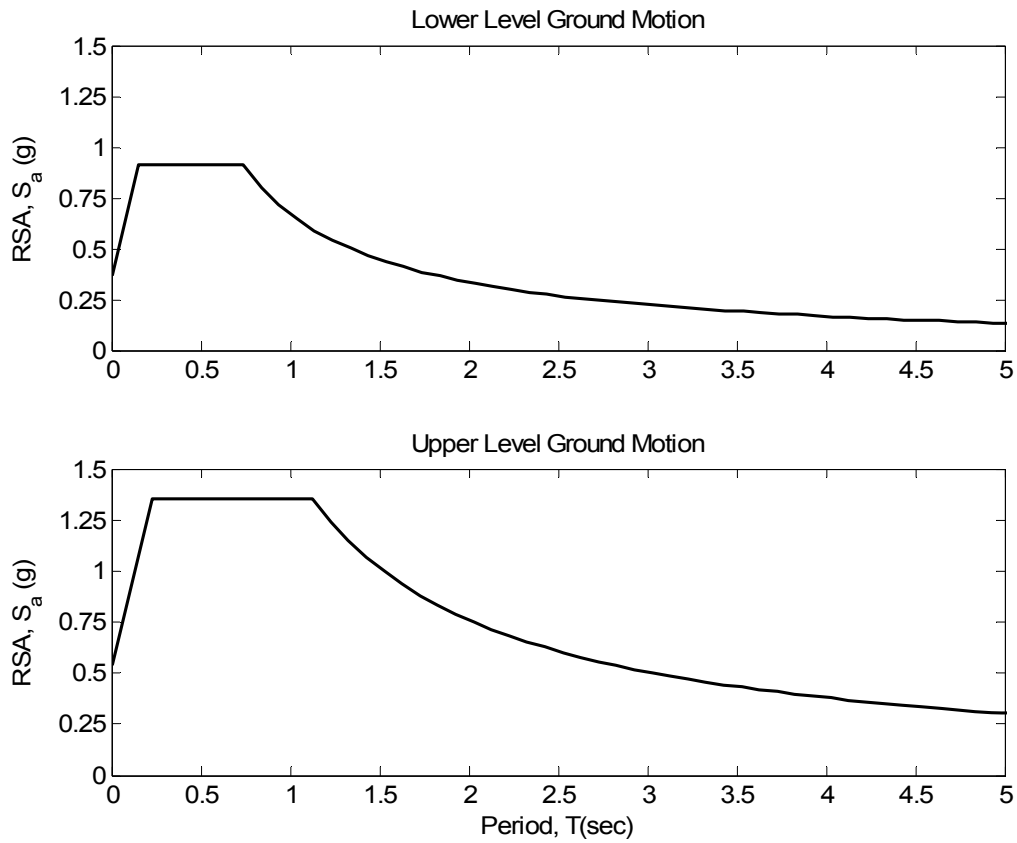

Figure 3A.1. Acceleration design spectra for LL and UL ground motions

Appendix 3B. Verification Studies of Pin-Hanger Element

Pin-hanger element in 2D:

The analytical force-deformation relation in a pin-hanger element considering geometric nonlinearities is found based on section properties and element deformation as follows, where the notation is illustrated in Figure 3B.1.

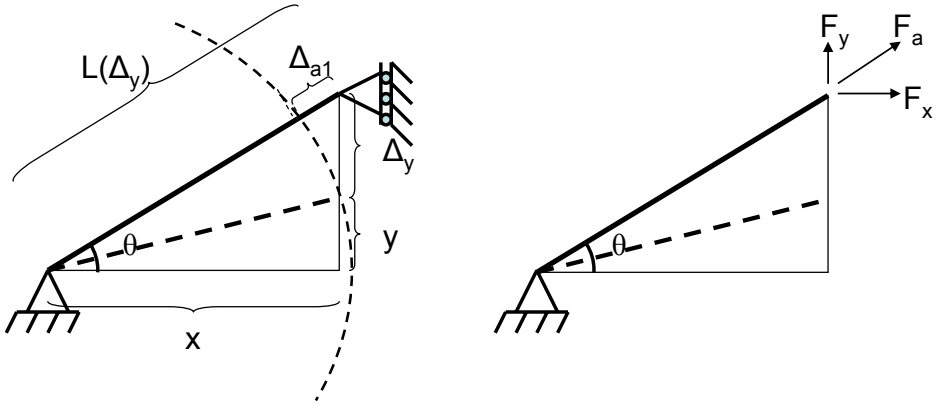

Figure 3B.1. Pin-hanger joint model for the analytical force-deformation derivation.

$$L(y) = \sqrt{x^2 + y^2}, \quad L(\Delta_y) = \sqrt{x^2 + (y + \Delta_y)^2}$$

$$\Delta_{a1} = L(\Delta_y) - L(y)$$

$$\varepsilon_{a1} = \frac{\Delta_{a1}}{L(y)},$$

$$F_a = EA\varepsilon_{a1}, \quad F_y = F_a \sin(\theta), \quad \sin(\theta) = \frac{(y + \Delta_y)}{L(\Delta_y)}$$

$$F_y = EA\frac{L(\Delta_y) - L(y)}{L(y)}\sin(\theta) = EA\frac{\sqrt{x^2 + (y + \Delta_y)^2} - \sqrt{x^2 + y^2}}{\sqrt{x^2 + (y + \Delta_y)^2}\sqrt{x^2 + y^2}}(y + \Delta_y)$$

Model properties:

The model shown in Figure 3B.2 has been implemented in LARSA and OpenSees for static and dynamic analyses.

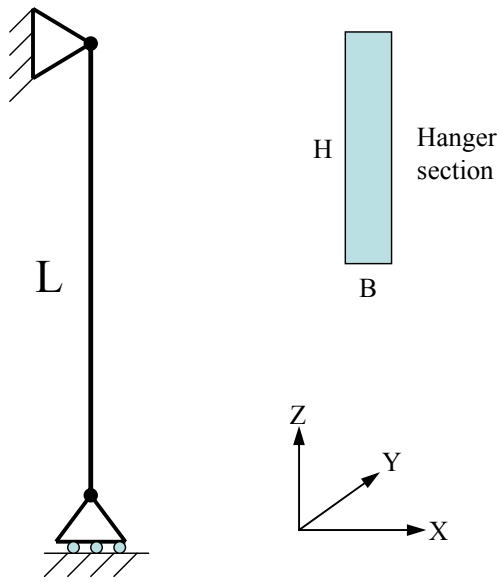

Figure 3B.2. Pin-hanger joint model in LARSA and OpenSees.

Section properties

$L_{Hanger} = 6$ *in*

$H_{Hanger} = 8$ *in*

$B_{Hanger} = 2$ *in*

Material: A36

***Static Cyclic Loading* (*displacement control*)**

A displacement controlled static analysis is conducted in LARSA and OpenSees where the displacement shown in Figure 3B.3 is imposed to the free moving end of the element.

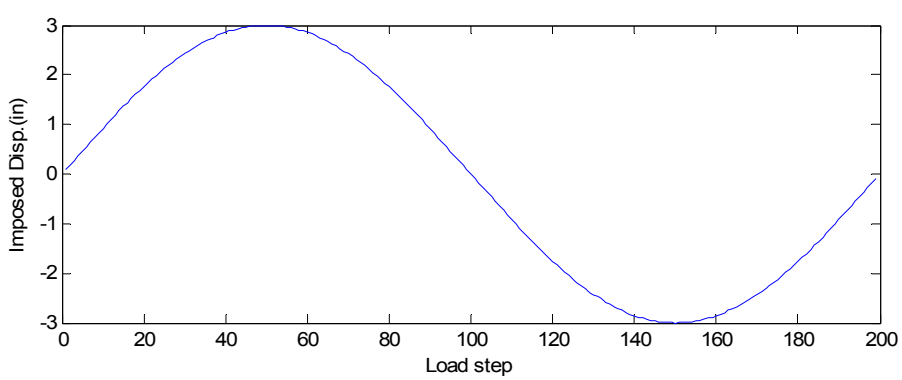

Figure 3B.3. Imposed end displacement.

Resulting force-deformation curves obtained from the analytical approach, LARSA and OpenSees numerical analyses are presented in Figure 3B.4. The force plotted is the x-direction component rather than the resultant axial force. A very good agreement in the results from different methods is observed.

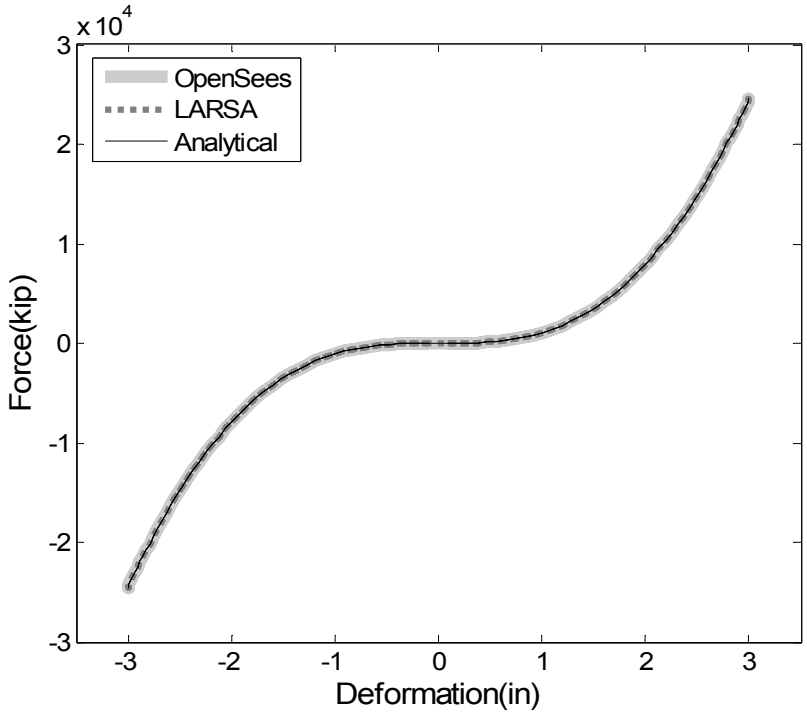

Figure 3B.4. Force-deformation curves for static cyclic loading.

***Dynamic Loading* (*input acceleration*)**

A concentrated mass (w = 100 kip) is attached to the bottom node (Figure 3B.2) which is free in the x-direction. The input acceleration is shown in Figure 3B.5.

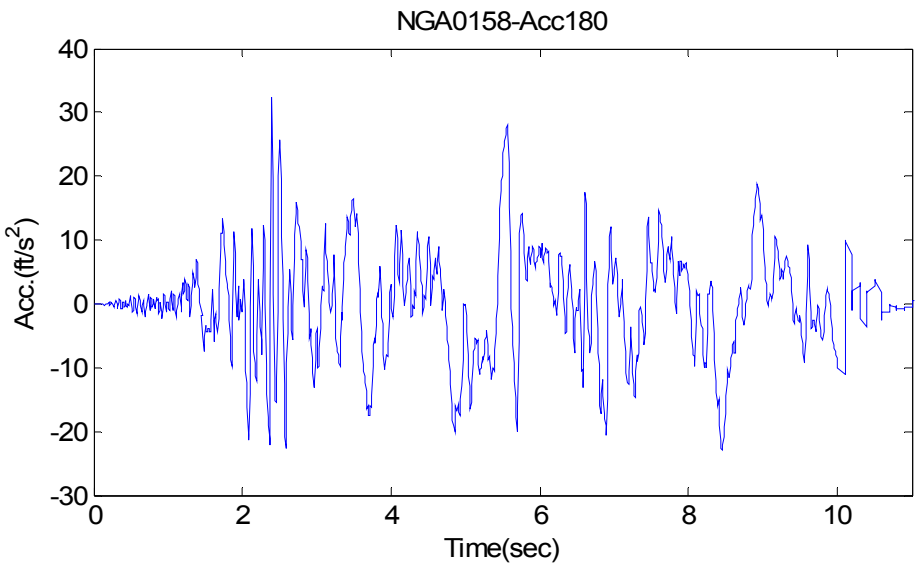

Figure 3B.5. Input acceleration in x-direction.

To check whether the models are correct and the same in LARSA and OpenSees, linear time history analysis is performed and displacement responses of the bottom node of the element (Figure 3B.2) are presented in Fig. 3B.6. The results from the two analysis programs match closely and are assumed to both be accurate.

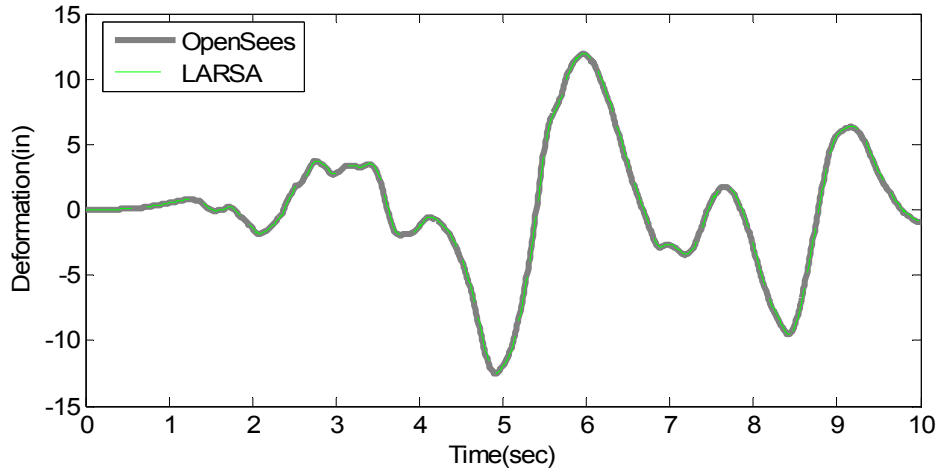

Figure 3B.6. Time history of the deformation response in X direction.

Geometrically nonlinear response history analysis is performed next. The force-deformation curves obtained from OpenSees and LARSA are compared to the analytically computed force-deformation in Figure 3B.7, and force and displacement versus time are plotted for OpenSees and LARSA in Figure 3B.8.

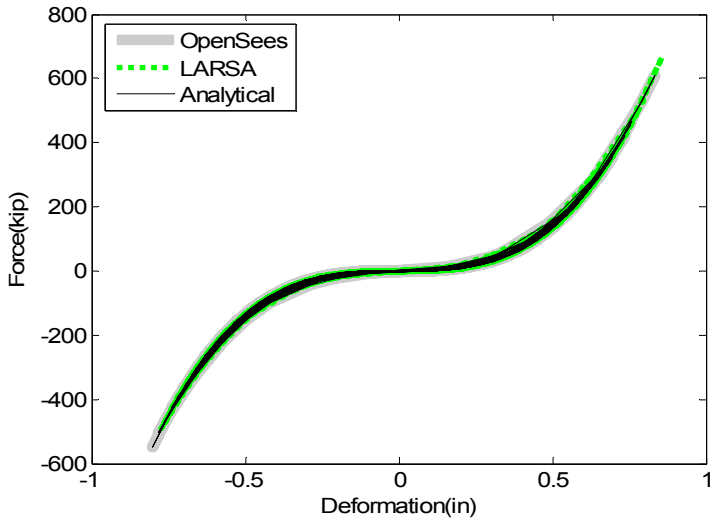

Figure 3B.7. Force-deformation curves for dynamic loading.

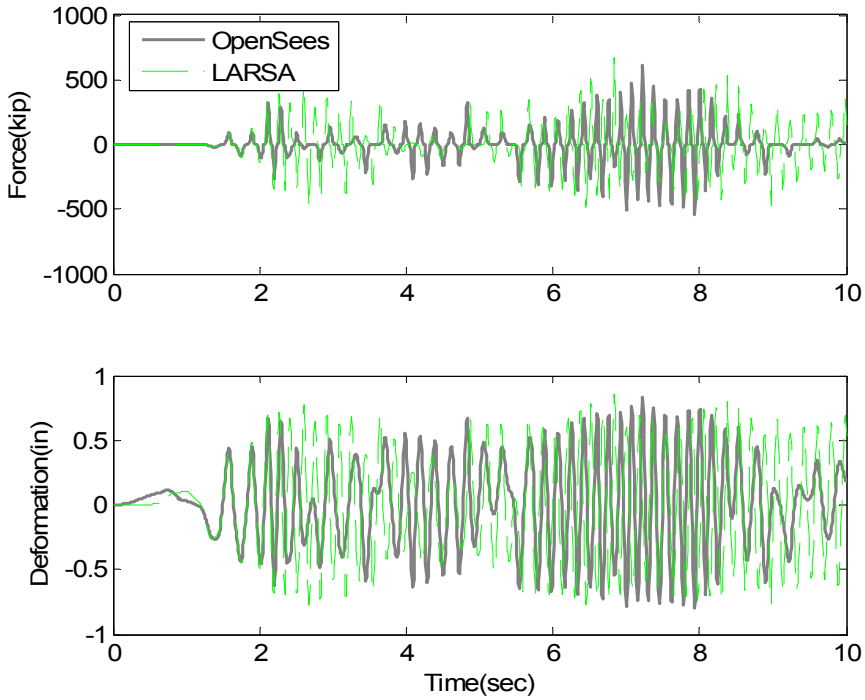

Figure 3B.8. Force and deformation response of the element in X direction versus time.

The force-deformation relations for both the OpenSees and LARSA models match the analytical force-deformation response (Figure 3B.7). However, time history responses of the element vary significantly from LARSA to OpenSees. For the first few seconds, the result from LARSA

matches the response obtained from OpenSees closely but afterwards they deviate significantly (Figure 3B.8). This suggests that one of the programs may be incorrect.

Pin-Hanger Element in 3D

The relation for the large deformation of a truss element in 2D is extended to 3D as follows.

$$L(x,y)=\sqrt{z^2+x^2+y^2},\quad L(x,y,\Delta_x,\Delta_y)=\sqrt{z^2+(x+\Delta_x)^2+(y+\Delta_y)^2}$$
$$\Delta_a=L(x,y,\Delta_x,\Delta_y)-L(x,y)$$
$$\varepsilon_a=\frac{\Delta_a}{L(x,y)},$$
$$F_a=EA\varepsilon_a,$$

$$F_x=F_a\cos(\theta_{y+\Delta_y,z})\sin(\theta_{x+\Delta_x,z}),\quad \cos(\theta_{y+\Delta_y,z})=\frac{z}{\sqrt{z^2+(y+\Delta_y)^2}},\quad \sin(\theta_{x+\Delta_x,z})=\frac{x+\Delta_x}{\sqrt{z^2+(x+\Delta_x)^2}}$$

$$F_x=EA\frac{L(x,y,\Delta_x,\Delta_y)-L(x,y)}{L(x,y)}\cos(\theta_{y+\Delta_y,z})\sin(\theta_{x+\Delta_x,z})$$
$$=EA\frac{\sqrt{z^2+(x+\Delta_x)^2+(y+\Delta_y)^2}-\sqrt{z^2+x^2+y^2}}{\sqrt{z^2+x^2+y^2}}\cdot\frac{z}{\sqrt{z^2+(y+\Delta_y)^2}}\cdot\frac{x+\Delta_x}{\sqrt{z^2+(x+\Delta_x)^2}}$$
$$F_y=F_a\cos(\theta_{x+\Delta_x,z})\sin(\theta_{y+\Delta_y,z}),\quad \sin(\theta_{y+\Delta_y,z})=\frac{y+\Delta_y}{\sqrt{z^2+(y+\Delta_y)^2}},\quad \cos(\theta_{x+\Delta_x,z})=\frac{z}{\sqrt{z^2+(x+\Delta_x)^2}}$$
$$F_y=EA\frac{L(x,y,\Delta_x,\Delta_y)-L(x,y)}{L(x,y)}\sin(\theta_{y+\Delta_y,z})\cos(\theta_{x+\Delta_x,z})$$
$$=EA\frac{\sqrt{z^2+(x+\Delta_x)^2+(y+\Delta_y)^2}-\sqrt{z^2+x^2+y^2}}{\sqrt{z^2+x^2+y^2}}\cdot\frac{y+\Delta_y}{\sqrt{z^2+(y+\Delta_y)^2}}\cdot\frac{z}{\sqrt{z^2+(x+\Delta_x)^2}}$$

The same model is used as in 2D tests, and the third dimension is included in the analysis. The previously defined acceleration input is used in the x-direction (Figure 3B.5), while the acceleration input of Figure 3B.9 is applied in the y-direction.

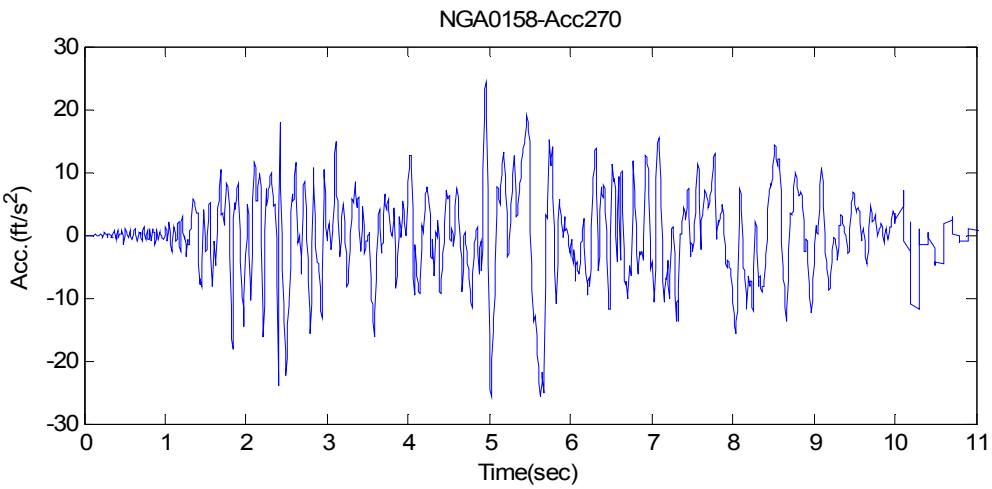

Figure 3B.9. Input acceleration in y-direction.

Force-deformation curves of the pin-hanger element in x and y-directions obtained from the analytical formula, LARSA, and OpenSees are presented in Figure 3B.10. A good agreement is observed between the results from different approaches. However as was the case in 2D analysis, time history responses of the element found from LARSA deviate from responses obtained from OpenSees after a few seconds (Figure 3B.11).

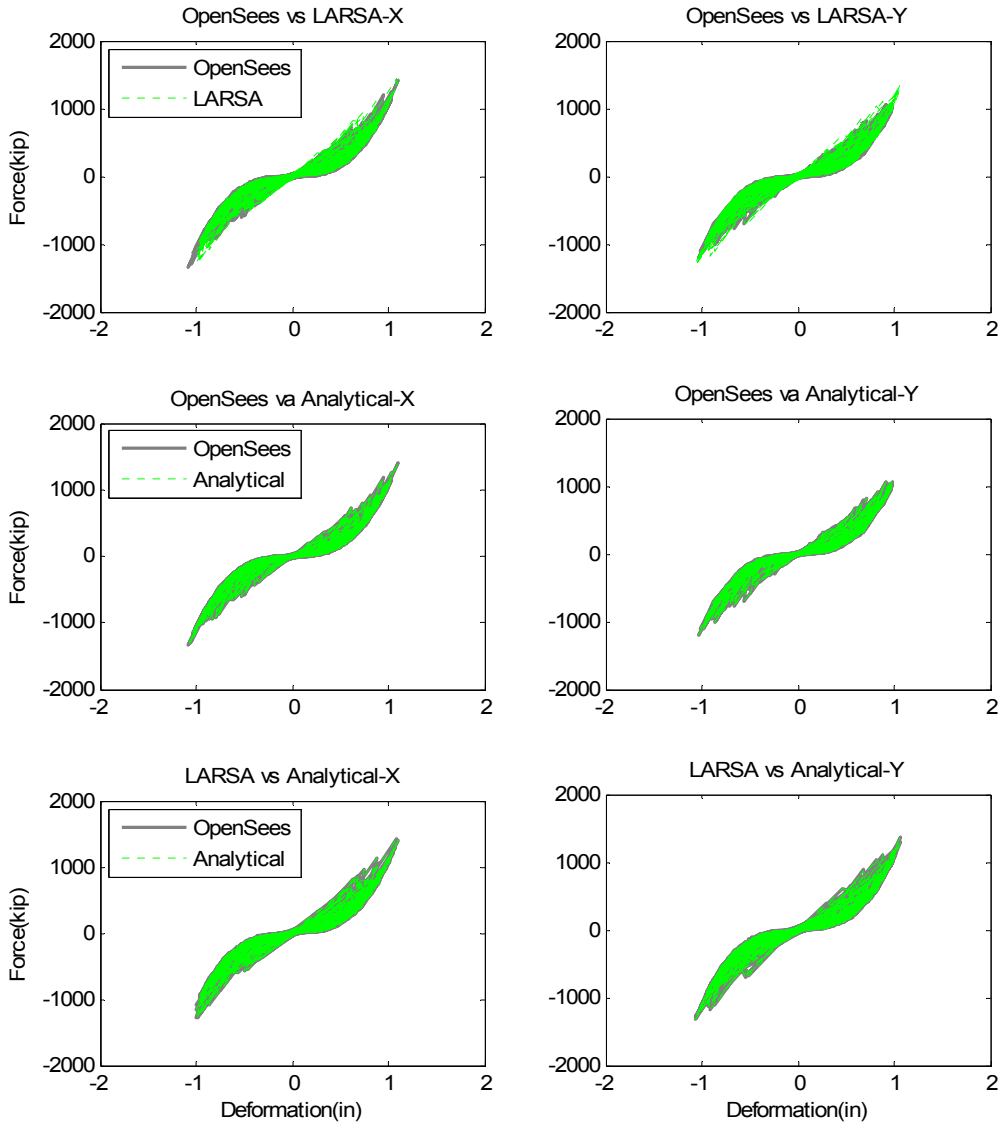

Figure 3B.10. Force-deformation curves for dynamic loading.

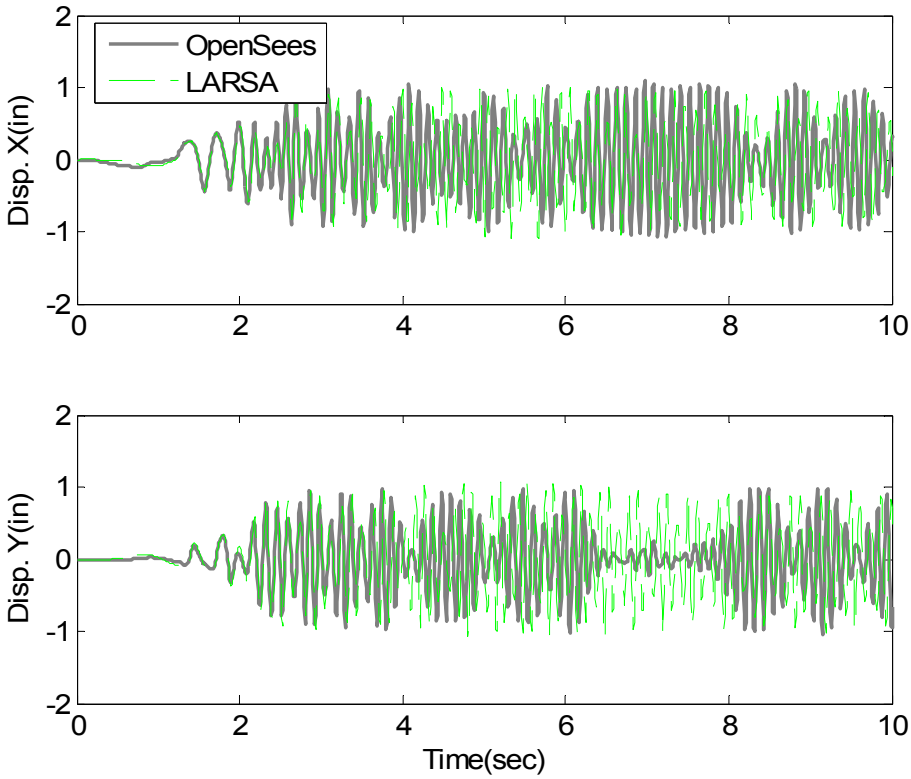

Figure 3B.11. X and y-deformation responses of the pin-hanger element versus time

Analysis of Pin-hanger Joint with Frame Elements

Model properties:

The interaction of frame elements with the pin-hanger joint system is investigated using the model shown in Figure 3B.12.

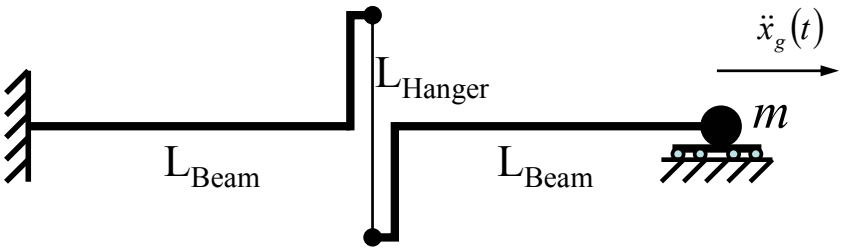

Figure 3B.12. Pin-hanger joint model with adjacent beam elements.

In this model, the properties of the hanger are the same as before and the section of beams and their dimension are as follows.

$L_{Beam} = 4\ ft$

Section: W16×50

$L_{Hanger} = 0.5\ ft$

w = 100 *kip*

Material: A36

In the model, the links connecting beams to hangers are rigid. The rigidity is imposed by choosing a very large elastic modulus for link elements, $E_{rigid\ link}$ = 2.9e8 kip/in^2 (= 10^4 E_{Beam}). The reaction force of the left end and displacement of the right node in X direction are presented in Figure 3B.13. The force-deformation behavior of the model in LARSA deviates from the expected, wherein the equilibrium point is shown to shift from 0 in to about -5 in (Figure 3B.13). However, only hysteretic material behavior could cause a residual displacement at zero force. Therefore, we conclude that the element in LARSA does not satisfy equilibrium for this case.

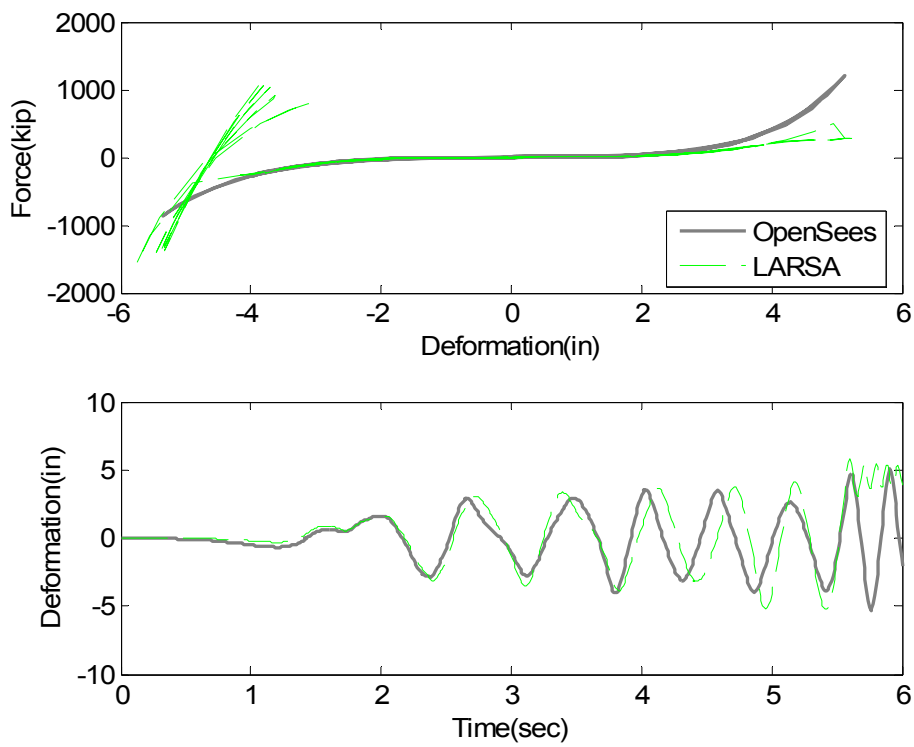

Figure 3B.13. Force-deformation and deformation time history response of the pin-hanger model with adjacent frame elements.

Appendix 3C. Modeling Considerations

Abutment Stiffness

L_{bridge}=1430.5 ft

R_{bridge}=1432.395 ft

$\theta/2$: = L_{bridge} / R_{bridge} =28.61^o

L=30 ft	Width of the backwall based on figure 1B.2
H: = 9.83 ft	Height of the abutment
C_p: = 40 kips	Capacity of the pile

The total capacity of the abutment-pile system in longitudinal direction is

$$P_{pLongComp} = p_p.H.L + N_p.C_p = \frac{2}{3} \times 9.83^2 \times 30 + 4 \times 40 = 2091.8 \quad kips$$

In tension, only piles contribute to the stiffness:

$$P_{pLongTen} = 4 \times 40 = 160 \quad kips$$

A similar procedure is applied in the transverse direction, but the transverse stiffness of the abutment is provided by wing walls. Priestley et al. (1996, Sec. 4.4.2) proposes to take the effective width as the length of the wing walls multiplied by a factor of 8/9 to account for differences in participation of both wing walls.

$L = \frac{8}{9} \times (2 \times 13) = 23.11 \quad ft$	Width of the wingwall
H_1: = 9.83 ft	Height of the abutment
H_2: =2.0 ft	Height of the abutment
H_{avg}: = 5.92 ft	Height of the abutment
C_p: = 40 kips	Capacity of the pile

The total capacity of the abutment-pile system in longitudinal direction is

$$P_{pTrans} = \frac{2}{3} \times 5.92^2 \times 23.11 + 4 \times 40 = 699.1 \quad kips$$

The global X direction in the model coincides with the longitudinal direction at the exact center of the bridge and the global Y direction is perpendicular to the X direction. As a consequence, at the far ends of the bridge, transformation is necessary to convert the longitudinal and transverse capacities to X and Y direction capacities. The transformation equations are given below. The force capacity of the abutment is different for tension and compression states, and they are indicated by the subscript "Ten" and "Comp" below. In each of these states, both the back wall and the wing wall contribute to the total capacity of the abutment in each direction, where they are shown by the subscript 1 for the back wall and with 2 for the wing wall. Considering these notations, the abutment capacities in X and Y directions are

$$P_{pXComp1} = P_{pLongComp} \times \cos(\theta/2) = 1836.4 \quad kips$$

$$P_{pXComp2} = P_{pTrans} \times \sin(\theta/2) = 334.7 \quad kips$$

$$P_{pXTen1} = P_{pLongTen} \times \cos(\theta/2) = 140.5 \quad kips$$

$$P_{pXTen2} = P_{pTrans} \times \sin(\theta/2) = 334.7 \quad kips$$

$$P_{pYComp1} = P_{pLongComp} \times \sin(\theta/2) = 1001.7 \quad kips$$

$$P_{pYComp2} = P_{pTrans} \times \cos(\theta/2) = 613.7 \quad kips$$

$$P_{pYTen1} = P_{pLongTen} \times \sin(\theta/2) = 76.6 \quad kips$$

$$P_{pYTen2} = P_{pTrans} \times \cos(\theta/2) = 613.7 \quad kips$$

$$\Delta_{yX} = 0.02H_{Long} = 0.02 \times 9.83 = 0.1966 \quad \text{ft}$$

$$\Delta_{yY} = 0.02H_{Trans} = 0.02 \times 5.92 = 0.1184 \quad \text{ft}$$

For boundary conditions, the abutment is assumed to be fully constrained in the vertical direction and for rotation around the longitudinal and transverse axes.

The following calculations indicate the yield displacements in the X and Y directions, which together with the capacities, can be used to determine the stiffnesses.

$$\Delta_{yX} = 0.02H_{Long} = 0.02 \times 9.83 = 0.1966 \quad \text{ft}$$

$$\Delta_{yY} = 0.02H_{Trans} = 0.02 \times 5.92 = 0.1184 \quad \text{ft}$$

The compression and tension stiffness are found as follows

$$K_{XComp} = P_{XComp1} / \Delta_{yX} + P_{XComp2} / \Delta_{yY} = 1013.97 \quad \text{kips/in}$$

$$K_{YComp} = P_{YComp1} / \Delta_{yX} + P_{YComp2} / \Delta_{yY} = 856.53 \quad \text{kips/in}$$

$$K_{XTen} = P_{XTen1} / \Delta_{yX} + P_{XTen2} / \Delta_{yY} = 295.13 \quad \text{kips/in}$$

$$K_{YTen} = P_{YTen1} / \Delta_{yX} + P_{YTen2} / \Delta_{yY} = 464.41 \quad \text{kips/in}$$

For boundary conditions, the abutment is assumed to be fully constrained in the vertical direction and for rotation around the longitudinal and transverse axes.

Material Property Assumptions for Section Analysis

```
fc = -1.4 ksi            # CONCRETE Compressive Strength
Ec = 57*sqrt(-fc)        # Concrete Elastic Modulus
Confined Concrete
Kfc = 1.3                # ratio of confined to unconfined concrete strength
fc1C = Kfc*fc            # CONFINED concrete (mander model), maximum stress
eps1C = 2*fc1C/Ec        # strain at maximum stress
fc2C = 0.2*fc1C          # ultimate stress
eps2C = 5*eps1C          # strain at ultimate stress
# unconfined concrete
fc1U = fc;               # UNCONFINED concrete (todeschini parabolic model), maximum stress
eps1U  = -0.003          # strain at maximum strength of unconfined concrete
fc2U = 0.2*fc1U          # ultimate stress
eps2U  = -0.01           # strain at ultimate stress
lambda = 0.1             # ratio between unloading slope at eps2 and initial slope Ec
# tensile-strength properties
ftC = -0.14*fc1C         # tensile strength +tension
ftU = -0.14*fc1U         # tensile strength +tension
Ets = $ftU/0.002         # tension softening stiffness

Fy = 24 ksi              # STEEL yield stress
Es = 29000ksi            # modulus of steel
```

Bs = 0.01	# strain-hardening ratio
R0 = 18	# control the transition from elastic to plastic branches
cR1 = 0.925	# control the transition from elastic to plastic branches
cR2 = 0.15	# control the transition from elastic to plastic branches

Bridge Natural Period and Mode Shapes

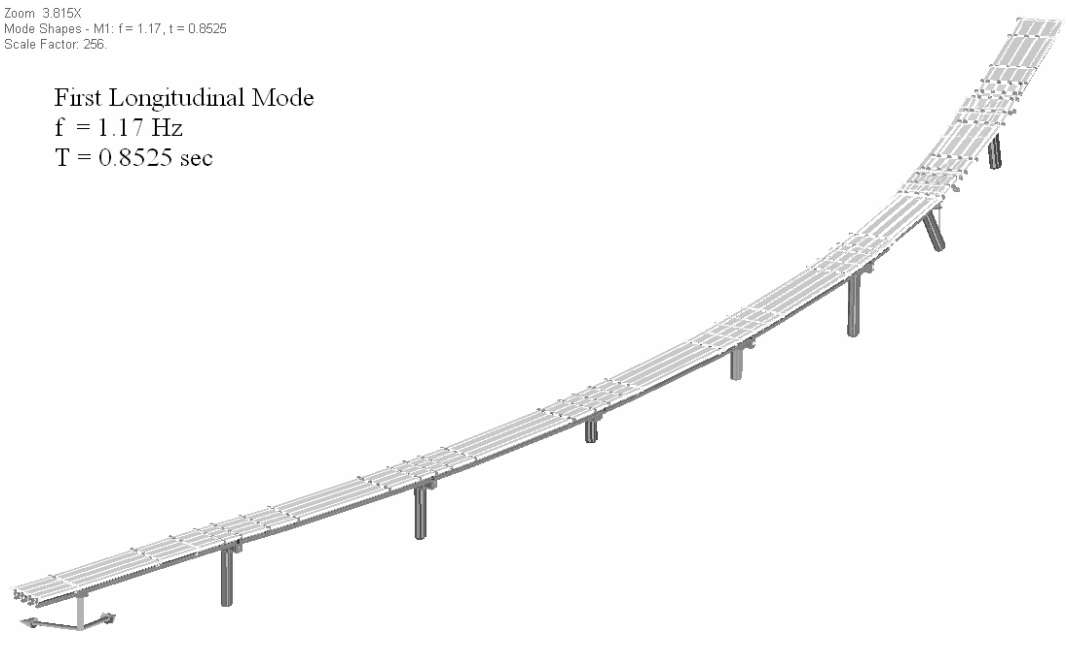

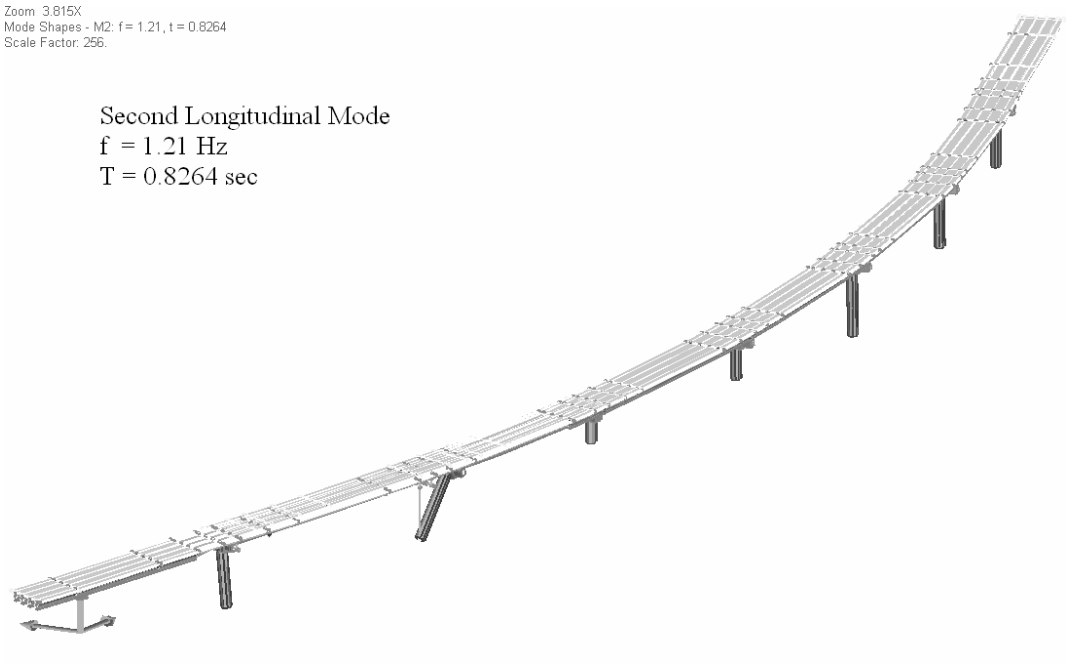

Figure 3C.1. Graphical depiction of first two mode shapes in the longitudinal direction

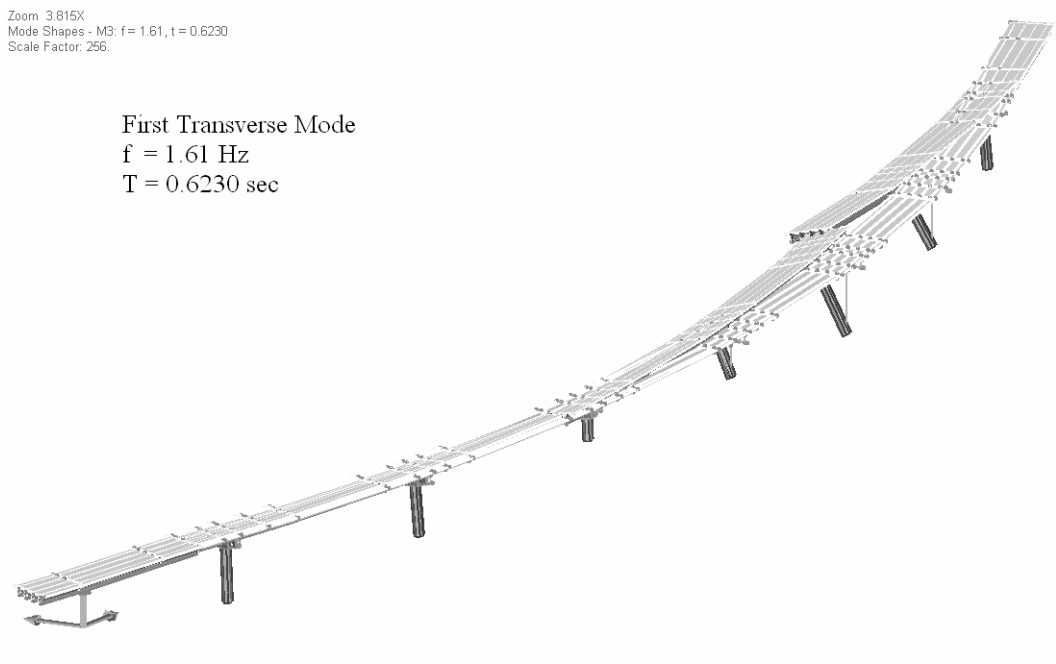

Figure 3C.2. Graphical depiction of first two mode shapes in the transverse direction

Appendix 3D. Restrainer Cable Design

Single-Step Non Iterative Method

Steps 1 and 2: Calculate maximum permissible displacement and displacement demand (mean demand from response history analysis) across the pin-hanger joint.

The displacement demand that produces yielding in the hanger and potential failure of the pin-hanger connection cannot be determined, because the vertical vibration of the hanger leads to inconsistent relation of the axial force and lateral hanger displacement over several ground motions. Therefore, the maximum permissible displacement is taken 3/2 of the mean observed displacement demand of the retrofitted bridge.

$D_r = 2.36$ in	Total displacement capacity of the restrainer cables at yield
$D_{rs} = 0.5$ in	Initial slack in the restrainer
$D_y = D_r - D_{rs} = 1.86$ in	Yield displacement in the restrainer cables
$D_{eq0} = 3.54$ in	Displacement demand at assumed hanger failure
$f_y = 176$ ksi	Yield strength of restrainer cables
E = 10000 ksi	Modulus of elasticity of restrainer cables

$A_r = 0.22\ in^2$ Area of an individual restrainer cable

$L_r = \frac{D_y E}{f_y} = \frac{1.86 \cdot 10000}{176}$ Required length of restrainer cable

$= 105$ inches (8.75 ft)

Step 3: Calculate restrainer stiffness

The required restrainer stiffness is based on the effective stiffness of the two adjacent span segments that the restrainers cross. The segment periods were determined by analysis of the free vibration response in the bridge longitudinal direction, which is more effective than eigenvalue analysis due to the asymmetry of the abutment stiffness and the difficulty of interpreting coupled lateral-torsional modes.

$W_1 = 2398$ kips Weight carried by bridge segment 1

$W_2 = 3373$ kips Weight carried by bridge segment 2

$W_3 = 2391$ kips Weight carried by bridge segment 3

$T_1 = 0.53$ sec Natural period of bridge segment 1

$T_2 = 0.36$ sec Natural period of bridge segment 2

$T_3 = 0.5$ sec Natural period of bridge segment 3

Note that the single step non-iterative method is permissible because the period ratios $T_2/T_1 = 0.68$ and $T_2/T_3 = 0.72$ both exceed the cutoff value of 0.6 (FHWA, 2006).

$\mu_1 = 3.30$ Target ductility in i_{th} span segment, approximated by the

$\mu_2 = 4.56$ average ductility demand observed during RHA of the

$\mu_3 = 3.11$ retrofitted bridge

$k_i = \frac{W_i}{g}\left(\frac{2\pi}{T_i}\right)^2 \frac{1}{\mu_i}$ Approximate stiffness of i_{th} span segment

$k_1 = (2398/386)\cdot(2\pi/0.53)^2/2 = 264.3$ kip/in

$k_2 = (3373/386)\cdot(2\pi/0.36)^2/2 = 583.6$ kip/in

$k_3 = (2391/386)\cdot(2\pi/0.50)^2/2 = 314.5$ kip/in

$$k_{eff} = \frac{k_i k_j}{(k_i + k_j)}$$ Effective stiffness across joint connecting spans i and j.

k_{eff1} = 264.3·583.6/(264.3+583.6) = 181.9 kip/in Hanger joint 2

k_{eff2} = 583.6·314.5/(583.6+314.5) = 204.4 kip/in Hanger joint 3

Recall that hanger joints 1 and 4 have been closed. The effective stiffness is essentially the restrainer stiffness, except that it has been altered by an amount dependent on the demand/capacity ratio of restrainer displacements.

$$k_r = k_{eff}\left(0.5 + \frac{0.5 - \eta^2}{\eta}\right)$$ Stiffness to be provided by the restrainers

$\eta = D_r/D_{eq0} = 2/3$ Ratio of restrainer displacement demand to capacity

kr_1 = 181.9·(0.5 + (0.5 - 0.667)/ 0.667) = 106.1 kip/in

kr_2 = 204.4·(0.5 + (0.5 - 0.667)/ 0.667) = 119.2 kip/in

Step 4: Calculate number of restrainer bars based on assumed strength, cross-sectional area of a single cable, stiffness and yield displacement. We opt for identical restrainer designs across hanger joints 2 and 3. Thus, we use the maximum value of k_{r1} and k_{r2} to determine the required number of bars.

$$N_r = \frac{k_r D_r}{F_y A_r} = \frac{119.2 \cdot 2.36}{176 \cdot 0.22} = 7.27$$

Minimum number of required bars = 8

REFERENCES

AASHTO, 2002, *Standard Specifications for Highway Bridges, Division I-A: Seismic Design*, 17th Edition, American Association of State Highway Transportation Officials, Washington, D. C.

Caltrans, (1995). *Bridge Memo to Designers Manual*, Sacramento, California.

DesRoches, R. and Fenves, G. L. 1998. Design Procedures for Hinge Restrainers and Hinge Seat Width for Multiple-Frame Briges, Technical Report MCEER-98-0013, Multidisciplinary Center for Earthquake Engineering Research, University at Buffalo.

El-Khoury, A., G. Washer, and T. A. Weigel, 1996. "Finite element modeling of a pin hanger connection", Proc., *Structural Materials Technology, an NDT Conference*, February 20-23, 1996, San Diego, California. Technomic Publishing Co., pp. 284-289.

Federal Highway Administration (FHWA), 2006, *Seismic Retrofitting Manual for Highway Structures: Part 1 – Bridges*, Publication No. FHWA-HRT-06-032, Department of Transportation, McLean, Virginia.

Jankowski, R., Wilde, K., and Fujino, Y., 1998. "Pounding of superstructure segments in isolated elevated bridges during earthquakes", Earthquake Engineering and Structural Dynamics, 27, 487-502.

Lai, Leon L-Y, 1997, "Seismic vulnerability of bridges containing pin-hanger connections", *Computing in civil engineering : Proc., Fourth Congress held in conjunction with A/E/C Systems,* Philadelphia, Pennsylvania, June 16-18, 1997. American Society of Civil Engineers, pp. 672-679.

McKenna, F. and Fenves, G., 2001. "The OpenSees Command Language Manual: version 1.2," Pacific Earthquake Engineering Center, Univ. of Calif., Berkeley. (http://opensees.berkeley.edu).

Multidisciplinary Center for Earthquake Engineering Research (MCEER), 2006, *Seismic Isolation of Highway Bridges,* Special Report MCEER-06-SP07, Buffalo, NY.

Pacific Earthquake Engineering Research Center. 25 Apr. 2009. <http://peer.berkeley.edu/nga/>

Priestley, M. J. N., Seible, F. and Calvi, G. M. (1996), *Seismic Design and Retrofit of Bridges*, John Wiley & Sons, New York, USA.

Scott, M. H. and G. L. Fenves, 2006. "Plastic hinge integration methods for force-based beam-column elements", Journal of Structural Engineering, ASCE, 132(2):244-252.

South, J. M., C. Hahin, R. O. Telford, 1992. *Analysis, inspection, and repair methods for pin connections on Illinois bridges.* Report no. FHWA-IL-PR-107, Illinois Dept. of Transportation, Bureau of Materials and Physical Research.

Wilson, N. and Ryan, K., 2009. *Seismic Retrofit Guidelines for Utah Highway Bridges.* Rep. No. FHWA-UT-09-06.